

MATRIX ISOLATION STUDY OF OZONE WITH HALOGEN-CONTAINING ALKANES

A thesis submitted in partial fulfilment of the requirements of the
degree of Doctor of Philosophy

by

Jonathan Roger Dann

Christopher Ingold Laboratories

University College London

University of London

1996

ProQuest Number: 10017225

All rights reserved

INFORMATION TO ALL USERS

The quality of this reproduction is dependent upon the quality of the copy submitted.

In the unlikely event that the author did not send a complete manuscript and there are missing pages, these will be noted. Also, if material had to be removed, a note will indicate the deletion.



ProQuest 10017225

Published by ProQuest LLC(2016). Copyright of the Dissertation is held by the Author.

All rights reserved.

This work is protected against unauthorized copying under Title 17, United States Code.
Microform Edition © ProQuest LLC.

ProQuest LLC
789 East Eisenhower Parkway
P.O. Box 1346
Ann Arbor, MI 48106-1346

ABSTRACT

The main aim of this research is to study, using Fourier-transform infrared spectroscopy, the photochemical reaction of ozone with some halogen-containing alkanes in low temperature matrices. The reactions between halogenated alkanes and ozone, studied in this thesis, can be applied to gas phase atmospheric research with regard to ozone depletion. One example, not expanded on in this thesis, is the search for ozone-friendly species (refrigerants, propellants etc.), especially since one of the provisions of the Montreal protocol is to phase-out such species.

Matrix reactions are carried out at low temperatures and, this means that the reactants are often effectively unable to react and, thus many 'reactive' or otherwise 'difficult to study' compounds can be stabilized and studied spectroscopically. In these experiments, the matrices must be photolysed in order to initiate a reaction; and we have used infrared, visible and ultraviolet irradiation to initiate reactions. By careful selection of the photolysis wavelength range used to irradiate the matrix it is possible to form different products and, thus reveal the photochemical reaction path.

The matrix environment also enables us to detect reactions that would not occur in the gas phase; in a matrix the species are held in close proximity to one another, allowing a variety of secondary reactions to occur, whilst, in the gas phase the primary products usually separate rapidly. This facet of a matrix reaction - by which the products are held closely together - has enabled us to study a range of nearest-neighbour complexes that were generated *in situ* by careful selection of the precursors.

Using matrix techniques, the reaction of ozone with halogen-containing compounds leads to the observations below.

In the cases of the single iodine-containing precursors ozone binds weakly with the iodine atom, and this modifies the photochemistry of ozone, allowing the effective dissociation of ozone. The transfer of an oxygen atom to the precursor leads to the formation of several new species. In addition to detecting these new species, it was

possible to determine wavelength-dependent photolysis pathways for these reactions.

The reaction of ozone with the halogen-containing precursors, studied in this thesis, leads invariably to the production of carbonyl complexes. The rigid nature of the matrix means that the spectra of these perturbed carbonyl complexes can be recorded, and the wavenumbers of specific bands compared between similar species. Similar comparisons are made between the carbon monoxide...Lewis acid complexes which tend to be produced after further photolysis of the carbonyl complexes. Trends are observed for these complexes in which the bands of the complex are shifted from those of the isolated species; this shift can be related to the Lewis acid strength of the perturber.

Finally, the carbonyl (COBrF), formed in the reaction of tribromofluoromethane with ozone, dissociates via an alternative mechanism to produce the radical-atom pair FCO and Br. The study of the subsequent reactions of these two might possibly have important implications with regard to processes occurring in the atmosphere.

ACKNOWLEDGMENTS

I must first thank Dr. Rob Withnall without whom the original impetus and apparatus for matrix experiments at U.C.L would not exist. Any mention of thanks, with regard equipment, would not be complete without thanking John Hill, Dave Knapp and the members of the workshop. Thanks also to my friends throughout the department, the Clark group, ULSAC and Prof. R.J.H. Clark who made the last few years an education. My special thanks go to Ian, for reading these chapters and for listening to my various research ideas, career aspirations etc.

And finally, to Vicky, my Mum, Nan, Tony and Pepper without whom the last seven years would have been a lot harder.

I gratefully acknowledge the financial support of the E.P.S.R.C. and UCL, and the ULIRS for use of the Bruker IFS 113v.

CONTENTS

ABSTRACT	ii
LIST OF FIGURES	viii
LIST OF TABLES	x
1. INTRODUCTION	1
1.1 MATRIX ISOLATION	1
1.2 IDEA FOR THIS STUDY	2
1.3 THESIS OUTLINE	3
2. EXPERIMENTAL	5
2.1 INTRODUCTION	5
2.2 PROPERTIES OF MATRICES	5
2.3 INFRARED SPECTROSCOPY	7
2.4 EXPERIMENTAL EQUIPMENT	14
2.4.1 Cryogenic & Gas handling equipment	14
2.4.2 Spectroscopic equipment	18
2.4.3 Photolysis equipment	18
2.5 EXPERIMENTAL TECHNIQUE	19
2.5.1 Preparation of precursors	19
2.5.2 Experiments performed on a matrix	20
2.5.3 Methodology of a typical experiment	23
3. REACTION OF ALKYL HALIDES WITH OZONE	25
3.1 INTRODUCTION	25
3.2 IODOETHANE, C ₂ H ₅ I	26
3.2.1 Results	27
3.2.2 Discussion	31
3.3 BROMOETHANE, C ₂ H ₅ Br	40
3.3.1 Results	40
3.3.2 Discussion	42

3.4	2-IODOPROPANE, (CH ₃) ₂ CHI	44
3.4.1	Results	44
3.4.2	Discussion	46
3.5	CONCLUDING REMARKS	52
4.	REACTION OF POLYFLUOROiodoethanes WITH OZONE	72
4.1	INTRODUCTION	72
4.2	PENTAFLUOROiodoethane, C ₂ F ₅ I	73
4.2.1	Results	74
4.2.2	Discussion	78
4.3	1,1,1-TRIFLUOROiodoethane, CF ₃ CH ₂ I	82
4.3.1	Results	83
4.3.2	Discussion	86
4.4	1,1,2,2-TETRAFLUOROiodoethane, CF ₂ HCF ₂ I	90
4.4.1	Results	90
4.4.2	Discussion	92
4.5	1,1,1,2-TETRAFLUOROiodoethane, CF ₃ CFHI	95
4.5.1	Results	95
4.5.2	Discussion	98
4.6	POLYFLUOROETHANAL...XI COMPLEXES	99
4.7	PHOTOCHEMICAL INTERCONVERSION	101
4.8	CONCLUDING REMARKS	104
5.	REACTION OF CHLOROiodomethane AND DIiodomethane	131
5.1	INTRODUCTION	131
5.2	CHLOROiodomethane, CH ₂ ClI	132
5.2.1	Results	133
5.2.2	Discussion	136
5.3	DIiodomethane, CH ₂ I ₂	143
5.3.1	Results	143
5.3.2	Discussion	144
5.4	COMPARISON OF THE Iodoso- SPECIES (Z-IO)	145

5.5	CONCLUDING REMARKS	147
6.	OXYGEN ATOMS WITH BROMOCHLOROMETHANES	161
6.1	INTRODUCTION	161
6.2	BROMOCHLOROMETHANE, CH ₂ BrCl	162
6.2.1	Results	162
6.2.3	Discussion	165
6.3	DIBROMOCHLOROMETHANE, CHBr ₂ Cl	172
6.3.1	Results	172
6.3.2	Discussion	175
6.4	CONCLUDING REMARKS	180
7.	TRIBROMOFLUOROMETHANE WITH OXYGEN ATOMS	193
7.1	INTRODUCTION.	193
7.2	RESULTS	194
7.3	DISCUSSION	197
7.4	CONCLUDING REMARKS	200
8.	CONCLUSIONS AND SUGGESTIONS FOR FUTURE WORK	208
8.1	CONCLUSION	208
8.2	SUGGESTIONS FOR FURTHER WORK	210
	APPENDIX A	216
	REFERENCES	217

LIST OF FIGURES

2.1. Schematic diagram of a Michelson interferometer	12
2.2. Schematic diagram of a Genzel interferometer	12
2.3. Diagram of the cryogenic cold window and shroud	15
2.4. Schematic diagram of the gas handling manifolds	17
3.1. Infrared spectra showing bands of the $C_2H_5I\cdots O_3$ complex.	64
3.2. Infrared spectra showing bands of iodoethane, C_2H_5IO	65
3.3. Infrared spectra showing bands of iodylethane, $C_2H_5IO_2$	66
3.4. FTIR spectra of C_2H_5OI , HOI and the $CH_3COH\cdots HI$ complex	67
3.5. Infrared spectra showing bands of the ethanal $\cdots HBr$ complex	68
3.6. Infrared spectra showing bands of 2-iodosopropane, $(CH_3)_2CHIO$	69
3.7. Infrared spectra showing bands of 2-iodylpropane, $(CH_3)_2CHIO_2$	70
3.8. Infrared spectra showing bands of the acetone $\cdots HI$ complex	71
4.1. FTIR spectra showing bands of iodosopentafluoroiodoethane, C_2F_5IO	122
4.2. The $\nu_{C=O}$ region of the complex $CF_3COF\cdots IF$	123
4.3. FTIR spectra showing bands of CF_3CH_2IO and of $CF_3COH\cdots HI$	124
4.4. Infrared spectra of iodyl-1,1,1-trifluoroethane, $CF_3CH_2IO_2$	125
4.5. Infrared spectra showing the $\nu_{C=O}$ bands of $CF_3COH\cdots HI$	126
4.6. FTIR spectra of CF_2HCF_2IO and $CF_2HCOF\cdots IF$	127
4.7. Infrared spectra showing the $\nu_{C=O}$ bands of $CF_2HCOF\cdots IF$	128
4.8. FTIR spectra of CF_3CFHIO , of CF_3CFHIO_2 , and of $CF_3COF\cdots HI$	129
4.9. FTIR spectra of the complexes $CF_3COF\cdots HI$ and $CF_3COH\cdots IF$	130
5.1. Infrared spectra showing bands of iodosochloromethane, $CH_2ClI^{18}O$	156
5.2. Infrared spectra of the band attributed to HOI	157
5.3. FTIR spectra showing the $\nu_{C=O}$ bands of the $COHCl\cdots HX$ complexes	158
5.4. Infrared spectra showing the ν_{HCl} and ν_{CO} bands of $OC(HCl)(HI)$	159
5.5. Plot of energy ν . C-I-O angle between CH_2ClIO and CH_2ClOI	160
6.1. FTIR spectra showing the $\nu_{C=O}$ bands assigned to $COHCl$ and $COHBr$	187
6.2. Plot of optical density ν . time for the reaction of CH_2BrCl with O_3	188
6.3. FTIR spectrum showing bands of the $(OC)(HCl)(HBr)$ complexes	189

6.4. The $\nu_{C=O}$ bands of COHCl, COHBr and COBrCl	190
6.5. Plot of optical density ν . time for the reaction of CHBr ₂ Cl with O ₃	191
6.6. Infrared spectra of various carbon monoxide complexes	192
7.1. Infrared spectra of CBr ₃ F, COBrF and FCO	205
7.2. Infrared spectra showing the conversion between COBrF and FCO...Br . .	206
7.3. Infrared spectra showing bands of COBrF, FCO and FC(O)O _x	207

LIST OF TABLES

3.1. Infrared bands of the molecular complex $C_2H_5I \cdots O_3$	53
3.2. Infrared bands of the molecular complex $C_2H_5I \cdots O_3$	54
3.3. Infrared bands of iodosoethane, C_2H_5IO	55
3.4. Infrared bands of iodylethane, $C_2H_5IO_2$	55
3.5. Infrared bands of HOI and CH_3CH_2OI	56
3.6. Infrared bands of ethanal, and ethanal \cdots HI complexes	57
3.7. Infrared bands of bromoethane	58
3.8. Infrared bands of the ethanal \cdots HBr complex.	59
3.9. Infrared bands of ethanal and ethanal \cdots HX complexes	60
3.10. Infrared bands of 2-iodopropane	61
3.11. Infrared bands of 2-iodosopropane, $(CH_3)_2CHIO$	62
3.12. Infrared bands of 2-iodylpropane, $(CH_3)_2CHIO_2$	62
3.13. Infrared bands assigned to hydrogen hypoiodide, HOI	62
3.14. Infrared bands assigned to acetone complexes	63
4.1. Infrared bands of pentafluoroiodoethane, C_2F_5I	105
4.2. Infrared bands of ozone in the complex, $C_2F_5I \cdots O_3$	106
4.3. Infrared bands of iodosopentafluoroiodoethane, C_2F_5IO	107
4.4. Infrared bands of iodylpentafluoroethane, $C_2F_5IO_2$	108
4.5. Infrared bands of hypoiodopentafluoroethane, C_2F_5OI	108
4.6. Infrared bands of the complex $CF_3CFO \cdots IF$	109
4.7. Infrared bands of 1,1,1-trifluoroiodoethane, CF_3CH_2I	110
4.8. Infrared bands of ozone in the $CF_3CH_2I \cdots O_3$ complex	111
4.9. Infrared bands of iodoso-1,1,1-trifluoroethane, CF_3CH_2IO	112
4.10. Infrared bands of iodyl-1,1,1-trifluoroethane, $CF_3CH_2IO_2$	112
4.11. Infrared bands of hypoiodo-1,1,1-trifluoroethane, CF_3CH_2OI	112
4.12. Infrared bands of the complex $CF_3CHO \cdots HI$	113
4.13. Infrared bands of 1,1,2,2-tetrafluoroiodoethane, CF_2HCF_2I	114
4.14. Infrared bands of ozone in the complex, $CF_2HCF_2I \cdots O_3$	115
4.15. Infrared bands of iodoso-1,1,2,2-tetrafluoroethane, CF_2HCF_2IO	115

4.16. Infrared bands of the complex $\text{CF}_2\text{HCFO}\cdots\text{IF}$	116
4.17. Infrared bands of 1,1,1,2-tetrafluoroiodoethane, CF_3CFHI	117
4.18. Infrared bands of ozone in the complex, $\text{CF}_3\text{CHFI}\cdots\text{O}_3$	118
4.19. Infrared bands of iodoso-1,1,1,2-tetrafluoroethane, CF_3CFHIO	119
4.20. Infrared bands of iodyl-1,1,1,2-tetrafluoroethane, $\text{CF}_3\text{CFHIO}_2$	119
4.21. Infrared bands of $\text{CF}_3\text{COF}\cdots\text{HI}$ and $\text{CF}_3\text{COH}\cdots\text{IF}$	120
4.22. Carbonyl bands of the complexes, $\text{CF}_3\text{COX}\cdots\text{XI}$ ($\text{X} = \text{H}$ or F)	121
5.1. The infrared bands of chloriodomethane, CH_2ClI	148
5.2. Infrared bands assigned to ozone in the $\text{CH}_2\text{ClI}\cdots\text{O}_3$ complex	149
5.3. Infrared bands of iodosochloromethane, CH_2ClIO	150
5.4. Infrared bands of hypiodochloromethane, H_2ClCOI	150
5.5. Infrared bands of the $\text{COHCl}\cdots\text{HI}$ complex	151
5.6 Infrared bands of the complex, $\text{OC}(\text{HCl})(\text{HI})$	151
5.7. Infrared bands of diiodomethane, CH_2I_2	152
5.8. Infrared bands of the products of reaction of CH_2I_2 with O atoms	154
5.9.a. Z-Matrix of iodosochloromethane, $\text{H}_2\text{ClC-I-O}$ (C-I-O angle $\sim 99^\circ$)	155
5.9.b. Z-Matrix of hypiodochloromethane, $\text{CH}_2\text{Cl-O-I}$ (C-I-O angle $\sim 28^\circ$)	155
5.9.c. Interatomic distances $r^{\text{a,b}}$ of CH_2ClIO and CH_2ClOI	155
6.1. Infrared bands of bromochloromethane, CH_2BrCl	181
6.2. IR bands of $\text{COHCl}\cdots\text{HBr}$, $\text{COHBr}\cdots\text{HCl}$ and COBrCl	182
6.3. Infrared bands of the $(\text{CO})(\text{HCl})(\text{HBr})$ complexes.	183
6.4. Infrared bands assigned to several $\text{COHCl}\cdots\text{XY}$ complexes.	183
6.5. Infrared bands of dibromochloromethane, CHBr_2Cl	184
6.6. IR bands of $\text{COHCl}\cdots\text{Br}_2$, $\text{COHBr}\cdots\text{BrCl}$ and $\text{COBrCl}\cdots\text{HBr}$	185
6.7. Infrared bands of the complexes $(\text{OC})(\text{HBr})(\text{BrCl})$ and $(\text{OC})(\text{HCl})(\text{Br}_2)$	186
7.1. Infrared bands of tribromofluoromethane, CBr_3F	202
7.2. Infrared bands of the products of the reaction of O atom with CBr_3F	203
7.3. Comparison of bands of COF_2 and $\text{COF}_2\cdots\text{X}$ ($\text{X} = \text{Br}_2, \text{IF}, \text{Cl}_2$)	204
8.1. The various species and complexes detected in this thesis	214
A.1. Bands of O_3 detected after co-deposition with other halocarbons	216

ABBREVIATIONS

Å	Angstroms
c.	circa
cm ⁻¹	wavenumber
δ	bending vibrational mode
ir	infrared
nm	nanometer
ν	stretching mode
ρ	rocking mode
τ	torsion
UV	ultraviolet
vac	vacuum
vis	visible
ω	wagging mode

to Vicky

Chapter 1

INTRODUCTION

1.1 MATRIX ISOLATION

Historical background

Pimentel¹ and Porter² are credited with separately carrying out the first matrix isolation experiments using inert gases as matrix media. Although, Lewis and Lipkin's³ phosphorescence studies of aromatic molecules in low temperature glassy media pre-date these and can probably be viewed as the first use of the technique. Pimentel has subsequently come to be regarded as the father of matrix isolation with his early spectroscopic investigations of photolytically produced radicals such as HNO⁴ and HCO⁵ paving the way for future experiments like this; in which species of interest are generated photolytically *in situ* in the matrix. Since the early studies of unstable intermediates and radicals, the matrix technique has been applied to a wide range of investigations including condensates from high temperature vapours, interstellar ices, isomerism, metal complexes, molecular complexes and even as a detector for HPLC. Whilst the early studies focused on the detection and generation of radicals and unstable intermediates, later workers began to study reactions occurring in matrices, typically between atoms and stable molecules. Various diatomic and triatomic species have been used to generate these atoms (N, S, F, Cl, Br, O etc.),⁶ ozone becoming the most common source - and that used in this study - of oxygen atoms. The results from these and numerous other matrix experiments have been well documented in a number of books^{7,8,9,10,11,12,13,14} and papers.^{15,16,17,18}

1.2 IDEA FOR THIS STUDY

The aim of this work is to study the reactions between ozone and halogen-containing hydrocarbons, primarily to observe and characterise novel intermediates, and to determine mechanisms for such processes. The reaction of halocarbons with ozone, in matrices, also has relevance to processes that may occur in the gas phase, and specifically in the atmosphere, since some of the precursors are currently used as pesticides or are related closely to commonly used ones.

As an aside, there has been a long standing interest in the reaction of oxygen atoms with iodine-containing alkanes, specifically iodomethane, with reports appearing each decade since the 1960's. The study of di-iodomethane and chloriodomethane, here, has continued the interest in iodinated methanes into the 1990's. The investigation of the reaction of ozone with iodine monochloride¹⁹ can be viewed as the precursor to this and to the studies with iodomethane²⁰ and trifluoriodomethane.²¹ Each experiment studied in this thesis has been motivated by and extends the research of a number of previous authors and, for clarity and space these considerations are mentioned within the relevant chapters.

Overview of the aims behind each precursor

The precursors and the way in which they react with ozone can be roughly split into two groups: those that contain one iodine atom; and those that do not (either containing more than one iodine atom or none at all). The first group (those containing a single iodine atom), began with iodoethane (chapter 3) as an extension to the previously studied iodomethane,²⁰ with the added possibility of observing differing reactions due to the increased carbon-chain length. The results from this study, specifically the detection of HOI, prompted the study of the rest of the species in chapters 3, 4 and 5. 2-Iodopropane (chapter 3) extended the carbon-chain length by a further carbon atom, and had the possibility that some steric effect might alter the products formed. The polyfluoroiodoethanes (chapter 4) were studied to help

clarify the mechanism proposed for the reaction of iodoethane with ozone in chapter 3. They are also an extension to the ozone/trifluoroiodomethane²¹ study. The investigations with chloriodomethane and di-iodomethane extended the study of iodinated methanes in a further direction by adding a second halogen atom (either Cl or I). In chapters 3-5 the species having the backbone structure X-CH₂I, where X = H,²⁰ Cl, I, CH₃ and CF₃, have now been studied.

The study of the second group, was motivated by two goals, the first being an attempt to detect Br-O_x bonds. The second, is to detect and compare the spectra of a number of carbonyl- and carbon monoxide-Lewis acid complexes. The first goal, motivated the initial study with bromoethane, and comparisons between the reactions of species having different halogen atoms were made. The second, was motivated by the detection of the carbonyl and carbon monoxide complexes reported as products of the reaction of ozone with iodinated methanes (chapter5). These suggested that a number of interesting complexes might be formed with other halogenated methanes and, thus bromochloromethane and dibromochloromethane (chapter 6) were treated with oxygen atoms and the products reported. Tribromofluoromethane (chapter 7) was a slight departure, in that knowledge of the way in which oxygen atoms react with halogenated alkanes was used to select CBr₃F as a precursor to form COBrF. The photochemical and thermal reactions of this product were subsequently studied in low temperature matrices. In chapters 3-7 the many carbonyl- and carbon monoxide-Lewis acid complexes reported, enable comparisons to be made between the spectra of the complexes having different Lewis acid groups but the same carbonyl, and *vice versa*.

1.3 THESIS OUTLINE

This thesis is divided into eight chapters with chapters 1 and 2 providing the reader with an overview of this matrix study, its place in the larger body of matrix type experiments and an understanding of the equipment and techniques involved. The contents and aims of chapters 3-7 are mentioned in more depth below. The chapters are arranged first in terms of similar chemical precursors, and secondly to form a

logical progression from one study to the next. Each of the chapters is self-contained in that all discussions, comparisons and conclusions pertaining to the study are given in the relevant chapter.

Chapter 3 reports the results of the reaction of ozone with iodoethane, bromoethane and 2-iodopropane. These reactions produce novel intermediates containing I-O bonds and some carbonyl complexes for which the geometry of the complex can be inferred from the wavenumber shifts of the detected bands. A mechanism for these reactions is proposed, based on the species that were detected.

Chapter 4 continues the study of iodine-containing precursors with the study of four polyfluoroiodoethanes, these precursors being chosen to provide a larger range of intermediate and final products, and to further study the mechanism.

Chapter 5 investigates two more iodine-containing precursors, but based around the one-carbon system. In this chapter the beginnings of a new thread are reported with the detection of complexes having different halogen atoms, e.g. COHX...HY and OC(HX)(HY), where X and Y are different halogen atoms.

Chapter 6 continues the work started in chapter 5 by examining the reaction of bromine- and chlorine-containing methanes with ozone. The products reported extend the number of known carbonyl- and carbon monoxide-complexes. The spectra of the species detected are compared with the spectra of the products detected after photolysis of the iodine-containing precursors.

Chapter 7 reports the products of the reaction of CBr₃F with ozone and their subsequent photochemical behaviour. The detected products confirm the proposed gas phase mechanism, as well as, the detection of several additional products.

Chapter 8 summarises the work reported in chapters 3-7, makes some general conclusions and provides some suggestions for modifications to the current study and for future work.

Chapter 2

EXPERIMENTAL

2.1 INTRODUCTION

The experimental methods and considerations undertaken to complete this research are mentioned in this chapter. These range from the choice of matrix material, of spectroscopic technique and, of experiments to be performed on the matrix. The experimental apparatus required to complete these experiments is reported, as are the technique and theory that are relevant to an understanding of their operation. The apparatus and technique reported is that currently used in this laboratory. A final section gives an outline of a typical experiment for the reference of future workers.

2.2 PROPERTIES OF MATRICES

An ideal matrix material will provide an inert, rigid support at the temperatures to be studied, it will also be spectroscopically transparent over the required regions. It should also be sufficiently volatile to enable it to be mixed with the precursors in the gas phase at room temperature. Thus species held in a matrix, under these conditions, are effectively 'trapped' and can be studied spectroscopically at leisure, on the timescale of conventional spectrometers. The ideal properties of matrix materials are discussed in more detail below.

Inertness. When attempting to study the reaction of two species in a matrix it is of particular importance that the matrix support material does not react with either precursor. It is for this reason that argon was chosen in this study, since other

possible fluorocarbon or relatively inert materials, i.e. N₂, might have reacted under the photolysis conditions used in these experiments. The inertness of a matrix material is also affected by its purity, since any nitrogen or halocarbon impurities would be expected to react with either ozone or the other precursor. For this reason all reagents and matrix materials were purchased at the highest purity possible, and where appropriate degassed and decanted by freeze-thaw techniques. Note: in some experiments oxygen was used as the matrix support with the intention that photolysis would rupture the O-O bond and create O atoms which would react with the other precursor in the matrix. It was hoped that the oxygen matrices would support the formation of differing products to those formed in ozone/argon matrices.

Rigidity. The rigidity of the matrix is important for two reasons. The first is that spectral collection is made more easy if a uniform rigid matrix is produced. The second is that a rigid, low temperature matrix will prevent most reactions from occurring. The rigidity prevents any bimolecular collisions from occurring, this increases the lifetime of any reactive intermediates, whilst the low temperature prevents any reactions that have any significant activation energy.

As a rough estimate matrix materials become sufficiently softened to allow diffusion at approximately half the melting point (*cf.* Tammann's rule used in solid-state studies), thus both argon and oxygen must be cooled to below 25 K, and ideally to ~ 14 K to meet the rigidity requirements.

Spectroscopy. Infrared spectroscopy is the technique of choice in these studies because of the ease of collection of spectra and the narrow band widths (~ 1 cm⁻¹) exhibited, which make identification of species from their spectra easier. Argon meets the matrix criteria of spectral transparency at the temperatures employed and over the spectral region (note: the transparency of some noble gases i.e. Xe, varies with temperature). The matrices were deposited slowly (~ 3 mmolh⁻¹) and at slightly elevated temperatures (~ 17 K) to improve the transparency of the matrices and hence the recorded spectra.

Volatility. For ease of preparation the matrices are best mixed in the gas phase at room temperature and, for this reason the chosen matrix material should be

sufficiently volatile at room temperature. This poses an alternative problem since the more volatile the matrix material, the lower the temperature required to 'freeze' the matrix on the cold window (see above - rigidity).

Thermal properties. The matrix material should be chosen, taking into account the thermodynamic properties of the matrix (Latent heat of fusion, lattice energy, and thermal conductivity) so as to minimise the heat produced in forming the matrix and maximise the ability of the matrix material to transfer heat. The latter is of particular importance since as the thickness of the matrix increases the excess energy must be removed through the matrix; a matrix material with poor thermal conductivity may experience localised warming and thus evaporation of the matrix. The rates at which the matrices are deposited can have a significant effect on these properties and, this is another reason for the slow deposition rate.

Other properties. The electrical properties and crystal structures of the matrix materials at low temperatures can have an effect on the recorded spectra. These phenomena are discussed in further detail elsewhere.⁸ Of interest to these studies is the possibility of multiple trapping sites that might give rise to additional bands in the spectra. These are reported for the ν_3 bands of ozone isolated in argon (see chapter 3).

2.3 INFRARED SPECTROSCOPY

Infrared spectroscopy has been used to study these matrices for two reasons. The first is that infrared provides vibrational information about the species in the matrix, and thus the species can be identified from their spectra. The second, is that infrared spectrometers are commercially available, and unlike other spectral techniques the radiation incident on the matrix does not damage the matrix, for example, with Raman spectroscopy the use of lasers can cause areas of the matrix to warm and thus evaporate, destroying the matrix. The collection of spectra is experimentally straight forward, unlike that for spectroscopies which collect reflected or scattered light. The

use of infrared and other spectroscopes is covered in a number of texts.^{6-13,22,23}

The infrared spectra of matrix isolated species usually have very narrow linewidth and only exhibit bands attributed to vibrations; any rotational component being removed because of the low temperature and rigidity of the matrix. The spectra are, for the most part, in very good agreement with the gas phase spectra; the isolation in the matrix approximates to that in the gas phase. The narrow linewidth of the bands makes isotopic substitutions easy to distinguish, this is very useful as it enables even small shifts between heavy isotopes to be observed. These advantages ease the identification of product species from their spectra.

The rest of this section provides a basic understanding of the origins of infrared spectra, and a description and discussion of the Fourier-transform spectrometer used in this work.

Underlying theory

The infrared absorption spectra recorded in this study arise from the vibrational motions of a molecule in its ground electronic state. The vibrating molecule absorbs in the infrared region of the spectrum, typically between 4500 and 400 cm^{-1} . The case of a diatomic molecule is used to illustrate the problem and to help to understand these vibrations in terms of the observed spectra. Nuclei move in a potential arising from electrostatic interactions between the particles (electrons and nuclei), this can be seen from the adiabatic Born-Oppenheimer approximation.

Due to the vast mass difference between the nuclei and electrons we can consider that the electron cloud adjusts adiabatically to any nuclear motion so as to minimise the potential energy of the system at any nuclear separation. The nuclei therefore effectively move in a potential arising from electrostatic interactions between the particles.

For a given potential, $V(r)$, where r is the separation between the particles, the problem is reduced to that of a single particle of mass, $\mu = m_1 m_2 / m_1 + m_2$ (the reduced

mass) moving in the same potential. To a good approximation most internuclear potentials can be considered to be harmonic for small displacements about the equilibrium position. In this case the problem has the exact classical analogue of two particles joined by a massless linear restoring spring. The frequency, ν , at which the system oscillates is found from the solution of the equation of motion.

$$\mu \frac{d^2r}{dt^2} = -k(r-r_0)$$

which has the solution

$$\nu = 1/2\pi (k/\mu)^{1/2}$$

where r_0 is the equilibrium separation and k is the force constant.

Classically an oscillating system will emit and absorb radiation at this resonant frequency. Classical mechanics can therefore go some way to explaining the general features of infrared spectra. If we are interested in the intensities of radiation, or specifically on selection rules then quantum mechanics is required.

Quantum mechanically a series of vibrational levels are predicted (equally spaced in the case of harmonic potential). Radiation is then seen as being associated with a transition between two levels. The Bohr frequency rule gives the frequency of light, ν , absorbed or emitted on the transition between two energy states, thus:

$$\Delta E = E' - E'' = h\nu$$

where ΔE is the change in energy between energy, E'' , of the ground state and E' of the excited state, and h is Planck's constant. A more detailed discussion of classical and quantum methods is discussed elsewhere.^{24,25}

Fourier-transform infrared spectroscopy (FTIR)

A Fourier-transform infrared spectrometer can be said to consist of four main components, the source, interferometer, sample compartment, and detector. In these experiments, a Globar source was used to supply the infrared radiation over the range 4500 - 400 cm^{-1} . The sample chamber is located after the interferometer and before the detector and can be evacuated - using a mechanical vacuum pump - to reduce the absorptions of water and carbon dioxide which would otherwise interfere with the spectrum. A liquid-nitrogen cooled mercury-cadmium-telluride (MCT) detector is used, this being the most sensitive available in the mid-IR region. A deuterated-triglyceride-sulphate (DTGS) detector is a common alternative to the MCT, however these are not as sensitive as the MCT detector, but have the advantage that they can be used at room temperature. The operation of the interferometer is discussed below. The Fourier-transform technique is described in a number of texts^{26,27,28,29} in addition to the description given below.

The interferometer. The basis of this device is to split the wavefront of the incident light into two parts at the beamsplitter. A time-dependent path difference is created between the two parts, which are then made to recombine at the beamsplitter. For a white light source a series of pulses are created at the point of zero path difference. The generation of these pulses of light, their subsequent detection and conversion into spectral information is discussed below.

A typical Michelson interferometer (Fig. 2.1) operates in the following manner. Light from the source is directed to the beamsplitter. At the beamsplitter 50% of the incident light is reflected onto a fixed mirror, while the other 50% is transmitted to a moving mirror. The two beams are reflected from the two mirrors and recombine and interfere at the beamsplitter - and again each beam is reflected or transmitted at the beamsplitter - with 50% of each beam combining and being transmitted to the detector. Upon recombination at the beamsplitter the path length travelled by the beams is altered by the moving mirror, and depending on this path difference between beams the interference may be either constructive or destructive. For path differences of integral wavelengths, $n\lambda$, the interference is constructive, while destructive

interference occurs for path differences of $(n + 1/2)\lambda$. It can then be shown that the intensity of the transmitted beam $I(\lambda)$, is a function of the optical path difference, x (cm), and this is given by the equation:

$$I'(x) = 0.5 I(\lambda) \{1 + \cos 2\pi x/\lambda\}$$

In the above equation, the modulated component $0.5 I(\lambda) \cos 2\pi x/\lambda$ is called the interferogram. The above equation can be rearranged in terms of wavenumbers, ν , ($\nu = 1/\lambda$) to the following:

$$I(x) = 0.5 I(\nu) \cos 2\pi x\nu$$

Spectral information can be obtained from this sinusoidal interferogram as the amplitude is directly proportional to the intensity of the transmitted beam, $I(\nu)$, and its wavelength is directly proportional to the wavelength of the source. With the continuous sources used (in the required spectral range) the interferogram is the integral of the contributions from all the wavelengths emitted from the source.

The Bruker IFS 113v employs a Genzel interferometer (Fig. 2.2), this has a different optical arrangement in which there are two stationary mirrors which are coplanar with a moving mirror positioned between them. This has the advantage that for a mirror displacement of x , the optical retardation changes by $4x$, compared with $2x$ for a standard Michelson interferometer. This occurs because the light is reflected from two sides of the moving mirror in a Genzel interferometer. Thus the light travels to the moving mirror from the fixed mirror and back again (distance of $2x$) and, this occurs for both sides, hence the $4x$ optical displacement.

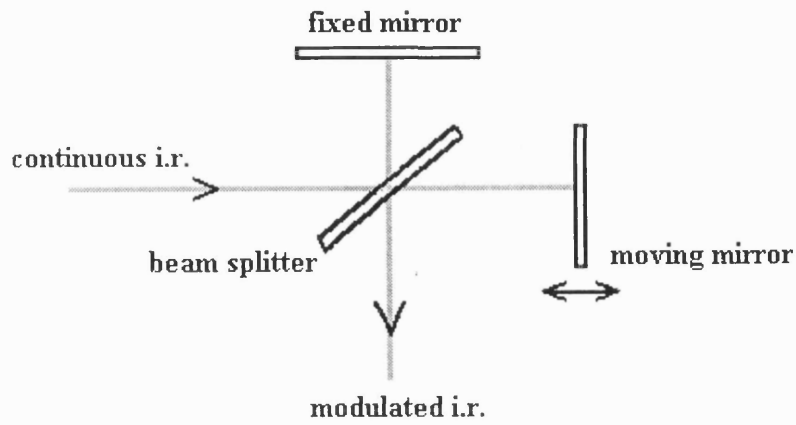


Figure 2.1. Schematic diagram of a Michelson interferometer.

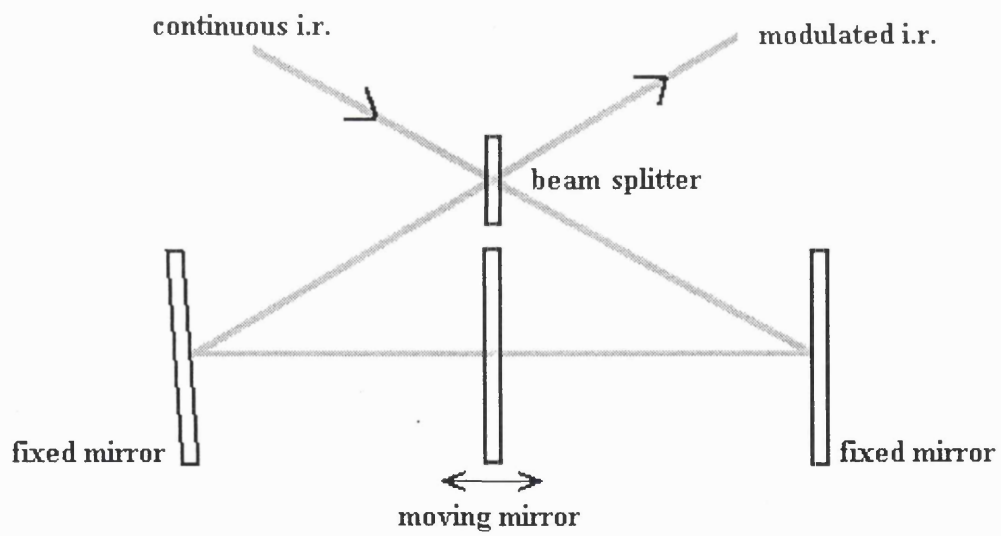


Figure 2.2. Schematic diagram of a Genzel interferometer.

Advantages of FTIR over dispersive infrared

Fourier-transform infrared spectroscopy has a number of important advantages over dispersive infrared spectroscopy. These being first Jaquinot's advantage, a measure of how much more throughput an interferometer gives due to an aperture being larger than the slits of a dispersive spectrometer. With the result that the optical throughput of an interferometer is greater than that of a dispersive spectrometer operating at the same resolution.

The second and most important advantage is Fellgett's (Multiplex) advantage. Acquisition of a spectrum of equal signal-to-noise, resolution, efficiency and source then it will take m times longer on a dispersive spectrometer. Where, m , the number of resolution elements is equal to the spectral width divided by the resolution. This advantage can be interpreted in another way - since we can see that the signal-to-noise ratio increases with $(n)^{1/2}$ (where n is the number of interferograms to be coadded) - this is that for equal data acquisition times the signal-to-noise ratio of measurements taken on a Fourier spectrometer will be $(m)^{1/2}$ times better than on a dispersive spectrometer. This advantage, due to the lack of a spatial wavelength selector (exit slit) in a Fourier spectrometer, is important for energy limited systems found with matrix experiments.

A third advantage, known as Connes advantage, relates to the intrinsic ability of the interferometer to record the frequency accurately, using a He-Ne laser which accurately measures the displacement of the moving mirror. This advantage enables the sample spectrum to be more accurately, and repeatably, referenced against a background spectrum and an absorbance or transmittance spectrum to be calculated. This is also important as it allows band wavenumbers to be known with confidence.

Another advantage occurs because the resolution of a FTIR spectrometer is related to the optical path difference between the moving and fixed mirrors. Thus higher resolutions are obtained by increasing the retardation of the moving mirror. In comparison, higher resolutions with dispersive spectrometers are achieved by using more dispersive gratings, or by using a series of gratings, which reduce the efficiency

of the spectrometer. This advantage makes a Fourier-transform spectrometer more suitable for high resolution infrared spectroscopy. Stray light has little effect upon the spectra recorded with FTIR spectrometers, in comparison stray light can cause an increase in the noise with dispersive spectrometers.

2.4 EXPERIMENTAL EQUIPMENT

The experimental equipment can be broken down into three component parts: (i) *cryogenic* and *gas handling* equipment, (ii) *spectroscopic* apparatus and (iii) *photolysis* apparatus. That is the means of generating matrix isolated species, their subsequent photolysis and the detection of the products of any reactions. Each of these three topics is discussed below.

2.4.1 CRYOGENIC AND GAS HANDLING EQUIPMENT

The cryogenic and gas handling apparatus is the hardware in which samples are initially 'matrix' isolated and subsequently irradiated and studied spectroscopically. The matrix deposition equipment and gas mixing apparatus will be discussed separately below. Vacuum technology and the types of different apparatus are well reported³⁰ and, a number of manufacturers provide very useful manuals³¹ for anyone contemplating the design and manufacture of an apparatus suitable for matrix experiments.

Matrix deposition equipment

The centre piece of the matrix experiment is the 'cold window', on which the matrix is formed, photolysed and studied spectroscopically. A schematic diagram of the apparatus necessary to perform these processes is shown in Fig. 2.3. The cold

window is housed within a vacuum shroud, which enables it to be cooled by means of an Air Products Displex DE 202 S closed-cycle He refrigerator. The cold window itself is made from caesium iodide, due to the spectral transparency (UV to far-ir) and thermal properties (good thermal conductivity and is resistant to thermal shock) of CsI. The cryostat and cold window are arranged vertically within the evacuable shroud, so that by rotation it may be placed in the correct alignment for either deposition, photolysis or spectral collection.

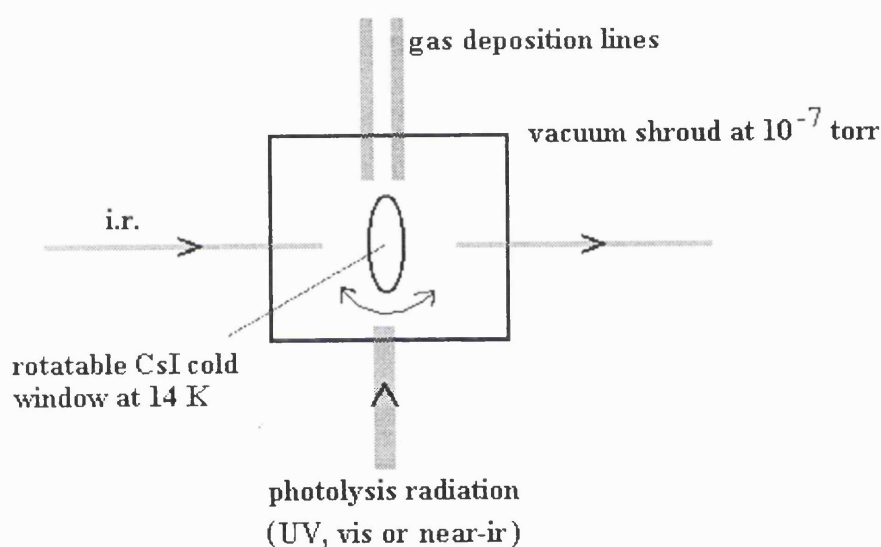


Figure 2.3 Shows a schematic of the cryogenic cold window and associated spectral and photolysis light paths, as well as the gas deposition lines.

The vacuum shroud, that houses the cryostat and cold window, has vacuum connections to an Edwards 63 mm Diffstak diffusion pump backed by an Edwards mechanical pump. This allows it to be evacuated to $\sim 10^{-7}$ torr. The shroud has two gland fittings through which steel capillary tubes are passed, these being directed so that the gaseous precursors can be sprayed onto the cold window. The shroud is fitted

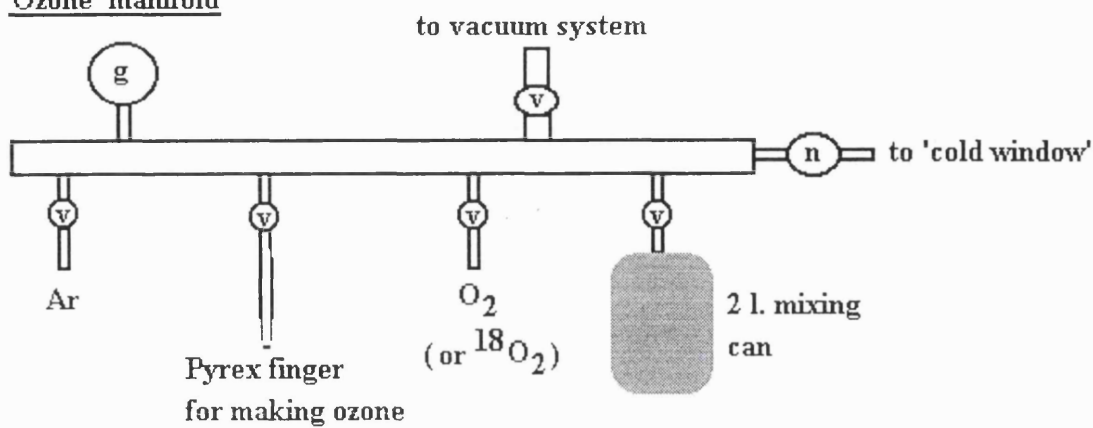
with three windows: two KBr windows for spectroscopic analysis, and a third made of quartz, for photolysis. The spectral windows (KBr), due to the design of the vacuum shroud, are 50 mm in diameter and thus KBr provides the required mechanical strength and transparency to infrared radiation that is required. It should be noted that while CsI windows transmit infrared radiation over a wider range, they are susceptible to 'creep', which is significant at this larger diameter in addition CsI windows of this diameter are significantly more expensive than KBr. However, CsI is a better choice for the cold window than KBr, because KBr is more susceptible to fracture due to temperature changes (thermal shock).

In addition to the requirements of the experiment mentioned above, the vacuum shroud has been designed to be reasonably compact, a feature that was important since it must fit into the sample chamber of the existing spectrometer. The shroud has been designed also to enable 180° reflectance and Raman scattering to be collected, although these spectra were not recorded in this work.

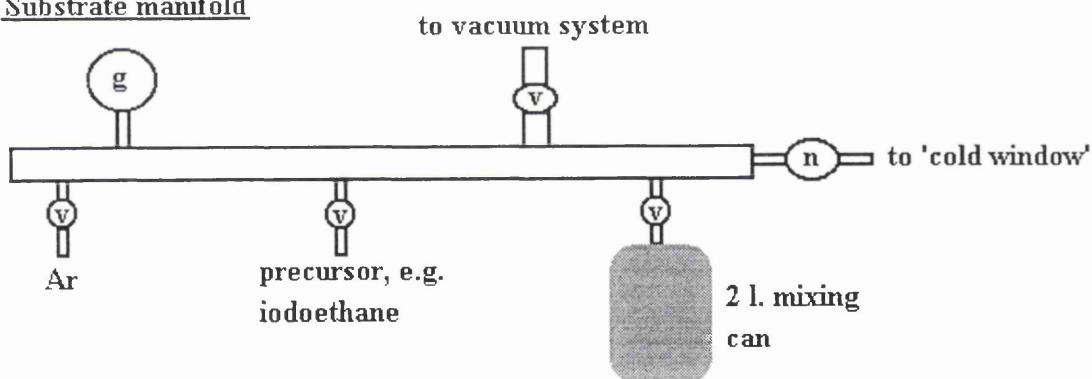
Gas handling apparatus

The apparatus includes two gas handling manifolds. These manifolds are used to prepare the gas, that contains the precursor and argon, to be deposited on the cold window and to meter the flow to the cold window. The manifolds are arranged as shown in the schematic (Fig. 2.4), with valves and appropriate connectors to enable evacuation of the manifolds, deposition of the gaseous mixes onto the cold window, and addition to the manifold of the various precursors to be used.

'Ozone' manifold



Substrate manifold



(v) - valve; (n) - needle valve; (g) - Bourdon type vacuum gauge.

Figure 2.4. Schematic diagram of the gas handling manifolds used to mix the precursors with argon and control the rate of deposition; one is used also to make ozone.

2.4.2 SPECTROSCOPIC EQUIPMENT

The deposited matrices are examined spectroscopically using an infrared spectrometer. The shroud and cryostat, seen previously, are arranged in the sample chamber of a Bruker model IFS 113v FT-IR spectrometer so that the radiation can be transmitted through the shroud windows and the CsI cold window itself. The spectrometer operates in the range 4000 - 560 cm^{-1} with a resolution of 1 cm^{-1} (higher resolution studies up to 0.25 cm^{-1} have been used). The spectrometer is equipped with a germanium-coated KBr beam splitter and liquid-nitrogen-cooled mercury-cadmium-telluride (MCT) detector. A typical spectrum consists of between 500 and 1000 scans. The interferograms recorded are coadded and converted to a single beam spectrum by a fast Fourier-transform algorithm²⁹ using a zero filling factor of times 2 and Happ-Genzel apodization.³² The spectrum of a deposited sample was then ratioed with a reference spectrum of the cold window before deposition to give a double-beam absorption spectrum.

2.4.3 PHOTOLYSIS EQUIPMENT

Photolysis of the matrices was achieved using an Oriel medium pressure xenon arc lamp, operating in the wavelength range 220 - 1000 nm, a 10 cm water filter was fitted to reduce the amount of infrared radiation incident on the matrix during photolysis; otherwise the matrix would warm. The wavelength of radiation incident on the matrix can be altered by the choice of a number of band pass and cut-off filters. The pass ranges were checked by collecting UV-vis transmission spectra of the filters using a Shimadzu UV-vis spectrometer over the range 200 - 1000 nm.

In these experiments photolysis is believed to excite the molecule causing either rearrangement of the molecule or dissociation, these processes are discussed in detail elsewhere.^{33,34,35}

2.5 EXPERIMENTAL TECHNIQUE

The experimental technique discussed below ranges from those used to prepare the precursors prior to deposition to the experiments actually performed on the matrix isolated samples themselves. Finally, in this section, the methodology of a typical experiment is given for the benefit of future workers within this laboratory

2.5.1 PREPARATION OF PRECURSORS

In this work two types of precursors are used; ozone and halogen-containing alkanes. All of the halogenated hydrocarbons were used with as high a purity as possible (often better than 99.9 % pure). Before use they were transferred directly into a suitable Pyrex storage flask fitted with a Youngs tap and Quickfit B14 ground glass socket. After this they were degassed by repeated freeze-thaw cycles at liquid nitrogen temperatures with the purity being tested by infrared spectroscopy.

The ozone used in these experiments is made by passing the high voltage static electric discharge from a Tesla coil through oxygen held in a Pyrex finger. The finger being immersed in liquid nitrogen to trap any ozone formed. Once sufficient ozone is formed it is subjected to freeze-thaw cycles to remove impurities as described above. The oxygen (zero grade) and argon used are supplied by British Oxygen Company. Isotopically substituted ozone is made in a similar fashion from 97.7 % $^{18}\text{O}_2$ (Enritech Enrichment Ltd.) and, mixed ozone ($^{16}\text{O}_{3-x}^{18}\text{O}_x$) is made from a 50:50 mixture of $^{16}\text{O}_2$ and $^{18}\text{O}_2$.

In these experiments a typical matrix reaction will be occurring between two substrates, with argon as the matrix material. In order that no thermal reactions occur (i.e. at room temperature in the gas phase) the substrates are diluted separately with argon in two different manifolds and deposited onto the CsI cold window where they mix. The diluted substrates are deposited at a rate of 3 mmolh^{-1} for 8 - 12 h. The gas to be deposited to form the matrix contains the precursor substrate, S, which must first be diluted to the required concentration with argon, typically the substrate to

argon ratio S/Ar ranged between 1:200 to 1:1000, this dilution was carried out in the gas handling manifolds using manometric techniques. The manifolds are evacuated and isolated and, since they have a known volume ($\sim 10 \text{ cm}^3$), a quantity of precursor can be added (e.g. 2 cm^3) to the manifold by opening the required valves and allowing the pressure to rise to 2/10 atm. A further valve can be opened to increase the volume of the manifold to 2 litres (i.e. 2 l can attached to manifold). A known fraction (in tenths atm) of argon is then added to achieve the desired S/Ar ratio. Note: the sensitivity of the vacuum gauges and the desired concentrations require the use of these manometric techniques. One alternative would be to use a single manifold ($\sim 2 \text{ l}$) and more sensitive vacuum gauges (e.g. Baratron type gauges).

2.5.2 EXPERIMENTS PERFORMED ON THE MATRICES

The types and nature of experiments that have and can be carried out on a matrix are discussed below. In these studies, wavelength-dependent photolysis and isotopic substitution have provided the greatest input.

Photolysis studies

Photolysis was required to initiate a reaction between ozone and the halogen-containing precursors in all the reactions reported below. Wavelength-dependent photolysis studies provide information as to the actual threshold wavelength required to initiate a reaction, and by irradiating the matrices with light of ever shortening wavelength a series of reaction intermediates may be observed, as well as the threshold at which they form. Studies have also been carried out in which the matrix is photolysed at a fixed wavelength for ever increasing time periods. Both time- and wavelength dependent studies have provided large amounts of information with regard placing the bands into groups having similar photolytic behaviour and hence belonging to the same species. The time-dependent photolysis studies can also be expanded to study the kinetics of the reactions, although this has not been used to any extent in these studies.

Warming studies

The purpose of warming the matrix is to reduce the rigidity of the matrix slightly, and allow some of the products in the matrix to diffuse and where possible form more stable geometries, for example, the geometry of the complex between ethanal and hydrogen iodide alters slightly after warming, to form a more thermally stable arrangement. Warming the matrix is carried out simply by selection of the required temperature using the temperature control unit, which semi-automatically adjusts the potential applied to the resistive wire wrapped around the cold head of the cryostat whilst monitoring the temperature. Both argon and oxygen matrices are warmed to 25 K for up to 25 min in these studies, this temperature is the upper limit for oxygen matrices, although with argon temperatures up to 35 K could be used before evaporation of the matrix became significant.

Substrate to argon ratio (S/Ar)

Generally the stoichiometric ratios of reactants is an integral part of the understanding of any reaction, however in low temperature matrices the deposition of matrices containing higher or lower concentrations may also result in aggregation and the detection of interesting spectra of such aggregate products.⁶⁻¹⁷ Experiments varying the S/Ar ratio are very simple to conduct, the precursors are simply diluted with argon to some known ratio and deposited; subsequent experiments would vary these ratios to produce matrices with increased or decreased ratios of one or both precursors. In these studies, the S/Ar ratio was usually chosen so as to produce clear spectra, with the precursors in reasonable concentrations so that reactions would occur. Various experiments in which one of the precursors was doubled in relation to the other showed no real difference in the products formed, however the spectra of the precursors exhibited the expected increase or decrease in intensity as would be expected by the associated change in concentration. The reason for this would appear to be statistical, since at the molecular level two precursors must be near to each other to react. The deposition creates a random array of precursors, and by increasing the amounts of precursors it simply increases the chances that two precursors would be

close enough to react.

Isotopic substitution

Isotopic substitution has been carried out on the precursors in this thesis. Primarily substitution of ^{16}O to ^{18}O with ozone was carried out, since so many of the detected species contain an oxygen atom. To a lesser extent deuterated samples have been used. At the simplest level, after ^{18}O substitution a band assignable to a molecular vibration that contains an oxygen atom should shift to lower wavenumber from its position for the ^{16}O isotopomer. Such a shift indicates that the band can be assigned to a mode that contains some contribution from an oxygen atom. The actual shift can provide more information as to the mode to which the band can be assigned. The isotopic shifts use the basic understanding that when an atom in a bond is substituted for one of different mass, the force constant of the bond in both isotopomers is constant and thus the shift in vibrational frequency is due to the difference in mass of the two isotopomers and the type of bond involved. Wavenumber shifts for various species and their calculation are discussed elsewhere.²⁴

Threshold energy calculation

The threshold energy required to cause a charge-transfer reaction to occur can be calculated by assuming point charges and values for the distances between the charges. The calculated energy can be subsequently converted into wavelengths which can be compared with the experimental wavelength used to cause the reaction to occur. The precise calculations and method are discussed in chapter 3.

2.5.3 METHODOLOGY OF A TYPICAL EXPERIMENT

This section contains the methodology of a typical ozone-halocarbon reaction, as carried out in this laboratory.

Equipment set up. This consists of evacuation of the gas handling manifolds, and cleaning and evacuation of the cryogenic equipment. The latter process requires that the vacuum shroud be removed and cleaned with solvents (usually methanol), and when appropriate re-polishing of the CsI cold window. The entire vacuum system (gas handling & cryogenic apparatus) takes approximately 2 h to evacuate to $\sim 10^{-7}$ torr.

Preparation of precursors. The precursors are degassed and mixed with argon in the gas handling apparatus. The time required to manufacture sufficient ozone (i.e. 2-4 cm³) - by the static discharge method - varies and is heavily dependent upon the passivation of the stainless steel manifolds (see chapter 8 for discussion of improvements).

Deposition. The matrices were deposited at ~ 3 mmolh⁻¹ and the nature of the apparatus was such that as deposition proceeded the backing pressure would reduce requiring the metering valves to be opened gradually during the deposition process. It was found empirically that the 'best' spectra were obtained from matrices in which the initial deposition rate was significantly less than 3 mmolh⁻¹ and, thus the following deposition regime was used in the majority of ozone/argon experiments. Deposition was begun at ~ 1 mmolh⁻¹ and over two hours the rate was gradually increased by opening the metering valves (at intervals of ~ 20 min); the increase in pressure in the vacuum chamber was used as one gauge of the speed of deposition, the other being the rate at which the pressure in the manifolds reduces. Over the next hour the metering valves were opened further at reduced intervals and finally, the valves were opened giving a flow rate of $\sim 5-6$ mmolh⁻¹ and the deposition was left running for a further 6-8 h. This last flow rate would decrease over the course of the deposition giving the required average flow rate.

Spectral collection. After collection of many spectra at resolutions exceeding 0.25 cm^{-1} and with 1000 scans, it became apparent that the time taken to collect spectra was an important parameter in these experiments, due to the desire to perform many photolysis and warming cycles on one matrix. To this end reducing the number of scans to between 500 and 750 and the resolution to 1 cm^{-1} reduced the collection time from $\sim 1.5\text{ h}$ to $\sim 25\text{ min}$ with no detrimental effect on the identification of spectral features. In addition, the interferometer design of the Bruker 113v enabled these spectra to be collected in approximately half the time of an FTIR instrument with a Michelson interferometer.

Photolysis and warming cycles. In general the matrices were photolysed for 30 min periods and warmed to 25 K for 25 min. The photolysis period of 30 min was found to be sufficient in the case of iodine-containing compounds to cause the reaction of $\sim 90\%$ of the precursors. The experiments in which the halogen atoms were bromine or chlorine required significantly longer photolysis periods (up to several hundred hours).

Overall experiment timings. The above constraints of preparation time, deposition time, spectral collection, photolysis and warming cycles determined the following typical experiment timing. At the beginning of a new experiment the equipment is checked (this is usually cleaned and evacuated at the end of the previous experiment) and the manufacture of ozone begun. During this time the other precursor is diluted with argon and, the cryostat is switched on and a background spectrum is recorded. After both precursors have been prepared, the deposition is begun, starting slowly at first, as mentioned above. After the full deposition period, usually 10-12 h, the first spectrum is collected. On the basis of earlier experiments (or experience) various wavelength- or time-dependent photolysis cycles and warming cycles are performed and, after each of these individual cycles an infrared spectrum is recorded. During the photolysis or warming cycles the spectra are processed and studied. Finally, at the end of the experiment the equipment (high vacuum pumps and cryostat) are switched off, and the matrix material evaporates. Once the 'cold' window has warmed to room temperature the window is cleaned and the equipment made ready for the next experiment.

Chapter 3

REACTION OF ALKYL HALIDES WITH OZONE

3.1 INTRODUCTION

Three alkyl halides are studied in this chapter, iodoethane (section 3.2), bromoethane (3.3) and 2-iodopropane (3.4), the idea being to detect any products that are formed after photolysis of the matrices and, by studying the iodo- and bromo-analogues, compare and contrast not only the photochemistry but the type and nature of the products formed. Additionally, by studying the reaction of ozone with 2-iodopropane a comparison of the one-, two-, and three-carbon alkyl iodides can be made. Additionally, 2-iodopropane, with the iodine atom in the 2-position, may react differently due to a steric effect.

The photolysis of ozone in low temperature (14-17 K) matrices is a well known source of atomic oxygen for transfer to substrate molecules. The photodissociation of ozone can occur by ultraviolet absorption in the intense Hartley continuum ($\lambda < 310$ nm) or by visible absorption in the weak Chappuis band (450 - 800 nm). In low temperature matrices, photolysis of ozone in the Chappuis band results in the formation molecular oxygen and ground state atomic oxygen, $O(^3P)$, while shorter wavelength irradiation into the Hartley continuum produces molecular oxygen and excited state atomic oxygen, $O(^1D)$. For a number of ozone substrate reactions, shorter wavelength radiation ($\lambda < 310$ nm) was required to initiate any reaction, e.g. ozone with diiodomethane and those haloalkanes studied in chapter 6 and 7. However, it has been reported that in the presence of certain substrates, photolysis with visible radiation can cause photodissociation of ozone and the transfer of an

oxygen atom to the substrate.¹⁹ This is accounted for by the formation of a charge transfer complex between ozone and the substrate. Molecular complexes of ozone of this type are known with iodine monochloride,¹⁹ iodomethane,²⁰ trifluoriodomethane,²¹ phosphine,³⁶ chlorine monofluoride,³⁷ arsenic and phosphorus trifluorides,³⁸ as well as sulphur trioxide.³⁹

Similar studies involving iodomethane and oxygen in an argon matrix⁴⁰ and iodomethane in a solid oxygen⁴¹ matrix have been carried out, which have led to the observation of radical species and to the formation of differing photoproducts from those found in the reaction with ozone. It has been observed⁴² that photolysis of a solid oxygen matrix with ultraviolet light leads to the formation of ozone via a process in which molecular oxygen is dissociated to ground state atomic oxygen, O(³P), which can then combine with another oxygen molecule to form ozone. Thus photolysis reactions in solid oxygen matrices can proceed via reaction between atomic oxygen, O(³P), and the substrate, or via reaction of the subsequently produced ozone with the substrate.

With species containing iodine¹⁹⁻²¹ it has been possible to form previously unknown inorganic monomeric iodoso- (ZIO), iodyl- (ZIO₂) and hypoiodo- (ZOI) compounds by photolysis of the substrate - ozone complex. Previous to the matrix isolation experiments there were only a very few known inorganic, aliphatic and aromatic compounds of these types.¹⁹

3.2 IODOETHANE, C₂H₅I

The study of the reaction of iodoethane and ozone was begun as an extension of the study by Andrews²⁰ et al. of iodomethane and ozone, the additional interest being that because of the second carbon atom a number of different reactions might be possible. As mentioned above, the reaction of ozone with the C-I bond might result in a number of IO_x species. Also, since the iodine atom is attached to the α-carbon and one possible reaction is the elimination of HI,⁴³ it might be possible to determine whether

the H atom is eliminated from the β -carbon producing ethene and HI, or from the α -carbon producing $\text{CH}_3\text{-CH}$ and HI. Additionally, the C-C bond might rupture producing CH_3 and CH_2I which could subsequently react with ozone to form a variety of products.

Whichever products were formed it was hoped to detect their characteristic infrared spectra and, in so doing, establish mechanisms for the reactions and where appropriate distinguish between them. The products were identified by employing deuterated iodoethane, $^{18}\text{O}_3$ and scrambled ozone ($^{16}\text{O}_{3-x}^{18}\text{O}_x$) made from 50:50 $^{16}\text{O}_2/^{18}\text{O}_2$.

3.2.1 RESULTS

The matrices containing iodoethane and ozone were diluted separately with argon at species-to-argon ($\text{C}_2\text{H}_5\text{I}/\text{Ar}$) ratios of between 1:100 and 1:400. Iodoethane was also deposited in a solid oxygen matrix ($\text{C}_2\text{H}_5\text{I}/\text{O}_2$ ratio = 1:150) and with oxygen in an argon matrix ($\text{C}_2\text{H}_5\text{I}/\text{O}_2/\text{Ar}$ = 1:2:400) in separate experiments. The deposition conditions (time, rate, temperature, etc.), procedure for collection of spectra, and the protocol for irradiation and warming the matrix are discussed in chapter 2.

The spectrum of isolated ozone^{42,44,45} deposited in an argon matrix was recorded and found to be in good agreement with those previously published. The spectrum of isolated iodoethane was also recorded (Table 3.1) and the bands assigned.

Iodoethane and ozone in argon

Deposition of the argon matrix containing ozone and iodoethane and its subsequent photolysis created a number of different products. The wavelength ranges chosen for the photolysis were selected so as to produce isolated photoproducts in a step-wise manner. The main photoproducts are associated with seven groups of

infrared bands (groups 1-7), the photochemical behaviour and structure of which are considered below.

Group 1. These bands were detected upon deposition of iodoethane and ozone in argon (Figure 3.1), and appeared as side bands to those attributable to the precursor molecules (Table 3.1 and 3.2). The group 1 bands all reduce in intensity upon irradiation with light of wavelength longer than 800 nm. This group has a weak band at 1100.8 cm^{-1} (the ν_1 band of O_3 absorbs at 1106.1 and 1104.4 cm^{-1}), and some strong absorptions at 1040.8, 1039.5, 1037.2, 1035.8, 1034.4, 1033.7, 1032.5 and 1031.7 cm^{-1} (near to those of isolated ozone the ν_3 band of which absorbs at 1040.5 and 1039.1 cm^{-1}) and a medium intensity band at 704.5 cm^{-1} (ν_2). Photolysis of the matrix with radiation of wavelengths of $\lambda > 650$ nm reduces the intensity of all these bands. On close inspection the ν_3 bands are split into two types according to their behaviour; those at 1040.8 and 1039.5 cm^{-1} are reduced by 30 %, while the others (between 1037.2 and 1031.7 cm^{-1}) are nearly destroyed. Further evidence for this can be seen (Table 3.2) in the reaction between iodoethane and mixed ozone ($^{16}\text{O}_{3-x}^{18}\text{O}_x$). Six sets of bands are observed for the mixed ozone, corresponding to the ozone isotopic mixes 16-16-16, 16-16-18, 18-16-18, 16-18-16, 16-18-18 and 18-18-18, and these were observed in the expected⁴⁴ 1:2:1:1:2:1 intensity ratio. Each of the sets exhibited three distinct types of band for the ν_3 mode, one assigned to isolated ozone and the other two to ozone involved in complex formation with iodoethane. The two bands of the ozone-iodoethane complex are shifted from their values for isolated ozone by between 3 - 4 cm^{-1} for the first band and 6 - 8 cm^{-1} for the second.

Strong bands at 1217.0 and 1208.8 cm^{-1} and a shoulder at 1206.4 cm^{-1} behaved in a similar fashion to the ozone bands; the 1217.0 cm^{-1} band reduced slightly on $\lambda > 650$ nm irradiation, while those at 1208.8 and 1206.4 cm^{-1} were destroyed. Thus the 1217.0 cm^{-1} band is assigned to a C-H motion of isolated iodoethane in argon (isolated iodoethane has a band at 1214.6 cm^{-1}), while the other two are assigned to C-H motions of iodoethane involved in the weak molecular complex with ozone. In these experiments it was noticed that photolysis of a matrix that had previously been irradiated ($\lambda > 650$ nm) with shorter wavelength radiation ($\lambda > 450$ nm) for short periods (up to 6 min) led to the reappearance of the two bands at 1208.8 and 1206.4

cm⁻¹ of the molecular complex; none reappeared that could be assigned to ozone. On further photolysis the intensities of these two bands decreased in proportion to the increase in intensity of group 3 bands (see later). None of the other bands attributed to the molecular complex was regenerated after having been destroyed by irradiation.

Experiments in which the C₂H₅I/O₃/Ar ratios were varied resulted in the observation that increasing the concentration caused an increase in the intensities of the group 1 bands, which appeared to arise from a 1:1 complex.

Group 2. Photolysis of the matrix containing the molecular complex (group 1) bands with near infrared radiation ($\lambda > 800$ nm) led to the growth of a new set of bands shown in Figure 3.2. These consist of a strong, sharp band at 717.0 cm⁻¹ and a sharp band at 1195.4 cm⁻¹, each of which is accompanied by weak side bands. Photolysis with radiation, $\lambda > 650$ nm increased the intensities of the group 2 bands by a factor of 5, and these bands appeared to be insensitive to radiation in the range 550 - 700 nm. Irradiation at wavelengths longer than 450 nm reduced the intensities of the group 2 bands slightly (5 - 10 %), while UV-vis radiation, $\lambda > 350$ nm, reduced the intensity by 50 %. Pyrex-filtered radiation ($\lambda > 290$ nm) destroyed all of the group 2 bands; these band wavenumbers and those for the isotopically substituted species in which ¹⁸O₃ replaces ¹⁶O₃ and C₂D₅I replaces C₂H₅I are listed in Table 3.3. The sharp band at 717.0 cm⁻¹ exhibits an ¹⁸O-shift of 35.7 cm⁻¹ and a near zero deuterium-shift (d-shift) for the ¹⁶O experiment and a d-shift of 0.9 cm⁻¹ for the ¹⁸O experiment; it appears as a doublet in the 50% ¹⁸O experiment, and is assigned to a I-O stretching vibration (predicted ¹⁸O shift for the diatomic I-O is 37 cm⁻¹). The sharp band at 1195.4 cm⁻¹ exhibits a small ¹⁸O shift of 3.7 cm⁻¹, but a much larger d-shift to 958.1 cm⁻¹ ($\nu_H / \nu_D = 1.248$) and is assigned to a perturbed C-H bending motion.

Group 3. Absorption bands for this group were first detected after irradiation at wavelengths longer than 650 nm. The bands occur as a doublet of doublets at 837.2, 829.3 and 803.1, 795.4 cm⁻¹ (Figure 3.3). Irradiation at wavelengths longer than 450 nm increases these band intensities by a factor of two. Group 3 bands are insensitive to 350 - 550 nm radiation. Irradiation with Pyrex-filtered light reduced the

intensities of the bands by 10 %. Quartz-filtered UV-vis light (240 - 1000 nm) reduced the intensities by 30 %. The four bands exhibit ^{18}O shift of between 39.5 and 41.3 cm^{-1} and d-shifts of $\leq 1.4 \text{ cm}^{-1}$. The experiment carried out with 50 % ^{18}O gave bands at 836.6, 829.3, 825.5, 818.7, 813.9, 801.4, 796.1, 789.3, 785.5, 772.0, 765.7, 761.4 and 754.1 cm^{-1} these (and those from the monoisotopic experiments) being assignable to symmetric or antisymmetric stretching vibrations (Table 3.4) of the monoisotopic I^{16}O_2 and I^{18}O_2 or the mixed $\text{I}^{16}\text{O}^{18}\text{O}$; hence the mode involves two oxygen atoms.

Group 4. These bands are formed after irradiation at $\lambda > 350 \text{ nm}$ (Table 3.5). The bands increased in intensity by 50 % after Pyrex-filtered irradiation, but reduced in intensity by 50 % after quartz-filtered irradiation. The group 4 infrared bands occurred at 3474.1 and 579.8 cm^{-1} . The band at 3474.1 cm^{-1} exhibited a large d-shift to 2565.2 cm^{-1} ($v_{\text{H}}/v_{\text{D}} = 1.354$) and a small ^{18}O -shift of 10.6 cm^{-1} and is assigned to an O-H stretching vibration. The 579.8 cm^{-1} band exhibited a small d-shifts of 5 cm^{-1} and ^{18}O -shift of 28.2 cm^{-1} (the predicted ^{18}O -shift for the O-I diatomic is 29 cm^{-1}) and, due to its similarities to bands observed for HOI,^{40,46} is assigned to an O-I stretch. In mixed-ozone ($^{16}\text{O}_{3-x}^{18}\text{O}_x$) experiments the bands all appeared as doublets corresponding to the monoisotopic species, and hence only one oxygen atom is involved in each of these vibrational modes.

Group 5. The group 5 bands are formed, like the group 4 bands, after irradiation at wavelengths, $\lambda > 350 \text{ nm}$, and they increase by approximately 50 % on Pyrex-filtered irradiation. Unlike the group 4 bands, however, group 5 bands are increased (by 10 %) on quartz-filtered irradiation. These bands are observed at 1106.0, 1076.7, 961.9 and 570.5 cm^{-1} (Table 3.4). The band at 1106.0 cm^{-1} exhibited a small ^{18}O -shift of 1.3 cm^{-1} and a small positive d-shift of 6.9 cm^{-1} and is assigned to a bending motion involving C-O-I. The band at 1076.7 cm^{-1} exhibited a d-shift of 1.4 cm^{-1} and a larger ^{18}O -shift of 51.1 cm^{-1} and on this basis is assigned to a C-O vibration (note: the predicted shift for the diatomic C-O is 28 cm^{-1}). The band at 961.9 cm^{-1} exhibited a large d-shift to 735.8 cm^{-1} ($v_{\text{H}}/v_{\text{D}} = 1.307$) and a small positive ^{18}O -shift of 0.5 cm^{-1} and is attributed to a C-H bending vibration. The band at 570.5 cm^{-1} exhibited a small d-shift of 4.9 cm^{-1} and ^{18}O -shift of 27.6 cm^{-1} and is assigned

to an O-I stretch. In mixed-ozone experiments the bands at 1106.0, 1076.7, 579.8 and 570.5 cm^{-1} all appeared as doublets corresponding to the monoisotopic species; hence each vibrational mode only involves one oxygen atom.

Group 6 and 7. The groups 6 and 7 bands (Table 3.6) were both formed weakly with irradiation at $\lambda > 350$ nm. The main group 6 and 7 absorption bands (Figure 4) occur at 1737.0, 1729.7, 1727.0, 1723.4, 1428.8, 1353.7, 1350.6 and 1122.3 cm^{-1} . Pyrex-filtered irradiation increased these band intensities by 3-4 times, and quartz-filtered irradiation increased them by a further 50 %. Warming the matrix caused the intensities of the bands between 1729.7 and 1723.4 cm^{-1} to increase at the expense of that at 1737.0 cm^{-1} , the bands that increased in intensities on sample warming being assigned to group 7, those that decreased being assigned to group 6.

Iodoethane in oxygen

Upon deposition the infrared spectrum of iodoethane in a solid oxygen matrix ($\text{C}_2\text{H}_5\text{I}/\text{O}_2 = 1:150$) showed bands assigned previously to iodoethane, but no new bands. Ultraviolet photolysis for 2 h led to the growth of some sharp bands (Table 3.6) at 3073.9, 3057.5, 2764.3, 2234.4, 1719.0, 1716.1, 1351.5, 1273.9, 1124.9, 1112.9 and 1103.2 cm^{-1} . No new bands were detected on Pyrex-filtered irradiation, and no ozone bands were observed after UV photolysis. Also no reaction was observed after UV photolysis of the argon matrix containing iodoethane and dioxygen ($\text{C}_2\text{H}_5\text{I}/\text{O}_2/\text{Ar} = 1:2:400$).

3.2.2 DISCUSSION

The major products will be identified for each of the band groups (1-7). The **Group 1** bands are assigned to $\text{C}_2\text{H}_5\text{I}/\text{O}_3$, a molecular complex formed upon the co-deposition of ozone/argon and iodoethane/argon. The complex is of a similar nature to those identified previously between ozone and other iodine-containing¹⁹⁻²¹ compounds. It is

believed to be a 1:1 complex as confirmed by the experiments in which the $C_2H_5I/O_3/Ar$ ratios were varied. The vibrational assignment is based on the similarity of the band intensities and wavenumbers (Table 3.1) to those of the isolated precursors. In the mixed ozone experiment six sets of bands were observed, providing evidence for ozone in the complex retaining its C_{2v} symmetry and for the bonding between iodoethane and ozone taking place via the central oxygen of ozone. The O-O angle in the ozone complex may be calculated⁴⁴ by taking ratios of the ν_3 bands of the isotopic variants, i.e. 16-18-16/16-16-16, 18-16-18/18-18-18, etc. However, where any angle change is small, a useful comparison can be made by examining the separation ($\Delta\nu$) between the ν_1 and ν_3 bands of ozone. This $\Delta\nu$ increases in the order isolated ozone⁴⁴ < C_2H_5I ⁴⁷ < CH_3I ²⁰ < CF_3I ²¹ < ICl .¹⁹ For the iodoethane...ozone complex $\Delta\nu$ is close to that of isolated ozone, indicating that the O-O-O geometry in both is similar.

The interaction between ozone and iodoethane is sufficient to change the photochemical behaviour of ozone in the matrix, making oxygen-oxygen bond cleavage possible with near infrared radiation. The irradiation corresponds to photolysis into the Chappuis band⁴⁸ (450 - 800 nm) of ozone, which corresponds to the transition $^1B_1 \leftarrow ^1A_1$ whereby an electron is promoted from a $p\sigma$ to a $p\pi$ orbital on either terminal oxygen atom. This is a very weak band and isolated ozone will only photodissociate on irradiation into this band with low probability;⁴⁹ in order to photodissociate isolated ozone effectively, it is necessary to irradiate with ultraviolet light (200 - 310 nm) into the Hartley band.³⁴ Thus the formation of the molecular complex alters the photochemistry of ozone in some subtle manner making the promotion of the electron more favourable and increases the probability of photodissociation. The first step is believed to be the production of the ion-pair $[C_2H_5I^+-O_3^-]^*$ via a charge transfer process, similar to that proposed for iodomethane-ozone²⁰ and phosphine-ozone.⁵⁰ The ion pair then transfers O^- to iodoethane to give the observed photolysis product. An estimate of the energy required to induce this charge transfer can be obtained from the relationship

$$E = I - A + C \quad (3.1)$$

where I = adiabatic ionization energy of the C_2H_5I donor ($I = 9.3$ eV for iodoethane⁵¹), A = electron affinity of the O_3 acceptor ($A = +1.9$ eV for ozone⁵²) and C = electrostatic potential energy of the $C_2H_5I^+O_3^-$ ion pair. Assuming $C_2H_5I^+$ and O_3^- to behave as point charges then $C = -e^2/r$ (eqn. 3.2) which, when substituted into equation 3.1, enables values of the energy threshold, E , to be calculated. Estimating the distance, r , to be 2.50 and 2.45 Å, E values of 1.64 and 1.50 eV, respectively, are calculated, which correspond to wavelengths of 756 and 800 nm, respectively; both of these are in good agreement with the threshold irradiation wavelengths used to the photolyze the complex.

Group 2. These bands were formed on photolysis with radiation at wavelengths longer than 800 nm (Figure 3.3). The band at 1195.4 cm^{-1} is characteristic of a C-H bending vibration, and that at 717.0 cm^{-1} is characteristic of an I-O vibration. The formation of new I-O stretching and C-H bending vibrations suggests that the species responsible for the group 2 bands is iodoethane, C_2H_5IO . By comparing the wavenumber of the I-O stretch of C_2H_5I-O (717.0 cm^{-1}) with those of CH_3I-O ²⁰ (723.7 cm^{-1}), CF_3I-O ²¹ (732.7 cm^{-1}) and $ClI-O$ ¹⁹ (779.1 cm^{-1}) a comparison of the effects of electron donating and withdrawing groups can be made (see chapter 5). The more electronegative substituent chlorine withdraws the electron density from the IO ($p-p$) π^* orbitals, while the methyl substituents tend to donate electron density.

Group 3. This group of bands was formed with radiation of wavelength longer than 650 nm and comprises a doublet of doublets at 837.2 (intensity = 0.11 abs units), 829.3 (0.21) and 803.1 (0.05), 795.4 (0.07) cm^{-1} . The former doublet is assigned to the antisymmetric IO_2 stretch and the second to the symmetric stretch on intensity grounds, and some of the bands observed in the mixed ozone experiment are assigned to stretches of the mixed isotopic species $I^{16}O^{18}O$. The wavenumber shifts between symmetric and antisymmetric stretches (ν_s and ν_a respectively) and between isotopes are in good agreement with these for IO_2 ^{19,20} species and ClO_2 .⁵³ The species responsible for group 3 bands is iodylethane, $C_2H_5IO_2$. For further identification a number of band shifts can be compared; (i) the difference between the symmetric and antisymmetric stretch of the IO_2 unit for a number of related compounds is as follows: O_2ICl ($\nu_a - \nu_s = 34.8$ cm^{-1}), O_2ICH_3 (33.9 cm^{-1}) and $O_2IC_2H_5$ (34 cm^{-1}). (ii) the

difference between the $\nu_s\text{IO}_2$ of ZIO_2 and the ν_{IO} of ZIO for species where $Z = \text{Cl}$, CH_3 or C_2H_5 is 65.6, 72.2 and 86.5 cm^{-1} respectively, and these values are similar to the differences between the $\nu_s\text{ClO}_2$ stretch of FClO_2 ⁵³ and the ν_{ClO} of FCIO .³⁷ These wavenumber shifts provide further evidence for the assignment of the group 2 species to an IO unit, and the group 3 species to an IO_2 unit.

Using the wavenumber separation between ν_{IO} , $\nu_s\text{IO}_2$ and $\nu_a\text{IO}_2$, assignments have been made for some of the bands observed by Walker *et al.*⁴⁶ for the products of the photochemically induced reaction between ozone and hydrogen iodide in a low temperature nitrogen matrix. Bands were observed at 781, 843 and 884 cm^{-1} and assigned to HIO_x species, and analogous bands for HI^{18}O_x were observed at 740, 766 and 792 cm^{-1} . By comparison of these bands with those detected in this experiment, these bands can be assigned to species similar in nature to those responsible for group 2 and 3 bands. Thus the bands are assigned as follows: The band at 781 cm^{-1} and its ^{18}O counterpart at 740 cm^{-1} are assigned to HIO . The ^{18}O isotopic shift (41 cm^{-1}) agrees well with that of other ZIO species. The band at 843 cm^{-1} is assigned to the symmetric stretch of HIO_2 and the band at 884 cm^{-1} to the antisymmetric stretch of HIO_2 . The observed shifts of ν_{IO} to $\nu_s\text{IO}_2$ (62 cm^{-1}) and $\nu_s\text{IO}_2$ to $\nu_a\text{IO}_2$ (41 cm^{-1}) are again in agreement with those of other ZIO_2 species. For the ^{18}O substituted species only the band at 792 cm^{-1} can be assigned to the symmetric stretch of HI^{18}O_2 . The band at 766 cm^{-1} for the ^{18}O species occurs too low in wavenumber to be attributed to either a symmetric or an antisymmetric stretch.

Groups 4 and 5. These two groups of bands (Table 3.5) were formed on irradiation $\lambda > 350$ nm. The band at 3474.1 cm^{-1} is assigned to an OH (alcohol) stretching vibration after the observation that there are no bands in the region 1700 - 1800 cm^{-1} that could be attributed to an acidic OH group. The band at 1106.0 cm^{-1} exhibited a positive d-shift and thus the COI bending motion must contain some hydrogen character. The 1076.7 cm^{-1} band shifted 51.1 cm^{-1} on ^{18}O substitution (predicted C-O diatomic shift = 28.0 cm^{-1}) indicating that the mode involves more than just carbon and oxygen, and this supports the assignment to a C-O vibration of the COI unit. The group 4 bands are assigned to an alcoholic OH stretch and an OI stretch, while the group 5 bands are assigned to a COI bend, CO stretch, CH_2 bend

and an OI stretch. Thus the species responsible for group 4 is hydrogen hypoiodide, HOI, and that for group 5 is hypoiodoethane, C₂H₅OI. The assignment of the OH stretch to HOI, and not to some alcohol such as CH₃CHIOH, was based on the shift to higher wavenumber of the OH band (to 3474.1 cm⁻¹) intermediate between the values for hydrogen hypoiodide (3417⁴⁰ and 3597⁴⁶ cm⁻¹) as compared to the alcohols ICH₂OH^{20,40} (3350 cm⁻¹) and methanol (3668.9 cm⁻¹).⁵⁴

Groups 6 and 7. These bands grew in intensities with shortening irradiation wavelengths and had infrared band wavenumbers similar to those of ethanal, but with small perturbations. The most diagnostic bands for these two groups occur in the C=O stretching region, between 1737.0 and 1723.4 cm⁻¹ (Figure 3.5). Groups 6 and 7 bands exhibited near identical photolytic behaviour. They can, however, be distinguished by warming the sample to 25 K for 10 min; thus in the $\nu_{\text{C=O}}$ region the bands between 1729.7 and 1723.4 cm⁻¹ (species 6) increased in intensities as the band at 1737.0 cm⁻¹ (species 7) decreased. Quartz-filtered radiation increases the yield of ethanal and produces a band at 2179 cm⁻¹ (deuterated analogue at 1560.3 cm⁻¹) and this band is attributed to hydrogen iodide, its wavenumber being very near to that of other hydrogen iodide complexes (*cf.* HI...C₂H₄ complex⁴³). The groups 6 and 7 bands arise from species which can be compared to similar methanal...hydrogen iodide²⁰ (1736.2 and 1729.9 cm⁻¹) and methanal...hydrogen hypoiodide⁴⁰ (1735, 1728 and 1722.5 cm⁻¹) complexes studied previously, the $\nu_{\text{C=O}}$ bands of which are shifted due to differing types of interaction between ethanal and HI or HOI. The group 6 bands are most likely to arise from a molecular pair complex, while the group 7 bands involve a hydrogen bond. In this study the complex is believed to be between ethanal and hydrogen iodide and hydrogen hypoiodide based on the proposed scheme (Summary 3.1) and the presence of four bands in the $\nu_{\text{C=O}}$ region. However, as the shift of the bands from the isolated value is very similar for HI and HOI no distinction can be made reliably on wavenumber shift alone. The situation is further made difficult by the observation of hydrogen iodide only after quartz-filtered photolysis (note: the low infrared absorption of hydrogen iodide may preclude its detection at longer wavelengths), and by the loss of HOI at this same photolysis wavelength, indicating that the presence of hydrogen iodide and hydrogen hypoiodide may be related.

Observation of the bands in the $\nu_{\text{C=O}}$ region during quartz photolysis gave no extra information on which distinction between a HI or HOI complex could be made.

Iodoethane in oxygen

The only bands detected upon deposition were those of iodoethane, which indicates that there was no molecular complex formed between iodoethane and molecular oxygen, unlike the situation arising with co-deposition of iodoethane and ozone. Of the product bands seen after UV irradiation, those at 2764.3, 1719.0, 1716.1, 1351.5, 1273.9, 1124.9, 1112.9 and 1103.2 cm^{-1} are assigned to ethanal formed via the reaction of iodoethane with oxygen atoms ($^3\text{P}_j$, $^1\text{D}_2$) arising from the photodissociated molecular oxygen. The sharpness of the doublet at 1719.0 and 1716.1 cm^{-1} and the further shift to lower wavenumbers is evidence for the C=O bond being more highly perturbed, probably by iodine. Comparisons of this experiment with that of diiodomethane in oxygen (see chapter 5) in which a methanal...iodine band was observed at 1723.3 cm^{-1} lends support to the idea that the above ethanal complex involves iodine.

Photochemical Interconversion

Based on the evidence that it is the perturbed ozone bands that are destroyed on irradiation and not those attributed to isolated ozone, it is believed that the photochemical reaction between ozone and iodoethane follows a step-wise, photoinduced pathway (see Summary 3.1). When ozone and iodoethane diluted separately with argon are co-deposited in a matrix, a molecular complex is formed. This is believed to be a charge transfer complex, and irradiation ($\lambda > 800 \text{ nm}$) into the charge transfer band produces an ion pair which then transfers negatively charged oxygen atoms to iodoethane, producing iodosoethane. This on subsequent shorter wavelength photolysis produced several products, hydrogen hypoiodide (HOI),

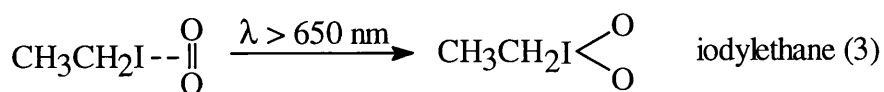
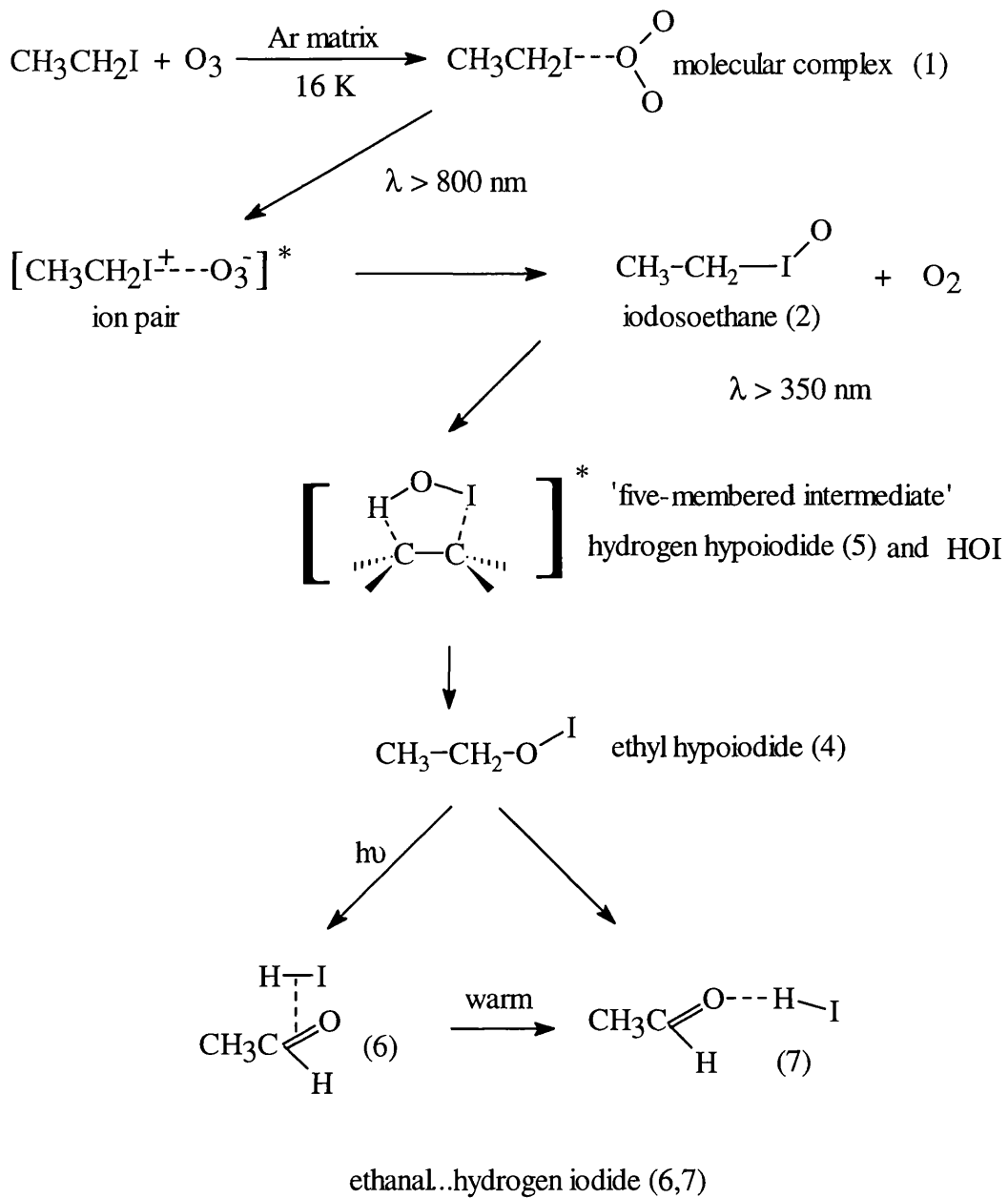
hypoiodoethane (C_2H_5OI) and ethanal (CH_3COH). A number of possible mechanisms can account for these products. In the first of these iodoethane dissociates to hydrogen hypoiodide and ethene (analogous to photolysis of iodoethane yielding ethene and HI),⁴³ with the subsequent reaction of ethene with oxygen atoms forming ethanal.⁵⁵ However, the observed behaviour of the products after Pyrex- and quartz-filtered irradiation supports a different mechanism. Since the bands associated with hypoiodoethane, hydrogen hypoiodide and ethanal all increased in intensities after Pyrex-filtered irradiation but, after quartz-filtered irradiation, bands for hydrogen iodide are produced while those of hydrogen hypoiodide are reduced; those for ethanal and hypoiodoethane increased. This observation tends to indicate that an alternative mechanism is occurring where HOI is formed first and is subsequently photolysed to form HI. At the time of writing this thesis we became aware of an analogous reaction performed by S.R. Leone⁵⁶ et al. in which HOI/DOI was detected by FT-IR emission spectroscopy in the reaction of $O(^3P)$ atoms with iodoethane. Using d_2 - and d_3 -iodoethane they determined that the mechanism involved addition of oxygen atoms to the iodine atom on the α -carbon and the subtraction of a hydrogen from the β -carbon of iodoethane, via a five-member ring intermediate. Thus this five-member intermediate would seem to be the first step in the mechanism, i.e. formed by a simple rearrangement of iodoethane. Unfortunately, Leone was unable to detect ethene as the other product, and this mechanism, while undoubtedly accounting for the presence of HOI, does not take account of the formation of hypoiodoethane and ethanal in these matrices. Thus it is proposed that the five-member ring intermediate is formed by rotation of the C-I-O bond of iodoethane. The five-member ring intermediate formed can be viewed as a close proximity complex between HOI and ethene. On shorter wavelength irradiation of the complex the OI unit rotates relative to the α -carbon and forms the -COI hypoiodo-species, with the H-atom rejoining the β -carbon. This hypoiodo-species now has the oxygen atom directly attached to the carbon atom and can further react to form ethanal with hydrogen iodide as its neighbour. The rearrangement of iodoethane (-CIO) to hypoiodoethane (-COI) is also supported by semi-empirical calculations (see chapter 5). The rearrangement can occur in either of two ways: the first involves the reduction of the C-I-O angle (of iodoethane) and elongation of the C-I bond until the appropriate geometry C-O-I (of hypoiodoethane)

is realised; the five-member ring geometry is intermediate between the two extremes, iodoso- and hypoiodo-. The second mechanism involves cleavage of the C-I bond in iodosoethane to form the radicals $C_2H_5\cdot$ and $OI\cdot$ which, due to their close proximity in the matrix, recombine to form hypoiodoethane. Of these two paths the former is favoured in this study (see Summary 3.1).

The production of the group 3 species, iodylethane, is believed to occur via the reaction between iodoethane and excited molecular oxygen, the presence of the two bands at 1208.8 and 1206.4 cm^{-1} providing tentative evidence for this. Whilst we have been able to identify the products and their threshold wavelengths of formation, we have not distinguished between possible competing mechanisms.

The photochemistry of the iodoethane-ozone complex is similar to that reported for the iodomethane-ozone complex,²⁰ except for the observation in this study of hydrogen hypoiodide. However the latter has been observed previously as a product in matrix experiments between iodomethane and molecular oxygen,^{40,41} and the related work of Leone⁵⁶ et al. confirms the detection of HOI.

SUMMARY 3.1



3.3 BROMOETHANE, C₂H₅Br

Bromoethane was studied with the intention of extending the known experiments of ozone with alkyl halides to include the bromo-analogue, C₂H₅Br. In this way comparisons with iodoethane can be made, specifically with regard to insertion of the carbon-halide bond by oxygen atoms, and to the detection of species containing C-Br-O_x and C-O-Br bonds. Bromoethane is related to the strongly ozone-depleting pesticide bromomethane, and a further investigation of these bromoalkanes might provide useful information. Additionally, if as expected bromoethane forms ethanal and hydrogen bromide complexes, these could be compared with those of ethanal and HI⁴⁷ and HF.⁵⁷

3.3.1 RESULTS

The spectra of isolated bromoethane in argon (1:400) and in solid oxygen have been recorded (Table 3.7). No previous matrix spectra of bromoethane are known and the bands detected are in good agreement to those reported for the liquid phase.⁵⁸

Bromoethane and ozone in argon

The spectrum of the matrix containing C₂H₅Br/O₃/Ar (1:1:400) is similar to that detected for isolated bromoethane above (Table 3.7) and isolated ozone⁴⁴ in argon, and no bands were detected that could be assigned to any complex formed. Photolysis of this matrix with Pyrex-filtered radiation was required before any bands were detected; quartz-filtered photolysis increased the intensities of these bands, but no additional product bands were detected.

Various experiments have been conducted to increase the yields and produce intermediate species containing BrO_x bonds, but with no success. These experiments

included varying the initial ratio of bromoethane/ozone/argon and photolysing the matrix during deposition. The first experiment produced spectra similar to those produced in the initial study, the only differences occurring with the intensities of the bands, due to increased or decreased concentration of the precursors. The second, produced only small quantities of ethanal, even after 16 h photolysis of a matrix containing O_3/O_2 (1:200) and C_2H_5Br/Ar (1:800).

The spectra detected (Table 3.8) gave rise to strong bands at 2995.6, 2987.8 and 2933.9 cm^{-1} and medium bands at 2873.3 cm^{-1} assigned to stretches of the CH_3 unit. The medium-weak band at 1717.0 cm^{-1} and its weak and medium-weak ^{18}O isotopomer bands at 1691.2 and 1686.8 cm^{-1} (^{18}O -shift = 30.2 cm^{-1}) are assigned to the carbonyl stretch. The medium-weak band at 1428.0 cm^{-1} with a small ^{18}O -shift of 2.4 cm^{-1} is assigned to the antisymmetric CH_3 bend, while a medium-weak band at 1354.3 cm^{-1} with an ^{18}O -shift of 2.0 cm^{-1} is assigned to the symmetric CH_3 bend. Medium-weak bands at 1138.3 and 1123.0 cm^{-1} (^{18}O isotopomer bands at 1127.6 and 1120.1 cm^{-1}) are assigned to the C-C-H bend. A number of very weak, broad bands at 899.6, 887.3 and 853.2 cm^{-1} (^{18}O isotopomer bands at 898.5 and 885.2 cm^{-1}) are assigned to the C-C stretch.

Bromoethane in oxygen

On deposition of bromoethane ($C_2H_5Br/O_2=$ 1:200) in solid oxygen, bands were detected (Table 3.7), which were similar to those detected for bromoethane in argon. Photolysis of this matrix with UV radiation ($\lambda > 240$ nm) for periods up to 10 h produced a number of bands (Table 3.8), which are assigned to modes similar to those detected in the experiment with ozone in argon. The most diagnostic bands occur at 1720.5 and 1713.7 cm^{-1} for the carbonyl stretch.

3.3.2 DISCUSSION

The formation of products in the photochemical reaction of bromoethane with ozone contrasts with that of iodoethane, in two ways. The first is that bromoethane requires ultraviolet radiation (Pyrex- and quartz-filtered photolysis) to initiate a reaction. The second difference is in the range and quantity of products. Thus with iodoethane, near-infrared irradiation produced more products than with bromoethane, for which only one product, the ethanal...HBr complex, was detected. Additionally the yield of products, determined by the intensities of the bands, is much lower than with iodoethane. This difference occurs due to the complex formation between ozone and iodoethane allowing ozone to transfer an oxygen atom on long (infrared) wavelength photolysis. Using eqns. 3.1 and 3.2 we can estimate the energy required to complete a charge-transfer process, similar to that proposed for iodoethane...ozone (I of bromoethane = 10.28 eV)⁵⁹ and, assuming a similar radii between the Br atom and ozone (2.45 Å) as between the I atom and ozone (see section 3.2.2), we can calculate a threshold energy, E , of 495 nm, which is inconsistent with the observed wavelengths needed to initiate a reaction with bromoethane. However, approaching the problem from the other side, if we use $\lambda_{\text{threshold}} = 300$ nm as an approximate threshold wavelength, then we calculate a distance, $r = 3.4$ Å, between the bromine atom and ozone, thus placing the two species significantly further apart which confirms the lack of complex formation.

In the case of bromoethane shorter wavelength irradiation ($\lambda \sim 300$ nm) is required to initiate a reaction, and thus even if these intermediates (having C-Br-O bonds) were formed they would be destroyed, as are the iodine analogues, to form ethanal. In gas phase experiments⁶⁰ between O(³P) atoms and bromoethane no HOBr was detected. The observation that Pyrex- and quartz-filtered irradiation produces similar products tends to indicate that both O(³P) and O(¹D) atoms react in a similar manner, via insertion into the C-Br bond, analogous to the insertion into C-I bonds seen above. However, since no species with either XC-Br-O or XC-O-Br bonds were detected we are still unsure as to the exact mechanism. An alternative mechanism would involve rupture of the C-Br bond of bromoethane and the subsequent reaction

of oxygen atoms with the ethyl radical. However, this seems unlikely for two reasons. First the bromine atom produced is likely to react with oxygen atoms and produce BrO,¹²⁵ for which no bands were detected. Secondly, the ethanal detected appears to be perturbed by HBr (see below) and, in the proposed alternative mechanism it seems unlikely that hydrogen bromide would form. These last two considerations and the observations made with iodoethane support the first mechanism, i.e. insertion of O atoms into the C-Br bond.

The main product observed in this study was ethanal (Table 3.8) but, in these experiments no bands assigned to HBr were detected. By comparison of the wavenumber shifts detected for this ethanal...HBr complex with those detected for the ethanal...HI complex formed in the reaction of iodoethane and ozone above, it is likely that the complex is perturbed by hydrogen bromide. A comparison of the $\nu_{\text{C=O}}$, δ_s CH₃ and δ_{CC} bands of these ethanal...HX species has been made (Table 3.9). For the carbonyl bands the shift, $\Delta\nu$, ($\Delta\nu = \nu_{\text{isolated}} + \nu_{\text{complex}}$) between the ethanal...HX complex and isolated ethanal is to lower wavenumbers (red-shift) for the hydric acids, HI ($\Delta\nu = 9.0, 16.3, 19.0$ and 22.6 cm^{-1}), HBr (29 cm^{-1}) and HF⁵⁷ (24 cm^{-1}), the last of these shifts-that detected for the HF complex-would have been expected to be larger than that of HBr. This difference can be accounted for by the nature of the experiment, whereby the precursors ethanal and HF were separately deposited and thus the possibility exists that HF forms two complexes with ethanal, the first (that observed) being a molecular-pair complex, while the second more perturbing complex (unobserved) involved a hydrogen-bond between the H atom of hydrogen fluoride and the carbonyl oxygen atom. The wavenumber shifts ($\nu_{\text{C=O}}$ bands) detected for these ethanal...HX complexes can be compared with those detected for the methanal...HX complexes; HF⁶¹ ($\Delta\nu = 10 \text{ cm}^{-1}$), HCl⁶¹ (12 cm^{-1}), HBr^{61,62} (17 or 14.3 cm^{-1}) and HI^{20,61} (16 or 6.1 and 12.4 cm^{-1}). Additionally, wavenumber shifts of approx. 4, 10 and 22 cm^{-1} were detected for the $\nu_{\text{C=O}}$ bands of CF₃COX...HI (X = F or H) complexes (see chapter 4), again in good agreement with the HI shifts reported above.

The bands of the symmetric CH₃ bend (δ_s CH₃) of these ethanal...HX complexes are shifted to higher wavenumbers; HI ($5.0, 1.9$ and 0.7 cm^{-1}), HBr (5.6 cm^{-1}) and HF⁵⁷ (4.3 cm^{-1}). Again the shift assigned to the species perturbed by HF

does not appear to fit the pattern set by HBr and HI, probably due to interference by the precursor ethanal bands. A further comparison of the C-C-H bend, shows bands blue shifted; HI by (6.6 cm⁻¹), HBr (22.6 and 7.3 cm⁻¹) and HF (13.3 cm⁻¹). In the case of HBr, the lower shift probably results from the H-bonded species whereby the carbonyl hydrogen is least perturbed.

3.4 2-IODOPROPANE, (CH₃)₂CHI

After studying the two-carbon system, iodoethane, it was decided to expand the alkane series by increasing the carbon chain length, and thus 2-iodopropane was studied. Due to the expected similarities with iodoethane, 2-iodopropane was chosen over 1-iodopropane. This gives the added possibility that it might be possible to produce either a ketone or aldehyde type final product, as well as similar I-O_x species seen previously.¹⁹⁻²¹ The α-carbon containing the iodine atom now has two methyl groups attached to it instead of one, as in the case of iodoethane. Due to the addition of this extra bulky methyl group some steric or electronic effects might alter the photochemistry or nature of the products detected. Detection of the various products is expected to enhance our understanding of the photochemical path, involved in these reactions, as well as yielding a number of novel species and complexes.

3.4.1 RESULTS

The spectra of an argon matrix containing 2-iodopropane ((CH₃)₂CHI/Ar = 1:500) were recorded (Table 3.10), and the major bands are assigned using iso-propane⁶³ as a guide.

2-Iodopropane and ozone in argon

Co-deposition of argon matrices containing 2-iodopropane and ozone, and their subsequent photolysis or warming, produced several bands which are grouped (1-5) according to their behaviour after these wavelength- and time-dependent photolysis cycles.

Group 1. These bands are detected after co-deposition of a matrix containing 2-iodopropane and ozone in argon ($(\text{CH}_3)_2\text{CHI}/\text{O}_3/\text{Ar} = 1:6:800$). On the whole the bands resemble those assigned to the precursors, 2-iodopropane (Table 3.10) and ozone,⁴⁴ except for a few minor wavenumber shifts. Photolysis of these group 1 bands with near-infrared radiation ($\lambda > 800$ nm) produced the group 2 bands. Further experiments varying the $(\text{CH}_3)_2\text{CHI}/\text{O}_3/\text{Ar}$ ratio had no effect on the products detected.

Group 2. Photolysis of a matrix containing ozone and 2-iodopropane with wavelengths longer than 800 nm resulted in the growth of these group 2 bands at the expense of the group 1 bands. Further irradiation of the matrix with shorter wavelength ($\lambda > 650$ and $\lambda > 410$ nm) radiation doubled the intensities of the bands after each cycle. However, UV-vis irradiation ($\lambda > 350$ nm) destroyed these bands and produced the group 4 and 5 bands. This group (Table 3.11) consists of medium and weak bands at 1200.1 and 1158.9 cm^{-1} (^{18}O at 1200.3, 1163.6 and 1156.8 cm^{-1}) assigned to perturbed C-H stretches. A medium band at 714.5 cm^{-1} (^{18}O at 690.8, 679.8 and 671.8 cm^{-1}) assigned to an I-O vibration (Fig. 3.6) based on the ^{18}O -shift of 34.7 cm^{-1} between the 714.5 cm^{-1} (^{16}O) and 679.8 cm^{-1} (^{18}O) bands.

Group 3. These bands are first detected very weakly after near-infrared ($\lambda > 650$ nm) photolysis. Further visible ($\lambda > 410$ nm) and UV-vis photolysis increased the intensities of these bands by 20 and 25 % respectively. Photolysis with Pyrex- and quartz- filtered radiation reduced the intensities of these bands. These bands (Table 3.12, Fig. 3.7) absorb between 833.0 and 792.7 cm^{-1} with the ^{18}O isotopomer bands absorbing between 794.0 and 747.2 cm^{-1} . Based on the ^{18}O -shifts of ~ 40 cm^{-1} and shifts between symmetric and antisymmetric stretches of ~ 34 cm^{-1} these bands are assigned to IO_2 stretching modes.

Group 4. This group of bands was detected after irradiation of the matrix with radiation of wavelengths longer than 350 nm, coinciding with the loss of the group 2 bands. These bands are destroyed by Pyrex-filtered photolysis. Weak bands for this group (Table 3.13) are detected at 3446.4 and 3445.3 cm^{-1} (^{18}O isotopomer at 3442.9 and 3434.5 cm^{-1}). On the basis of these ^{18}O -shifts (between 11.9 and 10.8 cm^{-1}), and their similarity to bands reported in section 3.2, assignment to O-H stretches is made. The other band in this group absorbs weakly at 578.8 cm^{-1} and with its ^{18}O -shift of 27.8 cm^{-1} is assigned to an O-I vibration.

Group 5 and 6. The bands assigned to these groups were first detected (Table 3.14) after photolysis with UV-vis radiation; Pyrex- and quartz-filtered irradiation increased the intensities of these bands. The bands detected are assigned as follows: those absorbing between 1723.2 and 1700.3 cm^{-1} are assigned to carbonyl stretches. Those in the range 1453.5 to 1419.0 cm^{-1} are assigned to antisymmetric CH_3 bends, while those between 1386.2 and 1351.3 cm^{-1} are assigned to symmetric CH_3 bends. Bands detected between 1231.6 and 1218.8 cm^{-1} in the $^{18}\text{O}_3$ experiment, are assigned to C-C stretches. Those between 1200.1 and 868.3 cm^{-1} are assigned to various CH_3 wagging and rocking motions. The medium-weak band at 767.7 cm^{-1} is assigned to another C-C stretch. Finally the weak bands at 630.9 and 621.9 cm^{-1} are assigned to the bending motion of the carbonyl oxygen atom, δ_{CCO} . Based on the wavenumbers of the bands detected it would appear that two complexes are present; differing by the geometric arrangement between the pair of species in the complex.

3.4.2 DISCUSSION

The bands detected are discussed below in terms of the groups 1-5 bands detected above. On co-deposition of 2-iodopropane and ozone in argon a number of bands were detected and these are assigned to **Group 1** (Table 3.10). These resemble bands detected for the isolated precursors and are assigned accordingly. Near-infrared photolysis reduced the intensities of the group 1 bands, forming the group 2 bands. Due to the similarity in behaviour of these group 1 bands after photolysis to those

detected in the reaction of ozone with iodoethane, this group is attributed to a weak complex between 2-iodopropane and ozone, $(\text{CH}_3)_2\text{CHI}\dots\text{O}_3$, similar in nature to the iodoethane...ozone complex detected in section 3.2. The loss of this complex after near-infrared photolysis ($\lambda > 800$ nm) suggests that, like the complex detected earlier,⁴⁷ the photolysis causes the transfer of an oxygen atom via a charge-transfer type complex. Using eqns. 3.1 and 3.2 seen above ($I = 9.26$ or 9.18 eV⁵⁹ for 2-iodopropane) and assuming a threshold wavelength, $\lambda_{\text{threshold}} = 800$ nm (1.5 eV), i.e. that observed to cause a reaction, we calculate the radius, r , between the O atom of ozone and the I atom of 2-iodopropane in the complex to be between 2.45 and 2.49 Å. These values are in good agreement with both the threshold wavelength actually used in these experiments and the calculated distance shown earlier for complexes with iodomethane,²⁰ phosphine³⁶ and iodoethane,⁴⁷ further supporting the assignment of these bands to this complex.

Group 2. This complex detected after near-infrared photolysis has bands (Table 3.11) at 1200.1 and 1158.9 cm^{-1} characteristic of a C-H bend, and at 714.5 cm^{-1} characteristic of an I-O stretch and on this basis it is considered to be the species 2-iodopropane, $(\text{CH}_3)_2\text{CHIO}$. The ν_{IO} band at 714.5 cm^{-1} is shifted to lower wavenumber than for either $\text{CH}_3\text{CH}_2\text{IO}$ ⁴⁷ (717.0 cm^{-1}) or CH_3IO ²⁰ (723.7 cm^{-1}). The band is shifted due to the electron donating effect of the second methyl group in 2-iodopropane (see the end of chapter 5 for a complete comparison of all the iodoso-species).

Group 3. The group 3 bands (Table 3.12) detected after visible photolysis are attributed to an IO_2 unit (Fig. 3.7) and thus are considered to arise from the species 2-iodylpropane, $(\text{CH}_3)_2\text{CHIO}_2$. The bands at 833.0, 827.7, 820.7 and 813.7 cm^{-1} are assigned to the antisymmetric I^{16}O_2 stretch, while those at 799.0, 795.0 and 792.7 cm^{-1} are assigned to the symmetric I^{16}O_2 stretch. In the $^{18}\text{O}_3$ experiments bands at 794.0 and 788.2 cm^{-1} having ^{18}O -shifts of ~ 40 cm^{-1} are assigned to the antisymmetric I^{18}O_2 stretch. ^{18}O isotopomer bands at 759.6, 755.6, 752.3 and 747.2 cm^{-1} likewise are assigned to the symmetric I^{18}O_2 stretch. Additionally, in the $^{18}\text{O}_3$ experiments weak bands were detected at 807.9 and 803.2 cm^{-1} and these are assigned to the antisymmetric stretch of the mixed isotopic unit, $\text{I}^{16}\text{O}^{18}\text{O}$. The wavenumber shifts

between the symmetric and antisymmetric stretch of these IO₂ unit ($\nu_a - \nu_s = 34$ and 32.7 cm^{-1}) and for the ¹⁸O isotopomer (34.4 to 32.6 cm^{-1}) are in good agreement with those seen for iodylethane ($\sim 34 \text{ cm}^{-1}$). An additional check on the identity of the group 2 and 3 species can be made by comparing the magnitudes of the separations between the ν_s of ZIO₂ and ν_{IO} of ZIO, in this case approx. 80 cm^{-1} which compares well with that of species in which Z = H,⁴⁶ Cl,¹⁹ CH₃,²⁰ and C₂H₅⁴⁷ ($62, 65.6, 72.2$ and 86.5 cm^{-1}).

Group 4. These bands formed after UV-vis ($\lambda > 350 \text{ nm}$) irradiation, are assigned (Table 3.13) to an O-H stretch and an O-I stretch and thus to hydrogen hypoiodide, HOI. The ν_{OI} band could possibly be assigned to the O-I vibration of the C-O-I unit, except that no other bands were detected that could be assigned to this hypoiodo-species. Given the species reported earlier in this chapter (and in chapter 4-5 later) it seems likely that 2-hypoiodopentane might be present. The detection of HOI here parallels the gas phase results of Leone⁶⁰ et al.

Group 5 and 6. These bands were first detected after photolysis, $\lambda > 350 \text{ nm}$, and they increased in intensities after each successively shorter wavelength (Pyrex- and quartz-filtered) irradiation cycle (Table 3.14). These bands represent the final group detected and the ultimate destination of the reaction path. Based on the similarity of the band positions to spectra previously detected this group of bands has been assigned to acetone.^{57,64,65} In this study the most diagnostic bands are those assignable to the carbonyl stretch, $\nu_{C=O}$. By examining the wavenumber shift relative to that of isolated acetone,⁶⁵ we are able to assign these bands to three acetone complexes in argon. The medium-weak band at 1723.2 cm^{-1} is $\nu_{C=O}$ band of acetone isolated in argon. The other carbonyl bands are assigned to two acetone-hydrogen iodide complexes, the first, medium band at 1719.2 cm^{-1} is attributed to a molecular pair complex (group 5), while the second, medium-to-weak bands at $1712.9, 1706.9$ and 1700.3 cm^{-1} are attributed to a complex involving a hydrogen bond between acetone and HI (group 6). Although no hydrogen iodide was detected in this study the bands can be compared to a separate study⁶⁵ in which acetone and HI were deposited separately, which resulted in the formation of similar complexes. In this work spectra recorded of matrices containing various initial ozone/2-iodopropane ratios

produced no additional bands, indicating that the complex is a 1:1 complex between HI and acetone formed from oxygen-atom addition to 2-iodopropane.

Several other acetone...HX complexes have been detected by co-deposition of the separate precursors, and the carbonyl band of these complexes exhibit the following shifts: acetone...HI⁶⁵ ($\Delta\nu = 8, 12$ and 17 cm^{-1}), HI^a (2.0, 10.3, 16.3 and 22.9 cm^{-1}), HCl⁶⁶ (14 and 27 cm^{-1}) and HF⁵⁷ (7 cm^{-1}) (where ^a denotes this work). The shift reported for the acetone...HF⁵⁷ complex is smaller than expected, due to there being at least two possible arrangements for the complex, with the reported complex exhibiting the smallest perturbation, and the more perturbing complex having not been reported; this behaviour was discussed above (section 3.3) for the ethanal...HF⁵⁷ complex. It is also useful to compare the wavenumber shifts of the carbonyl bands of the complexes of HI with methanal^{20,61} ($6.1, 12.4$ and 16 cm^{-1}), ethanal ($9.0, 16.3, 19.0$ and 22.6 cm^{-1})⁴⁷ and the polyfluoroethanals (chapter 4), CF₃COX ($\sim 4, 10$ and 22 cm^{-1}). The wavenumber shifts of the $\nu_{\text{C=O}}$ bands of all these carbonyl...HI complexes are in good agreement.

Photochemical Interconversion

The photochemical pathway (Summary 3.2) for the reaction of 2-iodopropane with ozone, is believed to be similar to that proposed for the analogous iodoethane reaction. The photolytic behaviour of the groups 1-6 is discussed below, as is the photochemical interconversion.

After co-deposition of 2-iodopropane and ozone in argon a weak complex is formed, (CH₃)₂CHI...O₃ (group 1). Near-infrared photolysis of this complex causes the transfer of an oxygen atom, via a charge-transfer type mechanism, and the formation of 2-iodosopropane, (CH₃)₂CHIO (group 2). Further UV-vis ($\lambda > 350\text{ nm}$) photolysis of 2-iodosopropane forms the group 4 species, HOI, and very possibly 2-hypoiodopropane, (CH₃)₂HCOI. This transfer, between iodoso- (Z-C-I-O) and hypoiodo-species (Z-C-O-I), proceeds via a five-member ring intermediate, which can be viewed as HOI in close proximity to the C=C bond of CH₃CH=CH₂ (see summary

3.2). The conversion begins by the C-I-O angle of the iodoso- species shortening, which places the O atom near enough to a of the terminal hydrogen atom to form a bond and hence HOI. The matrix environment prevents this five-member ring intermediate from separating into HOI and the alkene; at this stage HOI and the ethene would separate in the gas phase.⁶⁰ But, in the matrix a further rearrangement occurs, the C-I-O angle continues to shorten, to form the hypoiodo-species. This hypoiodo-species rapidly decays forming a C=O bond and the iodine atom abstracts a hydrogen atom from the α -carbon to form HI, and hence the complex $(\text{CH}_3)_2\text{C}=\text{O}\dots\text{HI}$. No direct spectral evidence for propene is detected either here in the matrix or in the gas phase. However, the detection of the final complex favours the proposed mechanism. The acetone...HI complex exists in two geometries, one in which the H-I and C=O bonds are parallel (group 5), and another in which the H atom of HI forms a hydrogen bond with the O atom of the carbonyl (group 6).

Finally, 2-iodylpropane, $(\text{CH}_3)_2\text{CHIO}_2$ (group 3), is formed under similar conditions to 2-iodosopropane (e.g. near-infrared radiation) however, unlike the iodoso-species, which are destroyed by UV-vis ($\lambda > 350$ nm) irradiation, shorter wavelength Pyrex-filtered photolysis is required to destroy the iodyl-species. 2-Iodylpropane is thought to form after a reaction between 2-iodopropane and molecular oxygen in an excited state.

3.5 CONCLUDING REMARKS

The co-deposition of the iodine-containing precursors (iodoethane⁴⁷ and 2-iodopropane) and ozone diluted in argon at low temperatures has led to the formation of weak molecular complex, $ZI...O_3$; these dramatically change the photochemistry of ozone, allowing dissociation to occur with near-infrared photolysis. Several novel intermediates are characterized by their infrared absorption bands and their photochemical behaviour. Assignments of the vibrational modes of the species are made in the text, and a proposed photochemical reaction path is shown (Summary 3.1 and 3.2) for the reactions occurring in a low temperature argon matrix.

The wavenumbers of bands assigned to the intermediates and complexes detected in this chapter are compared with those reported later in this thesis, both to confirm the identification of the species and to note trends in the spectra.

Table 3.1. Infrared bands /cm⁻¹ detected for iodoethane (and *d*_s) in the molecular complex C₂H₅I--O₃ (group 1) formed by co-deposition of ozone/argon and iodoethane/argon^a

C ₂ H ₅ I	H / ¹⁶ O ₃	H / ¹⁸ O ₃	D / ¹⁶ O ₃	D / ¹⁸ O ₃	assignment
3024.1w	3033.3w	3034.8w	2280.2w	2281.2w	site
3018.2w	3024.7w	3024.2w	2274.4w	2274.4w	v _a CH ₂
	2998.1sh		2250.8m	2250.8m	
2991.1s	2991.4s	2990.9m	2245.5m	2245.5m	
2982.9s	2984.2s	2983.7m	2233.4m	2231.0m	v _a CH ₃
			2231.0m		
2932.1s	2931.2s	2931.2m	2182.8m	2182.8m	v _s CH ₃
2926.2s	2927.3s	2926.8m	2177.0m	2177.0m	
2870.4s	2870.9s	2870.4m	2136.0m	2136.0m	2δ _a CH ₃
			2117.7m	2117.7m	
			2077.2m	2077.2m	
1457.1m	1459.6m	1460.0m	1151.4m	1150.5m	δ _s CH ₃
1444.0s	1445.1s	1444.1s	1148.1s	1148.1s	δ _a CH ₃
1378.1s	1378.3s	1379.5s	1066.6m	1066.1m	δ _s CH ₃
			1049.7s	1049.7s	
1214.6s	1217.0s	1217.0s	970.1s	970.6s	ωCH ₂
	1208.8s	1209.3s	968.2s	968s	
	1206.4sh	1206.9sh			
952.2ms	957.1m	957.6m	924.3mw	923.9w	v _{CC}
742.6m	746.4m	747.4m	742.6mw	743.0mw	τCH ₂
	739.1m	739.2m	733.9mw	733.4mw	
506.7m	505.3m				v _{Cl}

^a- s-sharp; mw-medium weak; m-medium; w-weak; sh-shoulder; δ-bend; v-stretch; τCH₂-twist; ω-wag; subscript s-symmetric; subscript a- antisymmetric.

Table 3.2. Infrared bands /cm⁻¹ attributed to ozone for matrix-isolated ¹⁶O_{x¹⁸O_{3-x} and iodoethane (and *d*₅) after deposition at 14 K}

ν_1 (ν_s)	ν_2 (δ)	ν_3 (ν_a)	assignment
1100.8w	704.5mw	1040.8m	site
		1039.5s	16-16-16
		1037.2^bs	complex
		1035.8sh	complex
		1034.4s	complex
		1033.7s	complex
		1032.5s	site
		1031.7sh	site
1091.7w	688.1m	1026.6 ^c ms	16-16-18
		1023.2sh	complex
		1020.3sh	complex
[1070.8] ^a	671.7mw	1017.9m	18-16-18
		1014.0sh	complex
		1009.9sh	complex
[1077.1]	696.7mw	1007.3m	16-18-16
		1003.4sh	complex
		1000.0sh	complex
1061w	680.8m	992.3s	18-18-16
		986.1sh	complex
1039.1w	664.9mw	983.2s	18-18-18
		979.3sh	complex
		976.6sh	complex
1100.3w	704.9m	1039.1s	¹⁶ O ₃ / <i>d</i> ₅
		1037.7s	
		1033.3s	
1039.6w	664.9m	982.2s	¹⁸ O ₃ / <i>d</i> ₅
		980.3s	
		976.4s	

^a- square brackets; values calculated for bands;⁴⁴ ^b- bold denotes those bands destroyed on irradiation with light of wavelengths longer than 650 nm; ^c- these ν_3 bands can be resolved at higher resolutions.⁴²

Table 3.3. Infrared bands /cm⁻¹ detected for iodosoethane, C₂H₅IO (group 2), formed after filtered xenon/mercury-arc irradiation (λ > 650 nm) of argon matrices containing ozone and iodoethane.

C ₂ H ₅ I ¹⁶ O	C ₂ H ₅ I ¹⁸ O	C ₂ D ₅ I ¹⁶ O	C ₂ D ₅ I ¹⁸ O	assignment
1200.6sh	1195.0sh	961.5sh		ωCH ₂
1195.4mw	1191.7mw	958.1mw	955.7w,br	
1191.7sh		955.2w,br		
717.0ms	681.3ms	717.0ms	680.4ms	ν _{IO}
711.3sh				
709.9sh				

Table 3.4. Infrared bands/cm⁻¹ detected for C₂H₅IO₂ (group 3) formed after filtered xenon/mercury-arc irradiation (λ > 450 nm) of argon matrices containing ozone and iodoethane.

C ₂ H ₅ -I ¹⁶ O ₂ (d ₅) ^a	C ₂ H ₅ -I ¹⁶ O _x ¹⁸ O _{2-x}	C ₂ H ₅ -I ¹⁸ O ₂ (d ₅)	assignment
837.2 (837.1)wm	836.6w		ν _a I ¹⁶ O ₂
829.3 (829.3)m	829.3sh		
825.4sh			ν _a I ¹⁶ O, ¹⁸ O
	825.5w		
	818.7w		
	813.9sh		
803.1 (802.8)wm	801.4sh		ν _s I ¹⁶ O ₂
795.4 (794.1)m			
	796.1w	797.0 (796.6)wm	ν _a I ¹⁸ O ₂
	789.3w	789.8 (789.3)m	
	785.5sh		ν _s I ¹⁶ O, ¹⁸ O
	772.0w		
	765.7w		
	761.4vw	762.3 (760.9)wm	ν _s I ¹⁸ O ₂
	754.1sh	754.1 (753.2)m	

(d₅)^a - deuterated analogues

Table 3.5. Infrared bands /cm⁻¹ of HOI (group 4) and CH₃CH₂OI (group 5), formed after photolysis for 30 min with radiation in the wavelength range 350 - 550 nm.

H / ¹⁶ O ₃	D / ¹⁶ O ₃	H / ¹⁸ O ₃	D / ¹⁸ O ₃	assignment
3474.1m	2565.2m	3463.5m	2549.8m	ν _{OH} (4) ^a
1106.0mw	1112.9w	1104.7w	1111.9w	δ _{C-O-I} (5)
1076.7w 1071.9w	1075.3w	1025.6w	1025.1w	ν _{CO} (5)
961.9m	735.8m	962.4mw	736.3m	δCH ₂ (5)
579.8m	574.8m	551.6m	548.7m	ν _{OI} (4)
570.5wm	565.6mw	542.9mw	539.1mw	ν _{OI} (5)

^a () group numbers.

Table 3.6. Infrared bands /cm⁻¹ of ethanal, CH₃CHO, and ethanal - hydrogen iodide molecular complexes (group 6 and 7) formed after ultraviolet photolysis for 30 min.

CH ₃ CHO	H/ ¹⁶ O ₃	H/ ¹⁸ O ₃	D/ ¹⁶ O ₃	D/ ¹⁸ O ₃	H/O ₂	assignment
2853.5w	2843.4w 2820.3w		2130.7w			vCH ₃
2758.5m 2734.9m	2762.4w 2739.7w 2734.9w		2082.5w 2064.2w		2764.3w	v _{CH}
	2179w	2177.5w	1560.4w	1560.3w		v _s HI
1746.0vs,br	1737.0s 1729.7s 1727.0sh 1723.4sh	1706.4m 1698.2m	1728.1m 1720.9m 1716.6m	1700.2m 1692.9m 1684.7m 1675.1m	1719.0m 1716.1m	v _{C=O}
1427.2m	1428.8m	1431.1m 1425.8m	1075.3m	1074.8m		δ _a CH ₃
1348.7m 1345.3sh	1353.7m 1350.6m 1349.4m	1354.0m	1023.7m	1021.7m	1351.5m	δ _s CH ₃
1115.7br	1122.3m	1121.5m	895.9m	893.0w	1124.9w 1112.9w 1103.2w	δ _{CCH}
878.5mw	877.5w,br	839.5w 826.0w	877.6mw 874.7mw 846.2mw	882.4w		v _{CC}
771.5m				729.1m		v _{O-O-P} ^a

^a - Out-of-plane vibration.

Table 3.7. Infrared bands /cm⁻¹ of bromoethane in a number of matrices at 14 K.

Ar	O ₂	O ₃ /Ar	¹⁸ O ₃ /Ar	assignment
3026.0mw	3023.7m	3026.6w	3025.8mw	v _a CH ₂
2995.7ms	3018.1m	2996.0m	2995.3m	
2987.1m	2989.7ms	2987.8m	2986.0m	v _a CH ₃
2977.6sh,mw	2977.9sh,m			v _s 'CH ₃
2967.8sh,w				v _s CH ₂
2934.1ms	2934.6m	2933.9m	2933.9m	v _s CH ₃
2901.0w	2902.4mw	2901.0w	2900.7w	2δ _s 'CH ₃
2873.1m	2874.0ms	2873.3m	2872.8w	2δ _a CH ₃
2835.1w	2836.8w		2834.7vw	2δCH ₂
2820.4w			2819.8vw	2δ _s CH ₃
2739.8w	2742.8w		2739.8w	
1457.9m	1460.2s	1458.5m	1458.4m	δ _s 'CH ₃
1446.0vs	1446.0s	1445.8s	1445.8s	δ _a CH ₃
1430.8w				δCH ₂
1379.2s	1381.4s	1380.0ms	1379.9m	δ _s CH ₃
1362.6mw	1364.3mw			
1354.0w	1353.9w			
1270.0w			1270.0w	
1257.4vs	1257.8vs	1257.4m	1257.3m	v _{CC} + v ₁₁
1245.5vs	1245.5vs	1245.5s	1245.5ms	ωCH ₂
1236.3mw	1236.6sh,m	1236.5w	1236.6sh,w	
1220.4w	1222.5w			
1062.3w	1064.9mw	1063.4vw	1063.9w	ρ CH ₃ ^a
	1053.6w			
1021.3w	1022.8w		1016.4w	ρ _⊥ CH ₃ ^a
1016.0w			1012.9w	
961.5vs	962vs	960.7s	961.5s	v _{CC}
952.5w	889.9vw	952.6w		
770.6sh,mw	773.3vs	774.8mw	773.9mw	τCH ₂
766.6m		766.6m	770.5mw	
			766.6mw	
	572.8vs		567.5s	v _{CBr}

^a - ρ_{||} and ρ_⊥ rock, parallel or perpendicular to plane of molecule.

Table 3.8. Infrared bands /cm⁻¹ assigned to ethanal...hydrogen bromide complex formed after pyrex-filtered photolysis of bromoethane in a number of matrices.

O ₂	¹⁶ O ₃ / Ar	¹⁸ O ₃ / Ar	assignment
	2995.6s 2987.8s 2933.9s 2873.3m		vCH ₃
2141.6m			v _s CO
1720.5s 1713.7sh,m 1698.5m,sh 1692.9sh,w	1717.0mw	1691.2w 1686.8mw	v _{C=O}
	1428.0mw	1425.6w	δ _a CH ₃
1354.1w	1354.3mw	1352.3br,mw	δ _s CH ₃
1306.3mw	1257.5s 1245.6s		
	1138.3w 1123.0mw	1127.6w 1120.1w	δ _{CCH}
1072.9vw 1036.9mw 1032.5mw		1025.1w 1020.7w 1016.8w	
	899.6vw,br 887.3vw,br 853.2vw,br	898.5vw 885.2vw	v _{CC}
655.7mw		658.1w	

Table 3.9. Infrared bands /cm⁻¹ assigned to modes of ethanal and ethanal...HX complexes in argon matrices at 14 K.

CH ₃ CHO ⁶⁴	CH ₃ CHO	...HF ⁵⁷	...HBr ^a	...HI ^b	assignment
1728	1746.0	1722	1717	1737.0 1729.7 1727.0 1723.4	v _{C=O}
1349	1348.7	1353	1354.3	1353.7 1350.6 1349.4	δ _s CH ₃
1111	1115.7	1129	1138.3 1123.0	1122.3	δ _{CCH}

^a- section 3.3; ^b- section 3.2.

Table 3.10. Infrared bands /cm⁻¹ detected for 2-iodopropane (group 1) in a number of matrices.

Ar	¹⁶ O ₃ / Ar	¹⁸ O ₃ / Ar	assignment
3007.0w	3006.6mw	3008.0s	ν _a CH ₃
	2991.3mw	2989.2m	
2987.5w	2986.6mw	2986.4ms	ν _s CH ₃
	2982.2mw	2983.0ms	
2966.2m	2966.2mw	2966.7s	
2928.9m	2929.0m	2929.1vs	ν _s CH ₃
	2924.3mw	2924.1sh,m	
2916.4w	2918.7w	2918.5wm 2912.9wm	
2901.2w	2902.7w	2902.5w	νCH ₃
2886.9w	2887.7w	2892.5m	
2875.3mw	2879.2w	2878.4mw	
	2867.7w	2868.4mw	
1464.4m	1463.3m	1463.1s	δ _a CH ₃
		1458.7mw	
1455.0m	1453.8m	1453.4ms	δ _s CH ₃
	1448.1w	1448.4mw	
1387.0m	1386.2m	1386.1m	δ _s CH ₃
1371.9m	1372.5ms	1372.1vs	
1210.9s	1211.6s	1211.6vw	ρ _{o-o-p} CH ₃
1208.0s	1207.8s	1207.8vs	
		1188.7m	
1148.0s	1149.1vs	1149.0vs	ρ _{o-o-p} CH ₃
		1144.9sh,mw	
1137.2vw	1137.7w	1137.9w	
		1133.3w	ρ _{o-o-p} CH ₃
1119.9vw	1120.0w	1121.7w	
		1061.4w	ρ _{i-p} CH ₃
		1050.8w	
	928.2w	928.3mw	ρ _{i-p} CH ₃
876.4m	875.8m	875.6s	
584w,br		588.7w	ν _{Cl}
		582.5w	
548.9w		550.7w 547.3w	

Table 3.11. Infrared bands /cm⁻¹ assigned to 2-iodopropane (group 2), formed after $\lambda > 650$ nm photolysis of an argon matrix containing ozone and 2-iodopropane.

(CH ₃) ₂ CHI- ¹⁶ O	(CH ₃) ₂ CHI- ¹⁸ O	assignment
1200.1m	1200.3m	δ_{CCH}
1158.9w	1163.6w	
	1156.8w	
714.5m	690.8w	ν_{IO}
	679.8m	
	671.8sh,w	

Table 3.12. Infrared bands /cm⁻¹ assigned to the 2-iodylpropane (group 3), formed after $\lambda > 650$ nm photolysis of an argon matrix containing ozone and 2-iodopropane.

(CH ₃) ₂ CHI ¹⁶ O ₂	(CH ₃) ₂ CHI ¹⁶ O ¹⁸ O	(CH ₃) ₂ CHI ¹⁸ O ₂	assignment
833.0m			$\nu_{\text{a}} \text{I}^{16}\text{O}_2$
827.7ms			
820.7m			
813.7m			
	807.9w		$\nu_{\text{a}} \text{I}^{16}\text{O}^{18}\text{O}$
	803.2w		
		794.0mw	$\nu_{\text{a}} \text{I}^{18}\text{O}_2$
		788.2mw	
799.0m			$\nu_{\text{s}} \text{I}^{16}\text{O}_2$
795.0m			
792.7m			
		759.6mw	$\nu_{\text{s}} \text{I}^{18}\text{O}_2$
		755.6w	
		752.3mw	
		747.2mw	

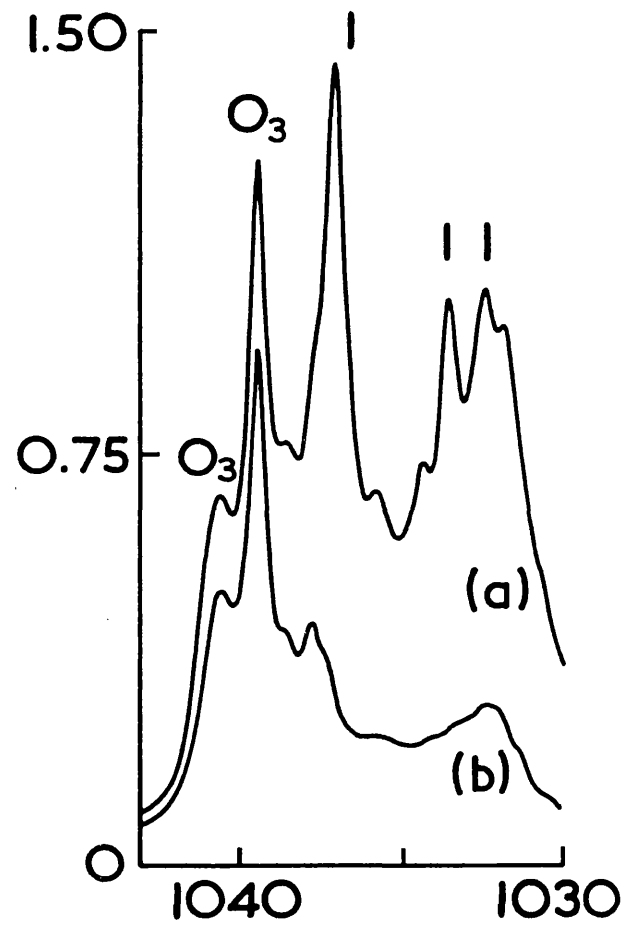
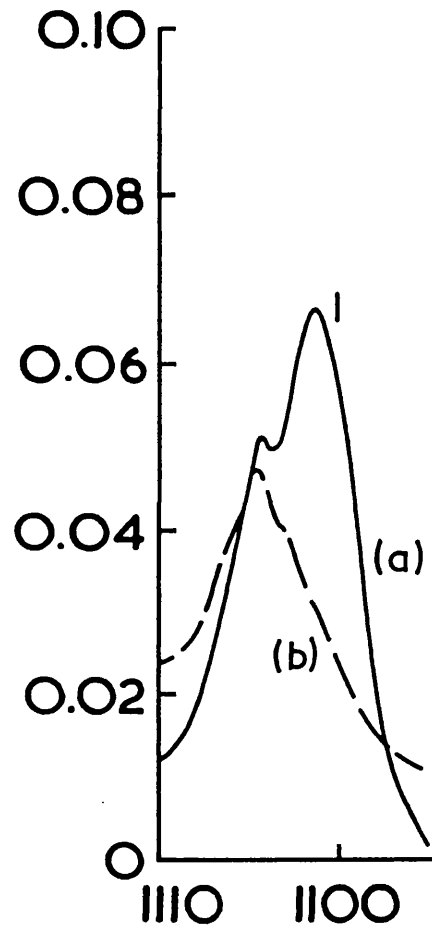
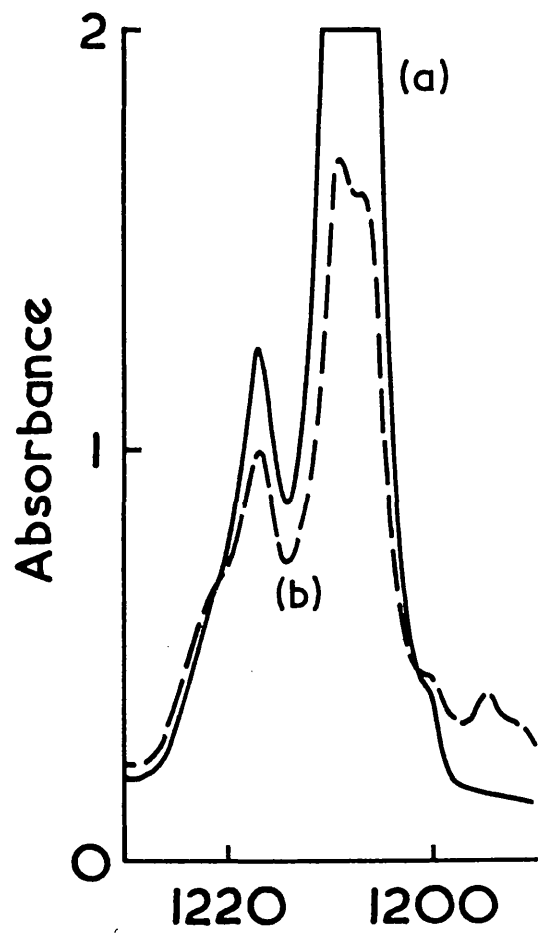
Table 3.13. Infrared bands /cm⁻¹ assigned to hydrogen hypoiodide, HOI (group 4), formed after photolysis, $\lambda > 350$ nm, of an argon matrix containing ozone and 2-iodopropane.

¹⁶ O ₃ /Ar	¹⁸ O ₃ /Ar	assignment
3446.4w	3442.9w	$\nu_{\text{OH}} \text{HOI}$
3445.3w	3434.5w	
578.8w	551.0mw	ν_{OI}

Table 3.14. Infrared bands /cm⁻¹ assigned to the acetone...HI species (group 5 and 6), formed after photolysis of 2-iodopropane and ozone in argon at 14 K, and those bands assigned to acetone⁶⁴ and the acetone...HF species⁵⁷ in argon.

acetone ⁶⁴	acetone..HF ⁵⁷	¹⁶ O ₃ /Ar	¹⁸ O ₃ /Ar	assignment
1722	1715	1723.2sh,mw 1719.2sh,m 1712.9m 1706.9mw 1700.3sh,w	1706.8w 1693.0mw 1687.7w 1683.2w 1675.3w	v _{C=O}
1429	1423	1453.5mw 1448.5mw 1444.0w 1422.1br,w 1419.0br,w	1442.8w 1439.3w 1426.1w	δ _a CH ₃
1361	1374	1386.2mw 1363.9w 1358.9vw 1355.8vw 1351.3vw	1381.4w 1377.1w 1362.8mw 1354.6w 1311.1w	δ _s CH ₃
1216	1242		1231.6w 1227.7w 1226.1w 1222.7w 1218.8w	v _{CC}
		1200.1m 1158.9m	1200.3m 1180.5w 1156.8mw	δCH ₃
1092	1097	1109.3w 1105.2w 1096.2w	1110.8w 1106.4mw 1101.6w	ρCH ₃
		933.6w 928.3w 925.0w	923.0mw	ωCH ₃
		914.0w 902.0w 875.7m 868.3m	914.3w 910.3w	ωCH ₃
		767.7mw		v _{CC}
529	556	630.9w 621.9w		δ _{CCO}

Figure 3.1. Infrared spectra of a matrix containing iodoethane/Ar = 1:400 and ozone/Ar = 1:400 samples at 16 K. Spectrum after (a) deposition and, (b) photolysis at $\lambda > 650$ nm for 30 min, showing the destruction of bands assigned to group 1. 1 - Group 1. Note the different scales on the intensity axes.



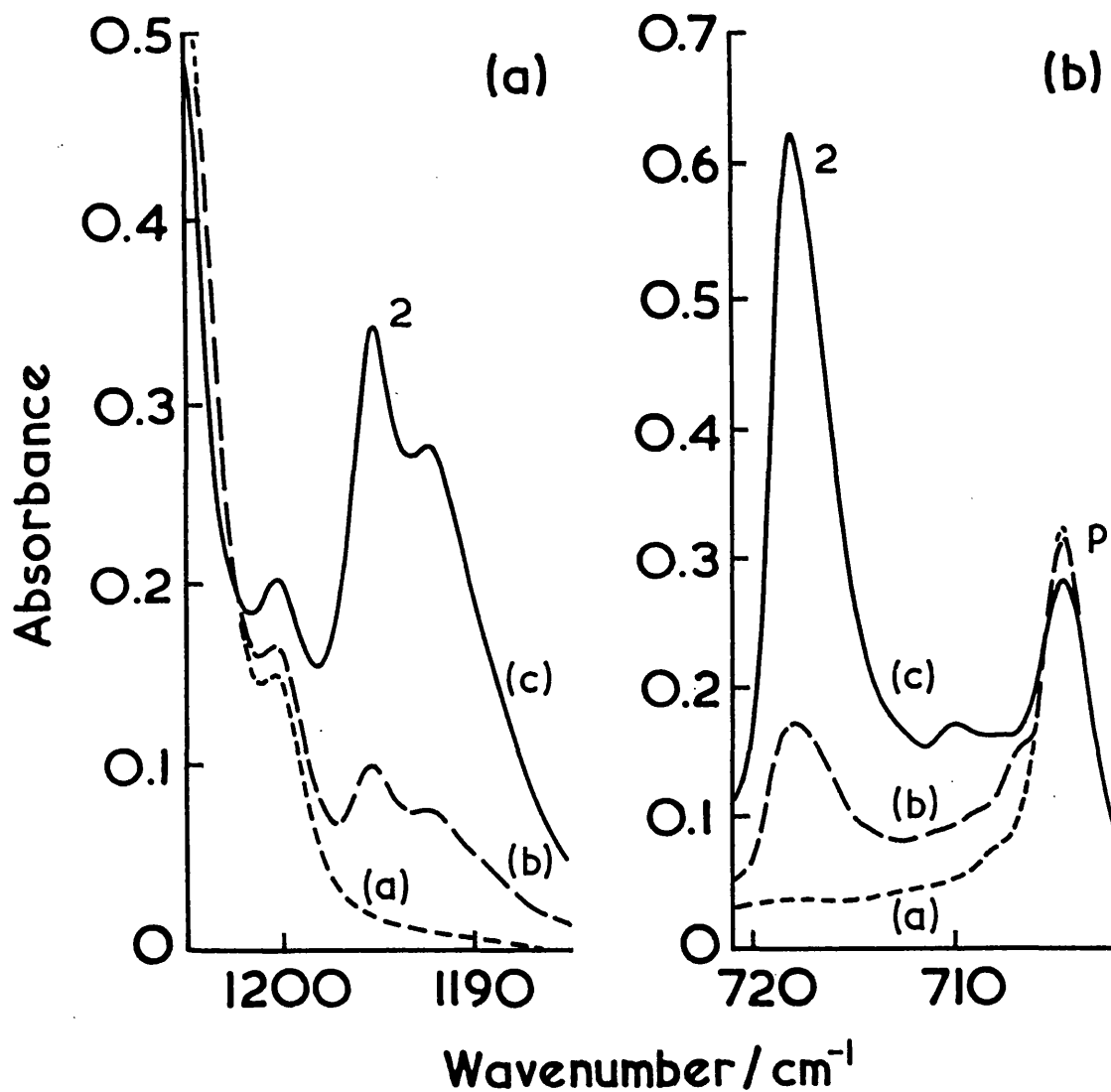


Figure 3.2. Infrared spectra of a matrix containing iodoethane/ozone/Ar (1:1:400) at 16 K. Spectrum after (a) deposition, (b) near-infrared radiation ($\lambda > 800$ nm) for 30 min and, (c) photolysis at $\lambda > 650$ nm for 30 min. Showing the growth of iodoethane. p - precursor; 2 - group 2. Note the different scales on the intensity axes.

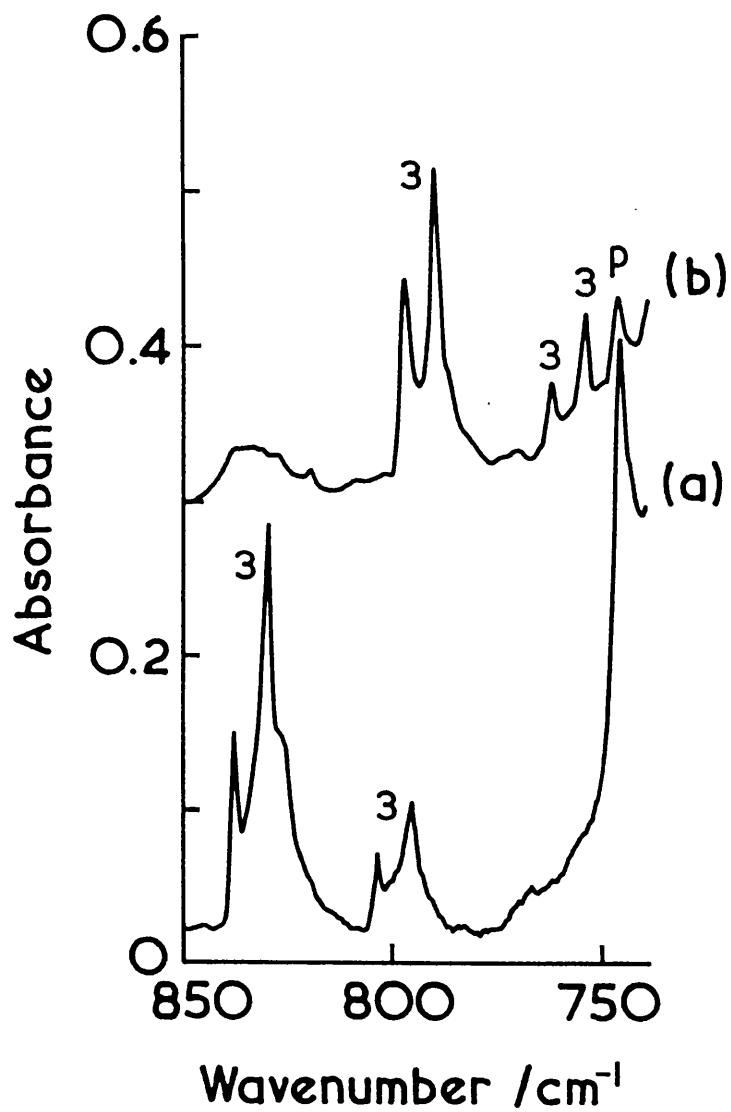
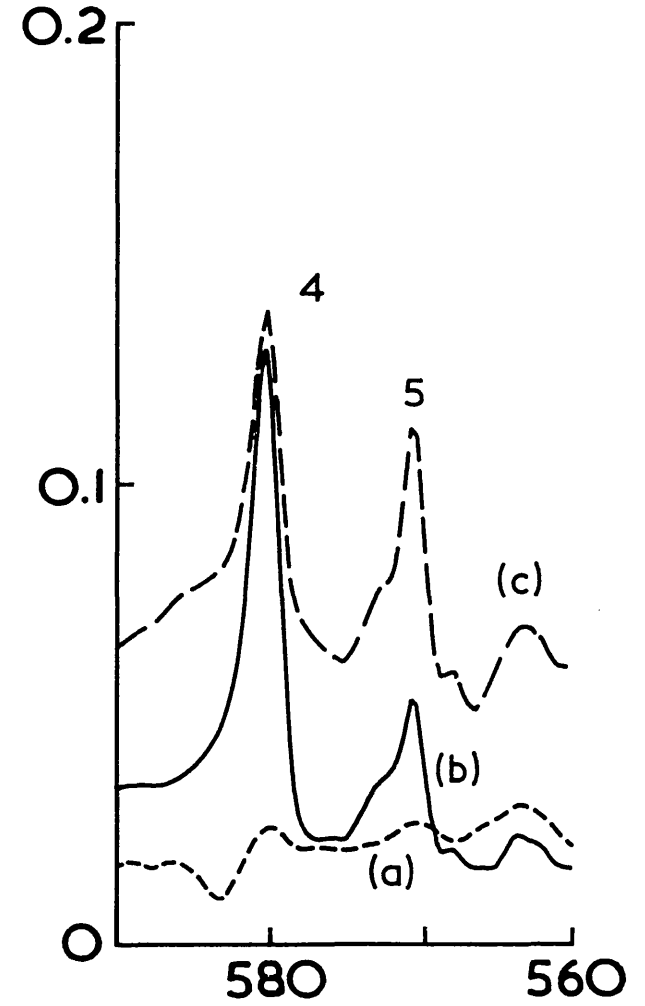
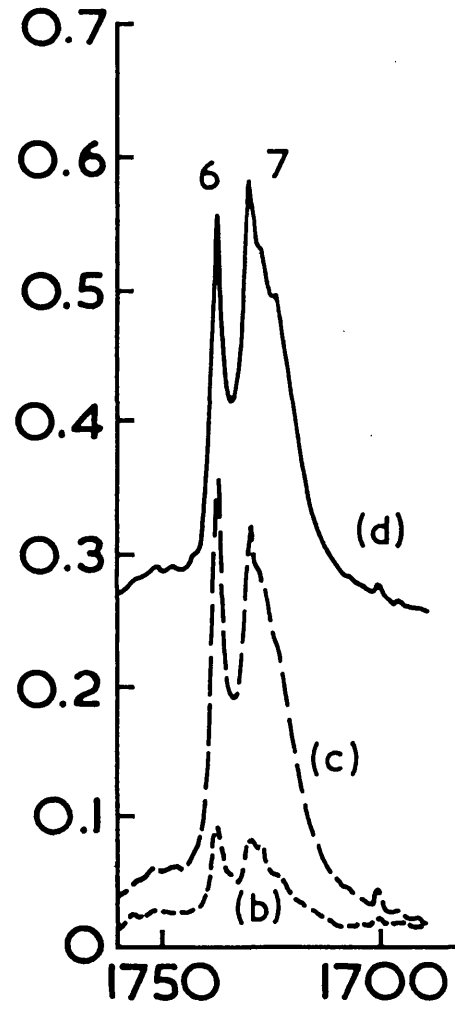
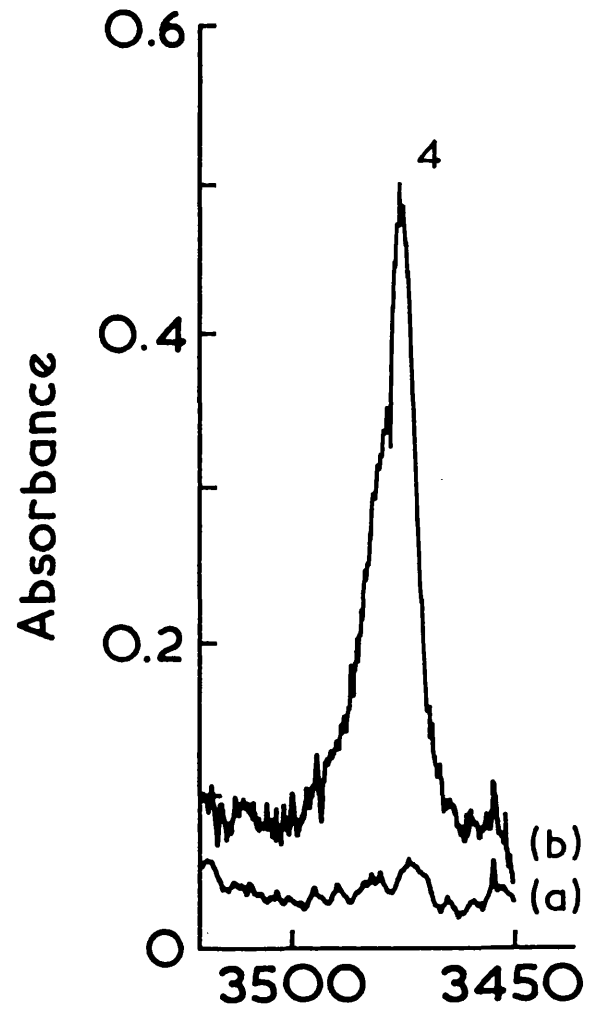


Figure 3.3. Infrared spectra in the region 850 - 740 cm^{-1} of matrices containing iodoethane/ozone/Ar (1/1/400) after photolysis for 30 min with radiation of wavelengths longer than 450 nm. Spectrum (a) isotopically normal and (b) 97% ^{18}O enriched, showing the group 3 bands. p - precursor.

Figure 3.4. Infrared spectra of matrices containing iodoethane/ozone/Ar (1:1:400) at 16 K. Spectrum after matrix had been (a) irradiated with wavelengths longer than 450 nm, (b) irradiated for 30 min in the wavelength range $350 > \lambda > 550$ nm, (c) irradiated with $\lambda > 240$ nm and, (d) warmed to 25 K for 10 min. Labels 4, 5, 6 and 7 relate to bands of groups 4, 5, 6 and 7. Note the different scales on the intensity axes.



Wavenumber / cm^{-1}

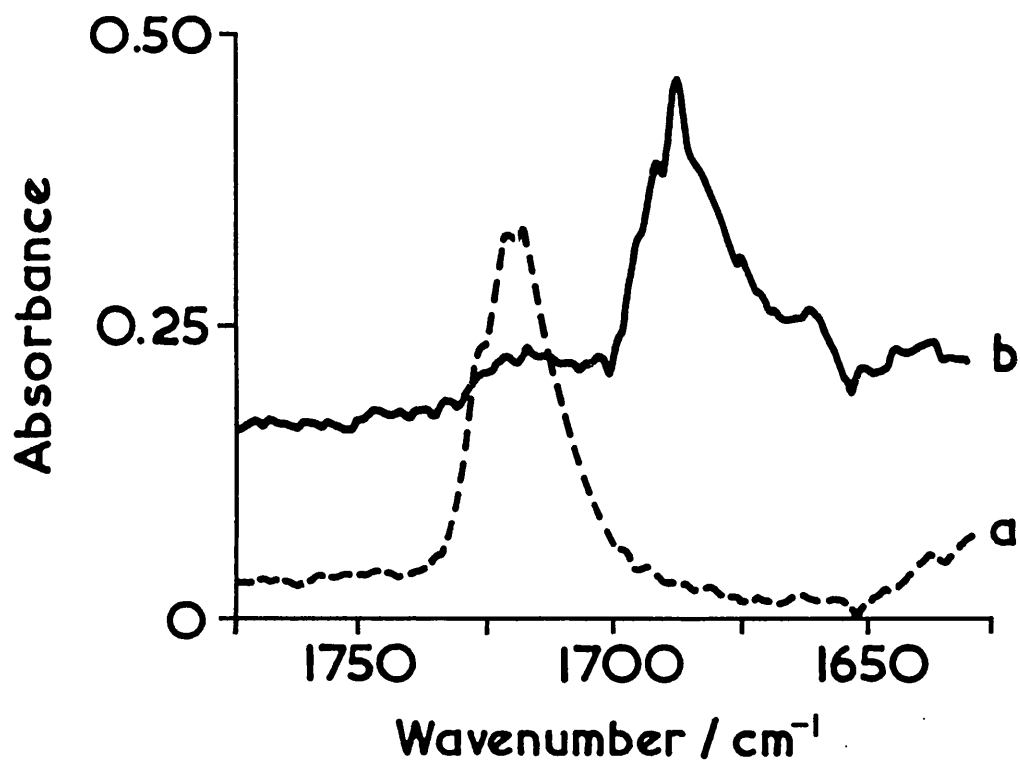


Figure 3.5. Infrared spectra in the $\nu_{C=O}$ region of the ethanal...HBr complex, detected after Pyrex-filtered ($\lambda > 290$ nm) irradiation of matrices containing bromoethane/ozone/Ar (1:1:400). Spectrum (a) normal isotopic ozone $\approx 99\%$ $^{16}\text{O}_3$ and (b) the ^{18}O isotopomer generated from $^{18}\text{O}_3$ ($\geq 97\%$ $^{18}\text{O}_2$).

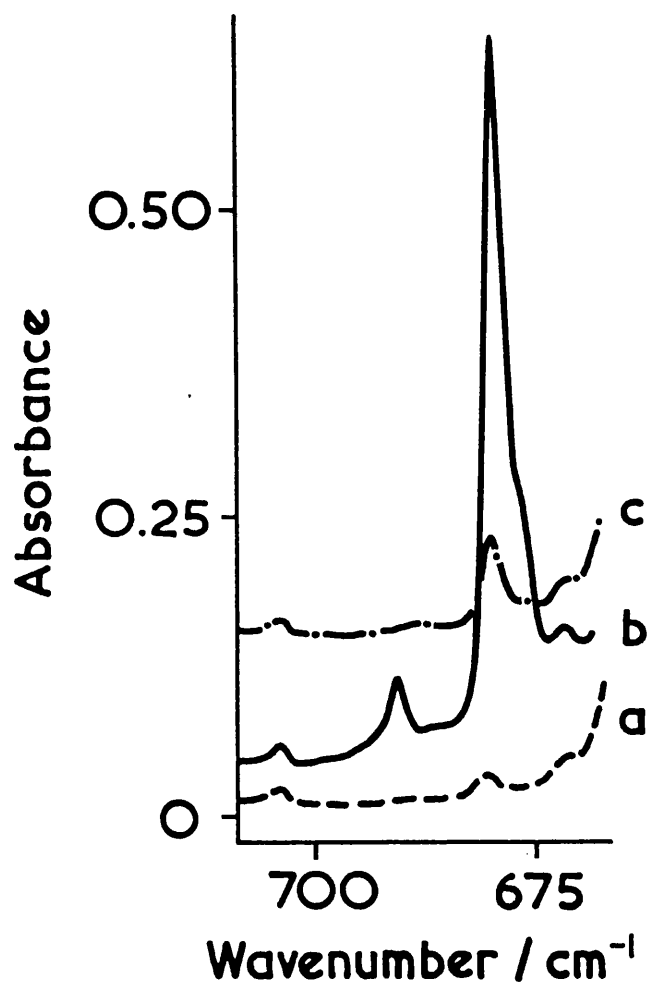


Figure 3.6. Infrared spectra in the ν_{10} region of a matrix containing 2-iodopropane/ $^{18}\text{O}_3/\text{Ar}$ (1:6:700) after (a) deposition, (b) infrared-photolysis ($\lambda > 650$ nm) and, (c) UV/vis photolysis ($\lambda > 350$ nm). The spectra show the band attributed to the I^{18}O stretch of 2-iodopropane, $(\text{CH}_3)_2\text{CHIO}$ (group 2).

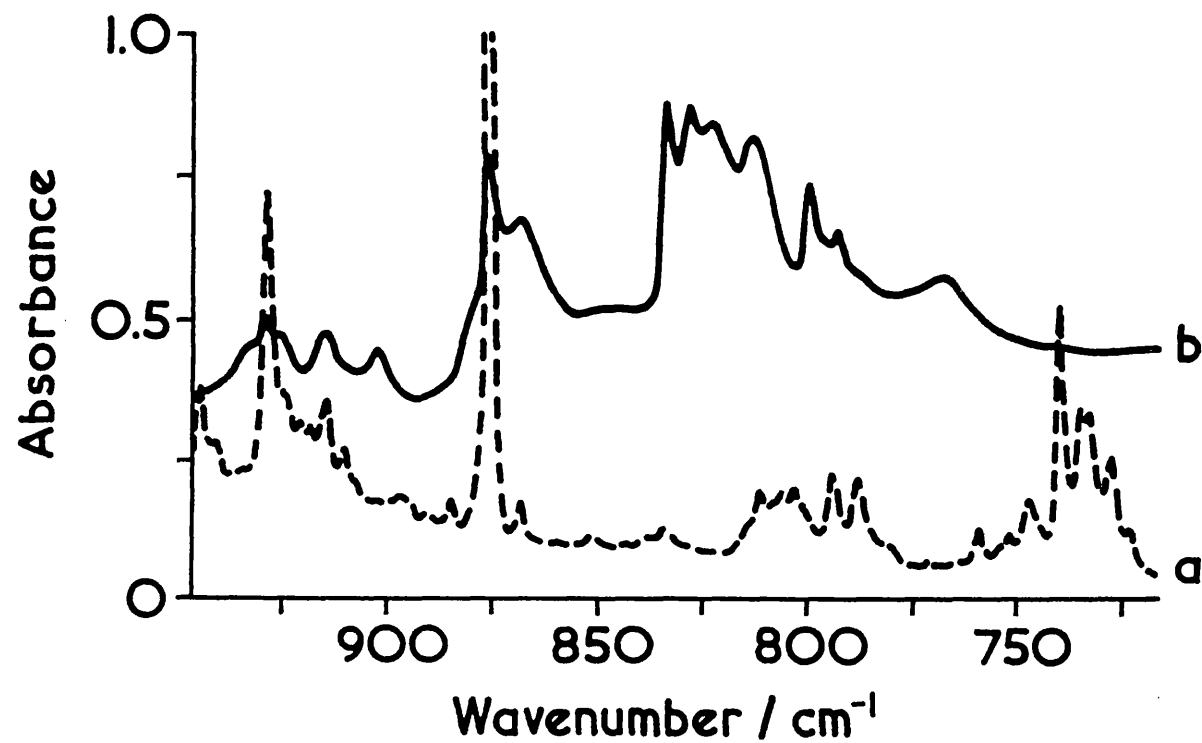


Figure 3.7. Infrared spectra in the region 950-725 cm^{-1} after UV-vis ($\lambda > 350 \text{ nm}$) photolysis of matrices containing (a) 2-iodopropane/ $^{18}\text{O}_3/\text{Ar}$ (1:6:800) and (b) 2-iodopropane/ $^{16}\text{O}_3/\text{Ar}$ (1:6:700). The spectra show the bands assigned to the group 3 species, 2-iodylpropane, $(\text{CH}_3)_2\text{CHIO}_2$.

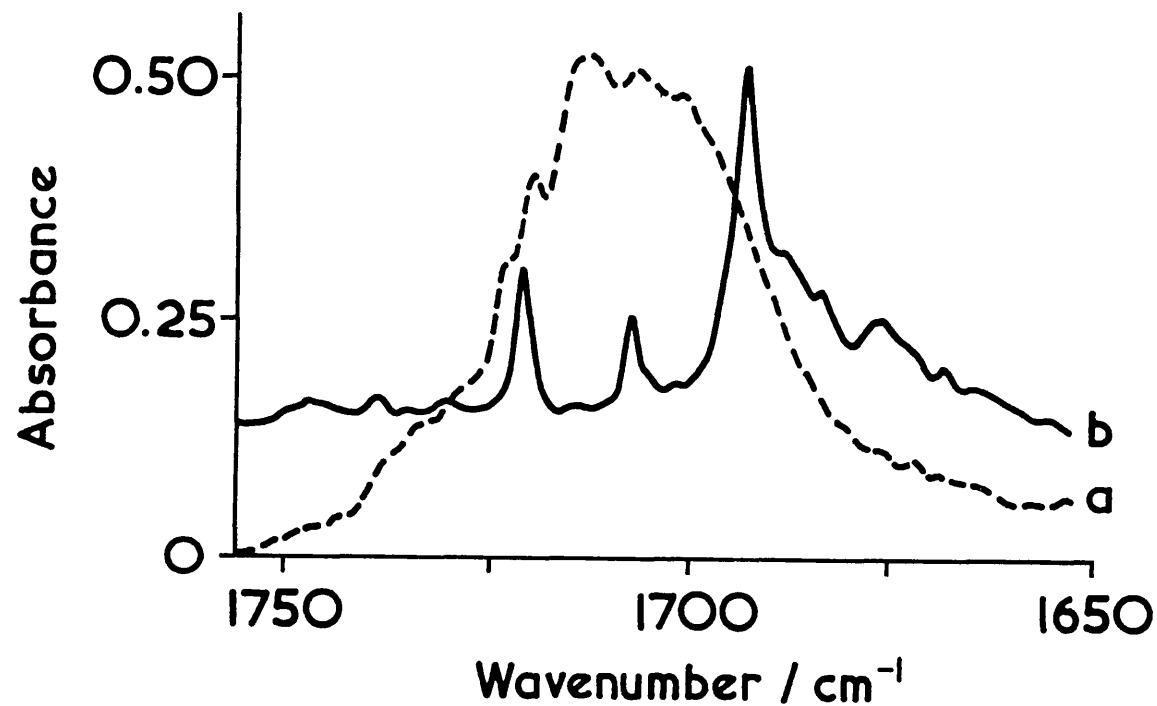


Figure 3.8. Infrared spectra in the $\nu_{C=O}$ region of the acetone...HI complex, detected after Pyrex-filtered ($\lambda > 290$ nm) irradiation of matrices containing 2-iodopropane/ozone/Ar (1:6:800). Spectrum of (a) normal isotopic ozone $\sim 99\%$ $^{16}\text{O}_3$ and (b) the ^{18}O isotopomer generated from $^{18}\text{O}_3$ ($\geq 97\%$ $^{18}\text{O}_2$).

Chapter 4

REACTION OF POLYFLUOROiodoethanes WITH OZONE

4.1 INTRODUCTION

The reaction of ozone with the four polyfluoroiodoethanes, pentafluoroiodoethane, 1,1,1-trifluoroiodoethane, 1,1,2,2-tetrafluoroiodoethane, and 1,1,1,2-tetrafluoroiodoethane (sections 4.2 to 4.5) has been studied in this chapter. The products of such reactions are expected to be fluoro-analogues of those reported in the reaction of iodoethane and ozone⁴⁷ (chapter 3), i.e. fluoro-species having -IO_x, -OI and -COX bonds. For example, if as expected, iodoso-species (Z-IO) are detected as products with each of the four precursors we will be able to compare both the photochemical and spectral behaviour with a range of such species reported in chapter 3 and elsewhere.¹⁹⁻²¹ The photochemical and spectral properties of the four precursors as well as the products of the reactions with ozone can be conveniently grouped into species having similar backbone structures. Thus both pentafluoroiodoethane and 1,1,2,2-tetrafluoroiodoethane have a X-CF₂I backbone structure, and it should be possible to compare the effect of various X groups for the species CF₃I²¹ (X = F), CF₃CF₂I (X = CF₃) and CF₂HCF₂I (X = CF₂H). Similarly, 1,1,1-trifluoroethane has a X-CH₂I backbone, and comparisons of X = H,²⁰ CH₃,^a CF₃^b and Cl^c can be made (^achapter 3; ^bthis chapter; ^cchapter 5). The precursor 1,1,1,2-tetrafluoroiodoethane is included in order to study the backbone structure X-CFHI, intermediate between the X-CH₂I and X-CF₂I structures. Additionally, comparisons can be made between the reactions of the species having the same X group (X = CF₃) but different backbone structures: -CH₂I, -CF₂I and -CFHI.

These four precursors were also chosen in order to study further the mechanism of the reaction of ozone with C_2X_3I species. It has been proposed that a five-membered ring intermediate⁵⁶ is formed in the gas phase reaction of ozone with iodoethane and thus, by studying the products of the reaction with, for example, CF_3CH_2I , it should be possible to determine whether the α - or β -carbon reaction predominates.

The polyfluoroiodoethanes may undergo additional reactions, e.g. Francis and Haszeldine⁶⁷ reported that the gas phase photolysis of perfluoroiodoalkanes, $CF_3(CF_2)_nI$, in oxygen produced carbonyl difluoride, COF_2 . Photolysis of trifluoroiodomethane in an oxygen/argon matrix has been shown to produce the radical CF_3O .⁶⁸ Also photolysis of ozone and tetrafluoroethene⁶⁹ was reported to produce carbonyl fluoride as the prime product, via C=C bond rupture and addition of an oxygen atom to the CF_2 species. It has also been shown that O_2 can add to CF_3 to form CF_3O_2 .^{70,71} Thus photolysis of these polyfluoroiodoethanes (chapter 4) may produce different products from those expected by simple extrapolation from the products reported with iodoethane (chapter 3).

4.2 PENTAFLUOROiodoETHANE, C_2F_5I

The photochemical reaction of C_2F_5I with ozone is expected to produce the fluoro-analogues of the $-IO_x$, $-OI$ and carbonyl species reported in the reaction of iodoethane with ozone⁴⁷ (chapter 3). Additional products might be detected as a result of C-C bond rupture and subsequent oxygen atom addition, similar to those reported for the gas phase reaction⁶⁷ of perfluoroiodoalkanes.

The products of the reaction of C_2F_5I with ozone can be compared with those of the reaction with precursors having the same backbone structure, $X-CF_2I$, i.e. CF_3I ($X = F$).²¹ In addition, the change in photochemistry between the reaction of ozone with CF_3I ²¹ and with C_2F_5I can be compared with the change observed in the

photochemistry between iodomethane²⁰ and iodoethane.⁴⁷

Finally, the hydrated iodoalkanes (chapter 3) are believed to react via a mechanism in which a five-member ring intermediate plays an important role. In this study it is hoped to provide evidence for a similar fluoro-intermediate.

4.2.1 RESULTS

After deposition of pentafluoroiodoethane in solid argon ($C_2F_5I/Ar = 1:400$) and solid oxygen ($C_2F_5I/O_2 = 1:200$) matrices at 14 K, the bands detected (Table 4.1) were found to be in good agreement with those detected previously for the liquid phase spectra.⁷² Ultraviolet ($\lambda > 240$ nm) photolysis of C_2F_5I isolated in argon for periods up to 1 h produced no detectable new bands. This supports the assumption that the reactions occur as a result of the reaction of O atoms or excited oxygen molecules with pentafluoroiodoethane, and not with some photodissociation product of pentafluoroiodoethane.

Pentafluoroiodoethane and ozone in argon

Co-deposition of argon matrices containing pentafluoroiodoethane ($C_2F_5I/Ar = 1:200$ to $1:400$) and ozone ($C_2F_5I/Ar = 1:200 - 1:1000$) and their subsequent photolysis produced a number of bands. These bands have been grouped (1-5) according to their behaviour after wavelength- and time-dependent photolysis or warming of the matrix.

Group 1. These bands are detected after co-deposition of pentafluoroiodoethane and ozone in argon matrices, and resemble those detected in the spectra of pentafluoroiodoethane (Table 4.1) and of ozone⁴⁴ isolated separately in argon. The most apparent wavenumber shifts occur for the bands attributed to ozone (Table 4.2). The ν_3 bands detected at 1039.5, 1033.8 and 1032.0 cm^{-1} in the $^{16}O_3$

experiment are attributed to ozone. The first to ozone isolated in argon and the second and third to an ozone...pentafluoroiodoethane complex. In the mixed-ozone experiments, $^{16}\text{O}_{3-x}^{18}\text{O}_x$, bands are assigned to the ν_2 and ν_3 fundamentals and the combination $\nu_1 + \nu_3$ of the six isotopomer variants of ozone (e.g. 16-16-16, 16-18-16 etc.). Additionally, bands are assigned to the weak ν_1 mode of for the 16-16-18, 16-18-16, 18-18-16 and 18-18-18 isotopomer variants. These group 1 bands reduced in intensity after near-infrared ($\lambda > 650$ nm) photolysis of the matrix.

Group 2. The group 2 bands were formed weakly after photolysis with near-infrared radiation ($\lambda > 650$ nm), while visible irradiation ($\lambda > 550$ nm and $\lambda > 410$ nm) increased the band intensities by 30 % after each successive 30 min cycle. However, UV-vis ($\lambda > 350$ nm) irradiation of the matrices destroyed the bands. The group 2 bands (Table 4.3) included a strong band assigned to a perturbed CF_2 stretch at 1090.7 cm^{-1} having a small ^{18}O -shift of 1.5 cm^{-1} . Weak bands assigned to perturbed stretches of the CF_2I unit were detected at 902.6 and 897.3 cm^{-1} and exhibited small ^{18}O -shifts of $< 0.9\text{ cm}^{-1}$. Very weak and weak bands at 867.0 and 845.7 cm^{-1} are assigned to the combination of the stretch of the CF_2I unit and CF_3 bend. A weak band at 738.7 cm^{-1} (Fig 4.1) having an ^{18}O -shift of 31.8 cm^{-1} is assigned to the I-O stretch. In the mixed-ozone experiments weak bands detected between 638.1 and 615.5 cm^{-1} and very weak bands between 535.3 and 527.2 cm^{-1} are assigned to perturbed CF_3 bends and C-I stretches, respectively. Additionally, in the mixed-ozone experiments a band was detected at 738.2 cm^{-1} but no ^{18}O isotopomer band was detected, probably because it was obscured by the ν_2 bands of the mixed-ozone precursor. The detection of bands for the ^{16}O and ^{18}O isotopomers suggests the presence of a single oxygen atom in this species.

Group 3. These bands were formed weakly after UV-vis ($\lambda > 350$ nm) photolysis of an argon matrix containing pentafluoroiodoethane and ozone (Table 4.4), and they appear to remain unchanged on subsequent shorter wavelength irradiation ($\lambda > 240$ nm). A single weak band was detected in the $^{16}\text{O}_3$ experiment at 812.1 cm^{-1} (between 818.7 and 759.2 cm^{-1} in the mixed ozone experiment, $^{16}\text{O}_{3-x}^{18}\text{O}_x$). These bands are thought to be characteristic of an IO_2 unit, based on the assignment methods

established in chapter 3 for an iodyl-species (see discussion for further assignment).

Group 4. Like the group 3 bands, this group was formed after UV-vis photolysis ($\lambda > 350$ nm) but, due to the low intensities (Table 4.5), no change in band intensity could be distinguished after subsequent photolysis at shorter wavelength. This group consists of medium bands assigned to C-O stretches detected at 968.7 and 961.5 cm^{-1} having ^{18}O -shifts of 13.0 and 8.2 cm^{-1} respectively. Weak bands at 583.9 cm^{-1} in the $^{16}\text{O}_3$ experiment, at 578.6 cm^{-1} in the $^{18}\text{O}_3$ experiment, and at 584.4, 581.0 and 577.4 cm^{-1} in the mixed-ozone experiments are assigned to O-I stretches, based on their similarity to bands reported in chapter 3.

Group 5. The bands detected for this group were first detected after UV-vis irradiation, Pyrex-filtered photolysis nearly quadrupled the intensities, whilst quartz-filtered irradiation increased the intensities by a further 50 % (Table 4.6). The most diagnostic bands for this group occur in the carbonyl stretching region (Fig. 4.2). For matrices deposited with 'high' precursor-to-argon concentrations ($\text{C}_2\text{F}_5\text{I}/\text{O}_3/\text{Ar} = 1:1:200$) three carbonyl bands were detected, at 1935.9, 1906.0 and 1886.8 cm^{-1} . The spectrum recorded after deposition of a matrix at a lower initial concentration (1:1:400) exhibited three groups of carbonyl bands, as above, in which the first group split into bands at 1938.4, 1936.4, 1933.9 cm^{-1} and, the second into bands at 1909.9, 1907.7, 1905.9 and 1901.2 cm^{-1} . Further experiments at different initial deposition ratios showed that the split pattern of bands was detected only when the concentration ratio of $\text{C}_2\text{F}_5\text{I}/\text{Ar}$ was 1:400 or greater (more dilute). After warming the matrix, the intensity of the band at 1886.8 cm^{-1} increased by 10 %, at the expense of a 10 % loss in the bands centred around 1936 cm^{-1} . Similar behaviour was noted for the bands of the ^{18}O -isotopomer.

Other bands for this group seemed to be unaffected by variations in the initial concentration ratios, and are assigned below. Of the remaining fundamentals, a strong band at 1327.0 cm^{-1} is assigned to the CF_3 stretch. Strong bands at 1267.2 and 1250.8 cm^{-1} (^{18}O at 1267.6, 1259.0 and 1240.6 cm^{-1}) are assigned to CF_3 stretches. A very strong band at 1197.7 cm^{-1} (^{18}O at 1197.7 and 1192.9 cm^{-1}) is assigned to a CF_2

stretch. A strong band at 1091.2 cm^{-1} (^{18}O at 1089.2 cm^{-1}) is assigned to the CF' stretch of the carbonyl fluorine atom ($-\text{COF}'$). Weak bands at 819.7 and 807.6 cm^{-1} , detected in the ^{18}O experiments, are assigned to C-C stretches. Medium and medium-weak bands at 769.6 and 762.3 cm^{-1} , respectively (^{18}O at 768.7 , 765.2 and 758.9 cm^{-1}), are assigned to the OCF' deformation; bands detected in the mixed-ozone experiment at 768.6 , 764.7 and 759.4 cm^{-1} confirm that only one oxygen atom is involved. A weak band, detected in the $^{18}\text{O}_3$ experiments, at 687.1 cm^{-1} is assigned to a CF_3 bend. A weak band detected at 596.5 cm^{-1} (^{18}O at 604.7 cm^{-1}) can be assigned to either a combination band (CF_3 bend and O-C-F' bend) or to the symmetric stretch of IF; the positive isotope shift indicates assignment to IF, the wavenumber shift being caused by differing geometries (see later). Strong bands at 1286.5 and 1282.6 cm^{-1} (^{18}O bands at 1276.8 and 1275.8 cm^{-1}) are assigned to the combination of C-C stretch and FCF bend, the former band being shifted slightly from a precursor band at 1287.4 cm^{-1} while the latter grows from an existing precursor band of medium intensity. A very strong, broad band (peak width $\sim 20\text{ cm}^{-1}$) at 1166 cm^{-1} (^{18}O at 1181.8 , 1177.5 and 1167.4 cm^{-1}) is assigned to the combination of an OCF' bend with an out-of-phase wag. A strong band at 1082.5 cm^{-1} (^{18}O at 1083.0 cm^{-1}) and two medium bands at 1067.6 and 1063.7 cm^{-1} (^{18}O at 1068.5 and 1064.6 cm^{-1}) are assigned to the combination of the CF_3 bend with an out-of-phase rock. A weak band at 644.7 cm^{-1} is assigned to the combination of an in-phase and an out-of-phase wag.

Pentafluoroiodoethane in oxygen

The spectra of pentafluoroiodoethane deposited in solid oxygen ($\text{C}_2\text{F}_5\text{I}/\text{O}_2 = 1:100$) resembles closely that in a solid argon matrix (Table 4.1). Photolysis of these oxygen matrices with quartz-filtered radiation was required before any new bands were detected (Table 4.6). The bands resemble those detected for group 5 above, and are assigned as follows. The bands detected at 1935.0 , 1905.1 , 1903.6 and 1887.7 cm^{-1} (relative intensities being 1:3:3:2), are assigned to the carbonyl stretch, those at

1251.3, 1196.81 and 1100.6 cm^{-1} are assigned to various C-F_x modes, those at 771.5 and 763.8 cm^{-1} are assigned to an OCF' bend, while those at 694.8 and 688.1 cm^{-1} are assigned to the CF₃ bend. Bands at 1180.9, 1173.6 and 1082.5 cm^{-1} are assigned to various combination bands.

In one experiment, Pyrex-filtered photolysis of a matrix containing C₂F₅I/O₂/Ar (1:10:1000) resulted in the detection of bands assigned to carbonyl stretches whose intensity increased on subsequent ultraviolet irradiation. Other weak bands were also detected at 983.8 and 965.0 cm^{-1} . Unusually, subsequent UV-vis photolysis produced weak bands at 633.3, 629.6, 608.8 and 581.4 cm^{-1} which could then be destroyed by Pyrex-filtered photolysis.

4.2.2 DISCUSSION

The bands detected after photolysis of pentafluoroiodoethane, with ozone (¹⁶O₃, ¹⁶O_{3-x}¹⁸O_x and ¹⁸O₃) in argon matrices and in an oxygen matrix are discussed below.

Group 1. The bands detected after co-deposition of pentafluoroiodoethane and ozone (Table 4.1 and 4.2) are assigned to modes of the precursors ozone⁴⁴ and C₂F₅I.⁷² The strong antisymmetric stretch (ν_3) exhibited shifts to 1033.8 and 1032.0 cm^{-1} ; these shifts are similar to those detected for ozone...precursor complexes discussed in chapter 3 (CH₃I,²⁰ CF₃I²¹ and C₂H₅I⁴⁷). In the mixed-ozone experiment, the detection of six sets of bands for the six isotopomer variants of ozone implies that ozone in the complex is symmetrically bound, i.e. via the central O atom. This contrasts with the ozone...trifluoriodomethane²¹ complex where eight sets of ν_3 bands were detected and thus the complex was believed to bind via one of the terminal oxygen atoms. A further difference between CF₃I²¹ and C₂F₅I occurs in the photochemistry, with the former requiring wavelengths of $\lambda > 470$ nm, while the latter only requires $\lambda > 650$ nm to initiate a reaction. The wavelengths required with pentafluoroiodoethane match closely those of the hydrated iodoalkanes: iodomethane,²⁰ iodoethane⁴⁷ and 2-

iodopropane. Like the reactions reported in chapter 3, the photochemical reaction is believed to proceed via a charge-transfer process and thus the difference in threshold wavelength is probably due to a difference in ionisation energies between pentafluoroiodoethane and trifluoroiodoethane.

Group 2. This group of bands formed after near-infrared photolysis (Table 4.3) as those of group 1 were destroyed. This group contains bands assigned to CF_2 stretch, the CF_2I unit, CF_3 deformations, IO (Fig. 4.1) and C-I stretches; the most diagnostic being the ν_{IO} at 738.7 cm^{-1} . This group has been attributed to iodosopentafluoroethane, $\text{C}_2\text{F}_5\text{IO}$. Comparisons of this with other iodoso-species, Z-IO, are made at the end of chapter 5.

Group 3. This group of bands (Table 4.4) detected after UV-vis photolysis is assigned using the assignment procedure used in chapter 3 for iodyl-type species (Z- IO_2). The band at 812.1 cm^{-1} detected in the $^{16}\text{O}_3$ experiments, is assigned to the antisymmetric I^{16}O_2 stretch, this band being intermediate between similar bands assigned to iodylethane ($837.2 - 825.4 \text{ cm}^{-1}$) and iodyltrifluoromethane^r (799 cm^{-1}). No bands were detected in the $^{16}\text{O}_3$ experiments that could be assigned to the symmetric stretch, due in part to the low absorbance and in part to the coincidence with the OCF' bend of tetrafluoroethanal between $760-770 \text{ cm}^{-1}$. In the mixed-ozone experiments, bands were detected at $818.7, 807.6, 799.9, 768.6, 764.7$ and 759.2 cm^{-1} . The predicted ^{18}O -shift of $\sim 40 \text{ cm}^{-1}$ (see chapter 3) enabled these bands to be assigned to the antisymmetric stretches of either I^{16}O_2 or I^{18}O_2 (Table 4.4). The presence of an IO_2 unit suggests the species iodylpentafluoroethane, $\text{C}_2\text{F}_5\text{IO}_2$. Like its hydrated counter-parts iodylpentafluoroethane is believed to be formed via reaction of pentafluoroiodoethane with an excited oxygen molecule, or possibly via reaction of iodosopentafluoroethane with an oxygen atom, the former mechanism being favoured in this work.

Group 4. Bands for this group were formed after UV-vis photolysis of the matrix, and are assigned to C-O and O-I stretches (Table 4.5). The bands assigned to the C-O stretches at 968.7 and 961.5 cm^{-1} exhibited ^{18}O -shifts of 13.0 and 8.2 cm^{-1}

respectively; in comparison to the predicted shift of 28 cm^{-1} for the pure harmonic stretch. However, these small shifts seem reasonable for the C-O stretch of a unit such as -C-O-X. The bands assigned to the O-I stretch have wavenumber shifts of 5.3 cm^{-1} between the ^{16}O and ^{18}O isotopomers (shift of 7.0 cm^{-1} between the bands detected in the mixed-ozone experiment). This suggests that the bands detected are those of the ^{16}O isotopomer, since we would expect to detect ^{18}O -shifts of $\sim 29\text{ cm}^{-1}$. It seems likely that the additional O-I bands detected in the mixed-ozone and $^{18}\text{O}_3$ experiments can be assigned to O-I stretches of different species rather than to different isotopomers. In comparison the ν_{OI} bands of HOI and $\text{C}_2\text{H}_5\text{OI}$ are separated by $\sim 9\text{ cm}^{-1}$ and thus it seems possible that the bands detected in this experiment could be attributed to ν_{OI} of the fluoro-analogues, $\text{CF}_3\text{CF}_2\text{OI}$ and FOI. The FOI species would be formed in much the same manner as HOI, formed in the iodoethane/ozone experiments, i.e. via a five-member ring intermediate. Unfortunately, no O-F stretching bands were detected (the ν_{OF} bands of the triatomics FON^{73,74,75} and FO₂^{76,77} absorb at 492 cm^{-1} and 584 cm^{-1} respectively) and thus the assignment of these ν_{OI} bands must remain tentative although reasonably convincing (*cf.* chapter 3).

Group 5. The group 5 bands were formed after UV-vis photolysis of the deposited matrices. The increase in group 4 and 5 band intensities after photolysis appeared to be at the expense of the group 2 bands, indicating that the species responsible for the group 4 and 5 bands are formed from the group 2 species, possibly in a step-wise manner (see photochemical interconversion, section 4.7). The group 5 bands continued to increase in intensity after Pyrex- and quartz-filtered photolysis, unlike the group 4 bands, providing further support for a step-wise reaction in which photolysis converts species 2 into species 4 and then 5.

The majority of the group 5 bands (Table 4.6) resemble those previously reported for CF_3COF in the gas phase^{78,79,80,81} and in an argon matrix,⁸² while the band at 596.5 cm^{-1} resembled those assigned to IF, reported previously in the gas phase,⁸³ isolated in an argon matrix,⁸⁴ and in the complex $\text{COF}_2\cdots\text{IF}$.²¹ Based on this spectral evidence the group 5 bands are attributed to the complex $\text{CF}_3\text{COF}\cdots\text{IF}$. The most

diagnostic bands are those assigned to the carbonyl stretch which may shed light on the geometry of the complex. Warming the matrix caused the intensity of the band at 1886.3 cm^{-1} to increase at the expense of those centred around 1936 cm^{-1} . Thus bands that increased in intensity have been assigned to a more thermally stable arrangement, involving a head-to-tail dipole-dipole interaction between the O and I atoms of CF_3COF and IF , while the other bands are assigned to a complex involving a molecular pair type complex with the C=O and I-F bonds parallel to each other. The wavenumbers of the various carbonyl bands of these two complexes, shed further light on the geometry of the complex. The $\nu_{\text{C=O}}$ band at 1886.3 cm^{-1} is shifted to lower wavenumber by 12.7 cm^{-1} from that for isolated CF_3COF isolated in argon, this shift being intermediate between those of 2.4 and 30 cm^{-1} detected for the two $\text{COF}_2\cdots\text{IF}^{21}$ complexes; these red-shifted bands represent the head-tail arrangement. Interestingly, in these experiments, the most intense carbonyl bands (those between 1901.2 and 1938.4 cm^{-1}) are shifted to higher wavenumber by between 2.2 and 39.4 cm^{-1} indicating a different interaction between IF and CF_3COF . It is proposed that the I-F bond and C=O bond lie parallel to each other, with the lone-pairs of the fluorine atom reinforcing the carbonyl bond in some manner. A comparison is made of the relative wavenumber shifts detected for the carbonyl bands of this and other carbonyl...Lewis acid complexes (section 4.6).

In these studies no bands were detected that could be attributed to carbonyl difluoride, COF_2 , the main product detected in the gas phase reaction of pentafluoroiodoethane⁶⁷ and oxygen atoms. Thus a different mechanism occurs in the matrix, most likely due to the rigid environment.

4.3 1,1,1-TRIFLUOROiodoethane, $\text{CF}_3\text{CH}_2\text{I}$

After studying the reaction of ozone with iodoethane⁴⁷ and pentafluoroiodoethane it was decided to extend the research area by studying a number of polyfluoroiodoethanes, and thus 1,1,1-trifluoroiodoethane. Using this precursor it should be possible to detect a number of new intermediates and product complexes, make comparisons between the spectra of these products, and use the information gained to clarify further the photochemical pathway for the reaction of ozone with these iodine-containing precursors.

The precursor $\text{CF}_3\text{CH}_2\text{I}$ has a backbone structure $\text{X}-\text{CH}_2\text{I}$ and thus the products formed can be compared with others having the same backbone, CH_3I ²⁰ ($\text{X} = \text{H}$), iodoethane⁴⁷ ($\text{X} = \text{CH}_3$), chloriodomethane and diiodomethane ($\text{X} = \text{Cl}$ and I see chapter 5). Comparisons between the species having the same X group (CF_3) but different backbones $-\text{CH}_2\text{I}$ (iodoethane), $-\text{CF}_2\text{I}$ (pentafluoroiodoethane) and $-\text{CFHI}$ (1,1,1,2-tetrafluoroiodoethane) can also be made.

With iodoethane and pentafluoroiodoethane it is not possible to determine from which carbon (α or β) the H or F came in the products HI , HOI , FI or FOI , but with $\text{CF}_3\text{CH}_2\text{I}$ the products formed will provide direct evidence for either the α - or β -carbon reaction; hence the presence of a five-member ring intermediate in these matrix experiments can be clarified (note: the presence of a five-member ring intermediate has been confirmed in the gas phase⁵⁶ reaction of iodoethane and ozone). As mentioned in chapter 3, whilst the five-membered ring intermediate accounts for the early products, it does not provide a clear route to the carbonyls detected in this study. If the five-member ring intermediate is a step in the mechanism, then $\text{CF}_3\text{CH}_2\text{I}$ should produce the fluoroalkene, $\text{CF}_2=\text{CH}_2$ and FOI . Subsequent O atom addition, and H/F atom migration across the double bond would lead to either CF_2HCOF or CH_2FCOH as the final carbonyls, and again detection of either of these will clarify the mechanism.

4.3.1 RESULTS

The spectra of argon or oxygen matrices containing 1,1,1-trifluoroiodoethane were recorded (Table 4.7) and found to be in good agreement with the gas phase spectra⁸⁵ recorded previously. Ultraviolet photolysis ($\lambda > 240$ nm) of $\text{CF}_3\text{CH}_2\text{I}$ isolated in argon for up to 2 h produced no new bands.

Trifluoroiodoethane and ozone in argon

The spectra of 1,1,1-trifluoroiodoethane ($\text{CF}_3\text{CH}_2\text{I}/\text{Ar} \sim 1:500$) and ozone ($\text{O}_3/\text{Ar} = 1:200-1:400$) co-deposited in argon has been recorded (Table 4.7) and is in good agreement with the spectra recorded for the isolated precursors 1,1,1-trifluoroiodoethane and ozone⁴⁴ except for slight shifts. The bands detected after deposition, subsequent wavelength- and time-dependent photolysis, or warming of the matrices are grouped (1-5) below.

Group 1. These bands were formed after co-deposition of the precursors. The most diagnostic shifts occur for the ν_3 bands of ozone (Table 4.8), which are shifted to 1033.0 cm^{-1} indicating an ozone... $\text{CF}_3\text{CH}_2\text{I}$ complex similar to those reported previously (see chapter). In the mixed-ozone experiments bands are assigned to the ν_2 and ν_3 modes and the combination, $\nu_1 + \nu_3$ for the six isotopomer variants. Additionally, some weak bands were detected at 1094.5, 1091.8 and 1090.3 cm^{-1} which are assigned to the symmetric stretch (ν_1) of the 16-16-18 ozone isotopomer.

Group 2. Photolysis of the group 1 bands with near-infrared radiation ($\lambda > 650$ nm) formed the group 2 bands. Visible photolysis ($\lambda > 450$ nm) doubled the intensities of these bands, while subsequent UV-vis photolysis ($\lambda > 350$ nm) reduced the intensities by 30 %, these bands being finally destroyed by Pyrex-filtered irradiation. The group 2 bands (Table 4.9) absorb at 1404.7, 1282.1, 1278.4, 1257.6, 1199.2, 732.4 and 727.1 cm^{-1} . The medium-weak band at 1404.7 cm^{-1} (^{18}O isotopomer

at 1406.0 cm⁻¹) is assigned to a perturbed CH₂ bend. The medium doublet of bands at 1282.1 and 1278.4 cm⁻¹ (¹⁸O at 1284.6, 1279.6 and 1278.6 cm⁻¹) are assigned to CH₂ wags. The strong bands at 1257.6 and 1199.2 cm⁻¹ (¹⁸O at 1257.0, 1244.1, 1240.4 and 1198.7 cm⁻¹) are assigned to CF₃ stretches. The medium-weak and weak bands at 732.4 and 727.1 cm⁻¹ having ¹⁸O-shifts of 37.2 and 38.4 cm⁻¹ respectively, are assigned to I-O stretches (Fig. 4.3). In the mixed-ozone experiments bands were detected that were assigned to either ¹⁶O or ¹⁸O isotopomers, confirming that only one O atom is involved in the species responsible for the group 2 bands.

Group 3. These bands are formed after visible photolysis ($\lambda > 450$ nm), and destroyed after quartz-filtered irradiation (Table 4.10). Photolysis with wavelengths intermediate between these two (e.g. visible) had little effect on the bands. In the ¹⁶O₃ experiments, weak bands were detected at 815.5 and 809.4 cm⁻¹ while in the mixed-ozone experiments a number of very weak bands were detected at 811.4, 808.4, 806.9, 787.5, 783.3, 781.0, 768.0 and 764.5 cm⁻¹. Finally in the ¹⁸O₃ experiments weak bands were detected at 811.9 and 805.4 cm⁻¹. These bands are assigned to stretches of the IO₂ unit.

Group 4. These bands were detected after UV-vis photolysis of the matrix and absorb (Table 4.11) very weakly at 588.2, 577.7 and 567.4 cm⁻¹. The wavenumbers suggest that they should be assigned to O-I stretches. A very weak band was detected at 3444 cm⁻¹ (intensity approx. double the rms noise) and is assigned to an O-H vibration, possibly of HOI.

Group 5. These group 5 bands are formed after UV-vis ($\lambda > 350$ nm) irradiation of the matrix, Pyrex-filtered irradiation doubling the intensities of the bands while quartz-filtered irradiation increased the intensities by approximately 30 % for every 30 min cycle. The bands detected (Table 4.12) are assigned as follows: a weak band at 2997.1 cm⁻¹ is assigned as a C-H stretch; a medium band at 1777.8 cm⁻¹ and its weak shoulders at 1784.5 and 1770.8 cm⁻¹ (Fig. 4.5) (¹⁸O at 1748.4, 1743.6 and 1729.1 cm⁻¹) are assigned to carbonyl stretches; a strong band at 1382.9 cm⁻¹ (¹⁸O at 1377.2 cm⁻¹) is assigned to the in-plane CH' bend. Strong bands at 1281.1 and 1277.3

cm^{-1} (^{18}O at 1256.6 cm^{-1}) are assigned to the symmetric CF_3 stretch, these bands absorbing near to those of the group 2 species; the photochemical behaviour indicates an overlap of these bands. Strong bands at 1198.2 , 1197.7 , 1195.3 and 1170.7 cm^{-1} and a medium-strong band at 1167.4 cm^{-1} (^{18}O at 1194.4 and 1173.9 cm^{-1}) are assigned to one of two antisymmetric CF_3 stretching modes. Weak and medium-weak bands at 974.5 and 958.1 cm^{-1} (^{18}O at 970.0 and 959.1 cm^{-1}) are assigned to the out-of-plane CH' bend (Fig. 4.3). The medium band 843.3 cm^{-1} and its weak shoulders at 851.3 and 836.6 cm^{-1} are assigned to C-C stretches. A very weak band at 598.5 cm^{-1} detected after quartz-filtered photolysis, is assigned tentatively to either an antisymmetric CF_3 bend, or to the ν_s of IF. Weak bands at 542.7 and 526.1 cm^{-1} are assigned to an antisymmetric CF_3 bending mode.

Additionally a number of combination and overtone bands were detected. A medium band at 1242.1 cm^{-1} (^{18}O at 1240.4 cm^{-1}) is assigned to the combination of C-C stretch and C-C=O bend. The weak band at 1079.1 cm^{-1} (^{18}O at 1077.7 cm^{-1}) is assigned to the combination of a C-C stretch and a CF_3 rock. A medium band 886.7 cm^{-1} is assigned to the first overtone of the C-C=O bend (δ_{CCO} at 431 cm^{-1}).⁸⁶ A weak band at 684.6 cm^{-1} detected after quartz-filtered photolysis, is assigned to the combination of the C-C=O bend and CF_3 rock. In the mixed-ozone experiments, bands were detected that could be assigned to either ^{16}O or ^{18}O isotopomers, confirming that only one oxygen atom is present. Unfortunately, in these studies, no bands were detected that could be assigned to hydrogen iodide.

1,1,1-Trifluoroiodoethane in oxygen

The spectra of $\text{CF}_3\text{CH}_2\text{I}$ deposited in solid oxygen ($\text{CF}_3\text{CH}_2\text{I}/\text{O}_2 = 1:400$) exhibited bands (Table 4.7) similar to those detected for the $\text{CF}_3\text{CH}_2\text{I}$ isolated in argon. Quartz-filtered photolysis was required before any product bands (Table 4.12) were detected. These bands at 1772.5 , 1384.3 , 1215.1 , 1177.5 , 1168.3 , 991.8 , 953.3 and 707.4 cm^{-1} are assigned based on their resemblance to the group 5 bands above.

In one study, photolysis of the matrix with Pyrex-filtered radiation for 15 h and quartz-filtered radiation for a further 4 h produced a weak band at 3492.3 cm^{-1} (Table 4.11) assigned to an O-H stretch, probably of the HOI species.

4.3.2 DISCUSSION

The bands detected above have been attributed to several species on the basis of their photochemical and thermal behaviour and their wavenumbers. These species and the groups of bands (1-5) to which they give rise are discussed below.

Group 1. These bands, formed after co-deposition of ozone and 1,1,1-trifluoroiodoethane are assigned to the weak molecular complex, $\text{CF}_3\text{CH}_2\text{I}\cdots\text{O}_3$. The ozone bands of the complex are the most diagnostic (Table 4.8), with those detected in the mixed-ozone experiments providing evidence for the ozone moiety binding through the central O atom, in the same manner as for the other ozone complexes detected in this work. The complex perturbs the photochemistry by allowing ozone to be dissociated after near-infrared irradiation ($\lambda > 650\text{ nm}$); this photodissociation occurs via a charge-transfer type mechanism similar to that reported in chapter 3.

Group 2. This group of bands was formed after near-infrared photolysis ($\lambda > 650\text{ nm}$), the bands increased in intensity after photolysis in the visible, but were reduced drastically after photolysis at $\lambda > 350\text{ nm}$. Finally, Pyrex-filtered photolysis destroyed this group of bands. The growth of these group 2 bands appeared to occur at the expense of the group 1 bands, indicating the first step in a step-wise mechanism. The bands detected for this group (Table 4.9) are assigned to a CH_2 bend, CH_2 wag, perturbed C-F stretches and an I-O stretch. These bands are attributed to iodoso-1,1,1-trifluoroethane, $\text{CF}_3\text{CH}_2\text{IO}$. The ^{18}O -shifts of 37.2 and 38.4 cm^{-1} for the ν_{IO} bands at 732.4 and 727.1 cm^{-1} respectively, are noteworthy since they are very close to the ^{18}O -shift predicted for I-O. A comparison of this iodoso-species with the others detected is carried out at the end of chapter 5.

Group 3. The group 3 bands were detected after visible photolysis and destroyed by quartz-filtered photolysis, and are assigned to various -IO_2 stretches (Table 4.10 and Fig. 4.5), and thus iodyl-1,1,1-trifluoroethane, $\text{CF}_3\text{CH}_2\text{IO}_2$. No other bands were detected for this species; however this is not surprising given the low intensities of the IO_2 bands, and the fact that any other bands would most likely overlap with the precursor bands. The bands assigned (Table 4.10) to the anti-symmetric and symmetric stretches of the various IO_2 isotopomer units, in the mixed-ozone experiment, support the conclusion that this unit contains two oxygen atoms. For comparison the weak bands at 815.5 and 809.4 cm^{-1} detected in the $^{16}\text{O}_3$ experiment and assigned to the $\nu_a\text{I}^{16}\text{O}_2$, are in good agreement with those of $\text{C}_2\text{F}_5\text{IO}_2$ (812.1 cm^{-1}), and are approximately intermediate between those of $\text{C}_2\text{H}_5\text{IO}_2$ ⁴⁷ (837.2 - 825.4 cm^{-1}) and CF_3IO_2 ²¹ (800 cm^{-1}). No other band, i.e. $\nu_s\text{I}^{16}\text{O}_2$, was detected for the ^{16}O isotopomer, probably due to its lower intensity versus that of the antisymmetric mode. However, in the mixed-ozone experiment a number of bands were detected at lower wavenumber and are assigned using the regime used in chapter 3 (i.e. ^{18}O -shift $\sim 40 \text{ cm}^{-1}$; $\nu_a\text{IO}_2 - \nu_s\text{IO}_2 \sim 34 \text{ cm}^{-1}$; ν_{10} (of ZIO) - $\nu_s\text{IO}_2$ (of ZIO₂) ~ 60 and 80 cm^{-1}). In addition the stretches of the mixed-unit, i.e. $\text{I}^{16}\text{O}^{18}\text{O}$, are assigned by assuming that the bands will absorb approximately half-way between the bands of the I^{16}O_2 and I^{18}O_2 units. Thus the bands detected at 787.5, 783.3 and 781.0 cm^{-1} are assigned to the $\nu_a\text{I}^{16}\text{O}^{18}\text{O}$, and those at 768.0 and 764.5 cm^{-1} to $\nu_s\text{I}^{18}\text{O}_2$. These assignments are confirmed since, the former absorb at too high a wavenumber to arise from the symmetric I^{16}O_2 stretch, while the latter are assigned using the separation between the ν_{10} of $\text{C}_2\text{F}_5\text{I}^{18}\text{O}$ (at 695.2 and 688.7 cm^{-1} group 2) and $\nu_s\text{IO}_2$ of $\text{C}_2\text{F}_5\text{I}^{18}\text{O}_2$ (768.0 and 764.5 cm^{-1} group 3), i.e. the shifts of 72.8 and 75.8 cm^{-1} respectively, are in good agreement with those reported in chapter 3.

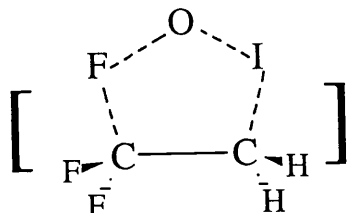
Group 4. These bands were detected after UV-vis photolysis at 588.2, 577.7 and 567.4 cm^{-1} (Table 4.11). The wavenumbers of these bands support their assignment to O-I stretches, possibly of $\text{CF}_3\text{CH}_2\text{OI}$, HOI or FOI . The tentative assignment, due to its low intensity, of the band at 3444 cm^{-1} (3492.3 cm^{-1} in the oxygen matrix) to the O-H vibration, indicates the presence of HOI . The detection

of FOI would be expected if the five-membered ring intermediate mechanism was occurring, but no ν_{OF} bands were detected (see section 4.2.2). The presence of HOI is accounted for by the reaction of HI, from $\text{CF}_3\text{CH}_2\text{I}$, with O atoms⁴⁶ this mechanism almost certainly operates in the oxygen matrix experiment in which over 19 h of photolysis was employed (see chapter 5 for similar product). This observation might also account for the disparity in which HOI was detected in the matrix reactions of iodomethane^{40,41} and molecular oxygen, in which long periods of ultraviolet photolysis were required, but not in the matrix²⁰ and gas phase⁶⁰ experiments using ozone to produce oxygen atoms. The lack of detection of FOI, and the tentative evidence for HI would at first tend to suggest that a five-membered ring intermediate was not formed; however, as will be discussed later, it is thought that the intermediate rapidly rotates around the α -carbon (i.e. the one that the I atom is attached to) to give the observed products.

Group 5. The bands detected for this group are in good agreement with those reported in the gas phase spectra of CF_3COH ⁸⁶ (Table 4.12). In addition to bands assigned to CF_3COH , a very weak band at 598.5 cm^{-1} detected after quartz-filtered photolysis, could be assigned to iodine monofluoride, IF.⁸⁴ However, this band could also reasonably be assigned to a vibration of trifluoroethanal and, as such, evidence for the presence of IF is tentative at best. No bands were detected for hydrogen iodide, but due to its low infrared absorbance this is not entirely unexpected, and the detection of HOI, mentioned above, provides support for the presence of hydrogen iodide. This group of bands is attributed to the complex $\text{CF}_3\text{COH}\dots\text{HI}$. The formation of this complex is supported by the detection of similar complexes earlier in this work (and later).

If iodine monofluoride were formed, it would do so via photodissociation of $\text{CF}_3\text{CH}_2\text{I}$ to yield $\text{CF}_2=\text{CH}_2$ and IF, analogous to the dissociation of iodoethane⁴³ yielding ethene and HI. If this process were to occur, subsequent O atom addition to $\text{CF}_2=\text{CH}_2$ would be expected to produce either CF_2HCOH or CH_2COF . Since CF_3COH was detected instead, a different mechanism must occur. It is thus believed that addition of O atoms to $\text{CF}_3\text{CH}_2\text{I}$ produces an iodoso-species, ZC-I-O, which

rearranges to produce a ring intermediate which can be viewed as FOI and $\text{CF}_2=\text{CH}_2$ in close proximity (see Summary 4).



FOI and $\text{F}_2\text{C}=\text{CH}_2$ forming a five-membered intermediate

This intermediate further rearranges by rotation of the C-I-O atoms to form a C-O-I arrangement of atoms (group 4) and subsequently dissociates to the carbonyl. Unlike the reaction of iodoethane and ozone, in which HOI was detected, no FOI is detected in this reaction because of the stronger C-F bonds. Additional studies using techniques more sensitive to the species FOI and $\text{CF}_2=\text{CH}_2$ are needed in order to clarify this part of the mechanism.

The reaction of ozone with $\text{CF}_3\text{CH}_2\text{I}$ has generated, *in situ*, some carbonyl complexes, $\text{CF}_3\text{COH}\dots\text{HI}$, if we compare the wavenumber shifts of the carbonyl bands of these complexes ($\Delta\nu = \nu_{\text{isolated}} - \nu_{\text{shifted}}$, where isolated $\text{CF}_3\text{COH}^{86}$ has an $\nu_{\text{C=O}}$ band at 1788 cm^{-1}), the following shifts are observed: the weak band at 1784.5 cm^{-1} ($\Delta\nu = 3.5\text{ cm}^{-1}$), the medium band at 1777.8 cm^{-1} (10.2 cm^{-1}) and the very weak band at 1770.8 cm^{-1} (22.2 cm^{-1}). These carbonyl shifts (between 3.5 and 22.2 cm^{-1}) are in good agreement with those found for complexes of HI with COH_2 ,^{20,61} (6 to 16 cm^{-1}), CH_3COH ,⁴⁷ (9.0 to 22.6 cm^{-1}), $(\text{CH}_3)_2\text{CO}$ ^{47,65} (2.0 to 22.9 cm^{-1}) and for the polyfluoroethanals detected in this chapter (see section 4.6).

4.4 1,1,2,2-TETRAFLUOROiodoethane, $\text{CF}_2\text{HCF}_2\text{I}$

The reaction of ozone with some polyfluorinated iodoethanes has been studied in the preceding sections with the intention of detecting a range of novel products and further elucidating the photochemical mechanism. In this section, $\text{CF}_2\text{HCF}_2\text{I}$ was chosen as it has a hydrogen atom on the β -carbon and might thus produce HOI as a product, confirming the presence of a five-member ring intermediate in the reaction path (ideally $\text{CH}_3\text{CF}_2\text{I}$ would have been used, but it was unavailable at the time the research was carried out).

The photochemical and spectroscopic properties of the products, in this reaction, can be compared with those of the reaction of CF_3I^{21} and $\text{C}_2\text{F}_5\text{I}$ with ozone, enabling a comparison of the X- CF_2I backbone species to be made. Additionally the X group, CF_2H , allows us to examine the effect of having a fully fluorinated CX_3 group, e.g. trifluoromethyl group (CF_3I ,²¹ $\text{CF}_3\text{CF}_2\text{I}$ and $\text{CF}_3\text{CH}_2\text{I}$).

4.4.1 RESULTS

The spectra of 1,1,2,2-tetrafluoroiodoethane isolated in argon ($\text{CF}_2\text{HCF}_2\text{I}/\text{Ar} = 1:400$) and in solid oxygen ($\text{CF}_2\text{HCF}_2\text{I}/\text{O}_2 = 1:300$) were recorded, and the bands assigned (Table 4.13) using the other polyfluoroiodoethanes as guides. As with the other species ultraviolet photolysis of $\text{CF}_2\text{HCF}_2\text{I}$ isolated in argon produced no new detectable products, confirming that those detected are formed as a result of the reaction of $\text{CF}_2\text{HCF}_2\text{I}$ with oxygen atoms or ozone, and not as the result of fragmentation of the precursor.

1,1,2,2-Tetrafluoroiodoethane and ozone in argon

The co-deposition of $\text{CF}_2\text{HCF}_2\text{I}$ and O_3 in argon ($\text{CF}_2\text{HCF}_2\text{I}/\text{O}_3/\text{Ar} = 1:2:400$), and the subsequent wavelength-dependent photolysis or warming of the matrix resulted in the detection of a number of bands as reported below.

Group 1. These bands, detected after deposition of the precursors, are assigned (Table 4.13 and 4.14) on the basis of their resemblance to bands of the isolated precursors, $\text{CF}_2\text{HCF}_2\text{I}$ (Table 4.13) and ozone.⁴⁴ The most diagnostic wavenumber shifts occur for the ozone bands, specifically the ν_3 bands, which exhibit similar shifts to those detected in the reaction of ozone with the other single iodine-containing compounds^{19-21,47} (chapters 3-5). In the mixed-ozone ($^{16}\text{O}_{3-x}^{18}\text{O}_x$) experiments six sets of bands were detected (Table 4.14) for the ν_3 band, indicating that six different isotopomers of ozone (e.g. 16-16-16, 16-16-18 etc.) were present. Near-infrared photolysis ($\lambda > 650$ nm) of matrices containing these group 1 bands produced the group 2 bands.

Group 2. These group 2 bands were formed after near-infrared photolysis. Visible photolysis ($\lambda > 410$ nm) increased the band intensities by 20 %, but UV-vis ($\lambda > 350$ nm) irradiation destroyed them. These bands (Table 4.15) arise as a medium-weak band at 1187.4 cm^{-1} (^{18}O isotopomers at 1175.4 , 1172.0 and 1168.1 cm^{-1}) assigned to a perturbed CF stretch, weak bands at 908.4 and 903.3 cm^{-1} (^{18}O at 908.6 , 903.7 and 850.5 cm^{-1}) assigned to stretches of the CF_2I unit, and a quartet of weak bands at 739.5 , 734.4 , 727.6 and 722.3 cm^{-1} (^{18}O at 691.4 and 680.6 cm^{-1}) assigned to I-O stretches (Fig. 4.6), based on the ^{18}O -shifts of 36.2 and 41.7 cm^{-1} between the ^{16}O bands at 727.6 and 722.3 cm^{-1} and the ^{18}O bands at 691.4 and 680.6 cm^{-1} . Unfortunately, no ^{18}O bands were detected that correspond to the two bands at 739.5 and 734.4 cm^{-1} . The weak bands at 562.8 and 534.4 cm^{-1} are assigned to a CF bend and a perturbed C-I stretch, respectively.

Group 3. These bands were formed after UV-vis irradiation and Pyrex- and quartz-filtered irradiation doubled their intensities after each photolysis cycle. These

bands (Table 4.16) are assigned as follows: strong bands at 1942.0, 1938.5 (^{18}O at 1906.8 cm^{-1}) and 1909.0 cm^{-1} (^{18}O at 1874.8 cm^{-1}) and medium-weak (Fig. 4.7) bands at 1888.3 and 1867.3 cm^{-1} (1861.7 cm^{-1}) are assigned to carbonyl stretches, based on their ^{18}O -shifts of c. 35 cm^{-1} . A medium band at 1329.1 cm^{-1} (^{18}O at 1329.3 cm^{-1}) is assigned to the antisymmetric stretch of the HCF_2 unit. The quintet of medium-weak, medium and strong bands at 1270.2, 1265.3, 1258.3, 1250.5 and 1246.5 cm^{-1} (^{18}O at 1269.9, 1265.5, 1249.9 and 1245.6 cm^{-1}) are assigned to a stretch of the HCF_2 unit. The medium-strong and medium bands at 1079.0 and 1064.2 cm^{-1} (^{18}O at 1078.4 and 1063.9 cm^{-1}) are assigned to the C-F' stretch of the fluorine attached of the carbonyl unit, $-\text{COF}'$. The medium band at 969.1 cm^{-1} is assigned to a HCF bend, and the weak pair of bands at 856.8 and 849.7 cm^{-1} are assigned to C-C stretches. Another pair of medium bands at 770.9 and 764.3 cm^{-1} (^{18}O at 767.1 and 760.0 cm^{-1}) are assigned to the OCF' bend, and the medium-weak pair of bands at 633.0 and 625.4 cm^{-1} are assigned to the HCF_2 bend. Finally a very weak band at 606.3 cm^{-1} detected in the ^{18}O experiments, is attributed to iodine monofluoride, IF.

Warming the matrix caused some bands to decrease in intensities while others, assigned to the same mode, are unaffected or increased in intensity slightly. The largest effect was detected for the carbonyl stretch for which warming reduced the intensities of the bands between 1942.0 and 1909.0 cm^{-1} by c. 20 %. Bands at 764.3 and 625.4 cm^{-1} assigned to the OCF' bend and HCF_2 bend, respectively, were also reduced slightly in intensities. Since both of these bands are members of a doublet of bands, and the other partner remained unchanged on warming (i.e. the bands at 770.9 and 633.0 cm^{-1}) there is evidence for the presence of two carbonyl...IF complexes (3a and 3b) differing by some interaction, most probably the bonding arrangement between the C=O bond of the carbonyl and IF.

4.4.2 DISCUSSION

The bands detected above are discussed below in terms of the groups 1-3. **Group 1.**

These bands are assigned (Table 4.13 and 4.14) to the complex, $\text{CF}_2\text{HCF}_2\text{I}\dots\text{O}_3$ formed after co-deposition of the precursors in argon. Like those ozone complexes detected previously^{19-21,47} (chapters 3-5) near-infrared photolysis causes the transfer of an oxygen atom from ozone to the iodine atom of the iodinated alkane to form the group 2 species, via a charge-transfer type process.

Group 2. The group 2 bands (Table 4.15) are assigned to a C-F stretch, a stretch of a CF_2I unit, a C-I stretch and a C-F bend similar in wavenumber to bands detected for the precursor, 1,1,2,2-tetrafluoroiodoethane. Additionally, bands attributable to I-O stretches are detected, and thus the assignment of the group 2 bands to the species iodoso-1,1,2,2-tetrafluoroethane, $\text{CF}_2\text{HCF}_2\text{IO}$, is made. The wavenumbers of these I-O stretches are in good agreement with the ν_{IO} stretches of the other hydrated and fluorinated iodoso-species (between approx. 714 and 740 cm^{-1}) detected previously^{20,21,47} (chapter 3-5), a comparison of which shall be made in chapter 5.

Group 3. These group 3 bands were first detected after UV-vis photolysis; photolysis at this wavelength destroyed the group 2 bands. These group 3 bands (Table 4.16) are assigned using $\text{CF}_3\text{COF}^{82}$ and $\text{CF}_3\text{COH}^{86}$ as guides, i.e. the detection of bands attributable to either the -COH or -COF unit should be diagnostic of the carbonyl species present. The bands between 1942.0 and 1867.3 cm^{-1} (^{18}O between 1906.8 and 1861.7 cm^{-1}) are assigned to the $\nu_{\text{C=O}}$ of $\text{CF}_3\text{COF}^{82}$ (1899 cm^{-1}) rather than to that of $\text{CF}_3\text{COH}^{86}$ (1788 cm^{-1}). In addition, the bands at 1079.0 and 1064.2 cm^{-1} are assigned to the $\nu_{\text{CF}'}$ and those at 770.9 and 764.3 cm^{-1} to the $\delta_{\text{OCF}'}$; this provides further evidence for a -COF' unit. No bands were detected that could be assigned to any C-H' bends. By examination of the bands detected and comparison of these with those of carbonyls having a -COF unit, it is clear that the species must be CF_2HCOF , 1,1,2-trifluoroethanal. In addition a very weak band at 606.3 cm^{-1} detected in the $^{18}\text{O}_3$ experiments, provides tentative evidence for the presence of IF, and hence the group 3 species is most likely the complex $\text{CF}_2\text{HCOF}\dots\text{IF}$. The wavenumber shifts of the $\nu_{\text{C=O}}$ bands are in good agreement with those of other carbonyl...IF complexes.

Warming the matrix provides information as to the geometry of the $\text{CF}_2\text{HCOF}\dots\text{IF}$ complex. After warming, many bands are reduced in intensity, the bands between 1942.0 and 1909.0 cm^{-1} ($\nu_{\text{C=O}}$) being reduced by 20 %, as are those at 764.3 and 625.4 cm^{-1} assigned to the OCF' bend and HCF_2 bend, respectively. Since for each of these modes additional bands were detected which remained unchanged after warming, there is evidence that the complex exists in two geometries distinguished by their thermal stabilities. Comparison with earlier experiments suggests that those bands that reduced in intensity after the sample was warmed can be attributed to a complex in which the IF and C=O bond of the carbonyl are parallel and have a molecular-pair type bond (species 3a), while those that are unchanged or increased in intensities be attributed to a complex in which the I atom of IF and the O atom of the carbonyl are attached in a head-to-tail type bond (3b). For both geometries of the complex the effect of IF on the wavenumbers of the carbonyl stretching bands can be compared with that of IF on other carbonyls reported previously; these comparisons are made in section 4.6 below. For these complexes, $\nu_{\text{C=O}}$ bands are detected that are shifted both to higher and to lower wavenumber from the $\nu_{\text{C=O}}$ band of the isolated carbonyl. Those which are red-shifted are assigned to the head-to-tail (3b) arrangement, while those blue-shifted are assigned to the molecular-pair complex (3a). The wavenumber shifts of the red- and blue-shifted bands are in very good agreement with those ^{of} other IF complexes (see section 4.6 for complete comparison), and this similarity serves to further confirm the presence of IF.

Photolysis of matrices containing the precursors $\text{CF}_2\text{HCF}_2\text{I}$ and O_3 has been shown to produce $\text{CF}_2\text{HCF}_2\text{IO}$ and the complex $\text{CF}_2\text{HCOF}\dots\text{IF}$. The bands assigned to the latter complex have been shown to increase at the expense of those assigned to the former, the iodoso species, providing evidence for a step-wise reaction path in which the C-I-O unit of $\text{CF}_2\text{HCF}_2\text{IO}$ rearranges to form a C-O-I unit, and subsequently a carbonyl C=O group. In this study no bands were detected that could be attributed to hypoiodo-type species, e.g. FOI, HOI, or $\text{CF}_2\text{HCF}_2\text{OI}$. However, detection of the final carbonyl complex confirms the interconversion expected (see section 4.7 for further discussion).

4.5 1,1,1,2-TETRAFLUOROiodoethane, CF₃CFHI

The mechanism of the photochemical reaction of ozone with iodine-containing compounds, described in the preceding chapters, has been elucidated for species having the backbone structures X-CH₂I and X-CF₂I. In this chapter 1,1,1,2-tetrafluoroiodoethane, having a backbone structure X-CFHI which is intermediate between those of X-CH₂I and X-CF₂I studied previously, is treated with ozone. This precursor has both a hydrogen and a fluorine atom on the α -carbon and, based on the previous reactions, either CF₃COF or CF₃COH is expected to be formed. Whichever carbonyl forms, it is expected to form a complex with the remainder of the precursor and hence either CF₃COF...HI or CF₃COH...IF; the wavenumbers of the bands assigned to these can be compared with those of other carbonyl...XI (where X = H or F) complexes. The photochemical reaction of CF₃CFHI with ozone can be compared with those of other iodine-containing compounds having a perfluoromethyl X group (CF₃), i.e. CF₃-CF₂I and CF₃-CH₂I.

4.5.1 RESULTS

The spectra of argon matrices containing 1,1,1,2-tetrafluoroiodoethane (CF₃CFHI/Ar = 1:600) were recorded and the bands detected are assigned (Table 4.17) using the previously studied polyfluoroiodoalkanes (sections 4.2-4.4) as guides. Ultraviolet photolysis of CF₃CFHI isolated in argon produced no new detectable bands.

1,1,1,2-Tetrafluoroiodoethane and ozone in argon

The spectra recorded after co-deposition of 1,1,1,2-tetrafluoroiodoethane (CF₃CFHI/Ar = 1:200) and ozone (O₃/Ar = 1:400) in argon exhibited a number of bands. Subsequent wavelength- and time-dependent photolysis and warming of the

matrices produced various bands which were detected and are grouped (1-5) below.

Group 1. Group 1 bands are detected after co-deposition of 1,1,1,2-tetrafluoroiodoethane and ozone in argon, and they resemble the bands assigned to the precursors, CF_3CFHI (Table 4.17) and ozone⁴⁴ (Table 4.18) except for minor perturbations. As with the earlier ozone complexes, the bands assigned to ozone exhibited the largest perturbations, and in the mixed-ozone experiments bands were detected for the six isotopomer variants of ozone. Again, like the other ozone complexes detected in these studies, efficient photolysis occurs with near-infrared radiation ($\lambda > 650$ nm) to form the group 2 bands.

Group 2. This group of bands was formed after near-infrared photolysis of an argon matrix containing the group 1 bands, various visible photolysis cycles ($\lambda > 550$ nm and $\lambda > 410$ nm) increased the band intensities, while shorter wavelength UV-vis ($\lambda > 350$ nm) irradiation destroyed the bands. The bands detected (Table 4.19) are assigned as follows: the medium-weak band at 1262.7 cm^{-1} (^{18}O -shift $< 0.7\text{ cm}^{-1}$) is assigned to a CF_3 stretch. In the mixed-ozone experiment, weak and medium bands at 1211.2 and 1206.3 cm^{-1} (^{18}O isotopomer at 1205.7 cm^{-1}) appeared as shoulders on existing precursor bands and are assigned to perturbed C-F stretches of the -CFHI unit. A very weak, broad band at 810.7 cm^{-1} is assigned to a C-C stretch. Weak bands at 732.0 and 726.0 cm^{-1} (^{18}O at 694.6 cm^{-1}) are assigned to I-O stretches (Fig. 4.8), this being confirmed by the ^{18}O -shift of 37.4 cm^{-1} for the ^{16}O band at 732.0 cm^{-1} . No definite assignments are made for the weak bands at 676.1 and 675.0 cm^{-1} detected in the mixed-ozone and $^{18}\text{O}_3$ experiments, respectively.

Group 3. These bands were formed very weakly after UV-vis ($\lambda > 350$ nm) photolysis of the matrix. The low intensities of these bands prevented any changes in band intensities from being detected after subsequent Pyrex- and quartz-filtered photolysis. The bands detected are assigned (Table 4.20 and Fig. 4.8) using the assignment regime established in chapter 3, e.g. $\nu_a\text{IO}_2 - \nu_s\text{IO}_2 \sim 34\text{ cm}^{-1}$ whilst the ^{18}O -shifts $\sim 40\text{ cm}^{-1}$. The very weak band at 815.8 cm^{-1} and weak bands at 810.2 and 805.1 cm^{-1} are assigned to the antisymmetric stretch of an I^{16}O_2 unit. In the mixed-

ozone experiments, very weak bands at 802.0 and 782.8 cm^{-1} (^{18}O at 801.1 cm^{-1}) are assigned to the antisymmetric stretch of the $\text{I}^{16}\text{O}^{18}\text{O}$ unit. Also detected in the mixed-ozone experiment are very weak bands at 757.5 and 751.7 cm^{-1} (^{18}O at 757.4 and 751.5 cm^{-1}) assigned to the symmetric stretch of the mixed isotopic $\text{I}^{16}\text{O}^{18}\text{O}$ unit. Other very weak bands at 771.1 and 768.0 cm^{-1} are assigned to the $\nu_s\text{I}^{16}\text{O}_2$ and $\nu_a\text{I}^{18}\text{O}_2$ stretches, respectively. Finally, bands at 747.2 and 742.1 cm^{-1} (^{18}O at 746.2, 741.6 and 735.7 cm^{-1}) are assigned to the symmetric I^{18}O_2 stretch. The assignment of some of these bands to the mixed-oxygen isotopomer unit, $\text{I}^{16}\text{O}^{18}\text{O}$, confirms the presence of two oxygen atoms.

Group 4. This group of bands was formed after UV-vis photolysis, and increased by c. 40 % and 20 % after subsequent Pyrex- and quartz-filtered photolysis, respectively. The bands detected are assigned (Table 4.21) as follows: medium, medium-strong and weak bands at 1894.2, 1888.5 and 1877.2 cm^{-1} respectively, are assigned to carbonyl stretches (Fig. 4.9), on account of the ^{18}O -shift of 35.3 cm^{-1} between the most intense ^{16}O band (1888.5 cm^{-1}) and the ^{18}O band at 1853.0 cm^{-1} . A weak band at 1336.3 cm^{-1} (^{18}O -shift of 2.8 cm^{-1}) is assigned to a CF_3 stretch. The medium band at 1247.3 cm^{-1} (^{18}O at 1259.4 and 1246.9 cm^{-1}) is assigned to another CF_3 stretch. The medium-weak and weak bands at 1092.6 and 1087.2 cm^{-1} respectively, (^{18}O at 1093.5, 1091.5 and 1089.2 cm^{-1}) are assigned to the C-F' stretch of the fluorine atom attached to the carbonyl unit, -COF'. Weak bands at 890.9 and 879.5 cm^{-1} (^{18}O at 878.4 cm^{-1}), detected in the mixed-ozone experiment, are assigned to C-C stretches. A medium-weak band at 690.5 cm^{-1} is assigned to a CF_3 bend, and a weak band at 603.6 cm^{-1} (^{18}O at 592.5 and 582.9 cm^{-1}) can be assigned to either a vibration described by the mixing of an OCF' bend and a CF_3 bend, or alternatively to the mixed halide, IF. A very weak band at 526.4 cm^{-1} is assigned to a FCF bend.

A number of combination and overtone bands are also detected, a weak band at 1409.2 cm^{-1} (^{18}O -shift of 0.6 cm^{-1}) being assigned to the first overtone of a CF_3 bend. A strong band at 1286.9 cm^{-1} is assigned to the combination of a C-C stretch and a FCF bend. A strong band at 1185.1 cm^{-1} and its weak shoulder at 1177.4 cm^{-1} (^{18}O at 1184.1 and 1178.3 cm^{-1}) are assigned to the combination of an OCF' bend and

an out-of-phase wag. A strong band at 1061.5 cm^{-1} (^{18}O at 1069.5 and 1054.1 cm^{-1}) is assigned to the combination of a CF_3 bend and an in-phase rock. Weak and very weak bands at 676.1 and 635.2 cm^{-1} are assigned to combinations of the in-phase and out-of-phase wags.

Group 5. The group 5 bands formed under similar photolytic conditions to the group 4 bands, except that the former have much the weaker intensities. The only distinguishable bands (Table 4.21 and Fig. 4.9) occurred in the carbonyl stretching region at 1826.0 , 1815.5 and 1792.0 cm^{-1} (^{18}O isotopomers at 1785.3 , 1778.7 and 1774.6 cm^{-1}). No other bands were detected for this group, though it is likely that many of these bands overlap with group 4 bands, specifically those assigned to CF_3 stretches or bends. Other bands (e.g. ν_{CH} and δ_{COH}) could not be detected, presumably due to the low concentrations of the group 5 species in the matrix.

4.5.2 DISCUSSION

The bands detected are discussed below in terms of the groups (1-5). **Group 1.** The group 1 bands, formed after co-deposition of the precursors resemble closely those assigned to the isolated precursors (Table 4.17 and 4.18); based on this wavenumber similarity and the photochemical behaviour, this group of bands is assigned to the complex, $\text{CF}_3\text{CFHI}\dots\text{O}_3$. Like the other ozone complexes, near-infrared photolysis causes an oxygen atom to be transferred from ozone to 1,1,1,2-tetrafluoroiodoethane, via a charge-transfer mechanism.

Groups 2 and 3. The group 2 bands, formed after near-infrared ($\lambda > 650\text{ nm}$) photolysis, exhibited bands assigned to a CF_3 stretch, a CHFI unit, a C-C stretch, and most diagnostically to I-O stretches (Table 4.19), and is assigned to iodoso-1,1,1,2-tetrafluoroethane, CF_3CFHIO . A comparison of the wavenumbers of the I-O stretch of this and other iodoso-species is made at the end of chapter 5.

The very weak group 3 bands (Table 4.20) are assigned to antisymmetric and

symmetric stretches of the $I^{16}O_2$, $I^{18}O_2$ and $I^{16}O^{18}O$ units based on the wavenumbers of the bands detected; as discussed above. Thus the presence of these IO_2 units suggests assignment of these bands to iodyl-1,1,1,2-tetrafluoroethane, CF_3CFHIO_2 .

Groups 4 and 5. Both the group 4 and 5 bands were formed after UV-vis irradiation of the matrix, the group 4 bands being the more intense. The bands detected (Table 4.21) are attributed, by comparison to those of CF_3COF ⁸² and CF_3COH ,⁸⁶ to the complexes $CF_3COF...HI$ (group 4) and $CF_3COH...IF$ (group 5). The most diagnostic bands for these complexes are those assigned to the $\nu_{C=O}$ stretch and a full comparison with those of the other carbonyl...XI (X = F or H) species is carried out below (section 4.6).

4.6 POLYFLUOROETHANAL...XI COMPLEXES (X = F or H)

The reaction of oxygen atoms with the four polyfluoroiodoethanes, studied in this chapter, has produced a number of polyfluorocarbonyls complexed with either HI or IF. Examination of the carbonyl bands (Table 4.22) of these carbonyl...Lewis acid complexes provides us with two pieces of information, first the wavenumber enables us to distinguish the environment of the carbonyl band, i.e. the Y species in the unit X-COY, and thus in this study we have distinguished between possible carbonyls having either the X-COH or X-COF units. This is very useful, since positive identification of the final products has enabled us to distinguish between possible competing mechanisms for their production. This method was of particular use in identifying the carbonyl formed after the reaction of ozone with 1,1,2,2-tetrafluoroiodoethane; the $\nu_{C=O}$ bands of CF_2HCOF resembled those of CF_3COF ⁸² (c. 1899 cm^{-1}) rather than those of CF_3COH ⁸⁶ (c. 1788 cm^{-1}).

Second, the wavenumber shift, ($\Delta = \nu_{\text{isolated}} - \nu_{\text{complexed}}$), of the complexed bands from those of the isolated carbonyl, can be used to distinguish between the complexes perturbed by IF or HI and, more importantly to supply information as to the geometry

and nature of the bonding between the carbonyl and the Lewis acid. For those cases in which HI is the Lewis acid, the $\nu_{\text{C=O}}$ bands are shifted to lower wavenumber e.g. those of $\text{CF}_3\text{COF}\dots\text{HI}$ are shifted by 4.8, 10.5 and 21.8 cm^{-1} and those of $\text{CF}_3\text{COH}\dots\text{HI}$ by 3.5, 10.2 and 22.2 cm^{-1} . For these complexes, the least shifted bands ($\Delta < 5 \text{ cm}^{-1}$) are assigned to a weak complex in which the HI has very little effect on the carbonyl. The medium shifted bands ($\Delta \sim 10 \text{ cm}^{-1}$) are attributed to a molecular pair complex between HI and the carbonyl (i.e. the H-I and the C=O bonds are parallel). Finally, the most perturbed bands ($\Delta > 20 \text{ cm}^{-1}$) are assigned to a complex involving a hydrogen bond between the H atom of hydrogen iodide and the oxygen atom of the carbonyl bond. For further comparison these wavenumber shifts can be compared to those detected previously for the $\nu_{\text{C=O}}$ bands of the carbonyl...HI complexes: $\text{COH}_2\dots\text{HI}$ ($\Delta\nu = 6.1$ and 12.4 cm^{-1})²⁰ (16 cm^{-1}),⁶¹ $\text{CH}_3\text{COH}\dots\text{HI}$ (9.0, 16.3, 19.0 and 22.6 cm^{-1})^{47,a} and $(\text{CH}_3)_2\text{CO}$ (8, 12 and 17 cm^{-1})⁶⁵ (2.0, 10.3, 16.3 and 22.9 cm^{-1})^a (where a = chapter 3).

For the complexes perturbed by IF, the $\nu_{\text{C=O}}$ bands are shifted both to higher and to lower wavenumbers, thus for the complex $\text{CF}_3\text{COF}\dots\text{IF}$ bands are blue-shifted by 39.4, 37.4, 34.9, 10.9, 8.7, 6.9, and 2.2 cm^{-1} and red-shifted by 12.7 cm^{-1} while for $\text{CF}_2\text{HCOF}\dots\text{IF}$ bands are blue-shifted by 43.0, 39.5 and 10.0 cm^{-1} and red-shifted by 10.7 and 31.7 cm^{-1} . For $\text{CF}_3\text{COH}\dots\text{IF}$ the bands are blue-shifted by 38.0, 27.5 and 4.0 cm^{-1} . First, the blue-shifted bands, can be split into three groups: (i) Δ between 30-40 cm^{-1} , (ii) $\Delta \sim 10 \text{ cm}^{-1}$ and (iii) $\Delta < 5 \text{ cm}^{-1}$. Whilst the red-shifted bands have shifts, Δ of approx. 10 cm^{-1} . Thus for the carbonyl...IF complexes there are three types of complex: two blue-shifted and one red-shifted (note: the bands blue-shifted by less than 5 cm^{-1} involve only a very weak complex). The bands with the largest blue-shift ($\Delta > 30 \text{ cm}^{-1}$) are assigned to a complex with the I-F bond parallel with the carbonyl bond (molecular pair complex), and it seems likely that the Lewis acid strengthens the carbonyl bond in some manner, probably via the fluorine atom donating electron density to the carbonyl bond. The other blue-shifted bands ($\Delta \sim 10 \text{ cm}^{-1}$) are assigned to a different geometry in which the interaction between the I-F bond and the carbonyl is weaker due to a smaller orbital overlap. Finally, the red-shifted bands are assigned

to a complex involving the head-tail, dipole-dipole interaction between the iodine of IF and oxygen atoms of the carbonyl. These red shifts, and especially the band shifted by 31.7 cm^{-1} detected for $\text{CF}_2\text{HCOF}\dots\text{IF}$, indicates that the IF complexes are at least as strong as their hydrogen iodide counterparts.

4.7 PHOTOCHEMICAL INTERCONVERSION

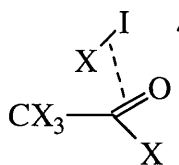
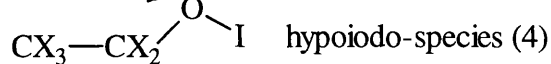
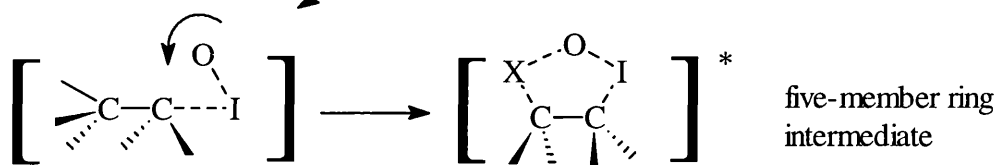
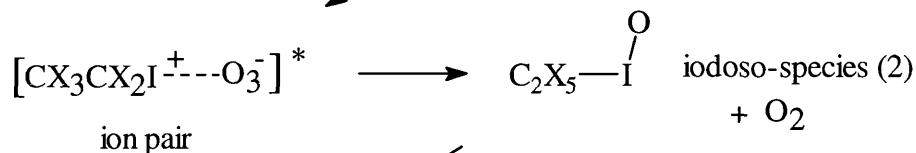
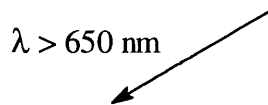
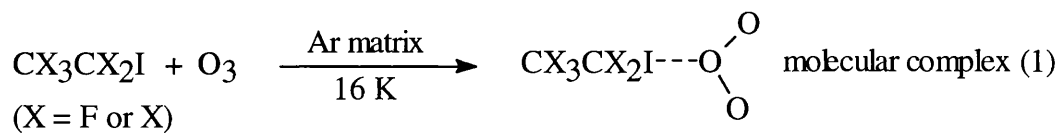
In chapter 3 a mechanism was proposed that accounts for the products of the reaction of ozone with iodoethane in an argon matrix⁴⁷ and in the gas phase.⁵⁶ One intermediate in the above mechanism, the five-membered ring intermediate, was not detected directly in either the matrix or the gas phase experiments and for this reason polyfluoroiodoethanes were studied in this chapter in order to further clarify the mechanism. In general, the mechanism was determined by grouping the detected bands by their wavelength-dependent behaviour. The bands in each group were subsequently assigned to species, and then these species were studied to determine the geometric changes (i.e. bond length/angles etc.) that would lead from one species to another. Thus by comparing the products detected in the reaction of ozone with these polyfluoroiodoethanes with those of iodoethane⁴⁷ (chapter 3) we have identified the following photochemical mechanism (see Summary 4). The first species detected after deposition is a weak complex between ozone and the iodine-containing precursor, e.g. $\text{C}_2\text{X}_3\text{I}\dots\text{O}_3$ ($\text{X} = \text{F}$ or H). The formation of this complex alters the photochemistry of ozone sufficiently, allowing the effective transfer of an O atom to the iodine-containing precursor after near-infrared photolysis ($\lambda > 650\text{ nm}$). This transfer of an oxygen atom occurs via a charge-transfer complex, and forms the second species, an iodoso-species ($\text{C}_2\text{X}_3\text{IO}$) having a C-I-O bond. These iodoso-species are stable to visible ($\lambda > 410\text{ nm}$) irradiation, but UV-vis photolysis ($\lambda > 350\text{ nm}$) destroys them, and forms easily identifiable carbonyl complexes. The mechanism of interconversion of these two species is of interest, since in the gas phase reaction of ozone with iodoethane⁵⁶ a five-membered ring intermediate was proposed which gave rise to HOI.

In these matrix reactions of ozone with these polyfluoroiodoethanes some hypiodo-species were detected, however not in the quantities seen with iodoethane (chapter 3). The aim in these studies was to detect bands that would provide evidence for the presence of a five-membered ring intermediate and hence species such as FOI and HOI as well as C_2X_3OI . The main doubt centred on whether the C-I-O bond rearranged to form a five-membered ring, or whether the re-arrangement was centred around the carbon atom containing the C-I bond. In fact the final rearrangement is believed to be a combination of both, in which the C-I-O rotates to form a weak five-membered ring intermediate; if the β -carbon has a H atoms attached (as with iodoethane) then HOI is detected, whereas if the β -carbon has F atoms then FOI is not detected due to the stronger C-F bond. In low temperature matrices the five-membered ring intermediate rotates further to bring the O atom close to the C atom (on which the I atom is attached) forming a new C-O bond and the hypiodo-species, Z-C-O-I. These hypiodo-species dissociate further to form the carbonyl complexes detected. In the gas phase the five-membered ring dissociates into the HOI and ethene (from iodoethane⁵⁶ and ozone), the difference with the matrix experiments being due to the solid nature of the matrix.

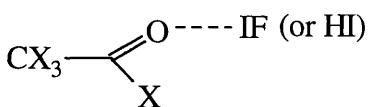
Fortunately, in these studies the detection of the final carbonyl proved very useful since this helped us to determine the mechanism without having to detect either the five-membered ring intermediate or the hypiodo-species. In the solid oxygen matrices, similar carbonyl...Lewis acid complexes were detected which suggests that the oxygen atoms produced are able to insert into the C-I bond in the same manner as those produced in the ozone experiments. The lack of intermediate products in these solid oxygen matrix experiments is accounted for by the shorter wavelength irradiation required to generate O atoms, which effectively destroys any intermediates which form.

A final group of species was detected after photolysis in the visible; these species resemble those detected in chapter 3 and are assigned to iodyl-species, $C_2X_3IO_2$. The low yields in these experiments was matched by the low yields reported for the reaction of ozone with trifluoroiodomethane.²¹

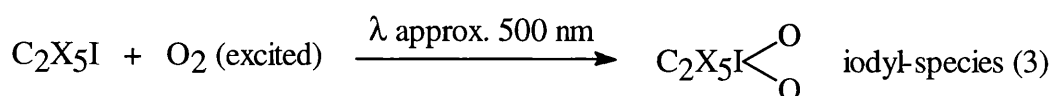
SUMMARY 4



molecular pair complex (5a)



dipole-dipole complex (5b) with IF
(or hydrogen bonded complex with HI)



4.8 CONCLUDING REMARKS

In studying this range of polyfluoroiodoalkanes many intermediates with various iodine-oxygen bonds have been detected as well as a number of complexes, thus adding greatly to the number of species of this type known.^{19-21,47} A mechanism (Summary 4) has been proposed to account for the species detected and to support the results of the gas phase⁶⁰ reactions.

Table 4.1. Infrared bands /cm⁻¹ detected for pentafluoroiodoethane in a number of matrices after deposition at 14 K.

Ar	O ₂	¹⁶ O ₃ /Ar	¹⁸ O ₃ /Ar	assignment
1335.2w	1334.2mw	1335.2m	1335.2m	vCF ₃ + ρCF ₂ I
1324.1vs	1322.1s	1323.1vs	1322.4vs	vCF ₃
1309.6w	1310.1mw	1310.1m	1309.6m	
1298.5w	1298.0mw	1298.5mw	1299.0mw	vCF ₃ + τ
		1289.3mw	1288.9m	
1286.9mw	1286.0ms	1287.4s	1286.9m	vCF ₂ I + ρCF ₂
1281.6w		1282.6ms	1283.1m	
1251.7w	1251.3mw	1251.7m	1251.7m	vCF ₃
		1231.5sh	1234.9s	
			1230.0s	
1224.3vs	1219.0vs	1213.2vs	1212.2vs	
1198.2mw	1196.8m	1198.2ms	1197.7m	vCF ₂ I + δ _{CCl}
1182.3mw	1188.1mw	1181.8s	1181.8s	vCF ₂ + τ
	1181.3m		1177.5m	
1155.5vs	1153.6vs	1154.5vs	1167.4mw	vCF ₂
1141.8mw	1142.8br,vs	1141.3vs	1152.9vs	
			1140.8s	
	1138.4vs	1137.0s	1136.0s	
1105.6vs	1102.5vs	1104.6vs	1103.2vs	vCF ₂
		1097.9vs		
		1097.0s		
1083.5w	1082.5mw	1083.5m	1083.0m	vCF ₂ I + ρCF ₂ I
1064.2w	1064.6w	1064.6mw	1064.6mw	
924.3vs	915.7vs	923.4sh		vCF ₂ I
919.5vs	907.0w	916.4vs	917.1vs	
897.3w	898.3m	897.3m	897.1m	
745.4 vs	745.0s	745.9vs	745.4s	v _{CC}
	740.6m		737.7w	
729.1w	730.0m	729.1m	729.1m	2vCF ₂
623.0m	622.5s	624.4s	624.4s	δCF ₃
590.7mw	590.7mw	591.1m	591.1m	
543.2s	543.0s	543.9br,vs	544.4s	

Table 4.2. Infrared bands /cm⁻¹ attributed to the ozone moiety in the complex, C₂F₅I...O₃, formed after co-deposition of pentafluoroiodoethane and ¹⁶O_{3-x}¹⁸O_x in an argon matrix at 14 K.

ν_1	ν_2	ν_3	$\nu_1 + \nu_3$	assignment
	703.9m	1039.5vs 1033.8vs 1032.0w	2140.3w 2138.5vw 2108.6mw 2100.4mw	16-16-16
1091.8mw 1090.4mw 1083.3w		1026.6w 1025.4vs 1022.6vs	2090.1mw 2087.3mw 2077.9w	16-16-18
1068.2vw		1017.4vs 1010.4s	2069.7w 2059.9mw 2057.2mw	18-16-18
1074.4vw		1006.1vs 1000.0s	2049.6mw 2047.1mw 2038.0w	16-18-16
1064.0sh,w 1061.6mw		991.1vs 988.7vs	2027.3mw 2024.6mw 2016.1w	18-18-16
1043.0w	667.8mw	982.1vs 976.9vs 962.9w	2006.4vw 1996.0mw 1985.0w	18-18-18

Table 4.3. Infrared bands /cm⁻¹ detected for iodosopentafluoroiodoethane, C₂F₅IO (group 2) detected after photolysis ($\lambda > 650$ nm) of pentafluoroiodoethane and ozone in argon at 14 K.

¹⁶ O ₃ /Ar	¹⁶ O _{3-x} ¹⁸ O _x /Ar	¹⁸ O ₃ /Ar	assignment
1090.7s		1089.2m	vCF ₂
902.6	902.2w		vCF ₂ I
897.3w	896.4w		
867.0vw			vCF ₂ I + δ CF ₃
845.7w			
738.7w	738.2w ^a	706.9w	v _{IO}
	638.w		δ CF ₃
	635.8w		
	615.5w		
	535.3vw		v _{Cl}
	531.4vw		
	527.2vw		

^a-¹⁸O isotopomer band obscured by that of the ozone precursor at 704 cm⁻¹

Table 4.4. Infrared bands /cm⁻¹ of iodylpentafluoroethane, C₂F₅IO₂ (group 3), detected after UV-vis (λ > 350 nm) photolysis of pentafluoroiodoethane and ozone in argon.

¹⁶ O ₃ /Ar	¹⁶ O _{3-x} ¹⁸ O _x /Ar	assignment
812.1w	818.7vw 807.6vw 799.9vw	v _a I ¹⁶ O ₂
a	768.6mw 764.7mw 759.2mw	v _a I ¹⁸ O ₂

a - obscured by OCF' bend of product group 5.

Table 4.5. Infrared bands /cm⁻¹ of hypiodopentafluoroethane, C₂F₅OI (group 4), detected after UV-vis (λ > 350 nm) photolysis of pentafluoroiodoethane and ozone in argon.

¹⁶ O ₃ /Ar	¹⁶ O _{3-x} ¹⁸ O _x /Ar	¹⁸ O ₃ /Ar	assignment
968.7m		955.7mw	v _{CO}
961.5m		953.3mw	
583.9w	584.4w 581.0w 577.4w	578.6mw	v _{OI}

Table 4.6. Infrared bands /cm⁻¹ of group 5 species, CF₃CFO...IF, detected after UV-vis photolysis ($\lambda > 350$ nm) of pentafluoroiodoethane with ozone in an argon matrix and in a solid oxygen matrix.

O ₂	¹⁶ O ₃ /Ar	¹⁸ O ₃ /Ar	assignment ^a
1935.0vw	1938.4ms 1936.4ms 1933.9ms	1904.7m 1903.4m	$\nu_{C=O}$
1905.1mw 1903.6mw	1909.9ms 1907.7s 1905.9s 1901.2sh,s	1875.7s 1862.8mw 1854.4mw	
1887.7w	1886.3mw 1327.0vs 1286.5s 1282.6s	1850.4sh,w 1276.8m 1275.8m	ν_{CF_3} $\nu_{CC} + \delta_{FCF}$
1251.3mw	1267.2s 1250.8vs	1267.6s 1259.0vs 1240.6s	ν_{CF_3}
1196.8ms	1197.7vs	1197.7s 1192.9s	ν_{FCF}
1180.9s 1173.6ms	1166vs	1181.8s 1177.5s 1167.4m	$\delta_{OCF'} + \omega_{i-ph}$
1100.6vs 1082.5m	1091.2vs 1082.5s 1067.6vs 1063.7m	1089.2s 1083.0s 1068.5s 1064.6s	$\nu_{CF'}$ $\delta_{CF_3} + \rho_{i-ph}$
		819.7w 807.6w	ν_{CC}
771.5w 763.8w	769.6m 762.3mw	768.7w 765.2w 758.9mw	$\delta_{OCF'}$
694.8vw 688.1vw		687.1w	δ_{CF_3}
	644.7w 596.5w	604.7w	$\omega_{i-ph} + \omega_{o-ph}$ δ_{FCF_2} or ν_s IF

^a- subscript i-ph = in-phase, subscript o-ph = out-of-phase.

Table 4.7. Infrared bands /cm⁻¹ detected after deposition of 1,1,1-trifluoroiodoethane in a variety of matrices at 14 K.

Ar	O ₂	¹⁶ O ₃ / Ar	¹⁸ O ₃ /Ar	assignment
3052.3w	3055.6w	3048.3w	3054.1w	v _a CH ₂
2998.9w	2996.7w	2990.0w	2990.0w	v _s CH ₂
1469.6w	1469.2m	1469.7wm	1470.6w	δCH ₂
1424.8ms	1427.2s	1425.3s	1426.3s	
	1404.6w	1408.0w	1406.5vw	
1378.1w	1375.2mw	1376.6w	1381.4vw	(ρ + δ) CH ₂
	1356.4mw	1359.3w	1361.7w	
1349.2w	1345.8mw	1344.3w	1349.1w	
1290br,vs	1291.8vs	1291.3s	1292.2vs	ωCH ₂
1260vs	1262.8vs	1263.3s	1265.2vs	vCF ₃
	1240.2w	1239.7w	1240.4vw	
1214.8s	1214.1s	1214.6s	1215.1s	v _{CF}
	1197.7w	1196.3w	1196.8vw	
1143.1s	1142.3s	1143.2mw	1144.2mw	v _s CF ₃
1131.4m	1131.2s	1131.7m	1132.2m	v _{CF}
1117.2s	1116.2vs	1114.3vs	1118.2vs	v _{CF}
	1093.6wm		1094.5w	
1053.9s	1055.5vs	1054.0s	1058.9s	δCH ₂
			1055.0vs	
842.6m	841.4s	842.4m	846.2w	v _{CC}
			842.8mw	
674.3m	674.1s	674.1m	675.5m	δCF ₃ , v _{CC}
629.2s	628.3s	629.2s	629.7s	δCF ₃
532.1w	534.7w	534.7w	535.2w	δCF ₃
		525.1w		
	515.4w	516.9w	516.9w	v _{Cl}

Table 4.8. Infrared bands /cm⁻¹ attributed to the ozone moiety in the CF₃CH₂I...O₃ complex (group 1), formed after co-deposition of 1,1,1-trifluoroiodoethane and ¹⁶O_{3-x}¹⁸O_x in an argon matrix.

ν_1	ν_2	ν_3	$\nu_1 + \nu_3$	assignment
1106.8m	703.7w	1039.5vs 1033.0s	2127.9w 2110.0mw 2108.1mw 2103.1w	16-16-16
1094.5w 1091.8w 1090.3w	687.6w	1025.6vs	2099.6w 2090.1mw	16-16-18
	675.7m	1016.8s 1010.3m	2087.3mw 2071.7vw	18-16-18
	696.1w 691.0vw	1005.8s 999.8m	2078.9w 2060.3w 2043.7w	16-18-16
	680.5w	991.6s 988.6sh,m 985.6s	2057.4w 2049.9mw 2047.5mw 2027.6mw	18-18-16
	664.4mw	982.1vs 976.3vs	2024.9mw 2017.2vw 2006.7w 1996.5mw 1993.5w 1986.8w	18-18-18

Table 4.9. Infrared bands /cm⁻¹ of the iodoso-1,1,1-trifluoroethane, CF₃CH₂IO (group 2) species detected after photolysis ($\lambda > 650$ nm) of 1,1,1-trifluoroiodoethane and ozone in an argon matrix at 14 K.

¹⁶ O ₃ /Ar	¹⁶ O _{3-x} ¹⁸ O _x /Ar	¹⁸ O ₃ /Ar	assignment
1404.7	1405.5mw	1406.0	δ CH ₂
1282.1m	1283.9m	1284.6m	ω CH ₂
1278.4m	1276.7m	1279.6m	
		1278.6m	
1257.6sh,s	1259.8m	1257.0s	ν CF ₃
	1256.7m	1244.1ms	
		1240.4m	
1199.2s	1199.7m	1198.7mw	ν CF ₃
	1111.2s		
732.4mw	732.5w	695.2w	ν _{IO}
727.1vw	727.6w	688.7vw	
	695.9w		
	687.4w		
	679.7vw		

Table 4.10. Infrared bands /cm⁻¹ of CF₃CH₂IO₂ (group 3), detected after photolysis ($\lambda > 450$ nm) of CF₃CH₂I and ozone in an argon matrix at 14 K.

¹⁶ O ₃ /Ar	¹⁶ O _{3-x} ¹⁸ O _x /Ar	¹⁸ O ₃ /Ar	assignment
815.5w	811.4vw	811.9w	ν_a I ¹⁶ O ₂
809.4w	808.4vw	805.4w	
	806.9vw		
	787.5vw		ν_a I ¹⁶ O ¹⁸ O
	783.3vw		
	781.0vw		
	768.0vw		ν_s I ¹⁸ O ₂
	764.5vw		

Table 4.11. Infrared bands /cm⁻¹ assigned to the group 4 species, hypoiodo-1,1,1-trifluoroethane (CF₃CH₂OI) and hydrogen hypoiodide (HOI).

O ₂	¹⁶ O ₃ /Ar	assignment
3492.3w	3444vw	ν_{OH}
	588.2vw	ν_{OI}
	577.7vw	
	567.4vw	

Table 4.12. Infrared bands /cm⁻¹ of the complex CF₃CHO...HI (group 5), detected after photolysis ($\lambda > 350$ nm) of 1,1,1-trifluoroiodoethane in a number of matrices.

O ₂	¹⁶ O ₃ /Ar	¹⁶ O _{3-x} ¹⁸ O _x /Ar	¹⁸ O ₃ /Ar	assignment
	2997.1w	2880.5vw		ν_{CH}
1772.5mw	1784.5w 1777.8m 1765.8vw	1783.7w 1778.0mw 1764.7vw 1748.0w 1743.9mw 1730.8vw	1748.4w 1743.6mw 1729.1vw	$\nu_{\text{C=O}}$
1384.3mw	1382.9s	1382.8mw 1377.4mw 1301.2ms	1377.2mw 1300.9m	$\delta_{\text{i-p}}\text{CH}$
	1281.1s 1277.3s	1283.9s 1277.0s	1256.6vs	$\nu_{\text{s}}\text{CF}_3$
	1242.1m	1240.4w	1240.4w	$\nu_{\text{CC}} + \delta_{\text{C-C=O}}$
1215.1s	1198.2s 1197.7s 1195.3s	1195.0s	1194.6s	$\nu_{\text{a}}\text{CF}_3$
1177.5m 1168.3m	1170.7s 1167.4sh,ms	1173.2ms 1171.4ms	1173.9vs	$\nu_{\text{a}}\text{CF}_3$
	1079.1w	1079.6w	1077.7vw	$\nu_{\text{CC}} + \rho\text{CF}_3$
991.8w 953.3w	974.5w 958.1mw	958.8w	970.0w 959.1vw	$\delta_{\text{o-o-p}}\text{CH}$
	886.7mw			$2\delta_{\text{C-C=O}}$
	851.3sh 843.3m 836.6sh	851.7vw	833.7w	ν_{CC}
707.4mw	684.6w	742.3w	695.3w 690.5vw 689.0vw	$\delta\text{CF}_3 + \delta_{\text{C-C=O}}$
	598.5vw 542.7w 526.1w			δCF_3

Table 4.13. Infrared bands /cm⁻¹ of 1,1,2,2-tetrafluoroiodoethane, CF₂HCF₂I, in a number of matrices after deposition at 14 K.

Ar	O ₂	¹⁶ O ₃ /Ar	¹⁸ O ₃ /Ar	assignment
		3039.1w		v _{CH}
		2987.7w	2983.0w	
		1413.7w	1414.0w	δ _{CHF}
1375vs	1387.9ms 1374.6s	1388.4wm 1374.7s	1388.7ms 1375.1vs	
1347.2m	1345.9ms 1342.7m 1339.2m	1346.1wm 1336.3w	1346.3mw 1337.1vw	vHCF ₂
1242.8w 1227.9s	1243.4wm 1226.4s 1211.7w	1242.6w 1225.3vs	1244br,w 1226.1s 1213.9sh,w	vCF ₂
1186.1w	1185.8w	1198.7w 1185.9br,w	1198.3vw 1186br,w	vHCF ₂
1140vs	1167.1w 1145br,vs	1163.3mw 1139.1s	1162.3mw 1145br,vs	vHCF ₂ vCF ₂
1123vs	1131.3vs 1122.4br,vs	1124br,vs 1115.0vs	1124br,vs 1114.3vs	
1103.1s	1101.8s	1104.1s	1104.7s 1103.0sh,s	v _{CF}
1049.2s	1076.7wm 1058.3wm 1050.6vs	1078.0w 1059.3w 1049.9s	1059.2w 1050.4vs	δ _{CHF} δCF ₂
	942.5vs 920.4wm	940.7vs 919.0w	940.4vs,br	δHCF ₂
	883.5w 835.5w	840.2w	883.3w 840.6w	vCF ₂ I
810.3vs	809.9s	810.1vs	810.9vs	v _{CC}
658.1m 656.4m 618.7m	656.3m 618.7m	658.7m 656.6m 618.9s	658.2m 656.3sh,m 618.8m	δHCF ₂
592.9s	586.3s 550.1mw		593.9vs 584.5s	δHCF ₂

Table 4.14. Infrared bands /cm⁻¹ assigned to the ozone moiety in the complex, CF₂HCF₂I...O₃ (group 1), formed after co-deposition of 1,1,2,2-tetrafluoroiodoethane and mixed isotopomer ozone (¹⁶O_{3-x}¹⁸O_x) in an argon matrix.

ν_1	ν_2	ν_3	$\nu_1 + \nu_3$	assignment
a	704.7m	1036.6br,vs	2111.2m 2108.3m 2099.6w	16-16-16
	691.4vw	1028.3w 1025.3mw	b	16-16-18
		1017.7w 1016.9w 1011.3w		18-16-18
		1005.9w 998.9w		16-18-16
	680.0vw	991.3mw		18-18-16
1039.6w	664.5m	977.3br,vs	1996.1m 1993.2m	18-18-18

^a- obscured by precursor bands; ^b- too weak to assign with confidence.

Table 4.15. Infrared bands /cm⁻¹ assigned to iodoso-1,1,2,2-tetrafluoroethane, CF₂HCF₂IO (group 2) formed after near-infrared ($\lambda > 650$ nm) irradiation of argon matrices containing CF₂HCF₂I and ozone in argon.

¹⁶ O ₃ /Ar	¹⁸ O ₃ /Ar	assignment
1187.4mw	1175.4w 1172.0w 1168.1w	ν_{CF}
908.4w 903.3w	908.6w 903.7w 850.5w	ν_{CF_2I}
739.5w 734.4w		ν_{IO}
727.6w ^a 722.3w ^a	691.4vw 680.6vw	
562.8w 534.4w		δ_{CF} ν_{CI}

^a- these are the most intense bands in this region.

Table 4.16. Infrared bands /cm⁻¹ assigned to the product, CF₂HCFO...IF (group 3) detected after 350 nm irradiation of an argon matrix containing the precursors 1,1,2,2-tetrafluoroiodoethane and ozone in argon.

¹⁶ O ₃ /Ar	¹⁸ O ₃ /Ar	assignment
1942.0s	1906.8m	v _{C=O}
1938.5s		
1909.0vs	1874.8s	
1888.3mw		
1867.3mw	1861.7w	
1329.1m	1329.3m	v _a HCF ₂
1270.2mw	1269.9sh,mw	v _s HCF ₂
1265.3mw	1265.5sh,mw	
1258.3m	1249.9m	
1250.5s	1245.6m	
1246.5ms		
	1178.4mw	δ _{OCF'} + ω
	1167.1w	
1079.0ms	1078.8m	v _{CF'}
1064.2m	1063.9w,br	
969.1m		δ _{HCF}
856.8mw		v _{CC}
849.7mw		
770.9m	767.1mw	δ _{OCF'}
764.3mw	760.0mw	
633.0mw	632.4w	δHCF ₂
625.4mw	625.5w	
	606.3vw	v _s IF

Table 4.17. Infrared bands /cm⁻¹ of 1,1,1,2-tetrafluoroiodoethane in a number of matrices after deposition at 14 K.

Ar	¹⁶ O ₃ /Ar	¹⁶ O _{3-x} ¹⁸ O _x /Ar	¹⁸ O ₃ /Ar	assignment
3013.2w	3015.8w		3014.1w 2879w	v _{CH}
1430.5mw	1430.2mw		1430.7w	δ _{CHF}
1368.3sh,s 1362.6vs 1353.5s	1360.3vs 1353.9s	1368.4m 1362.0s	1368.3s 1361.9vs 1353.7sh,s	vCF ₃
1294.7w 1286.8s 1274.9vs 1262.5m	1286.1ms 1273.0s 1263.1w	1287.5s 1277.2vs 1274.9vs 1262.3m	1286.7vs 1275br,vs 1262.3sh,w	vCF ₃
1250.6m 1249sh,m 1244.0mw 1235.0vs	1249.6mw 1244.2w 1234.2vs	1249.9w 1244.8w 1236.0ms 1206.1sh,m	1249.9mw 1235.6s	v _a CF ₃
1197.9br,vs 1164.3mw 1153.3mw	1195.0vs 1163.4w 1152.2w	1197.3vs 1163.9w 1153.5w	1196br,vs 1164.0w 1153.5w	v _s CF ₃
1126.2br,vs 1105.7mw	1122.4vs 1104.8w	1132.9sh,m 1125.9vs 1105.3w	1132.3sh,s 1124.0vs 1105.7s	v _{CFH}
1093.6ms 1092.1sh,ms 1086.6m 1077.1vs 1062.8s	1092.2mw 1086.8w 1073.7vs 1062.9s	1093.6mw 1091.5mw 1087.3w 1076.1s 1061.8mw	1093.5m 1086.5m 1075.8s 1069.8sh,m 1063.3m	v _{CF} δ _{CHF}
862.4vs 854.4m	861.8vs 854.6m	863.4mw 854.9w	863.2s 854.8mw	v _{CC}
703.5vs 683.7vs	703.3vs 684.2s	704.7s 684.2vs	705.2vs 684.3s	v _{Cl}
	658.2w	657.7w	652.9w	δCF ₃
567.2w 526.6w	566.9s	567.1m	567.2m	δCF ₃
522.2mw 516.5mw	522.4m 516.4m	522.1mw 516.5mw	521.9mw 516.4wm	v _{Cl}

Table 4.18. Infrared bands /cm⁻¹ attributed to the ozone moiety in the complex, CF₃CHFL...O₃ (group 1), formed after co-depositon of the precursors, 1,1,1,2-tetrafluoroiodoethane and mixed ozone (¹⁶O_{3-x}¹⁸O_x) in argon.

V ₁	V ₂	V ₃	V ₁ + V ₃	assignment
		1039.6s	2141.4mw	16-16-16
		1035.4vs	2111.2mw	
		1033.3w	2108.4m	
			2100.2sh,m	
		1025.7s	2090.4mw	16-16-18
		1023sh,w	2087.3mw	
			2083.3w	
		1016.9s	2078.8sh,w	18-16-18
		1010.4w	2073.1w	
		1006.2s	2060.2mw	16-18-16
		999.7w	2057.4mw	
			2050.0mw	
			2047.4mw	
			2042.7w	
		991.7s	2037.8w	18-18-16
		989.0sh,w	2027.6mw	
			2024.6mw	
			2021.3sh,w	
			2015.4w	
			2006.2w	
1042.4w	665.0m	982.4s	1996.2m	18-18-18
		978.0br,vs	1993.6m	
		957.5vw	1986.2sh,mw	

Table 4.19. Infrared bands /cm⁻¹ assigned to iodoso-1,1,1,2-tetrafluoroethane, CF₃CFHIO (group 2), detected after near-infrared photolysis ($\lambda > 650$ nm) of an argon matrix containing 1,1,1,2-tetrafluoroiodoethane and ozone.

¹⁶ O ₃ /Ar	¹⁶ O _{3-x} ¹⁸ O _x /Ar	¹⁸ O ₃ /Ar	assignment
1262.7mw	1262-1242br,w	1262.0mw	ν_{CF_3}
	1211.2sh,w 1206.3sh,m	1205.7sh,ms	ν_{CF} (-CFHI)
810.7br,vw			ν_{CC}
732.0w	732.9w	694.6w	ν_{IO}
726.0w	676.1w	675.0w	

Table 4.20. Infrared bands /cm⁻¹ assigned to iodyl-1,1,1,2-tetrafluoroethane, CF₃CFHIO₂ (group 3), detected after photolysis ($\lambda > 350$ nm) of an argon matrix containing 1,1,1,2-tetrafluoroiodoethane and ozone.

¹⁶ O ₃ /Ar	¹⁶ O _{3-x} ¹⁸ O _x /Ar	¹⁸ O ₃ /Ar	assignment
815.8br,vw		812.9vw	$\nu_a \text{I}^{16}\text{O}_2$
810.2w	809.1vw	808.6vw	
805.1w	805.3vw		
	802.0vw 782.8vvw	801.1w	$\nu_a \text{I}^{16}\text{O}^{18}\text{O}$
	777.1vvw		$\nu_s \text{I}^{16}\text{O}_2$
	768.0vvw		$\nu_a \text{I}^{18}\text{O}_2$
	757.5vw	757.4w	$\nu_s \text{I}^{16}\text{O}^{18}\text{O}$
	751.7vw	751.5vw	
	747.2vw	746.2vw	$\nu_s \text{I}^{18}\text{O}_2$
	742.1vw	741.6w 735.7w	

Table 4.21. Infrared bands /cm⁻¹ of the carbonyl complexes, CF₃COF...HI (group 4) and CF₃COH...IF (group 5), formed after UV-vis (λ > 350 nm) irradiation of an argon matrix containing 1,1,1,2-tetrafluoroiodoethane and ozone.

¹⁶ O ₃ /Ar	¹⁶ O _{3-x} ¹⁸ O _x /Ar	¹⁸ O ₃ /Ar	assignment
1894.2m	1894.8w		v _{C=O} CF ₃ COF
1888.5ms	1889.3m		
1877.2w	1877.6w		
	1853.2m	1853.0ms	
1826.0w	1826.2w		v _{C=O} CF ₃ COH
1815.5w	1815.2w		
1792.0w	1785.3mw	1785.3mw	
	1779.1vw	1778.7w	
	1774.8w	1774.6w	
1409.2w		1408.6mw	2δCF ₃
1336.3w	1334.4mw	1333.5mw	vCF ₃
1286.9s			v _{CC} + δ _{FCF}
		1259.4sh,w	vFCF ₂
1247.3m	1246.3m	1246.9m	
1185.1s	1185.0sh,w	1184.1ms	δ _{OCF'} + ω _{o-ph}
1177.4sh,w	1177.9sh,w	1178.3mw,sh	
1092.6mw	1091.7m	1093.5mw	v _{CF'}
1087.2w		1091.5mw	
		1089.2s	
	1069.2sh,w	1069.5ms	δ CF ₃ + ρ _{i-ph}
1061.5s	1064.2w		
	1053.8w	1054.1w	
	890.9w	878.4w	v _{CC}
	879.5w		
690.5mw	691.4sh,w		δCF ₃
676.1w			ω _{i-ph} + ω _{o-ph}
635.2vw			
603.6br,w		592.5w	δ _{OCF'} δFCF ₂ or v _s IF
		582.9w	
	526.4vw		δ _{FCF}

Table 4.22. Infrared bands /cm⁻¹ assigned to the carbonyl stretch of the polyfluoroethanals, CF₃COX (X = H or F) perturbed by either HI or IF.

complex	precursor	¹⁶ O	$\nu_{\text{isolated}} - \nu_{\text{complexed}}^a$
CF ₃ COF...IF	C ₂ F ₅ I	1938.4ms	-39.4
		1936.4ms	-37.4
		1933.9ms	-34.9
		1909.9ms	-10.9
		1907.7s	-8.7
		1905.9s	-6.9
		1901.2sh,s	-2.2
CF ₂ HCOF...IF	CF ₂ HCF ₂ I	1886.3mw	12.7
		1942.0s	-43.0
		1938.5s	-39.5
		1909.0vs	-10.0
		1888.3mw	10.7
CF ₃ COF...HI	CF ₃ CHFI	1867.3mw	31.7
		1894.2m	4.8
		1888.5ms	10.5
CF ₃ COH...IF	CF ₃ CHFI	1877.2w	21.8
		1826.0w	-38.0
		1815.5w	-27.5
CF ₃ COF...HI	CF ₃ CH ₂ I	1792.0w	-4.0
		1784.5w	3.5
		1777.8m	10.2
		1765.8vw	22.2

^a ν_{isolated} of CF₃COF⁸² = 1899 cm⁻¹, of CF₃COH is 1788 cm⁻¹, for CF₂HCOF use ν_{isolated} is 1899 cm⁻¹ (same as CF₃COF), +ve = shift to lower wavenumber, -ve = shift to higher wavenumber.

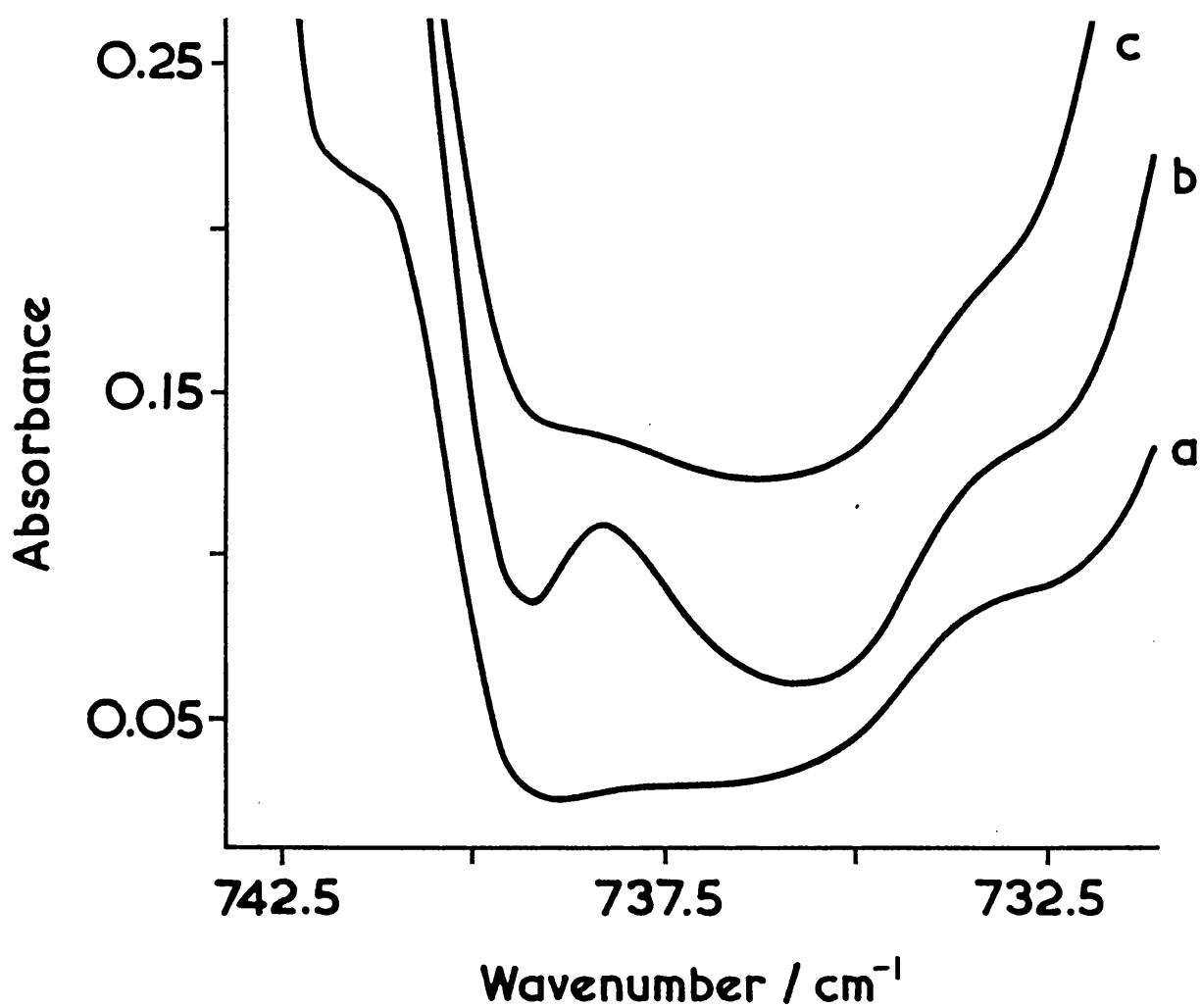


Figure 4.1. Infrared spectra in the range 742.5 and 732.5 cm⁻¹ of a matrix containing pentafluoroiodoethane and ozone in argon after (a) deposition at 14 K (b) near-infrared photolysis ($\lambda > 650$ nm) and (c) UV-vis ($\lambda > 350$ nm), showing the ν_{10} band of the group 2 species, iodosopentafluoroiodoethane.

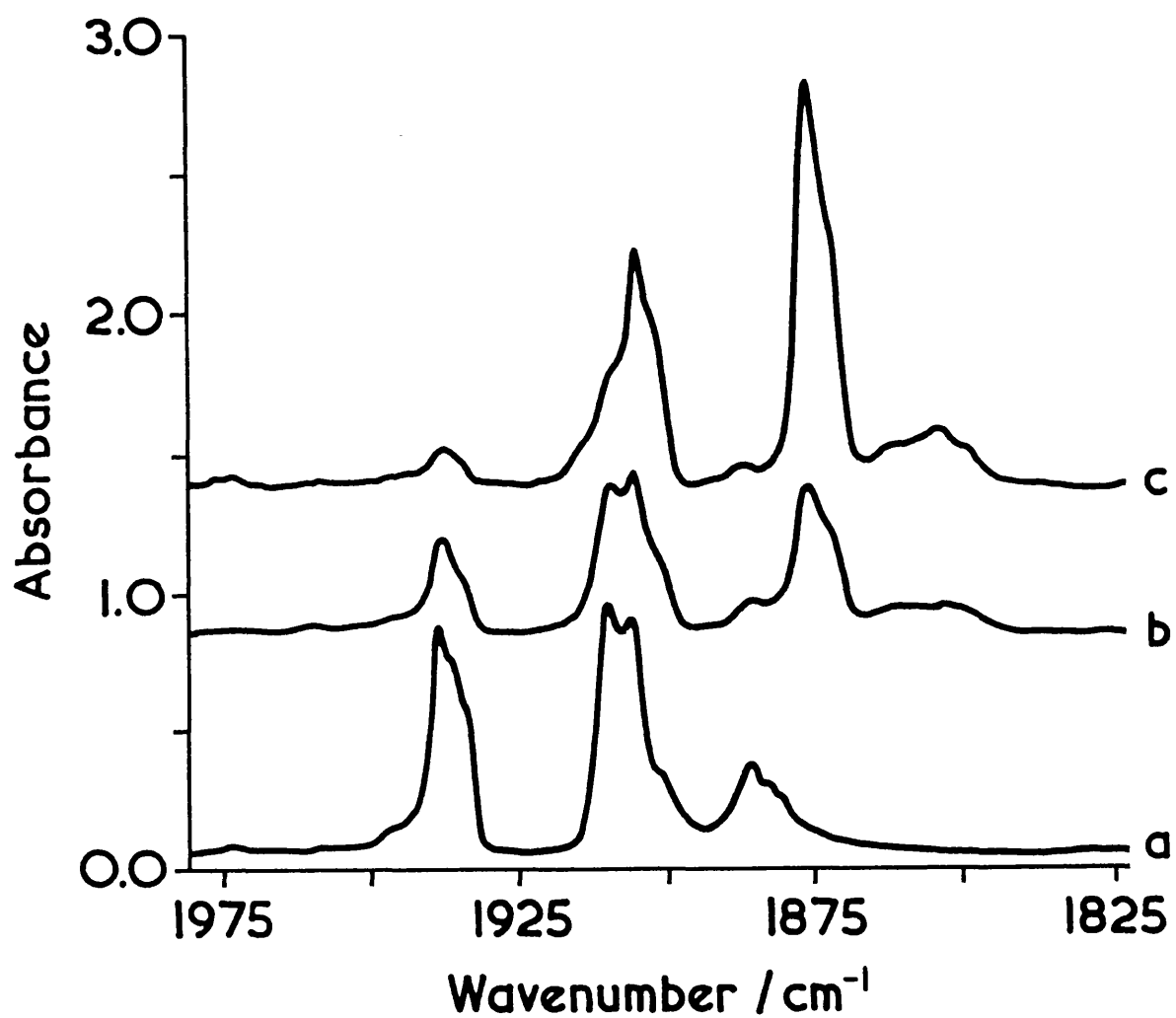


Figure 4.2. Infrared spectra in the $\nu_{C=O}$ region of the complex $\text{CF}_3\text{COF}\dots\text{IF}$ (group 5), detected after quartz-filtered photolysis of an argon matrix containing pentafluoroiodoethane and (a) ozone $^{16}\text{O}_3$, (b) mixed ozone $^{16}\text{O}_{3-x}^{18}\text{O}_x$ and (c) $^{18}\text{O}_3$ showing the ^{16}O - and ^{18}O -isotopomer.

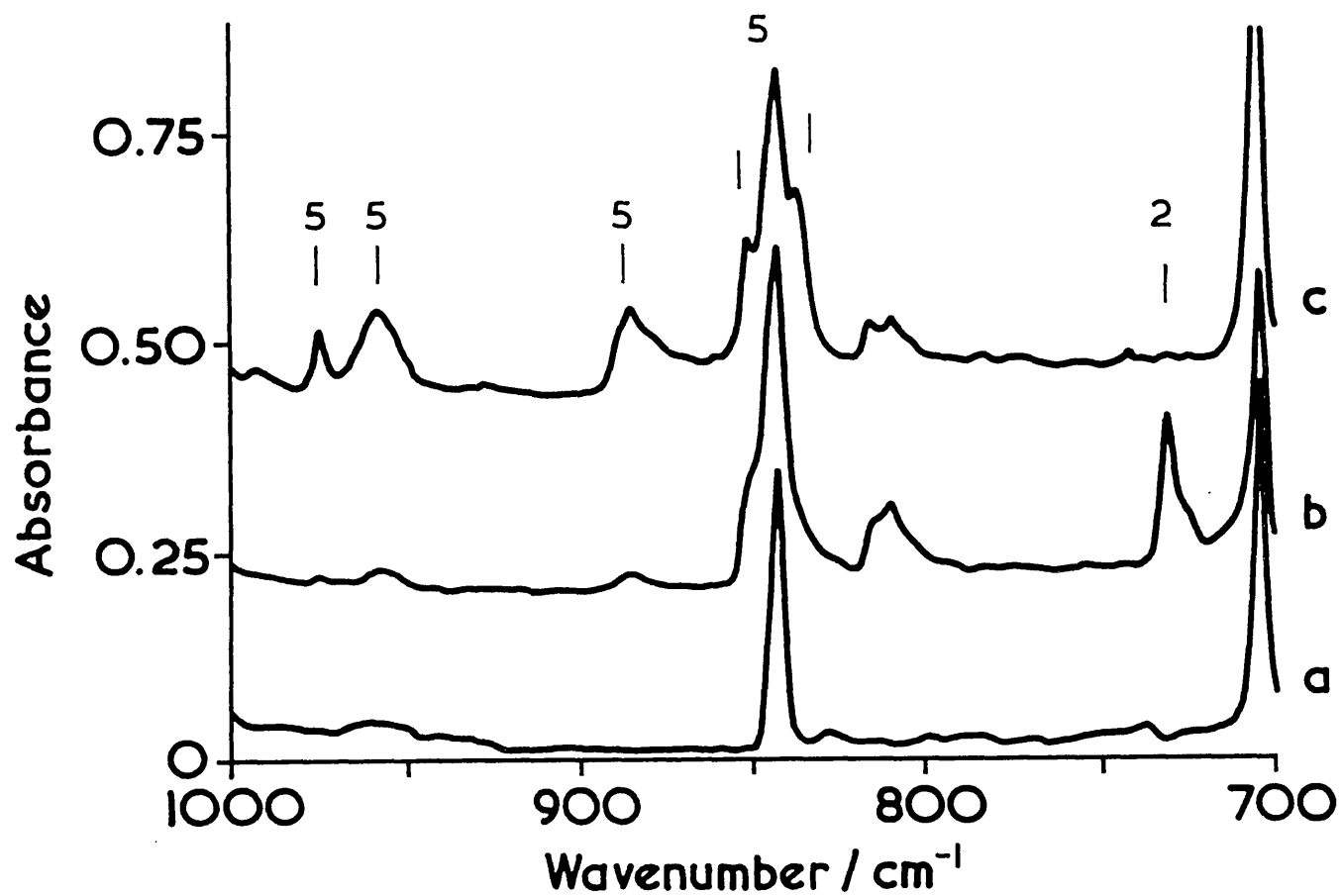


Figure 4.3. Infrared spectra in the range 1000 - 700 cm⁻¹ of a matrix containing CF₃CH₂I/O₃/Ar (2:5:1000) after (a) deposition (b) near-infrared photolysis ($\lambda > 650$ nm) and (c) quartz-filtered ($\lambda > 240$ nm) photolysis. This shows the growth and loss of the ν_{10} band of CF₃CH₂IO (group 2), and the growth of some bands of the complex, CF₃COH...HI (group 5).

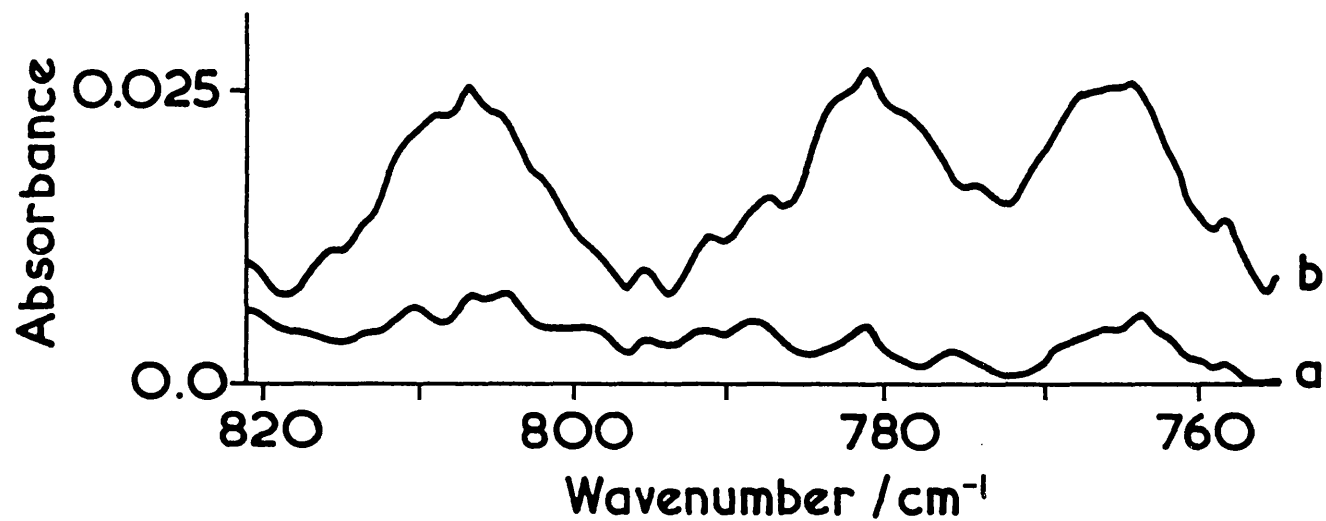


Figure 4.4. Infrared spectra in the IO₂ stretching region of a matrix containing CF₃CH₂I/¹⁶O_{3.ₓ}¹⁸O_ₓ/Ar (2:5:1000) after (a) deposition and (b) visible ($\lambda > 410$ nm) photolysis, showing bands assigned to iodyl-1,1,1-trifluoroethane, CF₃CH₂IO₂ (group 3).

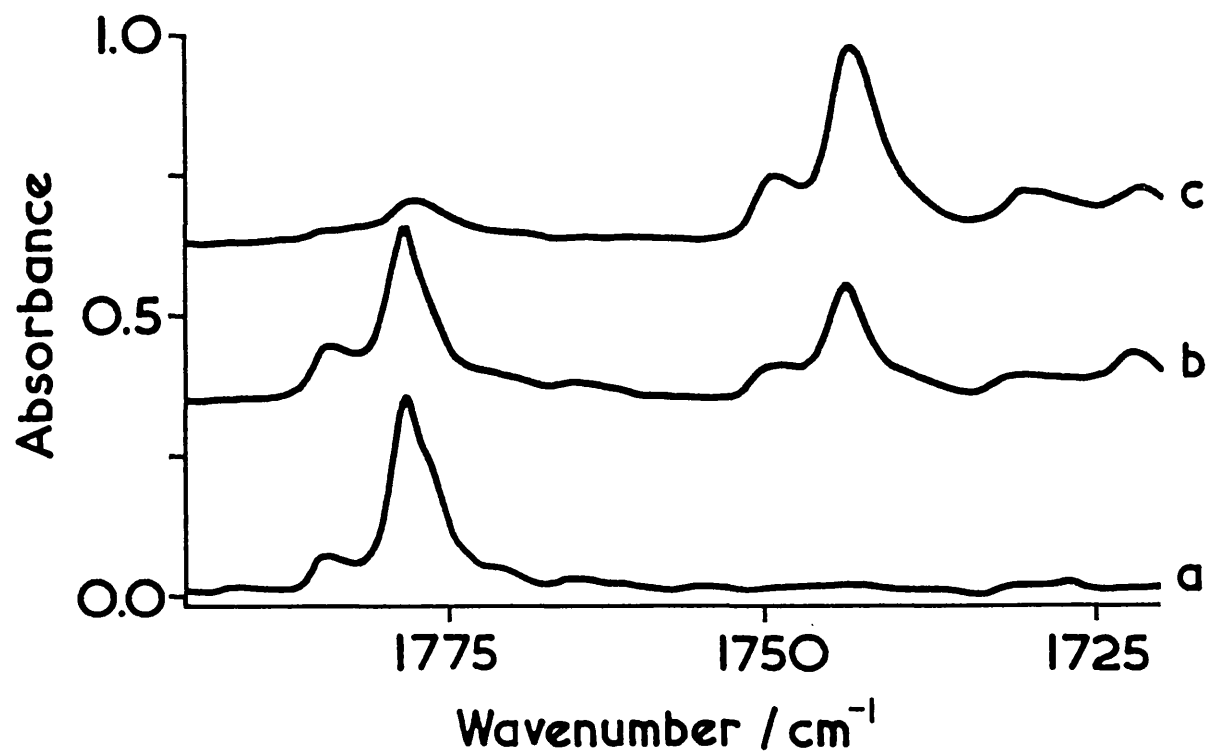


Figure 4.5. Infrared spectra detected after Pyrex-filtered photolysis of an argon matrix containing $\text{CF}_3\text{CH}_2\text{I}$ and (a) $^{16}\text{O}_3$ (b) $^{16}\text{O}_{3-x}^{18}\text{O}_x$ and (c) $^{18}\text{O}_3$ showing the $\nu_{\text{C}=\text{O}}$ bands of the ^{16}O - and ^{18}O -isotopomers of the complex $\text{CF}_3\text{COH}\cdots\text{HI}$ (group 5).

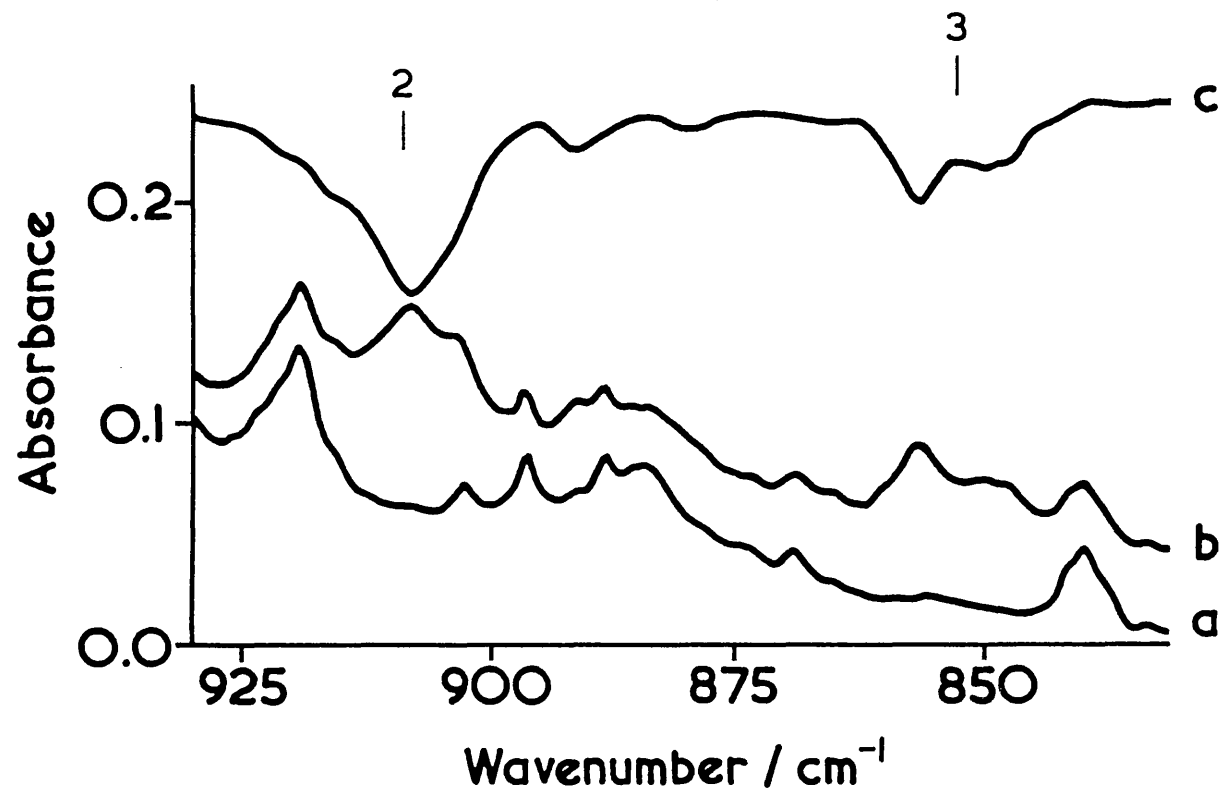


Figure 4.6. Infrared spectra of $\text{CF}_2\text{HCF}_2\text{I}/\text{O}_3/\text{Ar}$ (1:2:400) after (a) deposition (b) visible photolysis ($\lambda > 410$ nm) and (c) the subtraction spectrum of (a) and (b), showing bands assigned to iodoso-1,1,2,2-tetrafluoroethane, $\text{CF}_2\text{HCF}_2\text{IO}$ (group 2), and the complex $\text{CF}_2\text{HCOF}\dots\text{IF}$ (group 3).

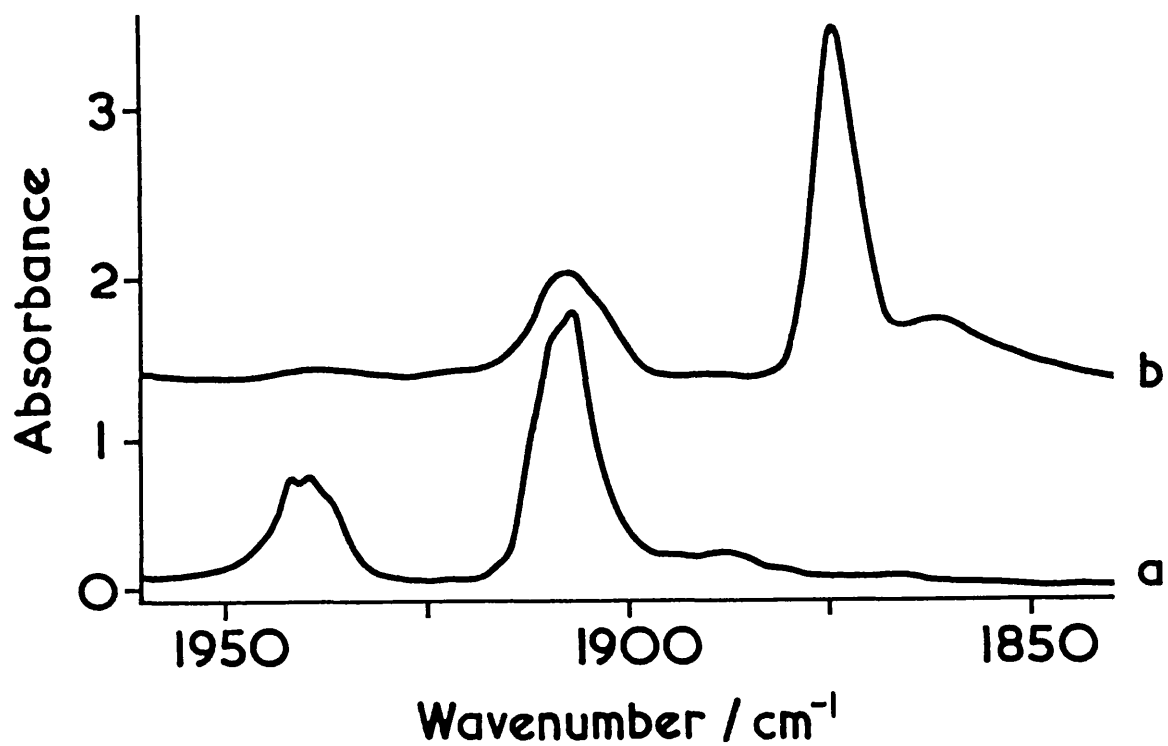


Figure 4.7. Infrared spectra after Pyrex-filtered irradiation of an argon matrix containing $\text{CF}_2\text{HCF}_2\text{I}$ and (a) $^{16}\text{O}_3$ and (b) $^{18}\text{O}_3$, showing the $\nu_{\text{C=O}}$ bands of the ^{16}O - and ^{18}O -isotopomers of the complex $\text{CF}_2\text{HCOF}\dots\text{IF}$ (group 3).

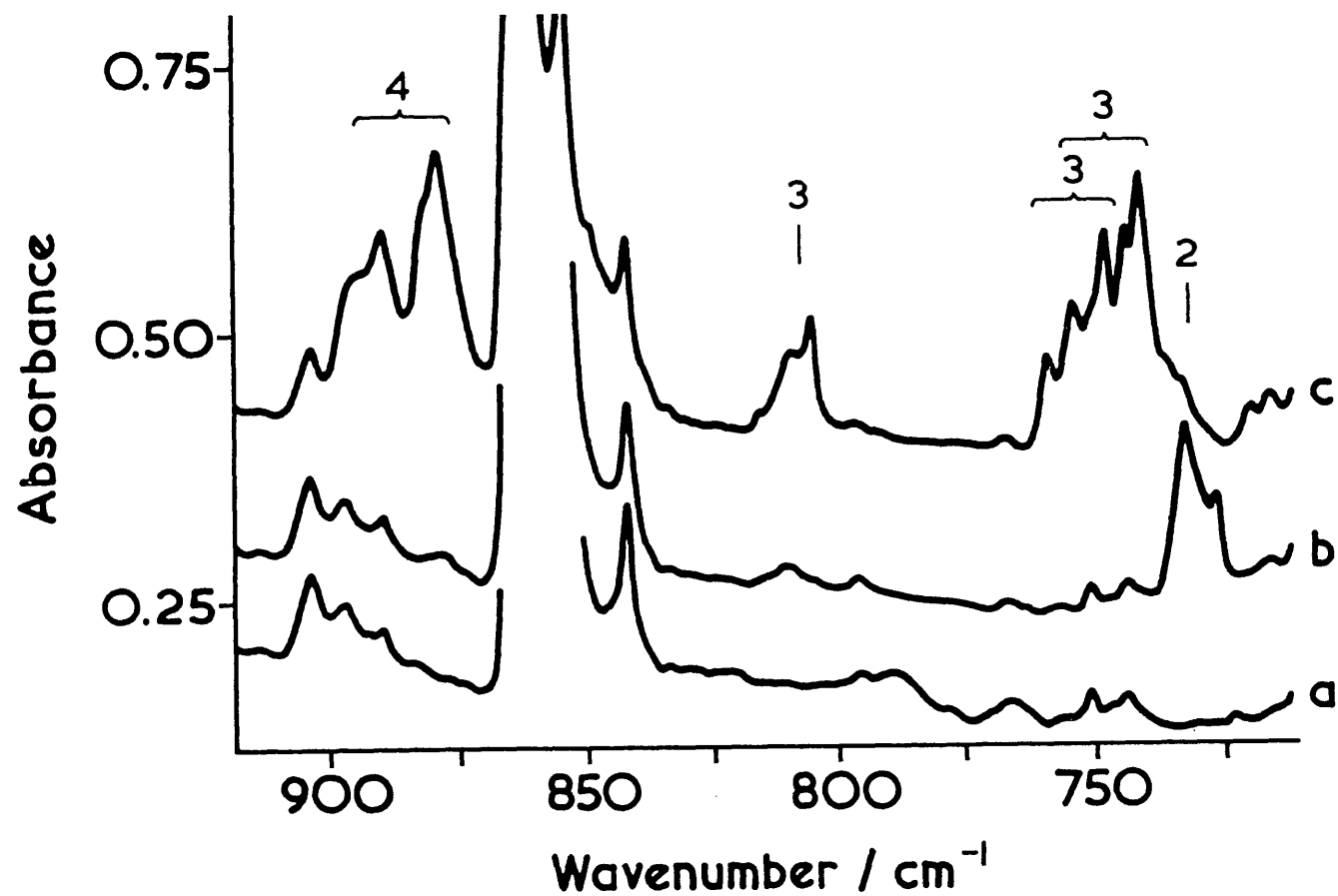


Figure 4.8. Infrared spectra in the region 900 - 725 cm^{-1} of a matrix containing $\text{CF}_3\text{CFHI}/^{16}\text{O}_{3-x}^{18}\text{O}_x/\text{Ar}$ (2:1:400) after (a) deposition (b) visible ($\lambda > 410 \text{ nm}$) photolysis and (c) Pyrex-filtered photolysis, showing the growth and loss of the ν_{10} band of CF_3CFHIO (group 2), growth of the νIO_2 bands of $\text{CF}_3\text{CFHIO}_2$ (group 3), and growth of some bands of the $\text{CF}_3\text{COF}\dots\text{HI}$ complex (group 4).

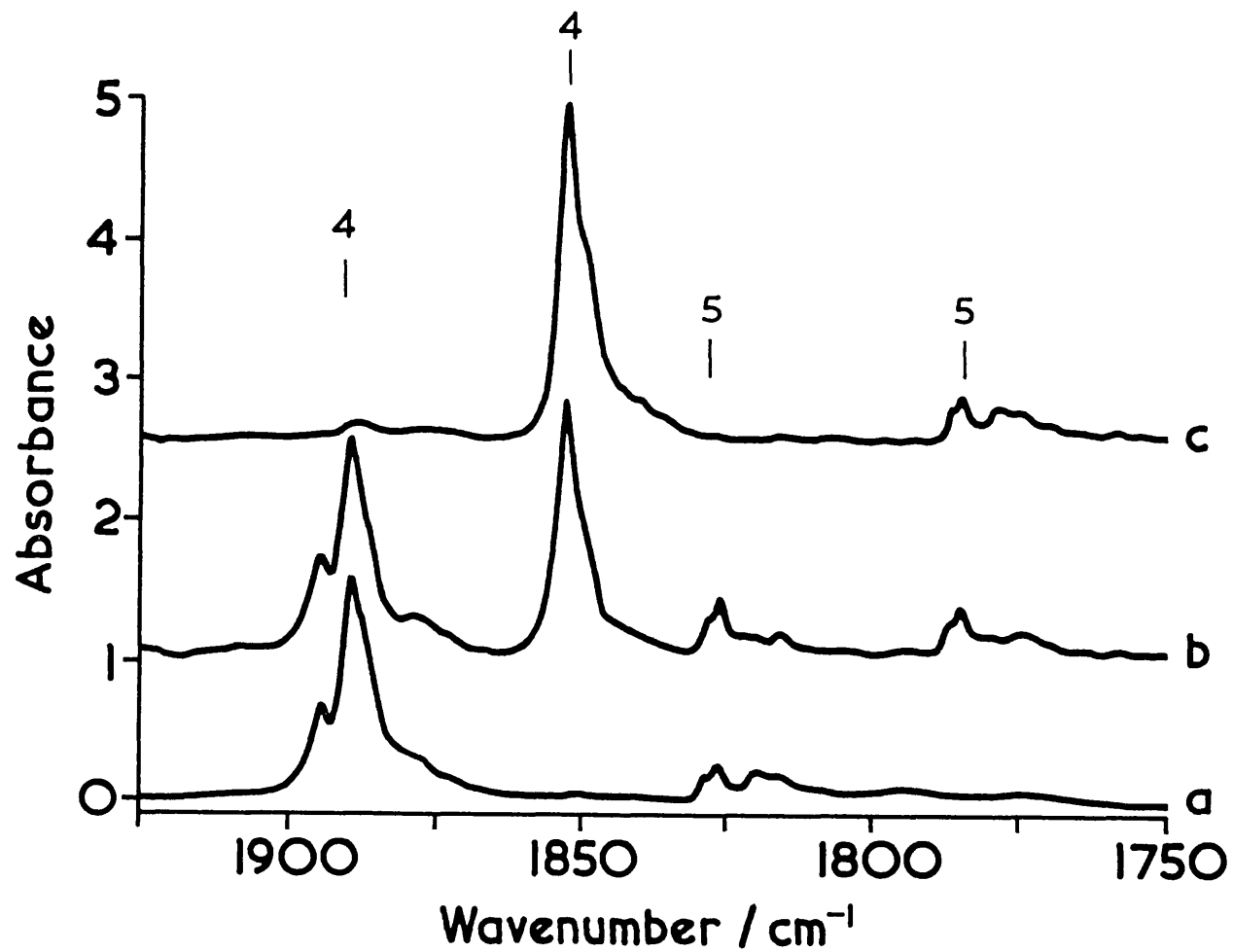


Figure 4.9. Infrared spectra recorded after Pyrex-filtered irradiation of argon matrices containing CF_3CFHI and (a) $^{16}\text{O}_3$ (b) $^{16}\text{O}_3$, $^{18}\text{O}_x$ and (c) $^{18}\text{O}_3$, showing the $\nu_{\text{C=O}}$ bands of the ^{16}O - and ^{18}O -isotopomers of the complexes $\text{CF}_3\text{COF}\dots\text{HI}$ (group 4) and $\text{CF}_3\text{COH}\dots\text{IF}$ (group 5).

Chapter 5

REACTION OF CHLOROIODOMETHANE AND DIIODOMETHANE WITH OZONE

5.1 INTRODUCTION

In the preceding chapters, a number of novel species and the photochemical interconversions between them have been identified. After studying the reaction of ozone with these two and three carbon, alkyl and polyfluoroalkyl iodides it was decided to study further some single carbon alkyl iodides, specifically those containing the backbone structure, X-CH₂I. It was hoped that these halogen-substituted methyl iodides would help to clarify the conflicting reports relating to the presence of hydrogen hypoiodide as a product of the reaction of oxygen atoms with iodomethane. Two photolysis studies, of iodomethane in an oxygen/argon⁴⁰ matrix and in solid oxygen,⁴¹ reported the presence of HOI. On the other hand, two other studies involving the reaction of ozone with iodomethane in an argon matrix²⁰ and in the gas phase⁶⁰ have reported no HOI. Thus whether or not hydrogen hypoiodide is detected as a product in these studies, should provide evidence for the reaction of alkyl halides with ozone occurring via a different mechanism to the reaction with oxygen atoms produced from O₂.

Additionally, the products of these species having the X-CH₂I backbone, can be compared with those reported in chapters 3 and 4, and thus the effect on the photochemistry and band wavenumber of some of the main bands i.e. ν_{10} , can be compared for the iodoso-species, X-CH₂-IO, where X = H,²⁰ CH₃,⁴⁷ CF₃,^a Cl^b and I^b (^a- see chapter 4; ^b- this chapter). Finally, the study of the reactions of these di-

substituted methanes, CH_2XY , with ozone can be combined with those of the halogenated methanes studied in chapter 6 with the aim of identifying a number of new and interesting carbonyl...Lewis acid and carbon monoxide...Lewis acid complexes.

5.2 CHLOROIODOMETHANE, CH_2ClI

Chloriodomethane is used as an agricultural pesticide and is believed to be a possible source of atmospheric iodine and hence, like other halocarbons, lead to the destruction of atmospheric ozone. Previously, in the matrix environment, ozone has been shown to form weak complexes with iodine-containing compounds (ICl ,¹⁹ CH_3I ,²⁰ CF_3I ,²¹ and those of chapters 3 and 4) and wavelength-dependent photolysis of these matrices produced a number of novel species containing iodine-oxygen bonds (X-IO , X-OI and X-IO_2). It has also been shown that shorter wavelength irradiation (usually Pyrex filtered) produces perturbed carbonyl species and that, in some cases, these carbonyl species dissociate further to form perturbed carbon monoxide complexes. In the case of chloriodomethane there are three possible carbonyl products, formyl chloride, COHCl , formaldehyde, COH_2 , and carbonyl chloride iodide, COCII , with each of these carbonyls being perturbed by the remainder of the starting material, i.e. HI , ICl and H_2 , respectively. The carbonyl and the remainder form carbonyl-Lewis acid type complexes, where the magnitude of the interaction can be inferred from the shift in wavenumber of the carbonyl bands. By detection of the products formed we can shed light on both the mechanism and the geometry of the complexes thus formed. In addition the products from these reactions can be compared with those of the halogenated methanes, CH_3I ,²⁰ CH_2Y_2 ,⁸⁷ ($\text{Y} = \text{Cl}, \text{Br}$), CHCl_3 ,⁸⁸ CH_2BrCl^a and CHBr_2Cl^a (^a- see chapter 6). Further photolysis, either for extended time periods or at shorter wavelengths, of these carbonyl-Lewis acid complexes may produce a range of carbon monoxide...Lewis acid complexes, $(\text{OC})_n(\text{XY})_m$, and again detection and comparison of these complexes with those previously reported would be of interest.

5.2.1 RESULTS

The spectra of chloriodomethane was recorded in an argon and an oxygen matrix (Table 5.1) and is in agreement with the vapour phase spectrum⁸⁹ recorded previously.

Chloriodomethane and ozone in argon

Co-deposition of chloriodomethane/argon ($\text{CH}_2\text{ClI}/\text{Ar} = 1:600$) and ozone/argon ($\text{O}_3/\text{Ar} = 1:300$) in matrices and the subsequent photolysis and warming of these matrices produced a variety of bands which have been grouped (1-5) according to their photolytic and thermal behaviour in the matrix.

Group 1. These bands were formed on co-deposition of chloriodomethane and ozone in argon matrices. The detected bands resemble those assigned, previously, to isolated chloriodomethane (Table 5.1) and ozone,⁴⁴ but with slight perturbations. The most apparent shifts occur to the bands assignable to the ozone moiety, and in particular the ν_3 bands detected at 1035.7 and 1033.3 cm^{-1} for the complex, which are shifted from the isolated (ν_3) band at 1039.1 cm^{-1} . In the mixed ozone experiment, $^{16}\text{O}_{3-x}^{18}\text{O}_x$, (Table 5.2) bands were detected for the ν_1 , ν_2 and ν_3 fundamentals, and for the combination, $\nu_1 + \nu_3$, of the six possible isotopomers (i.e. 16-16-16, 16-18-18, 18-18-18, etc.). This tends to indicate that the ozone moiety is bound via the central oxygen atom; retaining C_{2v} symmetry. In these studies, varying the initial $\text{CH}_2\text{ClI}/\text{O}_3/\text{Ar}$ ratios had no effect on the subsequent photochemical reactions, only on the relative intensities of the precursors. Near-infrared ($\lambda > 650 \text{ nm}$) photolysis of argon matrices containing these group 1 bands reduced their intensities, producing the group 2 bands.

Group 2. These bands are formed after near-infrared irradiation of argon matrices containing the group 1 bands. Shorter wavelength visible ($\lambda > 450 \text{ nm}$) irradiation increased the band intensities by a further 10 %, while subsequent shorter

wavelength UV-vis ($\lambda > 350$ nm) and Pyrex-filtered photolysis reduced the band intensities by 15 and 50 %, respectively. Finally, quartz-filtered irradiation destroyed the bands completely. The bands detected (Table 5.3) for this group have been assigned as follows: the medium band at 2962.0 cm^{-1} is assigned to a C-H stretch. A group of five medium intensity bands between 1215.1 and 1201.1 cm^{-1} are assigned to C-H bends. Two bands at 1198.7 and 1195.3 cm^{-1} which appear as shoulders on the existing C-H bands, are assigned to CH_2 wags. A broadening of the precursor band at 793.9 cm^{-1} indicates some perturbation of the CH_2 rock. A medium band at 748.1 cm^{-1} is assigned to a new C-Cl vibration. The strong precursor band at 731.7 cm^{-1} broadens and shifts to 723.5 cm^{-1} and exhibits a similar band at 690.0 cm^{-1} for the ^{18}O isotopomer, this band having an ^{18}O -shift of 33.5 cm^{-1} and a photochemical behaviour resembling bands reported in chapters 3 and 4, is assigned to an I-O stretch. A further three bands were detected between 542.9 and 528.9 cm^{-1} and are assigned to perturbed C-I vibrations. The bands detected in the $^{18}\text{O}_3$ and $^{16}\text{O}_{3-x}^{18}\text{O}_x$ experiments can be assigned to either ^{16}O or ^{18}O isotopomers, confirming the presence of only one oxygen atom in the species responsible for the group 2 bands.

Group 3. These bands are formed after visible ($\lambda > 450$ nm) irradiation they increased by a further 20 % after UV-vis photolysis, and are destroyed by Pyrex-filtered irradiation. These bands (Table 5.4) absorb at 1062.2 , 579.6 and 576.7 cm^{-1} . The medium band at 1062.2 cm^{-1} with an ^{18}O -shift of 27.4 cm^{-1} (predicted C-O diatomic shift is 28 cm^{-1}) is assigned to the C-O vibration some confusion surrounds this assignment, due to an additional band at 1054.5 cm^{-1} detected in the mixed ozone experiment, also assigned to a C-O stretch. The band at 576.7 cm^{-1} exhibited an ^{18}O -shift of 27.0 cm^{-1} (predicted O-I diatomic shift is 29 cm^{-1}), and is assigned to an O-I stretch, as is the weak shoulder band at 579.6 cm^{-1} . In the mixed ozone experiments two bands were detected at 578.6 and 554.5 cm^{-1} having an ^{18}O -shift of 24.1 cm^{-1} between the two, they are assigned to O-I stretches of the ^{16}O - and ^{18}O -isotopomers, respectively. Detection of bands attributable to O-I and C-O stretches in this group, suggests the presence of a C-O-I unit in the species responsible for these bands. After considerable photolysis (~ 20 h) a weak band around 3500 cm^{-1} was detected in the

$^{18}\text{O}_3$ experiment, which has been tentatively assigned to an O-H stretch of HOI.

Group 4. These bands are formed after visible photolysis they doubled in intensity after UV-vis photolysis, while subsequent Pyrex- and quartz-filtered irradiation increased the intensities of the bands by a further 100 % and 40 %, respectively. The bands for this group (Table 5.5) are assigned as follows: the band at 2987.6 cm^{-1} is assigned to a C-H stretch. The strong bands at 1778.3 and 1762.8 cm^{-1} and the weak band at 1769 cm^{-1} (^{18}O isotopomer bands at 1739.2 and 1721.4 cm^{-1}) are assigned to the carbonyl stretch (Fig. 5.3). The ^{18}O band at 1721.4 cm^{-1} exhibited a slight broadening on the high wavenumber side, deconvolution of this feature, using a curve fitting program, revealed its wavenumber to be 1728.3 cm^{-1} . These detected bands exhibit ^{18}O -shifts of between 39.1 and 42 cm^{-1} confirming their assignment to C=O stretches. In the mixed ozone experiment, bands were detected at 1778.3 , 1770.6 , 1761.9 , 1738.7 , 1730 and 1720.9 cm^{-1} these being assigned to either ^{16}O or ^{18}O isotopomers, confirming that only one oxygen atom is involved. Heating the matrix to 25 K for 20 min reduced slightly the intensity of the bands at 1778.3 and 1762.8 cm^{-1} while the intensity of the band at 1769 cm^{-1} increased.

The weak band at 1306.2 cm^{-1} is assigned to a C-H bend. The weak bands detected at 951.3 and 935.9 cm^{-1} for the ^{18}O isotopomer are assigned to the out-of-plane vibration of the molecule. The very strong, medium-weak and medium bands at 794.4 , 770 and 748.1 cm^{-1} respectively, are assigned to C-Cl stretches. In one set of experiments, weak bands were detected at 1756.6 and 1748.9 cm^{-1} (^{18}O at 1710.8 cm^{-1}) and these have been assigned to an additional carbonyl stretch, most likely from a different species, or complex, from that above.

Group 5. These bands formed weakly after visible irradiation, (Table 5.6, Fig. 5.4) and increased steadily (by 10-20 %) with each successive photolysis ($\lambda > 350$, 290 and 240 nm) cycle. This group comprised a medium band at 2787.5 cm^{-1} (^{18}O at 2790.4 cm^{-1}) assigned to a HCl stretch, and two other medium bands at 2151.5 and 2141.4 cm^{-1} having ^{18}O -shifts of 50.3 and 54.1 cm^{-1} respectively, which are assigned to C-O stretches of carbon monoxide (note: isolated CO in an argon matrix absorbs

at 2138.4 cm⁻¹).^{90,91}

Chloriodomethane in oxygen

After deposition of chloriodomethane in a solid oxygen matrix (CH₂ClI/O₂ = 1:150-200) at 14 K the infrared spectrum exhibited bands similar to those reported for chloriodomethane trapped in argon (Table 5.1). However, quartz-filtered photolysis was required before the following new bands were detected at 2985.2, 2140.1, 1773.0, 1747.9, 1307.2 and 792.2 cm⁻¹ these being assigned to bands similar to those reported for groups 4 and 5 above.

5.2.2 DISCUSSION

The various bands detected above have been grouped (1-5) according to their photolytic and thermal behaviour, and shall be discussed below.

Group 1. These bands are detected after co-deposition of CH₂ClI and O₃ in argon matrices, and resemble the bands detected for the isolated precursors (Table 5.1 and 5.2), except for small perturbations which are most apparent for the bands attributed to ozone. In the mixed isotopomer experiments, six sets of bands were assigned for each of the fundamental modes (only four for the weak ν_1 mode). These bands indicate that ozone has retained its symmetry (i.e. symmetric about the central O atom), and that any binding must therefore occur to the central oxygen atom. This spectral evidence, combined with the effective photodissociation after near-infrared photolysis producing the group 2 bands, suggests that the group 1 bands can be attributed to a weak ozone...chloriodomethane complex. This complex is believed to be very much like those ozone complexes detected in chapters 3, 4 and elsewhere,^{19-21,36,47} in that production of the group 2 bands occurs via a light-induced charge-transfer mechanism, transferring an oxygen atom from ozone to the iodine atom of chloriodomethane.

Group 2. These bands formed after near-infrared ($\lambda > 650$ nm) irradiation, and destroyed by Pyrex-filtered irradiation, are assigned to perturbed C-H stretches and bends, a C-Cl stretch, C-I stretches and most diagnostically an I-O stretch. The species accounting for these bands is iodosochloromethane, $\text{CH}_2\text{Cl-IO}$. A number of similar iodoso-species have been reported (chapter 3, 4, OICl ,¹⁹ CH_3IO ,²⁰ CF_3IO ,²¹ HIO ,⁴⁶ $\text{C}_2\text{H}_5\text{IO}$ ⁴⁷ and those of chapters 3 and 4) having this Z-IO structure. The nature of the Z group has an effect on the wavenumber of the ν_{IO} band, and this is discussed further in section 5.4, at the end of this chapter.

Group 3. These bands were formed, after UV-vis ($\lambda > 350$ nm) photolysis, at the expense of the group 2 bands, thus indicating some connection between the two groups. The bands detected (Table 5.4) are assigned to C-O and O-I stretches. On this basis a COI unit must be present, and hence the species hypiodochloromethane, $\text{CH}_2\text{Cl-OI}$. A number of other hypiodo-species (Z-OI) have been previously detected (see above for range of Z species), and this interconversion between the iodoso- and hypiodo-species has been studied using semi-empirical calculations MOPAC⁹² and shall be considered in more detail later (see Photochemical interconversion). Of prime interest here is the presence of hydrogen hypiodide and to a lesser extent chlorine hypiodide, ClOI ; the latter was not detected. Interestingly, the lack of any strong HOI bands in this experiment, matches the results reported for the reaction of ozone with iodomethane in argon matrices²⁰ and in the gas phase,⁶⁰ lending extra weight to the interconversion between the iodoso- and hypiodo-species to be proposed below. Other workers^{40,41} using O_2 as the oxygen atom source have, however, reported the detection of HOI, in the reactions with iodomethane. This formation of HOI, in the O_2 experiments, can be accounted for by the shorter wavelength ($\lambda < 280$ nm) photolysis, and increased photolysis times (1-2 h) required to produce O atoms in sufficient quantity from oxygen, which may cause iodomethane to photodissociate into CH_2 and HI. The hydrogen iodide then reacts with oxygen atoms to produce HOI.⁴⁶ This mechanism of producing HOI is the assumed route by which the weak ν_{OH} bands (Fig. 5.2) were formed in the $^{18}\text{O}_3$ experiment.

Group 4. These bands (Table 5.5) are assigned to formyl chloride,

COHCl.^{93,94} The most diagnostic bands occur in the carbonyl stretching region between 1710 and 1780 cm⁻¹ and, by their similarity to bands previously identified, it seems that the formyl chloride detected lies in at least three environments, i.e. isolated in argon, complexed with hydrogen iodide and lastly in a more perturbing environment, possibly with one or more hydric acids (HX). The strong band at 1778.3 cm⁻¹ (¹⁸O at 1739.2 cm⁻¹) is assigned to the $\nu_{C=O}$ band of formyl chloride isolated in argon. The bands at 1769 and 1762.8 cm⁻¹ (¹⁸O at 1728.3 and 1721.4 cm⁻¹) are attributed to the formyl chloride...HI complex. While the weak bands at 1756.6 and 1748.9 cm⁻¹ (¹⁸O at 1710.8 cm⁻¹) are attributed to a formyl chloride...HCl and a formyl chloride...(HCl)(HI) complex, respectively. These formyl chloride complexes can be compared with others reported previously, perturbed by HCl,⁸⁷ Cl₂⁸⁸ and with those detected in chapter 6 (HBr, Br₂, BrCl), where a complete comparison will be made. Unfortunately in these matrices no bands assignable to HI were detected, but this is not unusual given its low infrared absorption; the shifts of the $\nu_{C=O}$ band of COHCl...HI fit well into those of the formyl chloride complexes with HCl⁸⁷ and HBr (chapter 6).

The formation of formyl chloride as the only carbonyl product provides interesting information as to the favoured mechanism occurring in the matrix. Since we have been able to detect the iodoso- and hypoiodo-species we know that the reaction proceeds via O atom addition and subsequent insertion into the C-I bond. Thus the possible carbonyl products are limited to two: COHCl...HI or COH₂...ICl. *Ab initio* calculations of the products formed after O atom addition to CH₂X₂⁸⁷ (X = Cl or Br) predict that the abstraction of HX is the favoured path, and thus our result supports the calculations for a wider range of dihalide precursors.

Group 5. These bands are formed after visible irradiation, $\lambda > 450$ nm, and they increased steadily in intensity after photolysis at shorter wavelengths ($\lambda > 350$, 290, and 240 nm). Bands for this group have been assigned to stretches of CO and HCl, (Table 5.6, Fig. 5.4) suggesting a complex of the form (OC)_n(HX)_m. In previous studies⁹⁵ it has been suggested that it is possible to distinguish between the wavenumbers of the ν_{HCl} bands in the complex, OC...H-Cl^a...H-Cl^b, with the HCl in

the *a* position absorbing at c. 2790 cm⁻¹. Thus in this experiment the ν_{HCl} band at 2787.5 cm⁻¹ can be assigned to HCl in the *a* position of the complex. Similarly the wavenumber of the ν_{CO} band of this carbon monoxide complex can be compared with that of other carbon monoxide...hydrogen halide complexes, i.e. OC...HI⁹⁶ (2152, 2147.5 and 2137.5 cm⁻¹), OC...(HCl)₂⁸⁷ (2156.7 and 2155.6 cm⁻¹), OC...(HBr)₂^{87,96} (2153.1 cm⁻¹) and OC...HCl⁹⁶ (2151 cm⁻¹). The ν_{CO} band at 2151.5 cm⁻¹ detected in this study resembles closely that of carbon monoxide perturbed by either HCl or HI. Again, although no HI bands were detected, examination of the mechanism and stoichiometry of the reaction suggests that the group 5 bands can be attributed to the complex OC...HCl...HI. This assignment is supported further by the detection, reported in chapter 6, of an OC...HCl...HBr complex. The ν_{HCl} and ν_{CO} bands of this latter complex are more perturbed (i.e. the shift of the band wavenumber of the complex from that of the isolated species), due to the increased hydrogen bonding of HBr over HI.

Chloriodomethane in oxygen

The bands detected after UV ($\lambda > 240$ nm) photolysis of chloriodomethane in solid oxygen are assigned to formyl chloride and carbon monoxide (Table 5.5). The product bands detected suggest that a different mechanism may be occurring. In particular the carbonyl stretches at 1773.0 cm⁻¹ are assigned to formyl chloride isolated in argon and at 1747.9 cm⁻¹ to formyl chloride perturbed by both HCl and HI. The latter carbonyl band could have been attributed to formaldehyde, since isolated formaldehyde absorbs near 1742 cm⁻¹ but the most likely partner in the matrix, ICl, would have shifted the carbonyl band to around⁶² 1719 cm⁻¹ ruling out this assignment. The medium-weak band at 2140.1 cm⁻¹ is assigned to isolated carbon monoxide, again in a different matrix environment from that of the counterpart formed in the ozone experiments. These products (i.e. different formyl chloride and carbon monoxide complexes) may result from a different mechanism operating in solid

oxygen matrices. One such alternative process might involve photodecomposition of chloriodomethane ($\lambda \sim 266$ nm) producing excited CH_2Cl and I atoms,^{97,98} with these reacting with the oxygen atoms formed from dissociated oxygen. However, the dissociation of chloriodomethane as the first step seems unlikely since no dissociation products (CH_2 , ICl or HI) were detected. Additionally, during the photolysis ($\lambda > 240$ nm, 1-2 h) of chloriodomethane isolated in argon no photofragments were detected, further casting doubt on any process involving dissociation of chloriodomethane. As will be seen later (chapters 6 and 7), even after considerable photolysis times (> 100 h) no products were detected to indicate that C-halogen bond dissociation is occurring to any relevant extent in these reactions between haloalkanes and ozone or oxygen. Thus we must assume that the O atoms, produced from oxygen, insert into the C-I bond, and it is the harsher photolysis (UV radiation) conditions and different deposition characteristics of these oxygen matrix studies which favours the formation of either isolated formyl chloride or the formyl chloride...(HCl)(HI) complex.

Photochemical Interconversion

The first step in the photochemical interconversion (see Summary 5) is the formation of a weak complex between ozone and chloriodomethane formed after co-deposition of chloriodomethane and ozone in argon. This weak complex is believed to behave photochemically in the same manner as the ozone complexes^{19-21,36,47} previously detected (chapters 3 and 4), with near-infrared photolysis ($\lambda > 650$ nm) of the matrix causing the transfer of an oxygen atom from ozone to chloriodomethane via a charge-transfer type intermediate to produce the group 2 species, iodosochloromethane, $\text{CH}_2\text{Cl-IO}$.

Visible ($\lambda > 450$ nm) photolysis of the group 2 species causes a conversion into the group 3 species, hypiodochloromethane, $\text{CH}_2\text{Cl-OI}$. On shorter wavelength irradiation, these group 3 bands increased in intensities at the expense of group 2

bands, thus demonstrating a link between iodosochloromethane and hypiodochloromethane. The interconversion between the iodoso- (ZC-IO) and hypiodo-species (ZC-OI) has been the subject of semi-empirical calculations. Using MOPAC⁹² the change in the C-I-O angle between the two species was studied; ranging from 99° for the iodoso- to 28° for the hypiodo-species, revealing an energy barrier (Fig. 5.5 and Table 5.9) between the two structures at c. 55.° This transition, between the two, can be viewed as the C-I-O angle shortening until a new C-O bond is formed and the existing C-I bond ruptures to form ZC-OI. This transformation is corroborated by the increase of the C-I bond length from 2.12 Å to 2.82 Å and the decrease of the C-O bond length from 3.09 Å to 1.40 Å during the transformation from ZC-I-O to ZC-O-I. An alternative mechanism involving radicals has been proposed²⁰ for the conversion of CH₃IO to CH₃OI, in which the former dissociates into the radicals CH₃• and IO,• with subsequent rotation of IO• and recombination producing the hypiodo-species, CH₃OI. At this stage no evidence is available to distinguish between the two.

Further Pyrex-filtered photolysis destroyed the group 3 bands and produced the formyl chloride complexes (group 4). Since the C-O bond is already in place in group 3, the mechanism to form group 4 simply involves the rupture of the O-I bond and the formation of a new H-I bond to form the complex, COHCl...HI. This same photolysis wavelength, and subsequent shorter UV irradiation produced the group 5 carbon monoxide species, OC...HCl...HI. The structure of this complex is confirmed by comparison of the wavenumbers of the HCl bands, and can best be seen in the summary below.

5.3 DIODOMETHANE, CH₂I₂

The study of the photochemical reactions of diiodomethane in ozone/argon, and solid oxygen, matrices was carried out with the same aims in mind as the study of chloriodomethane. These were to study another precursor having the X-CH₂I backbone and to make comparisons with similar species. The study of diiodomethane also completes the study of the dihalomethanes, CH₂X₂⁸⁷ (X = Cl or Br) with ozone. The products of the dichloro- and dibromomethane reaction with ozone differed slightly; extra products were reported for the dibromo- cases. Thus it was hoped that a study of diiodomethane would clarify these observations. Additionally, since the favoured mechanism in both the dichloro- and dibromo- cases was the elimination of HX and the production of a formyl halide, it was hoped that the stabilising nature of the matrix might provide a route to formyl iodide, COHI.

5.3.1 RESULTS

Diiodomethane has a very low vapour pressure at room temperature, less than 1/20th of an atmosphere. At these low vapour pressures, and with the sensitivity of the measurement system, the calculated CH₂I₂/Ar ratios vary from 1:500 to 1:1500. After deposition of diiodomethane in argon and oxygen matrices a number of bands were detected and have been assigned using chloriodomethane and dibromomethane as guides (Table 5.7).

Diiodomethane with ozone/argon or in oxygen

Co-deposition of CH₂I₂ and ozone produced bands assignable to both precursors (Table 5.7). Unlike the monoiodinated alkanes (above), photolysis with visible radiation ($\lambda > 350$ nm) was required before even weak bands were detected

(Table 5.8). Pyrex- and quartz-filtered irradiation increased the intensity of these bands, but even after UV photolysis for 3 h the band intensities were still weak. Various experiments to increase the yield of products were tried, including photolysing the matrix during deposition, but these produced only weak product bands. The bands detected have been assigned to either carbon monoxide or methanal.

5.3.2 DISCUSSION

The reaction of ozone with diiodomethane differs markedly from the reaction with the mono-iodinated precursors. In the case of diiodomethane prolonged irradiation (up to 3 h) was required before any product bands were detected, in comparison with the photochemical reaction of ozone and iodoethane⁴⁷ in which bands were detected after near-infrared ($\lambda > 650$ nm) photolysis for 9 min. Unlike the single iodine-containing¹⁹⁻²¹ precursors, the formation of any complex between ozone and diiodomethane seems unlikely, given the photochemical behaviour. Possibly because of some steric hindrance caused by the large iodine group, although this seems unlikely given that the other X-CH₂I species having large groups, e.g. methyl- (chapter 3) or trifluoromethyl- (chapter 4) still formed complexes with ozone. For this reason it would have proved instructive to study bromiodomethane in order to study further the change in photochemistry occurring from CH₂ClI to CH₂I₂.

The possibility exists that diiodomethane reacts via an alternative mechanism to the single iodine-containing species, and one such possibility would involve the photodissociation ($\lambda \sim 300$ nm) of diiodomethane^{98,99} into CH₂I and I atoms, with either of these species subsequently reacting with oxygen atoms to form the products. However, the lack of detection of any of these products, and the observation that UV-vis ($\lambda > 350$ nm) photolysis produced some products tends to favour insertion of O atoms into the C-I bond, rather than dissociation of the C-I bond and subsequent attack of an O atom.

The methanal product detected follows the trend in the photochemical reaction of ozone with the dihalomethanes, CH_2X_2 , in which dichloromethane⁸⁷ produced only formyl chloride, while dibromomethane⁸⁷ produced both formyl bromide and formaldehyde, and diiodomethane produced only methanal. This trend mirrors the reduction in strength of the C-halogen and H-halogen bonds as one descends the group. It would be interesting to have additional *ab initio* calculations on the reaction of diiodomethane with O atoms in order to compare the results with those of the reaction with dibromo- and dichloromethane.⁸⁷ The wavenumbers detected for the carbonyl stretching bands of the methanal- I_2 complex (1720.7 cm^{-1}) can be compared with those of other methanal...halogen complexes; $\text{COH}_2\cdots\text{Br}_2$ (1727.7 cm^{-1})⁸⁷ and $\text{COH}_2\cdots\text{Cl}_2$ (1734.5 and 1732.4 cm^{-1}).⁶² These wavenumbers are shifted from $\nu_{\text{C=O}}$ of methanal^{100,101} (1742 cm^{-1}) and follow the trend of Lewis acid strength, where the stronger Lewis acids cause a larger wavenumber shift of the carbonyl band.

The detection of bands attributable to carbon monoxide is surprising since, under these photolysis conditions, methanal does not usually dissociate. Thus the detection of CO bands provides tentative evidence for the formation of formyl iodide, which is subsequently photodissociated to form carbon monoxide in a very rapid process. The wavenumber of the ν_{CO} band at 2149.9 cm^{-1} (isolated CO^{90} absorbs at 2138 cm^{-1}) suggests some perturbation of the carbon monoxide moiety, and possibly a $(\text{CO})_n(\text{HI})_m$ complex.

5.4 COMPARISON OF THE IODOSO- SPECIES (Z-IO)

Comparisons of the relative wavenumbers of the ν_{IO} bands of the iodoso-species reported in this thesis and elsewhere (ICl ,¹⁹ CH_3I^{20} and CF_3I^{21}) have been made in this section. In the first comparison of the three hydrated iodoalkanes, iodosomethane²⁰ $\text{H}_3\text{CI-O}$ (723.7 cm^{-1}), iodosoethane⁴⁷ $\text{C}_2\text{H}_5\text{I-O}$ (717.0 cm^{-1}), and 2-iodosopropane ($\text{CH}_3)_2\text{CHI-O}$ (714.5 cm^{-1}), we observe the trend in which the addition of methyl groups shifts the band to lower wavenumbers. This trend is caused by the methyl

groups donating electron density into the (p-p) π^* orbital of the I-O bond. We can use this trend to predict band positions, for example iodoso-tert-butane, $(\text{CH}_3)_3\text{C-IO}$, would be expected to absorb around 710 cm^{-1} since in this species there are three methyl groups donating electrons, rather than two in the case of 2-iodosopropane. Following this same line 1-iodosopropane, $\text{CH}_3\text{CH}_2\text{CH}_2\text{IO}$, would be expected to have an ν_{IO} band at $\sim 716\text{ cm}^{-1}$ intermediate between that of iodosoethane and 2-iodosopropane.

Further, the two perfluoroiodoalkanes, iodosopentafluoroethane, $\text{C}_2\text{F}_5\text{I-O}$, (738.7 cm^{-1}) and iodosotrifluoromethane, $\text{CF}_3\text{I-O}$,²¹ (732.7 cm^{-1}), can be compared in which the reverse trend is noted, in that adding extra trifluoromethyl groups shifts the ν_{IO} band to higher wavenumbers. This trend may be examined further by comparing iodoso-1,1,1-trifluoroethane, $\text{CF}_3\text{CH}_2\text{IO}$ (732.4 and 727.1 cm^{-1}) with iodosoethane (717.0 cm^{-1}), and again it is observed that replacing a methyl group with a trifluoromethyl group shifts the IO band to higher wavenumber. In chapter 4 the reactions of ozone with a number of other polyfluoroiodoethanes was studied in order to examine the effect of these fluorinated and hydrated methyl groups. Thus the species, iodoso-1,1,1,2-tetrafluoroethane, CF_3CFHIO , (732.0 and 726.0 cm^{-1}) and iodoso-1,1,2,2-tetrafluoroethane, $\text{CF}_2\text{HCF}_2\text{IO}$, (727.6 and 722.3 cm^{-1}) can be compared with those above. The IO band of iodoso-1,1,1,2-tetrafluoroethane absorbs within $\sim 1\text{ cm}^{-1}$ of the same band of $\text{CF}_3\text{CH}_2\text{IO}$, indicating that it is the trifluoromethyl group that has the greatest effect on the wavenumber of the ν_{IO} band and not the middle carbon group, i.e. CH_2 or CHF . Finally, comparison of iodoso-1,1,2,2-tetrafluoroethane, $\text{CF}_2\text{HCF}_2\text{IO}$, with the other iodoso-species is interesting as this species has an incomplete CX_3 group (i.e. not all H's of F's), and as expected the bands detected absorbed at lower wavenumber than those of any of the other polyfluoro-species, but higher than those of the hydrated iodoso-species. For completeness, the infrared bands of two other iodoso-species have been reported, absorbing at much higher wavenumbers: iodosochloride, ClI-O ,¹⁹ (779.1 cm^{-1}) and HIO (781 cm^{-1}).⁴⁶ The high wavenumber of ClIO has been accounted for by the strong electron withdrawing effect of the chlorine atom.²¹

5.5 CONCLUDING REMARKS

In this chapter, a number of novel iodoso- and hypiodo-intermediates have been detected by infrared spectroscopy as well as some formyl chloride, methanal and carbon monoxide complexes. All these species have been compared with other similar species, and where appropriate these complexes have enabled series of complexes to be studied, for example the formyl chloride...HX complexes.

We have also detected a dramatic change between the photochemistry of the mono- and di-iodinated methanes. This change does not appear to be due to any steric effects, and the exact reason is still unknown; the study of other di-iodo-species might yield further information, as would a further computational study. The use of the semi-empirical calculations to follow the change between iodoso- (XC-IO) and the hypiodo-species (XC-OI), demonstrates the use of such calculations, and others (*ab initio*), as complementary tools to these matrix studies.

Table 5.1. The infrared bands /cm⁻¹ of chloriodomethane, CH₂CI, trapped in a variety of matrices at 14 K.

Ar	O ₂	¹⁶ O ₃ /Ar	¹⁸ O ₃ /Ar	assignment
4448.1w	4434.6m	4435.6s	4464.0mw	($\delta + \nu_a$)CH ₂
4171.3w	4165.1m	4162.3s	4168.9mw	($\nu_a + \omega$)CH ₂
3727.2m		3846.3w	3857.9mw	($\nu_s + \rho$)CH ₂
3068.1m	3059.4m	3059.2vs	3070.0m	ν_a CH ₂
2996.7w	2989.0m	2990.0m	3001.6mw	ν_s CH ₂
	2582.5w	2584.5w	2589.3w	($\delta + \omega$)CH ₂
2179.0w	2180.4w	2178.5w	2183.8w	($\delta + \rho$)CH ₂
1598.9m	1594.1w		1470.2w	2 ρ CH ₂
1450.4w	1453.3w	1442.7w	1461.0w	2 ν_{CCI}
			1450.9w	
1398.8mw	1397.8m	1396.4s	1400.7mw	δ CH ₂
1384.8w	1386.7w	1385.3sh	1384.8w	ω CH ₂ + δ_{CCI} ^a
1374.2w	1372.8w		1356.4w	
1322.5w		1321.6m	1323.6mw	
1187.1s	1182.3s	1185.2vs	1186.7vs	ω CH ₂
1146.1mw	1146.6m	1145.7m	1141.3m	
1120.6mw	1118.7mw	1140.4m	1114.3w	
1103.7w		1114.3m	1104.7mw	
1065.6w	1049.7w	1066.1w	1061.8w	2 ν_{CI}
1050.7w				
942.7w	939.3m			$\nu_{\text{CCI}} + \delta_{\text{CCI}}$
924.3w	922.9m	923.9wm	923.9mw	
918.1w	917.1m	918.1sh	919.0w	
808.6w	806.7m			ρ CH ₂
792.2m	790.3s	793.9vs	792.2s	ν_{CCI}
		744.0s		
733.6vs	733.6vs	731.7s	735.6vs	
		728.1m		
540.0mw	541.0w	543.4w	541.0w	ν_{CI}

^a- $\delta_{\text{Cl-C-I}} \sim 200 \text{ cm}^{-1}$

Table 5.2. Infrared bands /cm⁻¹ assigned to ozone after deposition of mixed isotopomer ozone, ¹⁶O_{3-x}¹⁸O_x, and chloriodomethane in argon at 14 K.

ν_1	ν_2	ν_3	$\nu_1 + \nu_3$	assignment ^b
1105.2vw	704.0w	1039.1ms	2111.0w	16-16-16
		1035.7m	2108.1w	c
		1033.3m	2140.9sh	c
			2138.5w	
1090.2w	687.6w	1025.6s	2090.2w	16-16-18
		1019.8m	2087.3w	c
		1017.9m		c
	671.2vw	1016.4m	2059.9w	18-16-18
		1013.1mw	2057.0w	c
		1010.2mw		c
	696.3vw	1005.8m	2049.7w	16-18-16
		1002.4mw	2047.3vw	c
		1000.0mw		c
	1061.3w	680.4w	991.4s	2027.1w
<i>a</i>			2024.2w	c
986.5br,m				c
1040.1	667.8 w	982.2m		18-18-18
		978.8mw		c
		976.4mw		c

^a-obscured band; ^b-represents the isotopomer arrangement of ozone, ^c-complex bands.

Table 5.3. Infrared bands /cm⁻¹ of the group 2 species iodosochloromethane, CH₂ClIO, formed after near-infrared ($\lambda > 650$ nm) photolysis of an argon matrix containing chloriodomethane and ozone.

¹⁶ O ₃ /Ar	¹⁶ O _{3-x} ¹⁸ O _x /Ar	¹⁸ O ₃ /Ar	assignment
2962.0m	2966.8w 2960.1w	2965.9m 2959.1w	ν CH ₂
1215.1m 1211.2m 1205.4m 1202.6m 1201.1m,sh		1213.2mw	δ CH ₂
1198.7sh,m 1195.3sh,m			ω CH ₂
1157.7m	1156.7m	1157.2m	δ CH ₂
748.1m	755.1m	754.1ms	ν CCl
723.5s	728.3m 690.5m	690.0s	ν IO
542.9w 532.8w 528.9w		539.6w	ν Cl

Table 5.4. Infrared bands /cm⁻¹ of the group 3 species, hypoiodochloromethane, H₂ClCOI, formed after visible irradiation ($\lambda > 450$ nm).

¹⁶ O ₃ /Ar	¹⁶ O _{3-x} ¹⁸ O _x /Ar	¹⁸ O ₃ /Ar	assignment
1062.2m	1054.5w	1034.8m	ν CO
579.6sh,w 576.7w	578.6w 554.5w	549.7w	ν OI

Table 5.5. Infrared bands /cm⁻¹ of the group 4 species, formyl chloride and the formyl chloride...HI (HCl) complex.

O ₂	¹⁶ O ₃ /Ar	¹⁶ O _{3-x} ¹⁸ O _x /Ar	¹⁸ O ₃ /Ar	assignment ^a
2985.2mw	2987.6s	2967.3w 2959.6w 2945.0w		v _{CH}
1773.0m	1778.3s 1769w 1762.8s	1778.3m 1770.6w 1761.9s 1738.7m 1730vw 1720.9s	1739.2s 1728.3w ^b 1721.4vs	v _{C=O} ...Ar ...HI
1747.9s	1756.6w 1748.9w		1710.8sh 1686.2m	v _{C=O} ...HCl 2v _x
1307.2w	1306.2w 1244.5w	1311.0w 1308.6w 1242.1w	1311.0w 1142.3m	δ _{CH} δ _{CH}
			951.3w 935.9w	v _{o-o-p}
792.2s	794.4vs 770.0mw 748.1m	749.3s	799.0m 748.8s	v _{CCl}

^a- ...Ar, ...HI or ...HCl represents the second species in the formyl chloride...X complexes; ^b-band wavenumber deduced following deconvolution of the very strong band at 1721.4 cm.⁻¹

Table 5.6 Infrared bands /cm⁻¹ assigned to the carbon monoxide...HX complex, OC...HCl...HI (group 5).

O ₂	¹⁶ O ₃ /Ar	¹⁶ O _{3-x} ¹⁸ O _x /Ar	¹⁸ O ₃ /Ar	assignment	
		2787.5m	2789.9m	2790.4m	v _{HCl}
2142.8mw	2151.5m 2141.4m	2152.4m 2101.3m	2100.8m 2087.3m	v _{CO}	

Table 5.7. Infrared bands /cm⁻¹ of diiodomethane in various matrices at 14 K.

Ar	O ₂	¹⁶ O ₃ /Ar	¹⁸ O ₃ /Ar	assignment
3029.8mw		3029.5w		v _a CH ₂
2944vs	2967.8sh,s;2962.7s 2958.2ms; 2954.1s 2948.3ms; 2944.9ms 2935.3m; 2929.8m 2925.7m	2945vs		v _s CH ₂
2911.1sh,s 2902.9sh,m		2911.5s 2901.6ms		vCH ₂
2893.4sh,mw 2874.5s 2865.1s 2858.8s 2847.3m 2801.1w	2874.7m 2867.3m; 2862.5m	2893.5m 2865br,s 2849.0m 2801.8w		vCH ₂
2679.9w 2674.7w 2660.5w 2654.2w		2681.0w 2660.3w		
1466.8s 1462.6s 1452vs	1468.0w 1463.7w 1455.4s, 1451.9m 1449.1sh,mw	1467.1m 1462.9m 1454.6s ⁴ 1450vs		δCH ₂
1442.5sh,s 1431.4m	1442.8w 1432.2w	1442.3ms 1431.6m		
1359.8w 1355.5s 1343.2vs 1335.5w	1357.9w 1356.0w 1344.2w 1336.3w	1360.3w 1355.7ms 1343.3s 1335.6mw		δCH ₂
1271.5w	1274.2sh,mw 1271.9m 1265.6mw	1273.5sh,s 1271.1vs		
1263.0s	1262.4mw	1262.9s		
1217.8vs 1187.1w	1216.4m	1216.3vs 1187.7w	1188.7vw	ωCH ₂
1149.1w 1134.9m 1120.8w	1150.4vw 1135.1vw 1115.4s; 1113vs	1148.8w 1135.2w 1120.9w	1148.9vw 1112.7mw	

Table 5.7 contd.

1101.4ms	1102.0w	1101.1m	
1090.9w		1090.9m	
1076.0w		1075.6w	
1052.9w		1052.8w	
1032.0mw	1035.2w		
1017.0s	1017.1w	1016.6ms	
998.4s; 995.7s	999.0m	996.2vs	999.4w
941.7s	997.9m		992.0m
929.3m	926.3vw	922.6mw	
890.9vs	890.9mw	891.9s; 889.9s	
878.8mw	874.0w	878.9s;	
871.0s	872.1w	870.8m	
864.7s	862.2w	864.0sh,mw	
860.8s	860.3w	860.6m	
853.7m	854.0w	852.4mw	
820vs	821.4m	820vs	ρCH_2
808.7s	807.6w	808.1m	
804.0w		804.2w	
789.9w	788.7w	790.2w	
734vs	738.4s	736.5vs	733.2vw
720.6mw	712.2m	720.4w	718.3vw
689vs	690.5mw	689.6s	681.0w
		655.4w	657.9w
644.7m	644.5vw	643.1w	652.7w
	589.0m		587.8sh,w
	575.8w		581.8mw
	564.7w; 561.9w	564.5w	568.4w

Table 5.8. Infrared bands /cm⁻¹ of the products detected after quartz-filtered photolysis of diiodomethane in an ozone /Ar (¹⁶O₃ and ¹⁸O₃) and solid oxygen matrix.

O ₂	¹⁶ O ₃ /Ar	¹⁸ O ₃ /Ar	assignment
2149.9w		2094.1vw	v _{CO}
1734.4w	1720.7w	1706.1w	v _{C=O}
1719.2w		1693.5w	
1594.3w			
1498.9vw	1395br,vw		vCOH ₂
1496.6vw			
1491.2w			
1247vw ^a	1230.3vw		vCOH ₂
1130.4vw			
655.7vw		747.3vw	
617.9vw		696.0vw	
		687.6vw	

Table 5.9.a Z-Matrix^a of iodosochloromethane, H₂ClC-I-O (C-I-O angle ~ 99°) calculated using MOPAC^r (AM1 Hamiltonian).

atom number	chemical symbol	bond length /Å	bond angle /deg	torsional angle /deg	N _a	N _b	N _c
I	N _a	N _a :I	N _b :N _a :I	N _c :N _b :N _a :I			
1	C						
2	I	2.1			1		
3	O	1.94	98.80		2	1	
4	Cl	1.70	114.66	135.0	1	2	3
5	H	1.11	105.08	-103.0	1	2	3
6	H	1.11	105.20	15.0	1	2	3

^a- Z-matrix = matrix of atoms, bond lengths and bond angles.

Table 5.9.b Z-Matrix of hypiodochloromethane, CH₂Cl-O-I (C-I-O angle ~ 28°)

atom number	chemical symbol	bond length /Å	bond angle /deg	torsional angle /deg	N _a	N _b	N _c
I	N _a	N _a :I	N _b :N _a :I	N _c :N _b :N _a :I			
1	C						
2	I	2.82			1		
3	O	1.98	27.52		2	1	
4	Cl	1.76	147.39	-11.40	1	2	3
5	H	1.12	93.63	118.69	1	2	3
6	H	1.12	87.27	-129.09	1	2	3

Table 5.9.c Interatomic distances /Å^{a,b}

	C 1	I 2	O 3	Cl 4	H 5	H 6
C 1	0.00	2.12^a	3.09	1.70	1.11	1.11
I 2	2.82 ^b	0.00	1.94	3.23	2.64	2.64
O 3	<i>1.40</i>	<i>1.98</i>	0.00	4.48	3.62	2.86
Cl 4	<i>1.76</i>	<i>4.41</i>	<i>2.55</i>	0.00	2.34	2.32
H 5	<i>1.12</i>	<i>3.10</i>	<i>2.09</i>	<i>2.35</i>	0.00	1.84
H 6	<i>1.12</i>	<i>2.98</i>	<i>2.10</i>	<i>2.34</i>	<i>1.86</i>	0.00

^a- the interatomic distances in bold relate to iodosochloromethane (H₂ClC-I-O);^b- those in italics relate to hypiodochloromethane (H₂ClC-O-I).

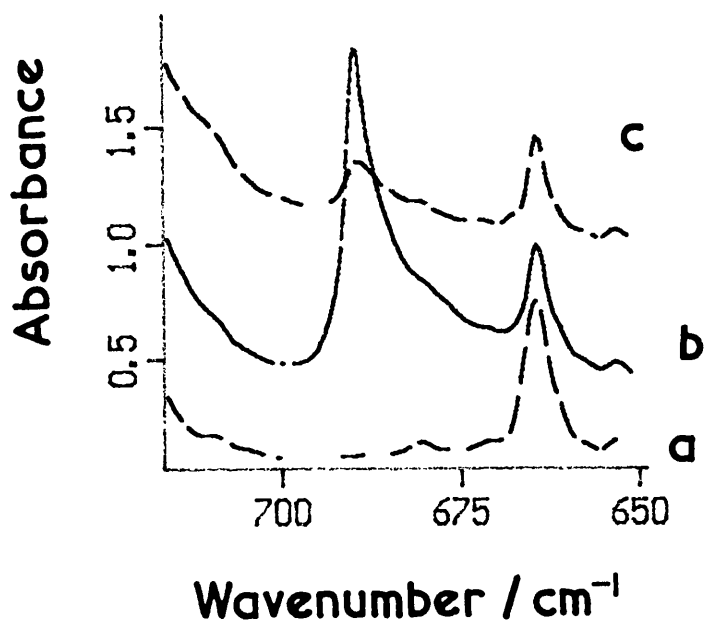


Figure 5.1. Infrared spectra of in the region 700-650 cm^{-1} of an argon matrix containing chloriodomethane and $^{18}\text{O}_3$ after (a) deposition, (b) near infrared photolysis ($\lambda > 650 \text{ nm}$) and (c) UV-vis photolysis ($\lambda > 350 \text{ nm}$) showing the $\text{I}-^{18}\text{O}$ band of the group 2 species iodosochloromethane, $\text{CH}_2\text{ClI}^{18}\text{O}$.

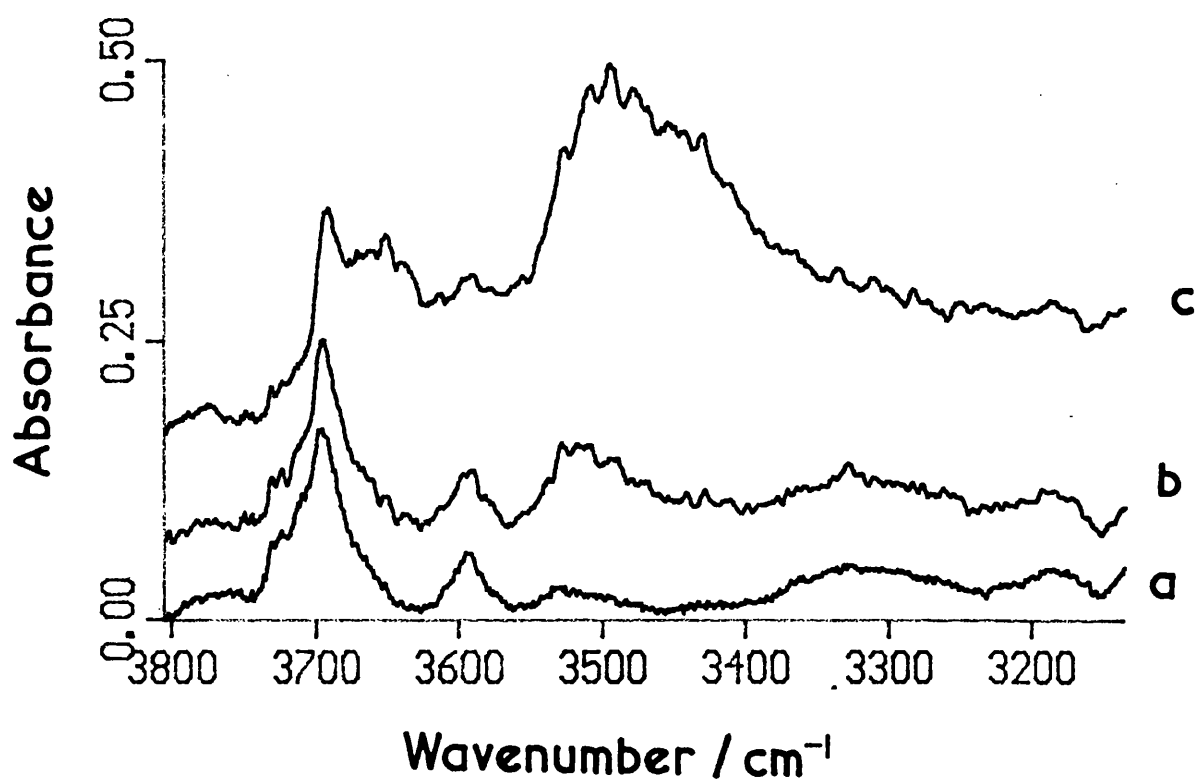


Figure 5.2. Infrared spectra of an argon matrix containing chloriodomethane and $^{18}\text{O}_3$ after (a) deposition, (b) visible photolysis ($\lambda > 450$ nm), and (c) Pyrex-filtered photolysis ($\lambda > 290$ nm). The spectra show the band attributed possibly to the ^{18}O -H stretch of hydrogen hypoiodide, HOI.

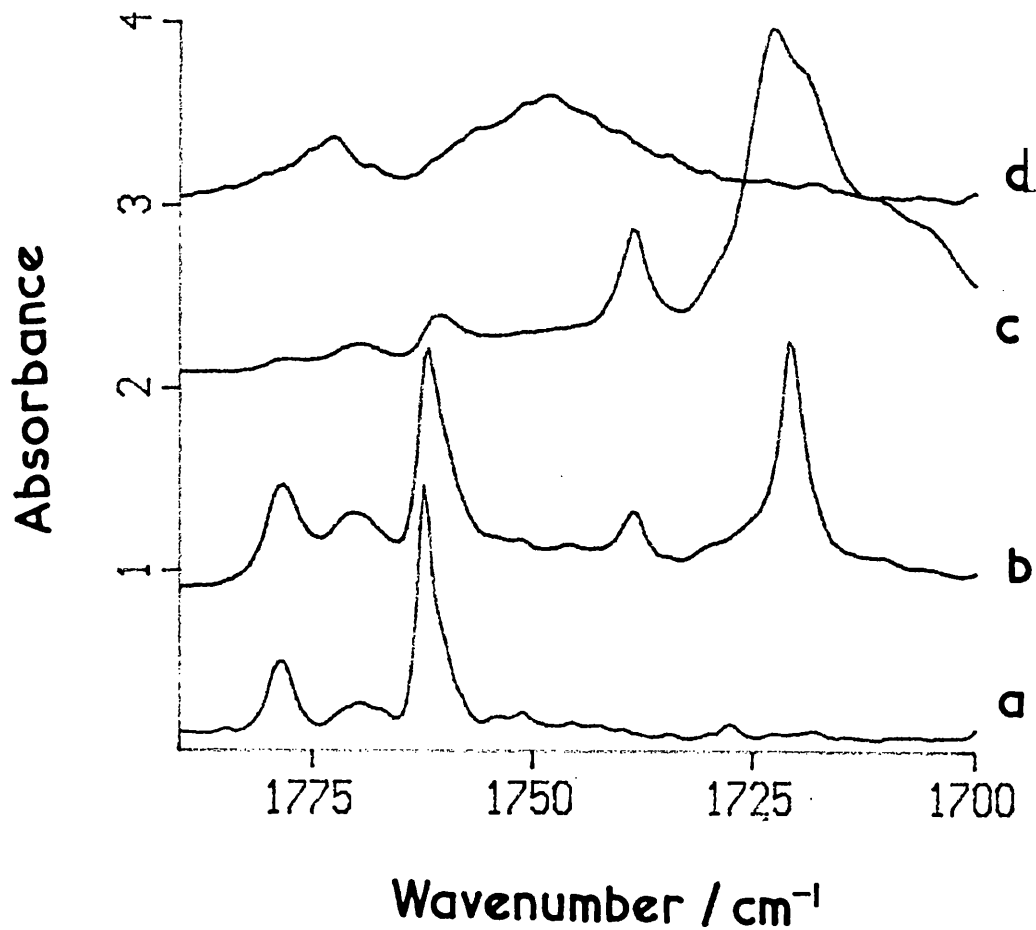


Figure 5.3. Infrared spectra recorded after Pyrex-filtered photolysis ($\lambda > 290$ nm) of chloriodomethane in the following matrices; (a) $^{16}\text{O}_3/\text{Ar}$, (b) $^{16}\text{O}_{3-x}^{18}\text{O}_x/\text{Ar}$, (c) $^{18}\text{O}_3/\text{Ar}$ and, (d) in a solid oxygen matrix. The spectra show the band attributed to the ^{16}O - and ^{18}O -isotopomers of the formyl chloride...HX complexes (group 4).

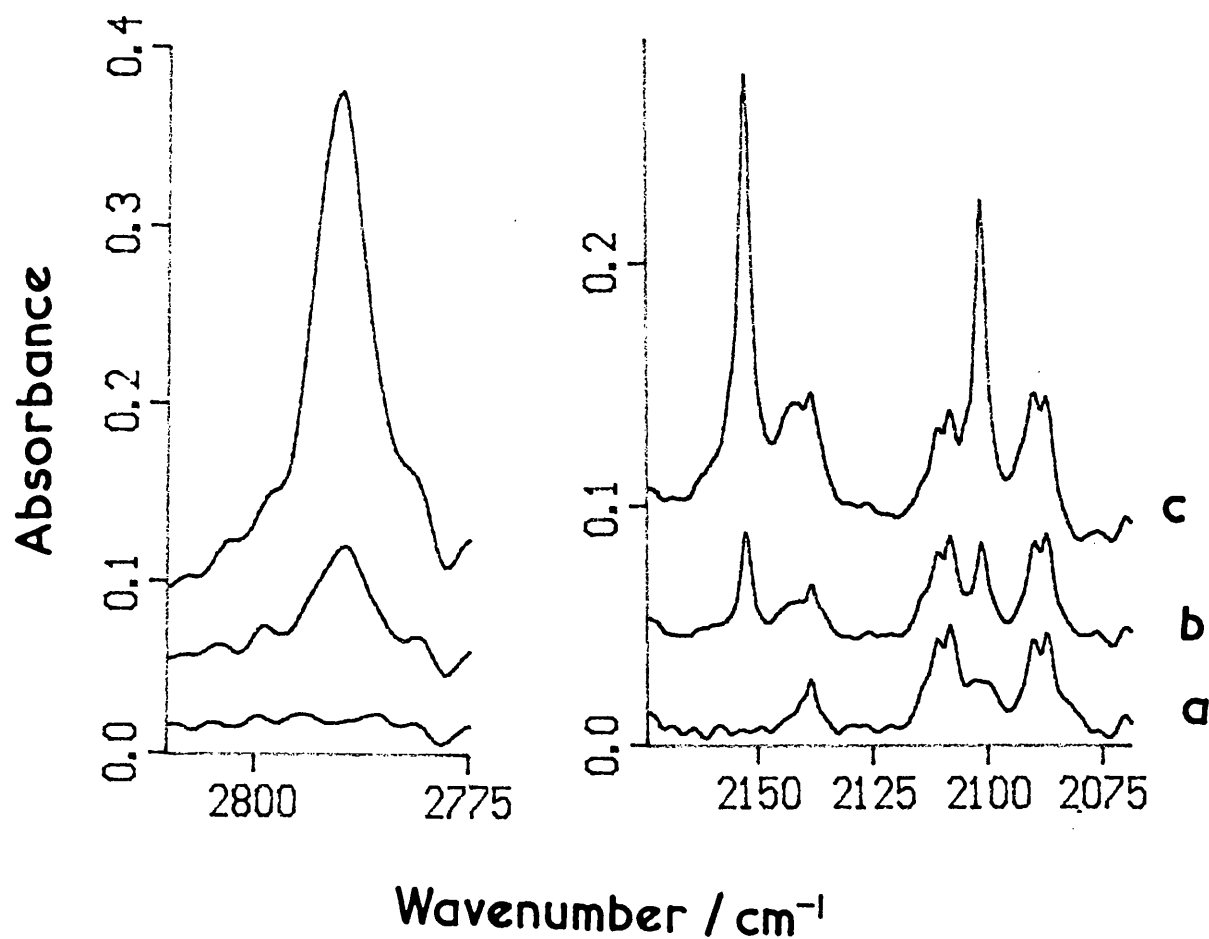


Figure 5.4. Infrared spectra of argon matrices containing CH_2ClI and $^{16}\text{O}_{3-x}^{18}\text{O}_x$ after (a) deposition, (b) visible photolysis ($\lambda > 410 \text{ nm}$) and, (c) Pyrex-filtered photolysis. The spectra shows the ν_{HCl} (2800-2775 cm^{-1}) and ν_{CO} regions (2175-2075 cm^{-1}).

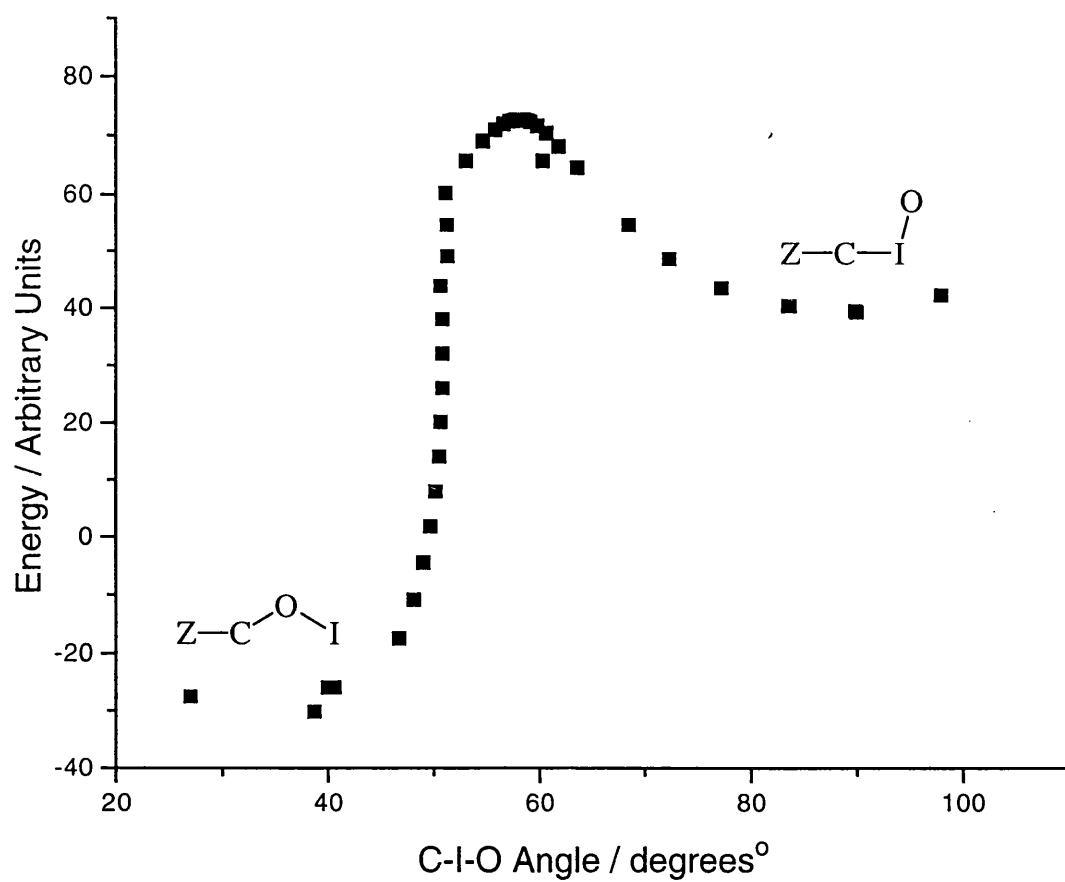


Figure 5.5. Plot of energy (arbitrary units) *versus* C-I-O angle (deg) calculated using MOPAC⁹² (AM1 Hamiltonian). The plot shows the energy path between the two species iodosochloromethane (C-I-O angle ~ 99°) and hypiodochloromethane (C-I-O ~ 28°) via a simple change in the position of the IO unit relative to the rest of the molecule.

Chapter 6

REACTION OF OXYGEN ATOMS WITH BROMOCHLOROMETHANES

6.1 INTRODUCTION

In earlier studies, the reaction of oxygen atoms with dihalomethanes and trihalomethanes has led to the production of carbonyl and carbon monoxide complexes. For the dichloro- and dibromomethanes⁸⁷ the favoured carbonyl product is formyl halide, perturbed by the hydracid, HX, and thus the complexes COHCl...HCl and COHBr...HBr, respectively, were detected. These carbonyl...HX complexes have been shown to dissociate after further photolysis to form carbon monoxide...hydracid complexes, $(CO)_n(HX)_m$. For the reaction of O atoms with dibromo-⁸⁷ and diiodomethane (chapter 5), methanal was also detected as a product. In a similar manner to the dihalomethanes, trichloromethane reacted with oxygen atoms and produced the formyl chloride...chlorine, COHCl...Cl₂, and carbonyl dichloride...hydrogen chloride, COCl₂...HCl, complexes. These carbonyl complexes dissociated further to complexes of carbon monoxide with chlorine and hydrogen chloride.

In this chapter the aim is to study the reaction of bromochloromethane, CH₂BrCl, and dibromochloromethane, CHBr₂Cl, with oxygen atoms, and to detect a range of carbonyl and carbon monoxide complexes for which comparisons can be made both between the complexes detected in this work and elsewhere.

6.2 BROMOCHLOROMETHANE, CH₂BrCl

Since bromochloromethane has two different halogen atoms, its reaction with oxygen atoms is expected to produce the complexes COHCl...HBr, COHBr...HCl and (CO)_n(HCl)(HBr); as well as the possibility that COH₂...BrCl and COBrCl...H₂ may be formed. These complexes can be compared with those detected after the reaction of O atoms with dichloromethane,⁸⁷ dibromomethane⁸⁷ and chloriodomethane (chapter 5) for example, it should be possible to compare the complexes of formyl chloride with HCl,⁸⁷ HBr (this chapter) and HI (chapter 5). In addition to these carbonyl complexes, a variety of carbon monoxide complexes are expected to be formed which, like the carbonyl complexes, can be compared with complexes seen elsewhere.^{95,96,102,103}

6.2.1 RESULTS

The spectra of CH₂BrCl in argon (CH₂BrCl/Ar = 1:500) and solid oxygen (CH₂BrCl/O₂ = 1:200) matrices are in good agreement (Table 6.1) with that reported for the liquid phase.^{104,105,106} Ultraviolet ($\lambda > 240$ nm) photolysis of CH₂BrCl in an argon matrix produced no new bands.

Bromochloromethane and ozone in argon

The spectra recorded after co-deposition of bromochloromethane and ozone in argon matrices (CH₂BrCl/O₃/Ar = 1:3:600) exhibited bands that could be assigned to either precursor, ozone⁴⁴ or CH₂BrCl (Table 6.1). Thus unlike the situation with iodoethane⁴⁷ (chapter 3) and the other single iodine-containing precursors, no initial complex was formed on deposition. UV-vis ($\lambda > 350$ nm) photolysis of these matrices for 40 min produced no detectable bands, while Pyrex-filtered photolysis, for similar periods, produced only weak bands. Quartz-filtered photolysis, for approx. 40 min,

doubled the intensities of the bands. The increase in intensities of bands seen after quartz-filtered photolysis is in part due to the higher photon throughput of the quartz-filtered arrangement over the Pyrex-filter arrangement. Various matrix experiments were performed in order to increase the intensities of the product bands; the first of these, varying the deposition ratio $\text{CH}_2\text{BrCl}/\text{O}_3/\text{Ar}$, made no difference to the photochemistry, only to the intensity of the precursor bands, due simply to the reduced or increased concentrations of precursors. The most diagnostic experiments concerned photolysis at fixed wavelengths, for varying time intervals. Using this technique the evolution of the products with time has been studied in order to elucidate the mechanism.

The following bands were detected after quartz-filtered photolysis (Tables 6.2 and 6.3) and they provide evidence for a range of complexes. For clarity the bands are grouped according to the product species to which they can be attributed, i.e. carbonyl, HCl, HBr or CO.

Carbonyl species. These bands are formed after photolysis with Pyrex- and quartz-filtered radiation (Table 6.3, Fig. 6.1). They increase in intensity as photolysis time increases, up to ~ 50 h at which point these bands begin to decrease in intensity (Fig. 6.2). It would appear from the band wavenumbers and photochemical behaviour that a number of carbonyl species have been detected. The first group of bands, attributed to the first carbonyl product, is assigned as follows: the strong band at 1756.6 cm^{-1} , its medium intensity shoulder at 1752.2 cm^{-1} and the weak band at 1748.8 cm^{-1} are assigned to carbonyl stretches. Weak bands at 1315.8 and 1313.6 cm^{-1} are assigned to C-H bends, while weak bands at 962.9 and 941.2 cm^{-1} are assigned to out-of-plane vibrations. Strong and medium bands at 745.1 and 742.4 cm^{-1} respectively, and medium-weak bands at 766 , 756.0 and 725.0 cm^{-1} are assigned to C-Cl stretches. Additional, weak combination bands were detected between 1190.0 and 1117.9 cm^{-1} . Detection of this first group of bands suggests that the carbonyl responsible is formyl chloride, COHCl .

A second group of bands, attributed to the second carbonyl, is detected having

much lower intensities even after similar photolysis conditions. These bands are detected as weak and very weak bands at 1801.5 and 1753.0 cm^{-1} respectively, assigned to carbonyl stretches. Weak bands at 1287.4, 1283.3, 1279.7 and 1272.6 cm^{-1} are assigned to C-H bends. A very weak band at 867.4 cm^{-1} is assigned to the out-of-plane vibration, and the very weak bands at 685.2 and 681.8 cm^{-1} to C-Br stretches. A very weak overtone band at 1775.7 cm^{-1} and combination bands at 1090.2 and 1067.0 cm^{-1} are also detected. This group of bands is attributed to formyl bromide, COHBr.

Finally, a weak band at 1817.3 cm^{-1} is assigned to a carbonyl stretch, while weak and medium-weak bands at 809.1, 805.2, 800.0 and 797.5 cm^{-1} are assigned to C-Cl stretches, this third group being attributed tentatively to carbonyl bromide chloride, COBrCl.

Hydrogen bromide species. These bands are formed after UV irradiation, and are detected in the HBr stretching region (Table 6.3, Fig. 6.3) as a strong band at 2507.3 cm^{-1} , a medium band at 2500.6 cm^{-1} and weak bands at 2492.0 and 2479.0 cm^{-1} . The wavenumber shifts of these bands from that of HBr¹⁰⁷ isolated in argon at 2560 cm^{-1} suggests that HBr is present in a number of different environments, and hence in different complexes. The exact nature of these complexes will be considered in the discussion.

Hydrogen chloride species. These bands are formed after UV photolysis and increased in intensities after each successive irradiation cycle. These bands were detected in the ν_{HCl} region as a strong band at 2783.6 cm^{-1} , a weak band at 2812.5 cm^{-1} and a very weak band at 2828.5 cm^{-1} (Table 6.3, Fig. 6.3). Like the HBr bands, the wavenumbers of these HCl bands relative to those of isolated HCl provides us with information about the relative environments. Thus as above it is considered that a number of complexes of the form $(\text{CO})_x(\text{HCl})_y(\text{HBr})_z$ may be present.

Carbon monoxide species. Like the HCl bands, these bands (Table 6.3 and Fig. 6.3) are formed after UV photolysis and they increased in intensities after successive irradiation cycles (Fig. 6.2). The spectra of these CO complexes gave rise

to a strong band at 2154.9 cm^{-1} and weak bands at 2149.0 , 2142.5 and 2138.1 cm^{-1} . The weak band at 2138.1 cm^{-1} has been assigned to isolated CO in an argon matrix,⁹⁰ while the remaining bands are assigned to one of the $(\text{CO})_x(\text{HCl})_y(\text{HBr})_z$ complexes.

6.2.2 DISCUSSION

The bands detected directly after co-deposition of the precursors, CH_2BrCl and ozone,⁴⁴ are assigned (Table 6.1) to modes of the precursors, with no bands of any complex being detected. Ultraviolet irradiation for tens of hours was required before any products were detected. This differs markedly from the reaction of ozone with the mono-iodinated precursors in which a complex with ozone was formed after deposition, and products were detected after ~ 10 - 20 min of near-infrared photolysis. The reaction of ozone with CH_2BrCl proceeds after Pyrex- and quartz-filtered photolysis, since these photolysis ranges dissociate ozone to produce both ground state and excited state oxygen atoms. It therefore seems likely that both atomic states of oxygen behave in a similar manner, i.e. insert into the weaker C-Br bond, like the reaction of ozone with the iodine-containing compounds (see chapters 3-5).

The bands detected after photolysis of bromochloromethane and ozone in argon matrices have been attributed to a number of species based on the wavenumbers of the bands. These species are discussed below.

Formyl chloride complexes. Various bands formed after Pyrex- and quartz-filtered irradiation are attributed to formyl chloride complexes. The most diagnostic bands are those assigned to the carbonyl stretch, in this case the strong band at 1756.6 cm^{-1} . The wavenumber of the carbonyl band and detection of a ν_{HBr} band, and their photochemical behaviour, support the assignment to the formyl chloride...hydrogen bromide complex, $\text{COHCl}\dots\text{HBr}$. For comparison we can compare the $\nu_{\text{C=O}}$ bands (Table 6.4) of the formyl chloride complexes with HCl (1756.7 , 1753 and 1751.3 cm^{-1})⁸⁷ and HI (1761.9 cm^{-1}).^{chapter 5} These bands shift to lower wavenumbers as the Lewis

acid strength increases, e.g. hydrogen chloride complexed with formyl chloride causes the carbonyl stretching band to shift the furthest (red shift) from the wavenumber of the band (1783 cm^{-1}) assigned to isolated formyl chloride⁸⁷ in argon.

Two other weaker $\nu_{\text{C=O}}$ bands were detected at 1781.5 and 1748.9 cm^{-1} and the first is assigned to formyl chloride isolated in argon, while the second is assigned to the carbonyl in a more highly perturbing environment, such as two hydracids the second hydracid coming from a second carbonyl complex. This latter band can be compared with a band detected at 1748.9 cm^{-1} in the spectrum of the reaction products of chloriodomethane with ozone (chapter 5) for which a similar assignment is given.

Formyl bromide complexes. These bands are formed under similar conditions to the formyl chloride complexes above, only with much lower intensities. Again the most diagnostic bands (Table 6.2) are those assigned to the carbonyl stretch, and in particular the medium band at 1753.0 cm^{-1} assigned to the complex $\text{COHBr}\dots\text{HCl}$. Comparison of this band with those assigned to the complex $\text{COHBr}\dots\text{HBr}$ (1756.3 and 1754.9 cm^{-1})⁸⁷ supports this assignment, and as expected the bands follow the trend of Lewis acid strength, i.e. the carbonyl bands are shifted further for the complex perturbed by HCl. Another weak carbonyl band at 1801.5 cm^{-1} has been attributed to formyl bromide isolated in argon.

Carbonyl bromide chloride complexes. Bands for this complex were detected at 1817.3 cm^{-1} and between $810\text{-}797\text{ cm}^{-1}$ and, being in good agreement with the previously reported gas phase¹⁰⁸ bands, are assigned to carbonyl bromide chloride, COBrCl . These bands are significantly weaker than those assigned to either formyl chloride or formyl bromide. Assuming that the carbonyl stretch of these three carbonyls have similar infrared absorption coefficients, then formyl chloride can be assumed to be present in the greatest quantity. This result parallels the gas phase reaction of bromochloromethane and ozone¹⁰⁹ in which the major product was formyl chloride ($> 70\%$).

We can also compare the range of products detected here with those detected in the dichloro- and dibromomethane⁸⁷ reactions with ozone; in all cases the

dissociation of HX and the formation of formyl halide is the favoured product. But, with dibromomethane, methanal was reported as a minor product, whereas in these studies no methanal was detected, and instead we detected evidence for carbonyl bromide chloride.

(OC)(HCl)(HBr) complex. Bands attributed to CO, HCl and HBr were detected and are attributed to either the complex OC...HCl...HBr or OC...HBr...HCl (Table 6.3). It has been previously reported⁹⁵ that for the complex OC...(HCl)^a...(HCl)^b distinct bands can be assigned for HCl, in either the *a* or *b* position in the complex, this being supported in a number of similar complexes.^{87,88,95,96,102,107} Thus HCl in the *a* position absorbs ^{at} 2791.3 to 2780.5 cm⁻¹ while in the *b* position between 2811.2 to 2803.0 cm⁻¹. For the complex, OC...(HBr)₂^{87,102} a similar behaviour has been noted with HBr bands in the *a* position absorbing at c. 2509.7 cm⁻¹ while in the *b* position at c. 2484.8 cm⁻¹. Thus the strong bands detected at 2783.6 and 2507.3 cm⁻¹ in this study are attributed to HCl in the *a* position and HBr in the *b* position of the complex OC...HCl...HBr. The band attributed to CO (2154.9 cm⁻¹) in this complex has a wavenumber intermediate between that of the CO band in the complexes⁸⁷ OC...(HCl)₂ and OC...(HBr)₂ at 2156 and 2153 cm⁻¹ respectively, providing further support for assignment to this complex. For comparison the wavenumbers of the HCl bands in the *a* position of the following complexes can be compared, OC...HCl...HCl,^{87,88,95,96,102,107} (2791.3 - 2780.5 cm⁻¹) OC...HCl...HBr^{ch.6} (2783.6 cm⁻¹) and OC...HCl...HI^{ch.5} (2787.5 cm⁻¹), again the trend is observed in which the stronger Lewis acid shifts the band to lower wavenumbers (i.e. more perturbed from isolated HCl¹⁰⁷ in argon at 2869 cm⁻¹). The HBr band in OC...HCl...HBr is shifted to lower wavenumbers (by 2.4 cm⁻¹) relative to that in OC...(HBr)₂ due to the greater perturbation of the accompanying HCl.

A second group of weak bands at 2812.5, 2479.0 and 2149.0 cm⁻¹ are attributed to HCl in the *b* position, HBr in the *a* position and CO, respectively, and hence the complex OC...HBr...HCl. As expected the relative wavenumbers of the HCl and HBr bands are in good agreement with the complexes reported above and the wavenumber shifts are in keeping with the new complex having different HX partners, these having

differing Lewis acid character

Other carbon monoxide complexes. The remaining HCl, HBr and CO bands are assigned as follows: the very weak HCl band at 2828.5 cm^{-1} is assigned to a one-to-one complex between HCl and CO, based on the similarity to bands detected previously.⁹⁶ The very weak CO band at 2142.5 cm^{-1} is assigned to a complex between two carbon monoxides and one hydricid, HX, i.e. $(\text{CO})_2(\text{HX})$, again due to its similarity to previously detected^{187,88,95,96,102,107} bands. The medium intensity HBr band at 2500.6 cm^{-1} would be expected to belong to one or other of the $\text{OC}\dots\text{HX}^a\dots\text{HX}^b$ complexes involving HCl and HBr in either *a* or *b* positions, however the wavenumber is intermediate between the two, and comparison of the relative intensities suggests that the bands arise from a third complex having a different geometric arrangement, i.e. $\text{HBr}\dots\text{CO}\dots\text{HCl}$.

Warming of the matrix to 25 K appeared to have no effect on any of these bands indicating that the complexes are formed in a thermally stable environment. This result supports the assumption, made here, that the two $(\text{OC})(\text{HCl})(\text{HBr})$ complexes exhibit a strongly hydrogen-bonded arrangement.

Photochemical Interconversion

The reaction of oxygen atoms with bromochloromethane is time-dependent in contrast to the wavelength-dependent reactions discussed in the previous three chapters. As can be seen in Fig. 6.2 (Summary 6.1) the reaction is a two step process in that for short-to-medium photolysis times (0 - 50 h) intermediates (carbonyl complexes) are formed but for longer photolysis times, (50 - 150 h), the intermediates decay to form the final products (carbon monoxide complexes). No evidence was detected for species having C-Br-O or C-O-Br bonds, unlike the reactions with the iodine-containing compounds^{19-21,47} (and chapters 3-5) in which evidence for C-IO_x and C-OI bonds was detected, or the reaction of SiHCCl_3 with O_3 ¹¹⁰ in which the

intermediate HOCCl_3 has been reported. There are a number of possible reactions that could lead to the observed products in this study, with the most likely of these involving O atoms, from ozone or oxygen, inserting into either the C-H, C-Cl or C-Br bonds. It would seem likely that an O atom would insert into the C-Br bond in preference to the C-Cl bond on bond energy grounds, however no distinction can be made between any of these insertions, except to note that the expected products from C-H insertion (COHCl , COHBr and COBrCl) match those detected, as compared to those of C-Br (COHCl and H_2CO) and C-Cl insertion (COHBr and H_2CO).

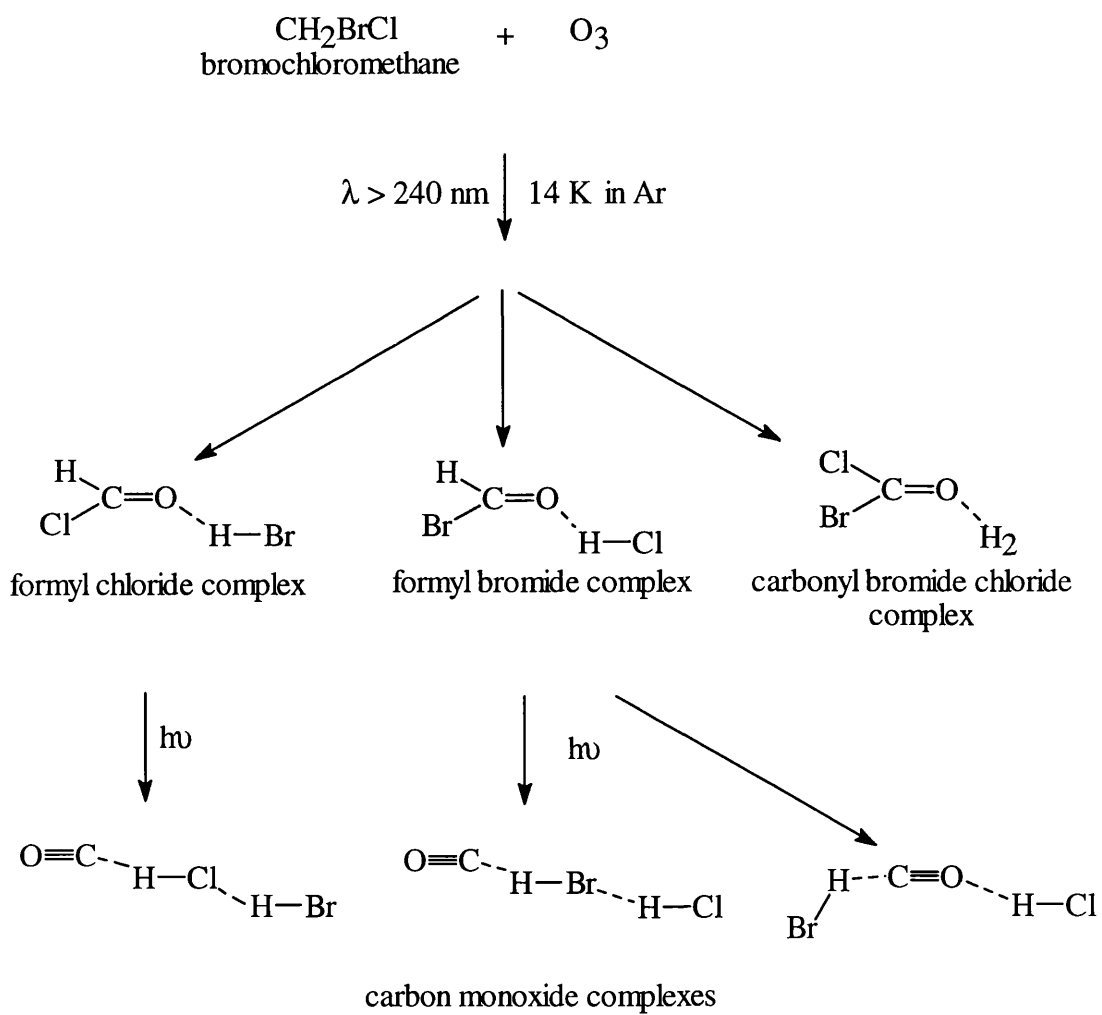
Alternatively, photodissociation of a C-halogen bond (probably Br) of CH_2BrCl to give CH_2Cl and Br atoms, with the latter reacting with oxygen atoms to form formyl chloride may occur. This mechanism may account for the very weak and weak bands at 826.5 and 817.3 cm^{-1} respectively which, although assigned to ν_{CCl} of COBrCl (Table 6.2) could possibly be attributed to CH_2Cl .¹¹¹ However, the lack of detection of bands assignable to BrO^{125} makes this mechanism seem unlikely. Previously, unidentified bands at 817 cm^{-1} were detected in the photochemical reaction of ozone with CHCl_3 ⁸⁸ and CHBr_2Cl (see later), and this band may be attributed to the radical CHCl .¹¹¹ But due to the low intensity any mechanism producing this band is minor at most. A final possibility is that an oxygen atom could add directly to the carbon atom of CH_2BrCl to form a five-centred intermediate which could subsequently rearrange to form a variety of products. This final possibility has not been considered in any great detail due to the broad range of previous studies in which insertion into the C-X bond ($X = \text{H}$ or halogen) seems to be the prevalent mechanism.

Previous *ab initio* calculations carried out for the reaction of $\text{CH}_2\text{Cl}_2/\text{CH}_2\text{Br}_2$ ⁸⁷ with oxygen atoms predicted that the carbonyl product $\text{COHX} \dots \text{HX}$ would be favoured over the product $\text{COX}_2 \dots \text{H}_2$ and over $\text{COH}_2 \dots \text{X}_2$. This calculation fits our experimental results in that the overwhelming product is $\text{COHCl} \dots \text{HBr}$, with low concentrations of $\text{COHBr} \dots \text{HCl}$ and $\text{COBrCl} \dots \text{H}_2$ being formed and no methanal being detected. Interestingly, for the reaction of dibromomethane⁸⁷ and diiodomethane (chapter 5) with O atoms, methanal is formed as an additional product; whilst in the case of CH_2I_2 formyl iodide was not directly detected. Thus there is some measure of disagreement

with theoretical work. Further calculations, e.g. CH_2BrCl , CH_2ClI and CH_2I_2 , might yield interesting results on their reliability for reactions involving C-X bonds (X = Cl, Br, I).

After long photolysis periods another type of product is formed which has been attributed to carbon monoxide...hydracid complexes, formed after dissociation of the formyl halide complexes. The detection of these carbon monoxide complexes confirms that these carbonyl complexes dissociate via molecular elimination to CO and HX. In chapter 7 an alternative dissociation path for carbonyls is discussed.

SUMMARY 6.1



6.3 DIBROMOCHLOROMETHANE, CHBr_2Cl

The reaction of oxygen atoms with dibromochloromethane has been studied. It is expected to produce both carbonyl and carbon monoxide complexes, as in the case of CH_2BrCl (above), CH_2ClI (chapter 5), CH_2Cl_2 ,⁸⁷ CH_2Br_2 ⁸⁷ and CHCl_3 .⁸⁸

6.3.1 RESULTS

The spectra of CHBr_2Cl in argon ($\text{CHBr}_2\text{Cl}/\text{Ar} = 1:450$) and solid oxygen ($\text{CHBr}_2\text{Cl}/\text{O}_2 = 1:150$) matrices were recorded (Table 6.5) and the bands assigned using bromochloromethane and other halomethanes as guides. Ultraviolet ($\lambda > 240$ nm) photolysis of dibromochloromethane in a solid argon matrix produced no new bands.

Dibromochloromethane and ozone in argon

Co-deposition of CHBr_2Cl and ozone in an argon matrix ($\text{O}_3/\text{CHBr}_2\text{Cl}/\text{Ar} = 2/1/400$) produced a number of bands (Table 6.5) that are attributed to either CHBr_2Cl or ozone;⁴⁴ no bands were detected that could be assigned to any complex formed between the two. Several additional experiments were carried out in which the $\text{CHBr}_2\text{Cl}/\text{Ar}$ ratio was varied, but no difference in the reactivity was detected, only an increase or decrease in the intensities of the bands directly related to the concentrations of the precursors in the matrix. Wavelength-dependent photolysis experiments were also carried out. Using UV-vis irradiation ($\lambda > 350$ nm) no new bands were detected, while Pyrex- and quartz-filtered irradiation produced bands having similar wavenumbers; for similar photolysis times the Pyrex-filtered irradiation cycles produced bands having weaker intensities than those detected after quartz-filtered photolysis. The most diagnostic experiments proved to be those time-

dependent studies in which the matrices were photolyzed at fixed wavelengths (quartz-filtered) for varying time periods. The bands detected are grouped into their respective species types, e.g. carbonyls, HCl, HBr and carbon monoxide, and are reported below.

Carbonyl species. A number of bands have been detected and attributed to various carbonyl species (Table 6.6), with the carbonyl stretch, $\nu_{\text{C=O}}$, being the most diagnostic feature in the spectra. It can be seen, Fig. 6.4 and 6.5, that there are four prominent carbonyl stretching bands at 1813.5, 1796.1, 1783.1 and 1753.7 cm^{-1} . The assignment of these and the other weaker bands is based upon their behaviour after time-dependent photolysis and warming of the matrix; thus after 25 h of UV photolysis all the bands increased in intensities. However, after continued photolysis (up to 120 h) the bands at 1779.7 and 1776.3 cm^{-1} reduced in intensities, the bands at 1817.4, 1801.4, 1796.1 and 1794.7 cm^{-1} increased, and the bands at 1813.5, 1783.1 and 1753.7 cm^{-1} remained unchanged. Other bands in the $\nu_{\text{C=O}}$ region were too weak to determine any change in band intensities.

Other bands were detected and are assigned as follows: weak bands at 1307.9, 1302.8 and 1298.5 cm^{-1} are assigned to the C-H bending mode of formyl chloride; after warming the matrix, the band at 1307.9 cm^{-1} is destroyed while the other two remained unchanged indicating the presence of two or more formyl chloride complexes distinguishable by their thermal behaviour. Other weak bands at 1285.9, 1279.7 and 1273.1 cm^{-1} are assigned to the C-H bend of formyl bromide. A group of medium to weak bands between 824.1 and 783.2 cm^{-1} are assigned to the C-Cl stretch of carbonyl bromide chloride. Weak bands at 716.9 and 712.7 cm^{-1} are assigned to the C-Cl stretch of formyl chloride. A weak band at 642.0 cm^{-1} is assigned to the C-Br stretch of formyl bromide. A number of combination bands are also detected, a medium intensity band at 1147.1 cm^{-1} is assigned to the combination of a C-Cl stretch and bend attributed to formyl chloride, while a very weak band at 1073.8 cm^{-1} is assigned to an equivalent combination attributed to formyl bromide. These last two bands, at 1147.1 and 1073.8 cm^{-1} may alternatively be assigned to combination bands attributable to carbonyl bromide chloride, but, given the existence of similar bands

attributed to formyl halide produced in the reaction of ozone with CH_2BrCl the earlier assignment is favoured. Finally, a very weak band at 626.8 cm^{-1} is assigned tentatively to the combination of BrCO and CBrCl bends of carbonyl bromide chloride.

These bands provide evidence for three carbonyl products formyl chloride, formyl bromide and carbonyl bromide chloride, with the bands for the last being the most intense. As has been seen above these carbonyl products are most likely to exist as complexes with the remainder from the precursor species, thus the three carbonyl complexes are $\text{COHCl}\dots\text{Br}_2$, $\text{COHBr}\dots\text{BrCl}$ and $\text{COBrCl}\dots\text{HBr}$.

Hydrogen chloride species. Four bands were detected (Fig. 6.6, Table 6.7) in the ν_{HCl} region. The medium and weak bands at 2813.5 and 2807.6 cm^{-1} respectively, are attributed to HCl in the complexes $\text{OC}\dots\text{X}^a\dots\text{HCl}^b$. The medium and weak bands at 2791.4 and 2794.6 cm^{-1} respectively, are attributed to HCl in the complexes $\text{OC}\dots\text{HCl}^a\dots\text{X}^b$. The detection of two bands assigned to a single complex suggests that two very similar complexes are formed having slightly different geometries.

Hydrogen bromide species. Five weak or very weak bands are detected (Fig. 6.6, Table 6.7) and attributed to HBr in various complexes. These HBr bands were detected with much lower intensities relative to those of HCl and CO ; in comparison the relative intensities of the HCl , HBr and CO bands were approximately equal in the CH_2BrCl experiment (section 6.2). The weak bands at 2510.4 , 2507.8 and 2496.7 cm^{-1} are assigned to HBr in complexes of the type $\text{OC}(\text{X})(\text{HBr})$, while the very weak bands at 2541.6 and 2525.2 cm^{-1} have been assigned to isolated HBr and to the 1:1 complex between CO and HBr , respectively.

Carbon monoxide species. These bands (Table 6.7 and Fig. 6.6) are assigned based on their wavenumber being near to that of isolated carbon monoxide⁹⁰ (2138 cm^{-1}) and that ^{the} carbon monoxide complexes, i.e. $(\text{CO})_n(\text{HX})_m$, have ν_{CO} bands shifted to higher wavenumbers, where the magnitude of the shift is dependent upon the HX species and the geometry of the complex. Thus the medium band at 2157.6 cm^{-1} is

assigned to carbon monoxide in the complex $\text{OC}\dots\text{HCl}\dots\text{Br}_2$, while the medium and medium-weak bands at 2153.1 and 2150.7 cm^{-1} respectively, are assigned to the complex $\text{OC}\dots\text{Br}_2\dots\text{HCl}$. The weak band at 2146.6 cm^{-1} is assigned to a complex such as $\text{BrCl}\dots\text{CO}\dots\text{HBr}$, while the weak bands at 2142.3 and 2138.0 cm^{-1} are assigned to $(\text{X})(\text{CO})_2$ ¹⁰² and isolated CO ,⁹⁰ respectively.

Comparing the intensities of these bands versus time (Fig. 6.5) provides us with the following observations. The HCl bands behave almost identically, e.g. they increased in intensities constantly throughout the entire photolysis period (120 h), indicating that they are formed as both a primary and a secondary product of the reaction. The HBr bands increased in intensities for the first 30 h of photolysis and then stopped increasing, indicating that they are formed as primary products. There are a number of carbon monoxide bands, some behaving differently, indicating the presence of more than one complex. The 2146.6 and 2138.0 cm^{-1} bands behave identically and increased at a rate intermediate between that of the HCl and HBr bands. The rate at which the bands at 2157.6, 2153.1 and 2150.7 cm^{-1} increase varied during the photolysis, possibly indicating that a number of different processes were occurring.

6.3.2 DISCUSSION

Several bands were detected and these are discussed below in terms of the species to which they can be attributed. The first of these was detected directly after deposition, and are attributed to the precursors CHBr_2Cl and O_3 , with no evidence for any complex formation. The lack of complex formation was also supported by the photolysis behaviour, whereby UV irradiation was required before any reaction was detected; if a complex had formed we would have expected the reaction to be initiated with much longer wavelength photolysis, i.e. visible or near-infrared (see chapters 3-5). Thus the reaction of ozone with CHBr_2Cl differs from the reaction with the mono-iodinated species in the photolysis times required to produce products, i.e. in this case

we require tens of hours of photolysis as opposed to minutes in the case of the iodinated alkanes.

Carbonyl bromide chloride complexes. Various bands of carbonyl bromide chloride were detected (Table 6.6) and these are in good agreement with the gas phase spectra.¹⁰⁸ Several $\nu_{\text{C=O}}$ bands were detected, and that at 1824.6 cm^{-1} is attributed to COBrCl isolated in argon, the least perturbed environment in the matrix. The other $\nu_{\text{C=O}}$ bands exhibit wavenumber shifts from this band of 4.9, 7.2, 11.1, 23.2, 28.5 and 29.9 cm^{-1} and are representative of complexes in increasingly perturbing matrix environments. The wavenumbers of these bands, and their shifts from the isolated band at 1824.6 cm^{-1} support the assignment to the complex COBrCl...HBr. These shifts are of a similar magnitude to those reported, above, for carbonyls perturbed by HBr. The possibility exists that the three weak bands at 1824.6, 1819.7 and 1817.4 cm^{-1} detected after 25 h photolysis could be assigned to the carbonyl stretch of COBr₂...HCl, these being in reasonable agreement with the gas phase $\nu_{\text{C=O}}$ band of COBr₂¹¹² at 1828 cm^{-1} however the formation of this complex seems unlikely since it requires the rupture of the two strongest bonds (C-H and C-Cl) while leaving the weaker C-Br bonds intact.

Formyl chloride complexes. These formyl chloride complexes can be most easily distinguished via the carbonyl stretches (Table 6.6 and Fig. 6.4). Thus the weak band at 1779.7 cm^{-1} is assigned to formyl chloride isolated in argon, while the weak band at 1768.1 cm^{-1} is assigned to formyl chloride perturbed by bromine. This band can be compared with the $\nu_{\text{C=O}}$ band of the formyl chloride...Cl₂⁸⁸ complex at 1780.6, 1775.7 and 1760 cm^{-1} for which the wavenumber shift is greater for the stronger Lewis acid. The medium band at 1753.7 cm^{-1} is assigned to formyl chloride in a strongly perturbing environment, probably by at least two Lewis acid species, arising when two neighbouring carbonyls overlap.

Formyl bromide complexes. Like the formyl chloride complexes above, the carbonyl stretch is the most diagnostic band and thus the band at 1783.1 cm^{-1} (Table 6.6 and Fig. 6.4) is assigned to the complex COHBr...BrCl. This band is shifted from

the isolated precursor at 1801.5 cm^{-1} (Table 6.2) by 18.4 cm^{-1} in reasonable agreement to those detected for formyl chloride complexed with chlorine (2.9 , 7.8 and 23.5 cm^{-1})⁸⁸ and bromine^{ch.6} (15.4 cm^{-1}).

(OC)(HCl)(Br₂) complexes. Utilising previous results (section 6.2) in which the position *a* or *b* of HCl can be distinguished in complexes such as $\text{OC}\dots\text{X}^a\dots\text{X}^b$ using the wavenumber of the ν_{HCl} band, the following complexes are identified. The first complex, $\text{CO}\dots\text{Br}_2\dots\text{HCl}$, has ν_{HCl} and ν_{CO} bands at 2813.5 , 2807.6 , 2153.1 and 2150.7 cm^{-1} . The second group of similar bands at 2794.6 , 2791.4 and 2157.6 cm^{-1} are attributed to the complex $\text{OC}\dots\text{HCl}\dots\text{Br}_2$. The bands of the two complexes absorb with similar intensities, and since no evidence for the complex $\text{COBr}_2\dots\text{HCl}$ was detected, it is believed that the two complexes form from photodissociated $\text{COHCl}\dots\text{Br}_2$. The different geometries occur because bromine does not favour a head-to-tail arrangement such as in the $\text{OC}\dots\text{HCl}\dots\text{HBr}$ complexes (section 6.2).

(OC)(BrCl)(HBr) complexes. The bands at 2510.4 and 2507.8 cm^{-1} are assigned to HBr in the complex $\text{OC}\dots\text{BrCl}\dots\text{HBr}$ based on the wavenumbers of the HBr bands in comparison to those of the other carbon monoxide...HBr complexes reported above and elsewhere.^{87,88,95,96,102,107} The bands at 2496.7 and 2146.6 cm^{-1} are assigned to ν_{HBr} and ν_{CO} in the complex $\text{BrCl}\dots\text{OC}\dots\text{HBr}$. These complexes are formed only weakly, possibly from the photodissociation of formyl bromide...BrCl complex or carbonyl bromide chloride...HBr complex. No distinction in mechanism is possible but, given the low intensity of these bands, the latter is favoured since the bands attributed to carbonyl bromide chloride increased in intensity throughout the photolysis periods, indicating that any process that might reduce the band intensity was occurring to only a minute extent. The low intensities of the bands of this carbon monoxide complex is in agreement with a minor process destroying the carbonyl bromide chloride complex.

Other carbon monoxide species. These bands (Table 6.7) are attributed to various species as follows: the very weak band at 2541.6 cm^{-1} is assigned to isolated HBr in argon. The very weak and weak bands at 2525.2 and 2142.3 cm^{-1} are assigned

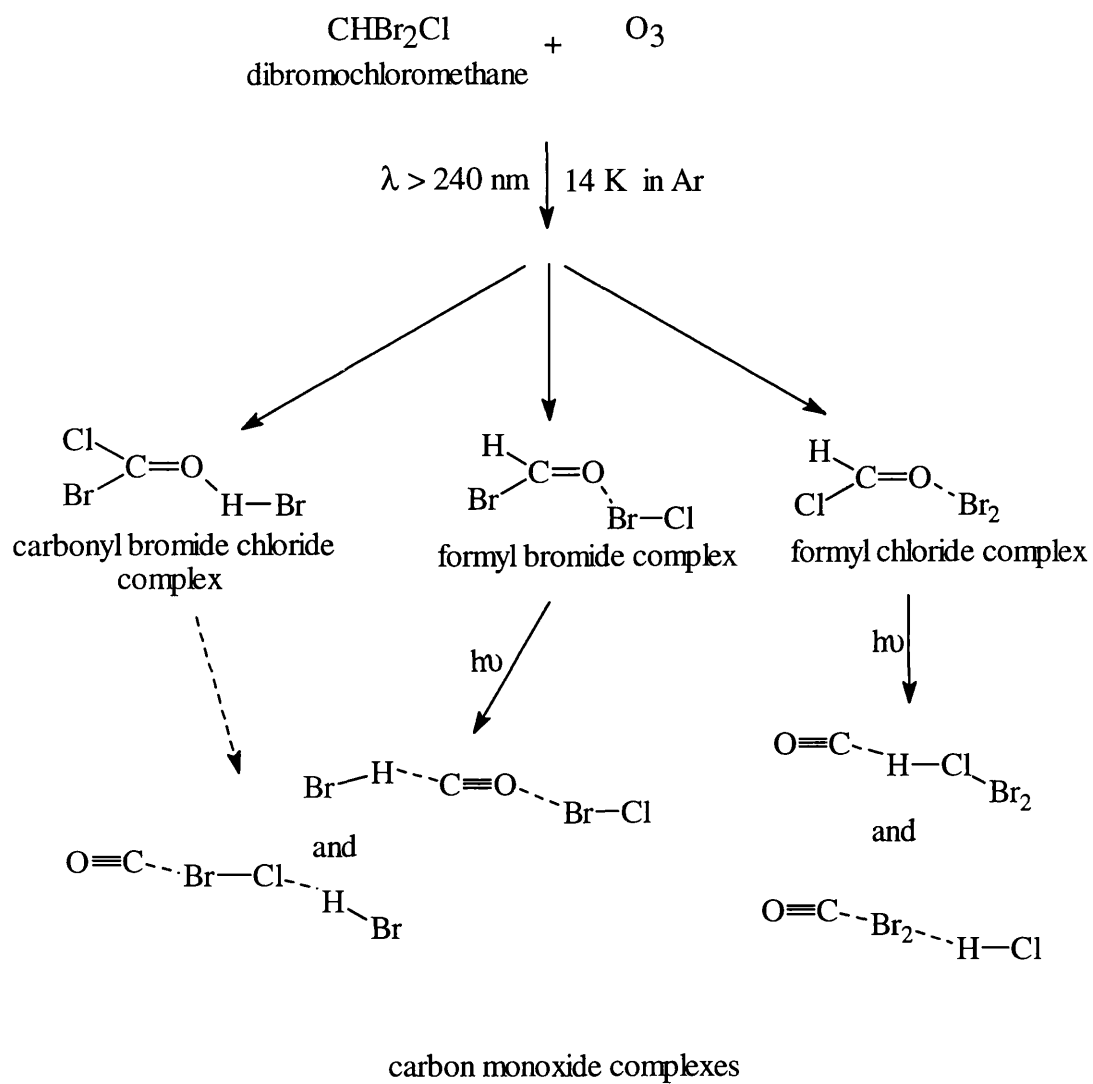
to ν_{HBr} and ν_{CO} , respectively, and attributed to a complex of the type $(\text{CO})_n(\text{HBr})_m$ where n is most likely equal to 2.

Photochemical Interconversion

In the reaction of dibromochloromethane with oxygen atoms, three carbonyl products are detected, COBrCl , COHCl and COHBr . These carbonyls dissociated after further photolysis to form a number of carbon monoxide complexes (see Summary 6.2). Assuming that the $\nu_{\text{C=O}}$ bands of the three carbonyls have similar infrared absorption coefficients, we can reasonably assume that the complexes are formed in approximately equal quantities. As with bromochloromethane (above) there are three possible bonds that the O atoms could insert into, C-Br, C-Cl or C-H. Insertion into the C-Br bond accounts for all the carbonyl products detected. This insertion into the weakest C-X bond follows the behaviour expected after studying the iodinated alkanes (chapters 3-5), but differs from that seen with bromochloromethane, in which C-H insertion accounts for all the observed products. If we consider the reaction of oxygen atoms with the dihalomethanes⁸⁷ where abstraction of HX is the favoured path, and trichloromethane⁸⁸ in which the favoured product is $\text{COCl}_2 \dots \text{HCl}$, with $\text{COHCl} \dots \text{Cl}_2$ as a minor product, we see that the reaction of CHBr_2Cl behaves as expected.

The carbon monoxide complexes are formed after dissociation of the various carbonyl complexes as discussed above; thus $\text{COBrCl} \dots \text{HBr}$ and $\text{COHBr} \dots \text{BrCl}$ dissociate into the complexes $\text{OC} \dots \text{BrCl} \dots \text{HBr}$ and $\text{BrCl} \dots \text{CO} \dots \text{HBr}$. While $\text{COHCl} \dots \text{Br}_2$ dissociates into the two complexes $\text{OC} \dots \text{HCl} \dots \text{Br}_2$ and $\text{OC} \dots \text{Br}_2 \dots \text{HCl}$.

SUMMARY 6.2



6.4 CONCLUDING REMARKS

The photochemical reaction of ozone with both CH_2BrCl and CHBr_2Cl has shown that the transfer of oxygen atoms occurs, leading to the formation of carbonyl species, which subsequently dissociate further to form carbon monoxide complexes. The carbonyl...Lewis acid and carbon monoxide...Lewis acid complexes thus produced are novel and can be compared with similar complexes. A mechanism accounting for the reactivity of these species is still elusive.

Table 6.1. Infrared bands /cm⁻¹ assigned to bromochloromethane, CH₂BrCl, deposited in an ozone /argon and an oxygen matrix at 14 K.

O ₂	O ₃ / Ar	assignment
3067.0w	3077.7w	v _a CH ₂
3061.4w	3040.6vw	
	3006.4w	v _s CH ₂
2998.1w	2997.7w	
	1465.8w	δ _{H-C-Cl} + v ₆ ^a
1420.1mw	1457.1w	
1415.7mw	1415.2w	δCH ₂
1411.4mw		
1381.8mw	1371.9w	δ _i CH ₂ ^b + v ₆
1368.3mw		
1346.9mw	1346.7w	
1338.3mw	1321.2w	
1330.0mw	1307.7w	
1319.9w		
1230vs	1230.9s	δ _{H-C-Cl}
	1229.0s	
	1197.5w	2v _{CBr}
	1130.7w	δ _i CH ₂
	1125.3w	
	1076.3w	v ₆ + ρCH ₂
	1070.0w	
1051.0w	1059.6w	
	903.6w	v _{CCl} + v _{CBr}
	896.9w	
	889.6w	
854.4w	856.8sh	ρCH ₂
853.0m	849.1m	
738vs	747.7s	v _{CCl}
	740.3s	
	738vs	
	732.5vs	
	711.5w	
613.5s	658.2w	v _{CBr}
	612vs	

^a- the band assigned to the v₆ mode is assumed to absorb at 240 cm.⁻¹

Table 6.2. Infrared bands /cm⁻¹ attributed to the carbonyl products of the photochemical reaction ($\lambda > 240$ nm) of CH₂BrCl with ozone in argon at 14 K.

complex	$\nu_{\text{C=O}}$	δ_{CH}	$\nu_{\text{o-o-p}}$	ν_{CCl}	ν_{CBr}
COHCl...HBr	1761.8w	1315.8w	962.9w	766m,br	
	1756.6s	1313.6vw	941.2w	756.0mw	
	1748.9w	1302.8vw ^a		745.1s	
				742.4s	
				740.3s	
COHCl...Ar	1781.5vw				
COHBr...HCl	1753.0m,sh	1287.4w	867.4vw		685.2vw
		1283.3w			681.8vw
		1279.7w			
		1272.6w			
COHBr...Ar	1801.5w				
COBrCl	1817.3vw			826.5vw	
				817.3w	
				809.1w	
				805.2mw	
				800.0w	
				797.5mw	
combinations:					
$2\nu_6$ COHBr			1775.7vw		
$\nu_{\text{CCl}} + \nu_5^{\text{b}}$ COHCl			1190.0w		
			1153.9w		
			1117.9w		
$\nu_{\text{CBr}} + \nu_5$ COHBr			1090.2w		
			1067.0w		

^a- Obscured by precursor band; ^b- $\nu_5 \sim 460$ cm.⁻¹

Table 6.3. Infrared bands /cm⁻¹ assigned HCl, HBr and CO in several complexes, detected after photolysis ($\lambda > 240$ nm) of ozone and bromochloromethane in argon matrices at 14 K.

complex	ν_{HCl}	ν_{HBr}	ν_{CO}
HCl...CO	2828.5vw		
OC...HBr...HCl	2812.5w	2492.0w 2479.0w	2149.0w
OC...HCl...HBr	2783.6s	2507.3s	2154.9s
HCl...CO...HBr		2500.6m	2156.7m
(CO) ₂ HX			2142.5vw
CO			2138.1w

Table 6.4. Infrared bands /cm⁻¹ assigned to the formyl chloride moiety in several complexes.

complex ^a	ν_{CH}	$\nu_{\text{C=O}}$	δ_{CH}	ν_{CCl}	δ_{CCl}	$\nu_{\text{o-o-p}}$
COHCl ⁸⁸	2933.5	1783.5	1307.0	738.6	458.0	932.3
...Cl ₂ ⁸⁸		1780.6				
...Br ₂ ^b		1779.7 1768.1	1307.9 1302.8 1298.5			
...HI ^c	2987.6	1778.3 1762.8	1306.2			935.9
...HBr ^d		1761.8 1756.6	1315.8 1313.6 1302.8	766- 740.3		941.2
...HCl ⁸⁷	2960.5	1756.7 1754.6 1751.3		753		

^a- complexes in descending order of increasing perturbation, i.e. COHCl...HCl complex is the most perturbed; ^b- formed from CHBr₂Cl (this chapter); ^c- formed from CH₂ClI (chapter 5); ^d- formed from CH₂BrCl (this chapter).

Table 6.5. Infrared bands /cm⁻¹ detected for CHBr₂Cl after deposition with ozone in argon matrices, and in solid oxygen matrices at 14 K.

O ₂	O ₃ /Ar	assignment
3057.2mw	3070.5w 3058.9m 3040.1w	v _{CH}
1360.9w	1361.2mw 1353.9w	v _{CH}
1315.7w	1321.2w 1308.6mw	
1216.3w 1197.9m	1217.0wm 1198.7ms	
1154.1m	1160.1m 1155.3ms 1147.1w,sh	δ _{CH}
1092.2vw	1092.1w	
751.0s 737.0s	751.7s 737.1s 730.0w	v _{CCl}
669.9s	670.7vs 647.6w	
572.1ms	573.3s 529.5w	v _{CBr}

Table 6.6. Infrared bands /cm⁻¹ assigned to the carbonyl products detected after photolysis ($\lambda > 240$ nm) of ozone and CHBr₂Cl in argon at 14 K.

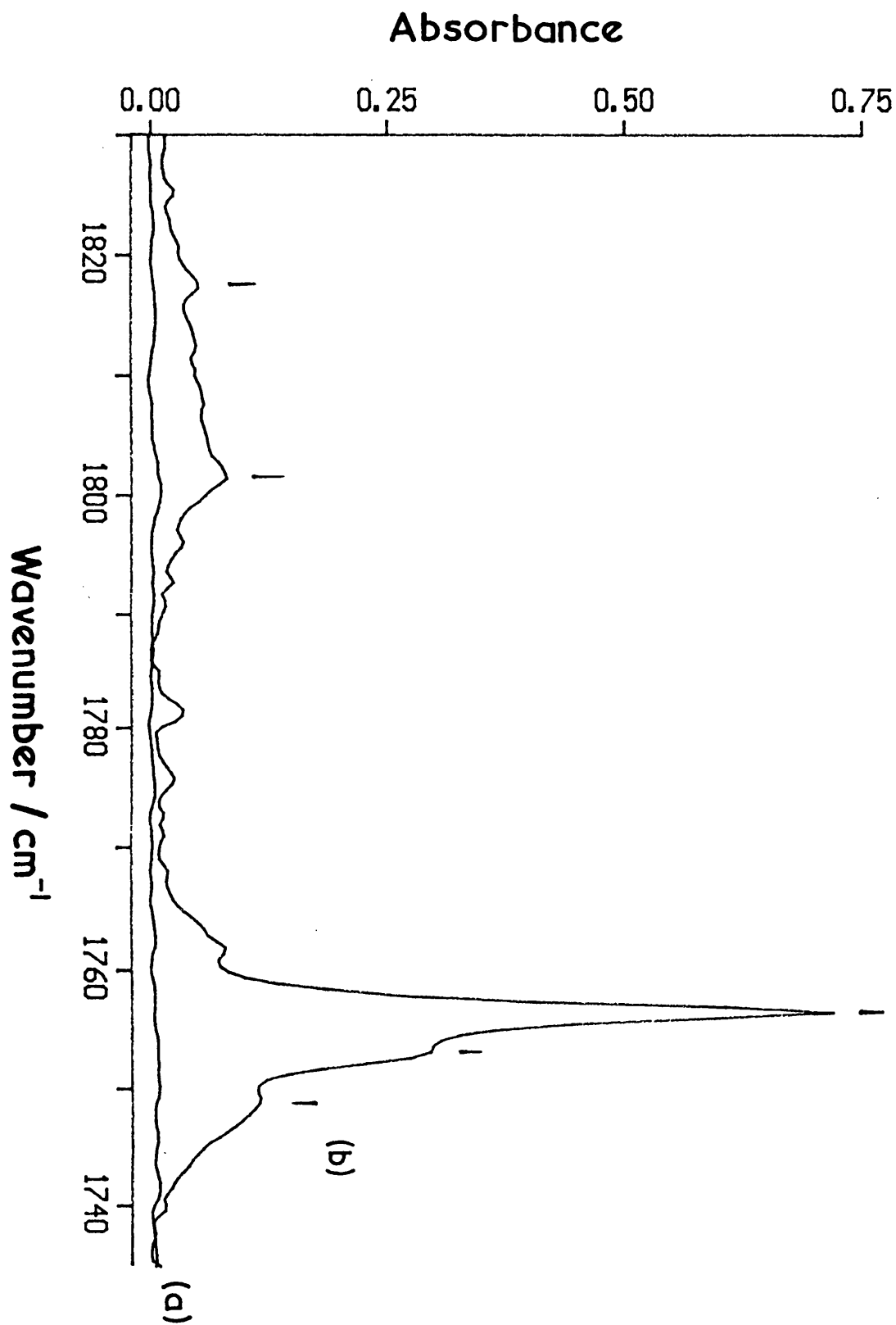
complex	$\nu_{\text{C=O}}$	δ_{CH}	ν_{CCl}	ν_{CBr}	others
COBrCl...Ar	1824.6w 1819.7w,sh 1817.4w				
COBrCl...HBr	1813.5m 1801.4m 1796.1ms 1794.7sh,m		824.1mw 820.7m 814.9m 812.0m 805.7m 797.0mw 791.2mw		626.8vw ^e
COHBr...BrCl	1783.1m 1776.3sh,w ^b	1285.9w 1279.7w 1273.1mw		642.0w d	1073.8vw ^f
COHCl...Ar ...Br ₂	1779.7sh,w 1768.1w	1307.9w	c		
COHCl...(HX) ₂ ^a	1753.7m	1302.8w 1298.5w	716.9w 712.7w		1147.1m ^g

^a- HX from nearest neighbour; ^b- $2\nu_6$ of COHBr; ^c- ν_{CCl} bands obscured by those of precursor at 750 cm⁻¹; ^d- ν_{CBr} bands of COHBr are obscured by those of precursor at 670.7 cm⁻¹; ^e- combination $\nu_{\text{CO}} + \delta_{\text{CBrCl}}$; ^f- combination $\nu_{\text{CBr}} + \nu_5$; ^g- combination $\nu_{\text{CCl}} + \nu_5$.

Table 6.7. Infrared bands /cm⁻¹ assigned to the ν_{HCl} , ν_{HBr} and ν_{CO} of the carbon monoxide complexes detected after UV photolysis ($\lambda > 240$ nm) of ozone and CHBr_2Cl in argon at 14 K.

complex	ν_{HCl}	ν_{HBr}	ν_{CO}
OC...(Br ₂)...HCl	2813.5m 2807.6w		2153.1m 2150.7mw
OC..HCl...(Br ₂)	2794.6w 2791.4m		2157.6m
HBr...Ar		2541.6vw	
(HBr) _n (CO) _m		2525.2vw	2142.3sh,w
OC...BrCl...HBr		2510.4w 2507.8w	
BrCl...CO...HBr		2496.7w	2146.6w
CO...Ar			2138.0w

Figure. 6.1. Infrared spectrum in the $\nu_{\text{C=O}}$ region of an argon matrix containing CH_2BrCl and ozone after (a) deposition and (b) photolysis with UV ($\lambda > 240 \text{ nm}$) radiation for 71 h, showing bands assigned to COHCl and COHBr .



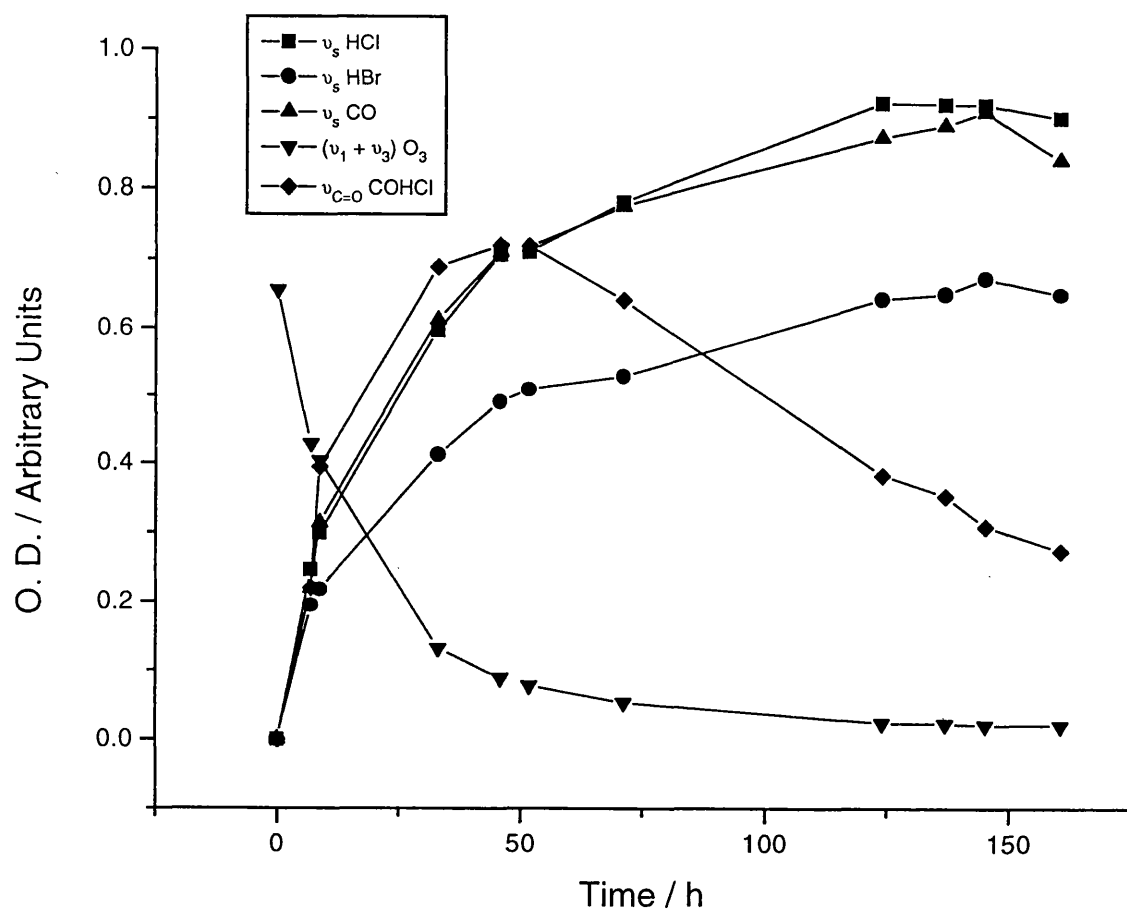


Figure. 6.2. Plot of optical density (arbitrary units) *versus* time (h) showing the destruction of the ozone ($\nu_1 + \nu_3$) band, the formation and destruction of the carbonyl band of COHCl, and the growth of the ν_{HCl} , ν_{HBr} and ν_{CO} bands.

Figure. 6.3. Infrared spectrum of an argon matrix containing CH_2BrCl and ozone after (a) deposition and (b) quartz-filtered ($\lambda > 240 \text{ nm}$) photolysis for 160 h, showing bands in the ν_{HCl} ($2850 - 2775 \text{ cm}^{-1}$), ν_{HBr} ($2510 - 2480 \text{ cm}^{-1}$) and ν_{CO} regions ($2170 - 2140 \text{ cm}^{-1}$) attributed to the various carbon monoxide complexes.

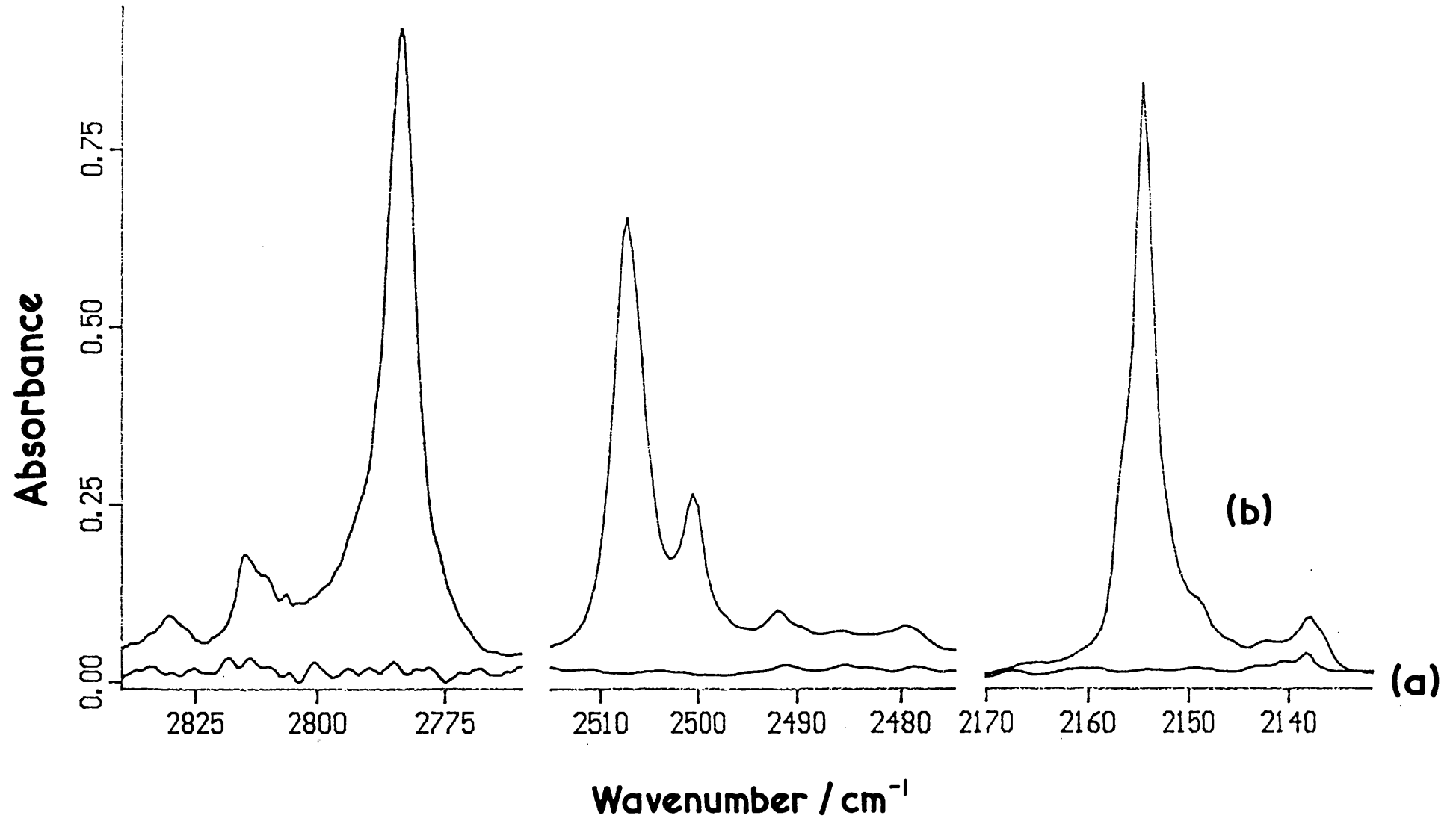


Figure. 6.4. Infrared spectrum of an argon matrix containing CHBr_2Cl and ozone after (a) deposition, (b) UV photolysis for 25 h and (c) UV photolysis for 115 h, showing bands in the $\nu_{\text{C=O}}$ region attributed to the carbonyls COHCl , COHBr and COBrCl .

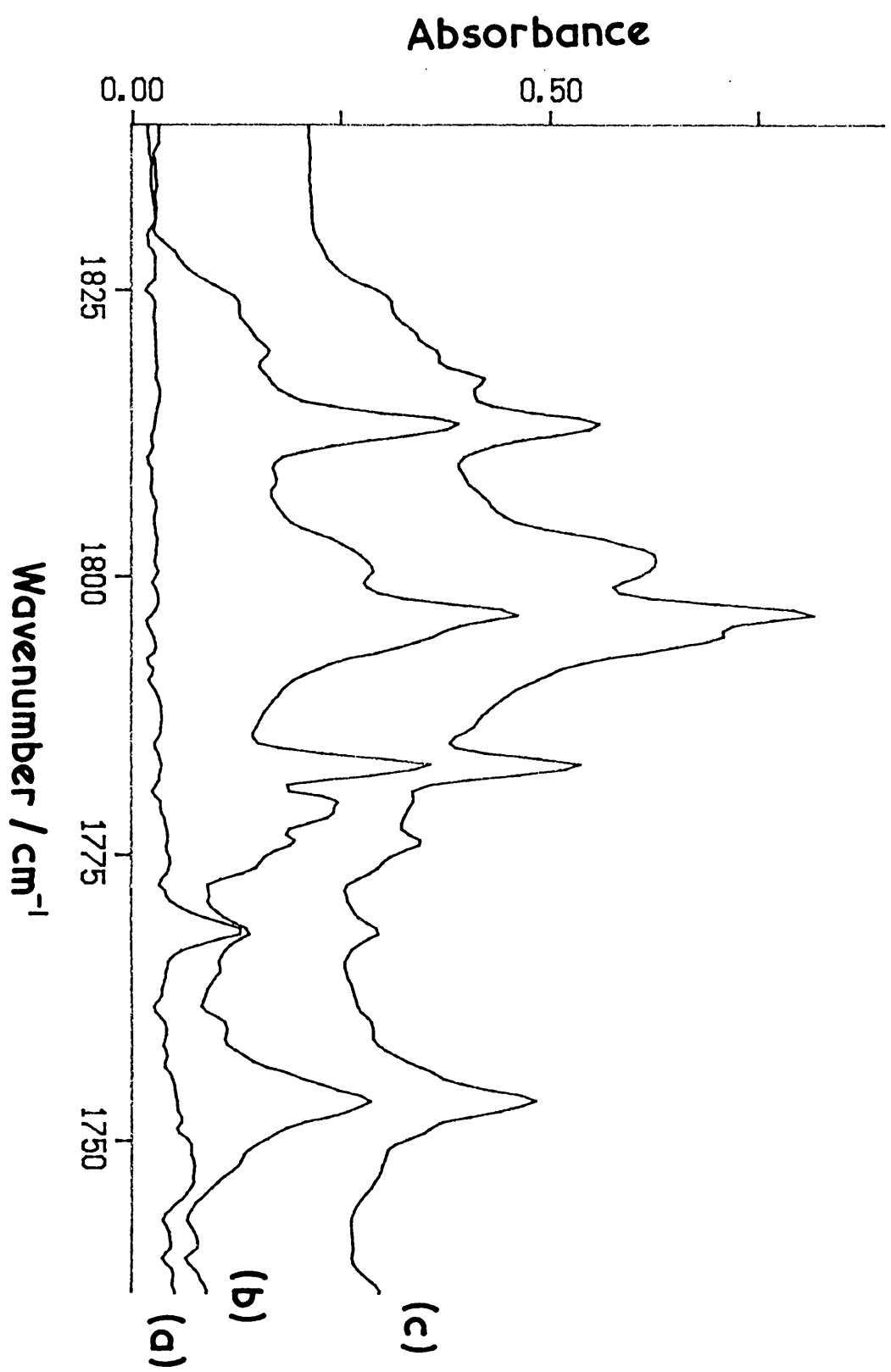


Figure. 6.5. Plot of optical density (arbitrary units) *versus* time (h), showing in (i) growth of the ν_{HCl} and ν_{HBr} bands, (ii) growth of ν_{CO} bands and, (iii) growth and loss of the $\nu_{\text{C=O}}$ bands of the various COXY carbonyls.

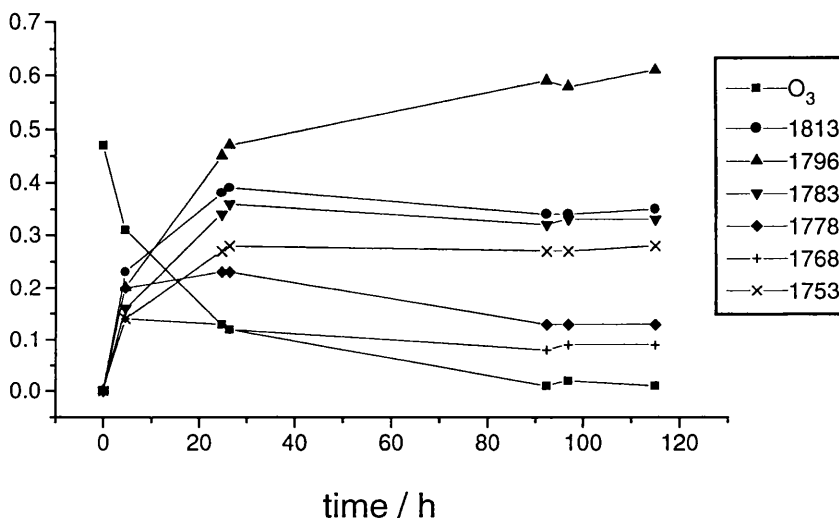
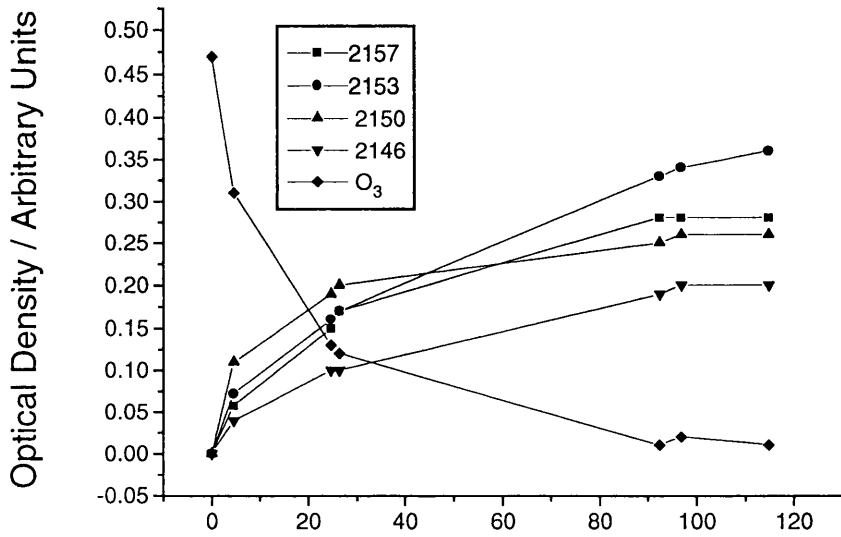
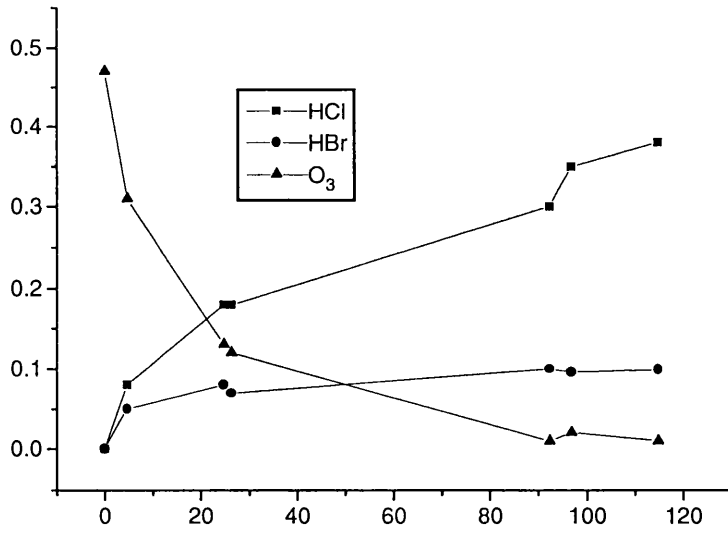
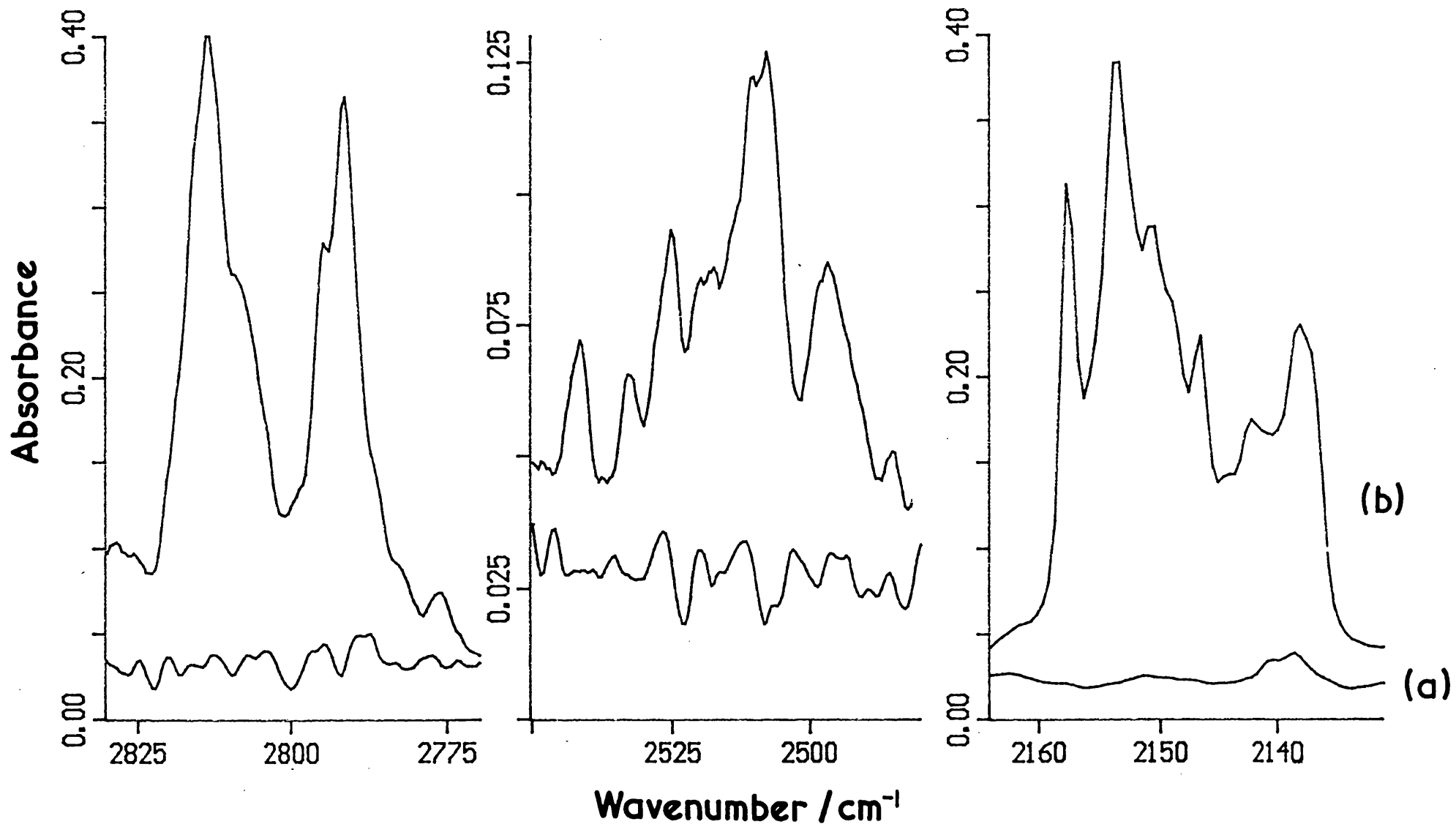


Figure. 6.6. Infrared spectrum of an argon matrix containing CHBr_2Cl and ozone after (a) deposition and (b) quartz-filtered ($\lambda > 240 \text{ nm}$) photolysis for 115 h, showing bands in the regions ν_{HCl} ($2825 - 2775 \text{ cm}^{-1}$), ν_{HBr} ($2550 - 2475 \text{ cm}^{-1}$) and ν_{CO} ($2160 - 2130 \text{ cm}^{-1}$) attributed to the various carbon monoxide complexes.



Chapter 7

REACTION OF TRIBROMOFLUOROMETHANE WITH OXYGEN ATOMS

7.1 INTRODUCTION

In this chapter the photo-oxidation of tribromofluoromethane isolated in an ozone/argon and oxygen matrix has been studied. Previous matrix studies have shown that reaction of halogenated methanes with ozone or oxygen provides a successful means for generating a range of products. In this case photolysis of ozone or oxygen in the matrix is expected to produce O atoms which will react with CBr_3F to produce carbonyl bromide fluoride, COBrF , perturbed by bromine. Continued photolysis of matrices containing these carbonyl species will result in dissociation of these carbonyls, either to a carbon monoxide...dihalide complex or to a radical-atom type complex via C-halogen bond rupture. The exact products will be dependent upon the various bond energies and reaction barriers involved. Recent gas phase studies of the infrared spectrum of COBrF^{113} and of the photolysis products,¹¹⁴ have provided indirect evidence for the formation of the FCO radical and Br atoms via the second process, in preference to the formation of carbon monoxide...BrF complex. In the matrix we may be able to 'trap' the reactive FCO radical and thus confirm its presence as a product of photodissociation of COBrF . In addition, by detecting any further reaction of the FCO radical and Br atom in the matrix, light may be shed on some important environmental processes. In particular FCO radicals may trap bromine atoms and hence remove them from the ozone-depleting BrO_x catalytic cycle. Also, the FCO radicals may undergo reactions with O or O_2 and thus it may be possible to detect

peroxides of the form FC(O)O_x ($x = 1$ or 2),^{115,116,117,118} or they may combine with each other to form COF_2 . Thus it is expected that a number of novel complexes may be detected, and that by observing the photochemical and thermal interconversion of the species detected we may be able to provide an insight into a possibly important reaction.

7.2 RESULTS

The matrix spectra of CBr_3F in solid argon are very similar to that reported for CBr_3F liquid,^{119,120} and are assigned accordingly (Table 7.1). Quartz-filtered, ultraviolet photolysis ($\lambda > 240$ nm) of isolated CBr_3F in an argon matrix, for up to 30 h, produced no new bands, although radiation of these wavelengths is capable of dissociating a CBr bond.¹²¹

Tribromonfluoromethane and ozone in argon

The spectra of CBr_3F with ozone ($^{16}\text{O}_3$ or $^{18}\text{O}_3$) ($\text{O}_3/\text{CBr}_3\text{F}/\text{Ar} = 3:2:1200$) in argon (Table 7.1, Fig. 7.1) show similar bands to those observed for isolated CBr_3F (above) and for ozone.⁴⁴ Tens of hours of photolysis (quartz-filtered) was required before any significant product was detected (Fig. 7.1). Pyrex- ($\lambda > 290$ nm) and blue/green-filtered ($\lambda > 350$ nm) photolysis produced no detectable products. However given the length of time required to detect products with quartz-filtered photolysis, significantly longer Pyrex-filtered photolysis would have been needed to detect any products, since there is no evidence to suggest that $\text{O}(^3\text{P})$ atoms are any less able than $\text{O}(^1\text{D})$ atoms at insertion into the CBr bond.

The product bands detected are assigned (Table 7.2, Figs. 7.1 and 7.2), and their behaviour on warming and further photolysis is studied. The bands detected are placed into one of four groups based on this behaviour; the most significant changes

in intensity occurred in the $\nu_{\text{C=O}}$ region.

Group 1. These bands are formed on irradiation in the UV: on warming the sample, the band intensities increased by 100 %, while on photolysis with visible radiation they decreased by 50 %. The bands lie at 1839.3, 1077.2, 1070.0, 1067.1, 728.3, 723.1, 719.9, 712.5 and 621.0 cm^{-1} and are assigned to modes of the species COBrF perturbed by Br_2 . The medium band at 1839.3 cm^{-1} exhibited an ^{18}O -shift of 40.3 cm^{-1} and is assigned to the carbonyl stretch of COBrF. The medium intensity triplet of bands at 1077.2, 1070.0 and 1067.1 cm^{-1} (^{18}O isotopomer at 1060 cm^{-1}) are assigned to the CF stretching mode of COBrF. The weak band at 728.3 cm^{-1} is assigned to the combination of C-Br stretch and rock of COBrF, while those at 723.1, 719.9 and 712.5 cm^{-1} (^{18}O isotopomers at 722.1 and 719.7 cm^{-1}) are assigned to the F-C-O bending mode. The weak band at 621.0 cm^{-1} (^{18}O isotopomer at 618.5 cm^{-1}) is assigned to the out-of-plane bending mode of COBrF which overlaps with the bending mode of FCO (group 3).

Group 2. These weak bands are similarly formed on UV irradiation; but they are not affected either by sample warming or by photolysis with visible radiation. One member of this group is detected at 1864.4 cm^{-1} (^{18}O isotopomer at 1825.5 cm^{-1}), the observed ^{18}O -shift of 38.9 cm^{-1} providing evidence for its assignment to the carbonyl stretch of COBrF isolated in argon.

Group 3. These bands, which are formed on UV irradiation of the sample, are reduced in intensity by 40 % on warming of the sample, but increased in intensities by photolysis with visible radiation. The group 3 bands absorb at 1857.3, 1851.6 and 621.0 cm^{-1} and are assigned as follows: the bands at 1857.3 and 1851.6 cm^{-1} (^{18}O at 1817.3 and 1810.1 cm^{-1}) are assigned as CO stretches of FCO, while the band at 621.0 cm^{-1} (^{18}O at 612.4 cm^{-1}) is assigned to the bending mode of FCO, which overlaps as indicated earlier, with the group 1 band, out-of-plane bending mode of COBrF.

The group 3 behaviour is directly related to that of the group 1; both are formed after UV irradiation and, on warming the sample, the growth of group 1 bands appears to be at the expense of group 3 bands. Subsequent visible irradiation reversed

the process, causing an increase in the intensities of the group 3 bands at the expense of group 1 bands.

Group 4. The fourth group is formed weakly on initial photolysis with UV radiation while, due to the low intensities of the bands, warming or photolysis with visible radiation appears to have no effect. The 1844.3 cm^{-1} band in this group is assigned tentatively to either FC(O)O_2 or FC(O)O . No ^{18}O isotopomer bands were detected.

Tribromofluoromethane in oxygen

In this series of experiments CBr_3F deposited in oxygen ($\text{CBr}_3\text{F}/\text{O}_2 = 1:200$) resulted in the formation of a similar number of bands (Table 7.1) to that detected for CBr_3F isolated in argon (*vide supra*). Quartz-filtered photolysis ($\lambda > 240\text{ nm}$) was required to initiate a reaction in this matrix, since wavelengths shorter than 280 nm are required to dissociate O_2 .⁴⁵ This photolysis range yielded a number of bands (Table 7.2), which are arranged into groups 1-5 in a similar way as for the ozone experiments, seen earlier (note the detection of a fifth group). Again the most diagnostic bands occur in the $\nu_{\text{C=O}}$ region (Fig. 7.3).

Group 1 and 2. In this series of experiments, bands were also detected at similar wavenumbers to those reported in the ozone experiments, groups 1 and 2 bands being likewise assigned to modes of COBrF either isolated or perturbed by Br_2 (Table 7.2). However extra bands were observed here: one at 1111.9 cm^{-1} is assigned to the combination, F-C-O bend and C-Br stretch, and one at 729.1 cm^{-1} to the combination of C-Br stretch and rock of $\text{COBrF}\dots\text{Br}_2$. From these two combination bands, the C-Br stretch and rock band wavenumbers may be calculated to occur at 392.4 and 336.7 cm^{-1} respectively.^{113,122}

Group 3 and 4. The group 3 bands behave exactly as those seen earlier, with absorptions at 1857.8 , 1853.0 , 1852.0 and 620.6 cm^{-1} . The band at 1857.8 cm^{-1} is

assigned to CO stretch of the FCO radical, with the two medium-weak bands at 1853.0 and 1852.0 cm^{-1} being assigned to similar bands of FCO perturbed more strongly. The 620.6 cm^{-1} band is assigned (as before) to the bending mode of FCO. The medium-weak group 4 bands at 1850.6 and 1848.4 cm^{-1} are tentatively assigned to the carbonyl stretch of the FC(O)O_x peroxides ($x = 1$ or 2).

Group 5. With prolonged photolysis (70 h) a fifth group of very-weak bands was detected at 1934.5 and 1905.8 cm^{-1} and these are assigned to the overtone $2\nu_s\text{CF}_2$ and $\nu_{\text{C=O}}$ modes of COF_2 perturbed by Br_2 , respectively (Table 7.3).

7.3 DISCUSSION

Ultraviolet radiation is necessary in order to cause a reaction between either ozone or molecular oxygen and CBr_3F . This can be compared to the dramatic change detected for the ozone complexes with the iodine-containing compounds ICl ,¹⁹ CH_3I ,²⁰ CF_3I ,²¹ and $\text{C}_2\text{H}_5\text{I}$,⁴⁷ where a reaction can be initiated on irradiation in the visible and infrared region. Photolysis of either ozone⁴⁴ or molecular oxygen⁴⁵ with UV radiation is capable of producing both excited state $\text{O}(^1\text{D})$ and ground state $\text{O}(^3\text{P})$ atoms (Summary 7-reaction 1). It is believed that these atoms insert into the C-Br bond, in a manner analogous to the insertion into the C-I bond^{19-21,47} (and chapters 3-5). Thus the initial reaction between CBr_3F and oxygen atoms proceeds via insertion of O atoms into the C-Br bond to yield the carbonyl bromide fluoride, COBrF , via an intermediate such as $[\text{Br}_2\text{FC-O-Br}]^*$ (reaction 2). An alternative reaction involving cleavage of C-Br to yield $\text{CBr}_2\text{F} + \text{Br}$ atoms, of which the latter could then react with oxygen atoms to yield BrO , is not believed to occur in these matrix experiments; there is no spectral evidence for either CBr_2F (absorbing^{123,124} at 1136 and 782 cm^{-1}) or for the BrO ¹²⁵ species. However, a similar reaction involving the chlorine analogue, CCl_3F , is known to yield ClO as well as the carbonyl.¹²⁶ The bands detected are assigned to one of the product groups 1-5.

Group 1 and 2. The groups 1 and 2 bands are assigned to COBrF, either isolated in argon or perturbed by bromine, on account of their similarities to those of COBrF.^{113,122} The COBrF...Br₂ species is a charge transfer complex, with the oxygen atom of the carbonyl transferring electrons to the σ^* antibonding molecular orbital of bromine. The extent of the charge transfer manifests itself as a shift in the $\nu_{\text{C=O}}$ bands. In this case the bands of the complex are shifted by an average of 26 cm⁻¹ from the values for the isolated carbonyl, which shift can be compared to that of bromine on the other carbonyls COF₂ (7.7 cm⁻¹), COH₂ (14.8 cm⁻¹)⁸⁷ and COCIF (27 cm⁻¹).¹²⁷ This transfer is least for the carbonyl difluoride complex, for which the highly electronegative fluorine atoms remove electron density from the C=O bond.

Group 3. The group 3 bands are assigned to modes of the radical FCO, the C=O stretching band of which has been detected for both ¹⁶O and ¹⁸O isotopomers at 1857.3 and 1817.3 cm⁻¹ and is in good agreement with the published spectra.¹²⁸ Although no band attributable to the C-F stretch of FCO (1023.0 cm⁻¹)¹²⁸ was detected in this study, that for the bend was detected for both the ¹⁶O and ¹⁸O species at 621.0 and 612.4 cm⁻¹ respectively. The FCO radical is formed from the dissociation of carbonyl bromide fluoride (reaction 3) induced by visible irradiation. This step has been calculated by *ab initio*¹¹⁴ methods to dominate over that of molecular elimination of CO and FBr. On warming the matrix to 25 K, there is an increase in the intensities of the COBrF bands and a decrease in those of the FCO bands, this being accounted for by the thermal recombination of the radical and atom as shown in reaction 4. Thus a link between COBrF and FCO has been established: photolysis of COBrF with visible radiation produces FCO and Br atoms, while warming these two products in a matrix causes them to combine and reform COBrF (reaction 4). A similar reaction occurs in the gas phase, in which formyl bromide, COHBr, and bromine atoms are formed photochemically from the formyl radical,¹²⁹ CHO, and bromine. This result provides some support for the possibility that thermal recombination may occur.

Group 4. The previously unidentified weak group 4 bands detected in the ¹⁶O₃/Ar experiment in the $\nu_{\text{C=O}}$ region at 1844.3 cm⁻¹ (1850.6 and 1848.4 cm⁻¹ in the O₂ experiment) may arise from vibrations of one or other of the peroxide radicals

FC(O)O_x (x = 1 or 2), for which molecular orbital *ab initio* calculations¹¹⁶ have provided tentative band assignments. These peroxides are formed when the FCO radical reacts with either O atoms or O₂, the latter reaction being the faster¹¹⁸ (reaction 5). These peroxides are stabilised in the oxygen matrix (Fig. 7.3) as evidenced by the increased intensities of their $\nu_{C=O}$ bands relative to the group 1 and 3 bands.

Another reaction, between FCO radicals and BrO could lead to the formation of FC(O)O and Br atoms, hence regenerating the bromine atom. Given the tentative nature of the assignments in this group to either FC(O)O or FC(O)O₂, this last reaction must remain speculative at most, it might prove extremely informative to carry out *ab initio* calculations on this reaction, since it provides a possible route for regeneration of bromine atoms.

Group 5. Prolonged photolysis, in a solid oxygen matrix, resulted in the detection of group 5 bands at 1934.5 and 1905.8 cm⁻¹ and assignment to modes of COF₂. This compound is formed via the 'hot' F₂C₂O₂ intermediate^{130,131} when two FCO radicals combine (reaction 6). This reaction would also have produced CO, but the yields were too low to permit detection. The observation that COF₂ is only formed in low yields even on prolonged (70 h) photolysis is interesting as it allows a comparison of the COBrF to FCO + Br reaction in the gas phase and in an argon matrix; in the former, recombination of radicals is so fast that the stable carbonyl COF₂ is formed, while in a low temperature matrix the likelihood of radicals recombining is dramatically reduced by the cold, rigid environment which stabilises the FCO radical.

Alternatively, the COF₂ detected might result from the reaction of an impurity with oxygen atoms. If the impurity were CF₂Br₂ it would be expected, by analogy with CF₂Cl₂,¹⁰³ to react with oxygen atoms and form COF₂ and Br₂. Whilst this second reaction cannot be overlooked, any impurity would be present in only minute concentrations, the combination of two FCO radicals to form COF₂ is the favoured mechanism based on the gas phase¹¹⁴ observations.

The bands observed at 1934.5 and 1905.8 cm⁻¹ are assigned to the Fermi

doublet $2\nu_s\text{CF}_2$ and $\nu_{\text{C=O}}$, respectively, for the complex $\text{COF}_2\cdots\text{Br}_2$. The bands are shifted in comparison with their values for uncomplexed COF_2 by amounts ($\Delta\nu$) comparable to the shifts found for $\text{COF}_2\cdots\text{Cl}_2$ and $\text{COF}_2\cdots\text{IF}$ (Table 7.3). The shifts follows the trend of Lewis acid character.

7.4 CONCLUDING REMARKS

It has been demonstrated that CBr_3F reacts with oxygen atoms to yield COBrF (see Summary), and that the photodissociation of this carbonyl can be studied in a matrix without interference from precursors. The radical FCO has been detected directly in this work as a product of the photolysis of COBrF , whereas gas phase studies themselves have led only to the detection of COF_2 . The present results thus remove any doubt as to the preferred chemical path, as predicted and inferred by Francisco *et al.*¹¹⁶ The observed thermal reaction between FCO and Br atoms to reform COBrF , suggests that FCO may be an important reagent in the atmosphere on account of its ability to remove the Br atoms responsible for the destruction of ozone, and hence COBrF could act as a reservoir for Br atoms.

Tentative infrared evidence is also provided for the FC(O)O_x peroxides. Bands of the complexes, $\text{COBrF}\cdots\text{Br}_2$ and $\text{COF}_2\cdots\text{Br}_2$ have been detected and are compared with wavenumber shifts detected for other such dihalogen complexes.

SUMMARY 7

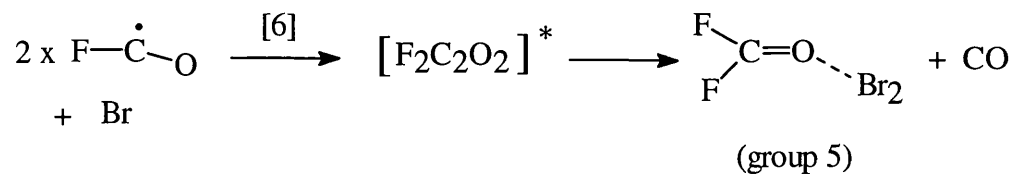
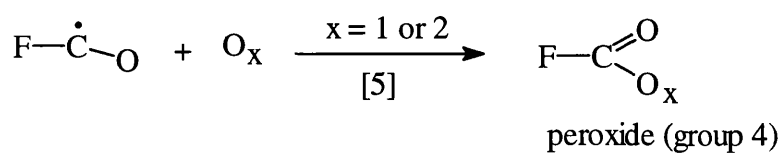
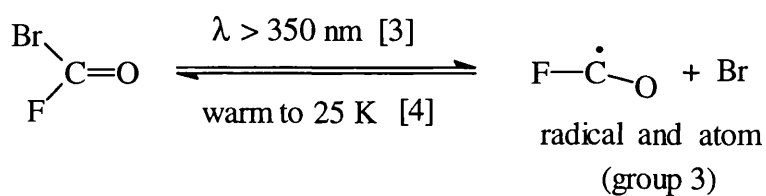
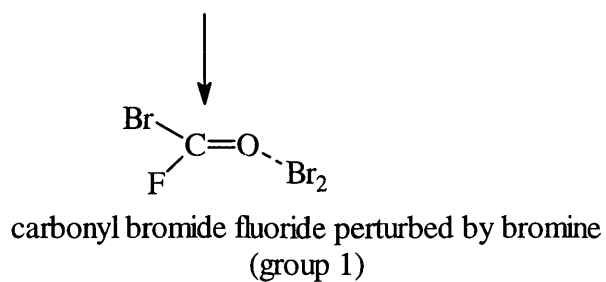
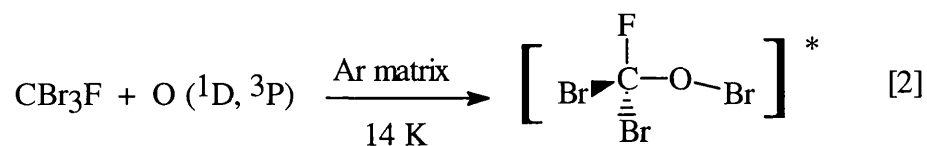
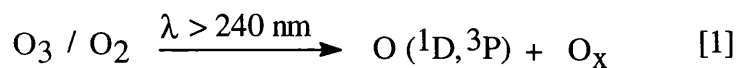


Table 7.1. Infrared bands /cm⁻¹ of CBr₃F in a number of matrix environments.

Ar	O ₂	¹⁶ O ₃ / Ar	¹⁸ O ₃ / Ar	assignment	
		2110.0m	1995.3m	v _s + v _a	O ₃
		2108.3m	1992.4m		
		2099.7w			
		1104.3w		v _s	O ₃
1058vs	1065.7ms	1069.0w ^a	1069.7sh	v _{CF}	CBr ₃ F
	1064.7ms	1060.3m	1059vs		
	1060.3s	1055.8w			
	1057.4m				
	1053.1m				
1034.3w			1034.3w	v _{CBr} + ρ	CBr ₃ F
		1036vs ^b	1026.1w	v _a	O ₃
		1025.4w	1017.4w		
			999.1w		
			982vs		
747vs	749vs	744.0s	747vs	v _{CBr}	CBr ₃ F
719.9m	724.6w		722.1w		
712.7s	710.2w		720.0w		
			712.7s		
	705.0mw	703.5m	670.2vw	δ _{O-O-O}	O ₃
704.0s	705.0mw		703.8s	v ₂ + v ₅	CBr ₃ F

^a- This band probably overlaps with a product band, as its intensity initially increases then decreases on prolonged photolysis; ^b- Photolysis changed the broad band at 1036 cm⁻¹ to a complex band structure with peaks at 1039.1, 1034.8 and 1032.8 cm⁻¹.

Table 7.2. Infrared bands /cm⁻¹ of the products of the oxygen atom oxidation of CBr₃F.

O ₂	¹⁶ O ₃ / Ar	¹⁸ O ₃ / Ar	assignment	
2115.3 2108.1			v _s + v _a	O ₃
1934.5vw ^a 1905.8vw ^a			2v _s CF ₂ v _{C=O}	COF ₂ ...Br ₂
1865.8w 1859.8w	1864.4w	1825.5w	v _{C=O}	COBrF
1857.8m 1853.0mw 1852.0mw	1857.3m 1851.6w	1817.3m 1810.1mw	v _{C=O}	FCO
1850.6mw 1848.4mw	1844.3w		v _{C=O}	FC(O)O _x
1839.5mw	1839.3m	1799.0mw 1796.1mw	v _{C=O}	COBrF...Br ₂
1111.9w			δ _{FCO} + v _{CBr}	COBrF...Br ₂
1104.2vw			v _s	O ₃
1079.6w 1073.0w 1063.8s 1057.0m 1054.0m	1077.2m 1070.0m 1067.1m	1060vs ^b	v _{CF}	COBrF...Br ₂
1036.7s 1030.9w			v _a	O ₃
729.1vw	728.3w		v _{CBr} + ρ	COBrF...Br ₂
721.4sh 719.5mw 702.5w	723.1w 719.9w 712.5w	722.1m 719.7s	δ _{FCO}	COBrF...Br ₂
620.6w	621.0w ^a	618.5w 612.4vw	v _{o-o-p} δ _{FCO}	COBrF...Br ₂ FCO
392.4 ^c			v _{CBr}	COBrF
336.7 ^c			v ₅	COBrF

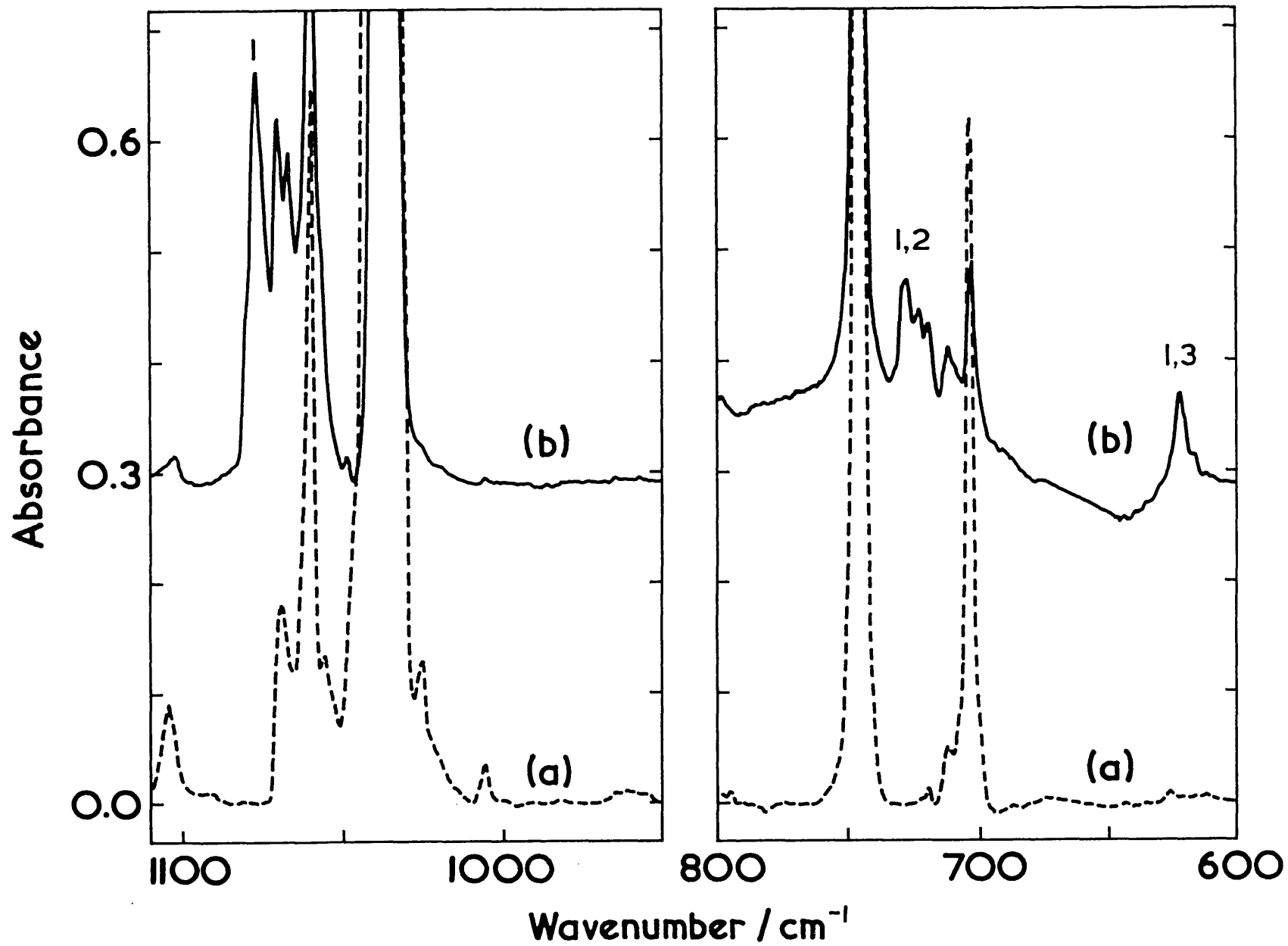
^a- After 70 h photolysis; ^b- overlap with a precursor band; ^c- deduced from the wavenumbers of combination bands.

Table 7.3. Comparison of infrared bands /cm⁻¹ detected for uncomplexed and complexed COF₂ in argon matrices.

	COF ₂ ⁸⁸		COF ₂ ...Cl ₂ ⁸⁸		COF ₂ ...IF ²¹		COF ₂ ...Br ₂	
	v	v	Δv	v	Δv	v	Δv	
2.v _s CF ₂	1941.4	1940.2	1.2	1938.9 1968.2	2.5 26.8 ^a	1934.5	6.9	
v _{C=O}	1913.5	1911.1	2.4	1911.2 1883.4	2.3 30.1 ^a	1905.8	7.7	

^a- The higher value of Δv pertains to a more strongly perturbed geometric arrangement in the matrix.²¹

Figure 7.1. Infrared spectrum of CBr_3F and $^{16}\text{O}_3$ in an argon matrix after (a) deposition and (b) photolysis with UV radiation for approximately 70 h, showing group bands 1 - 4 of the product.



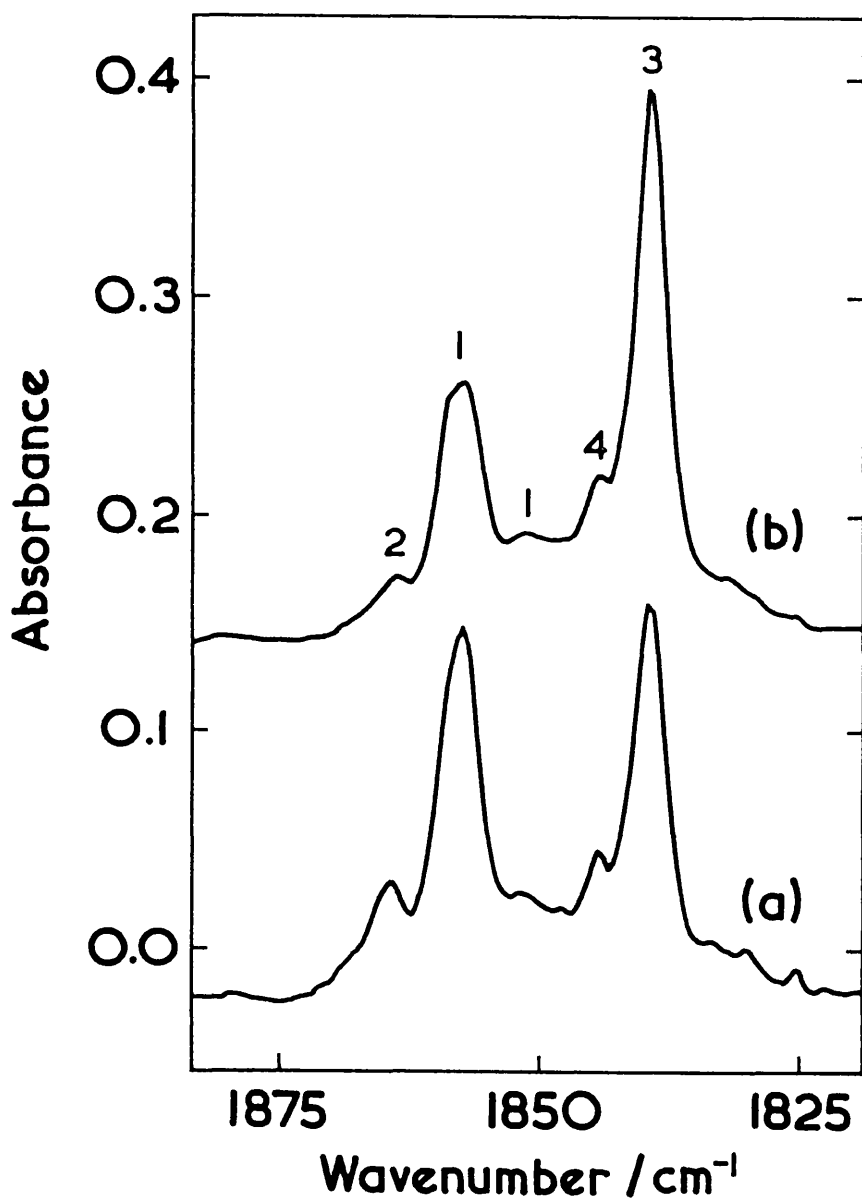


Figure 7.2. Infrared spectrum of CBr₃F and ¹⁶O₃ in an argon matrix after (a) UV photolysis ($\lambda > 240$ nm) for 70 h and (b) warming to 25 K for 20 min.

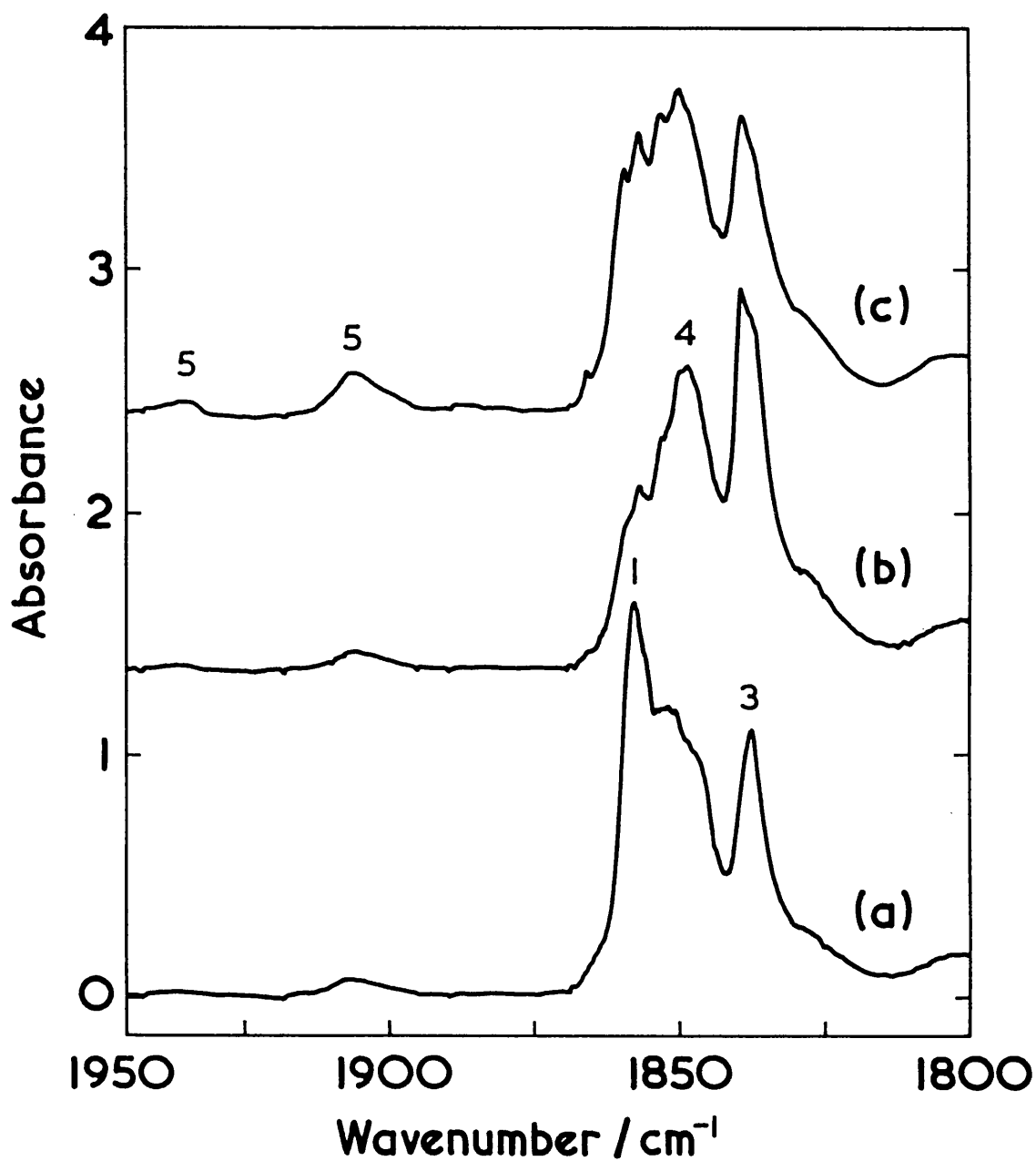


Figure 7.3. Infrared spectrum of the $\nu_{\text{C}=\text{O}}$ region of a solid oxygen matrix containing CBr_3F , taken after (a) UV photolysis ($\lambda > 240 \text{ nm}$) for 20 h, (b) warming to 25 K for 25 min, and (c) visible photolysis ($\lambda > 350 \text{ nm}$) for 15 h, showing group bands 1-5 of the product.

Chapter 8

CONCLUSIONS AND SUGGESTIONS FOR FUTURE WORK

8.1 CONCLUSION

In this thesis, the matrix isolation technique has been used to study a number of reactions, and thus many 'reactive' intermediates and weak complexes have been reported as have some photochemical mechanisms. All of these were possible because of the properties (see chapter 1) of low temperature matrices. The themes linking the five results/discussion chapters have been mentioned previously (chapter 1) and it is sufficient to recall here that the first three chapters (3-5) involve the study of ozone with a variety of iodine-containing precursors. The various precursors were chosen to study (i) the varying reactions occurring with different carbon chain lengths, (ii) the photochemical mechanism occurring and (iii) the effects of different methyl- and trifluoromethyl-groups on the spectra of the products. Chapters 5 and 6 reported the study of di-substituted methanes and the subsequent formyl halide...Lewis acid and carbon monoxide...Lewis acid complexes. In chapter 7 a recent gas phase experiment¹¹⁴ was repeated in the matrix environment enabling some of the elusive products to be detected (due to the different prevailing conditions).

The reactions of ozone with a range of halogenated alkanes have been studied in the preceding five chapters (3-7). All of these reactions were initiated photochemically, and in a number of cases additional re-combinations occurred after warming the sample in the matrix. The species detected are summarised below by simple reference to species types (e.g. iodoso-, iodyl- etc.); and in Table 8.1, by

chapter.

Iodoso-species (Z-IO). The following eight novel iodoso-species were detected: iodosoethane,^{47,ch.3} 2-iodosopropane,^{ch.3} iodosopentafluoroiodoethane,^{ch.4} iodoso-1,1,1-trifluoroethane,^{ch.4} iodoso-1,1,2,2-tetrafluoroiodoethane,^{ch.4} iodoso-1,1,1,2-tetrafluoroiodoethane^{ch.4} and iodosochloromethane^{ch.5}

Iodyl-species (Z-IO₂). Evidence has been presented for the following eight iodyl-species: iodylethane,^{47,ch.3} 2-iodylpropane,^{ch.3} iodylpentafluoroiodoethane,^{ch.4} iodyl-1,1,1-trifluoroethane,^{ch.4} iodyl-1,1,2,2-tetrafluoroiodoethane,^{ch.4} iodyl-1,1,1,2-tetrafluoroiodoethane^{ch.4} and iodylchloromethane.^{ch.5}

Hypoiodo-species (Z-OI). Tentative evidence has been presented (chapters 3-5) for several of these hydrated and polyfluorinated species. The detection of these hypoiodo-species helps to elucidate the mechanism, and in particular the rearrangement that is responsible for the final carbonyl species.

Carbonyl...Lewis acid complexes. The reaction of ozone with halogen-containing alkanes tends to result in the production of carbonyl...Lewis acid complexes, and in the course of this work eighteen have been detected. Useful comparisons can be made between the spectra of complexes having similar Lewis acids but different carbonyls and vice versa. The complexes detected are: CH₃COH...HI⁴⁷/HBr,^{ch.3} (CH₃)CO...HI,^{ch.3} CF₃COF...IF/HI,^{ch.4} CF₃COH...HI/IF,^{ch.4} CF₂HCOF...IF,^{ch.4} COHCl...HI^{ch.5}/HBr^{ch.6}/Br₂,^{ch.6} COH₂...I₂,^{ch.5} COHBr...HCl/BrCl,^{ch.6} COBrCl...H₂/HBr,^{ch.6} COBrF...Br₂,^{ch.7} and COF₂...Br₂.^{ch.7} The spectra and geometries of these complexes have been compared with similar complexes detected elsewhere (see relevant chapters).

Carbon monoxide complexes. These complexes are formed as a result of photodissociation of halogenated methanals. The complexes detected were OC...HCl...X (where X = HI,^{ch.5} HBr^{ch.6} and Br₂^{ch.6}), OC...X...HCl (where X = HBr and Br₂),^{ch.6} OC...X...HBr (where X = HCl and BrCl),^{ch.6} BrCl...CO...HBr,^{ch.6} HBr...CO...HCl,^{ch.6} and a number of (CO)_n(HX)_m^{ch.6} complexes (where X = Cl or Br).

These complexes are of interest since previously only complexes having similar HX groups, i.e. CO...HX...HX, have been detected, whereas in this study we have detected those having different hydracid groups.

Other complexes. The peroxides FC(O)O_x ^{ch.7} and the radical-atom pair FCO...Br ^{ch.7} were reported as secondary products of the reaction of ozone with CBr_3F . These two complexes provide useful information as to the preferred mechanism occurring in the reactions (chapter 7).

Mechanisms. Finally, in this thesis, by detection of the products after either time- or wavelength-dependent photolysis a number of reaction mechanisms have been proposed; there being two main types in this thesis. The first, is the wavelength-dependent transfer of an O atom from ozone to the iodine-atom of the precursor. Matrix isolation techniques are the only way in which the initial 'intermediates' could be detected, and hence the above mechanisms solved. The second type of mechanism involved the reaction of O atoms with a halogen-containing alkane and the formation of a carbonyl species. These matrix experiments enable the detection of the products and the distinction between possible competing dissociation paths to be made; see chapters 6 and 7 and the difference in dissociation path of formyl halides and carbonyl bromide fluoride.

8.2 SUGGESTIONS FOR FURTHER WORK

Improvements to current experiment

Improvements to the current experimental apparatus can be split into two groups: (i) spectroscopic and (ii) general apparatus. Dealing first with the spectral improvements, alignment of the spectrometer (either to use the near-ir or far-ir capabilities of the instrument) and use of the correct ir-transmitting windows would allow the entire infrared region, from near-to-far, to be recorded this change would

enlarge the number of species that could be studied. If the vacuum shroud and sample chamber were re-designed into a hexagon having four ports (4 spectral windows, 1 quartz, and the deposition inlets) it would be possible to collect spectra of adjoining regions with the same sample. The vacuum shroud and deposition apparatus could be modified to allow the 'sample cell' to be transported between spectrometers (e.g. UV-vis and Raman) and this would further the range of species that could be studied, in addition to providing increased electronic and vibrational information. At present the vacuum shroud can be used to collect both transmission infrared spectra and 180° reflection spectra, either UV-vis or Raman.

In addition to the adaption of spectral ports of the vacuum shroud, provision could be made for vacuum-UV photolysis of the matrices, either by replacement of the quartz window with a suitable vac-UV window (for instance LiF or MgF₂), or by use of a 'blind' argon discharge sustained by a microwave cavity, which could replace one of the existing deposition ports, or an additional port could be added for these purposes. Various improvements to the layout of the deposition and gas handling lines could be made, in particular using wider but shorter tubing would improve pumping efficiency and by reducing the effective wall area should make the production of ozone more efficient.

Future experiments

The study of the reaction of ozone with some additional precursors would provide useful comparisons with those studied in this thesis (note: these are mentioned where appropriate in the text). Referring to chapter 3, and the discussion of iodospecies at the end of chapter 5, a number of iodine-containing compounds could be studied to confirm the expected wavenumbers of the I-O bands of such species. The study, in chapter 4, of the fluoro-analogues of iodoethane would have benefited from the study of CH₃CF₂I, but this was unavailable at the time and thus CHF₂CF₂I was used as a replacement, since it had one hydrogen on the carbon atom not

containing the iodine atom. Other two carbon iodine-containing systems such as iodoethene, H_2CCHI , and iodoacetylene, HCCI , might be studied to determine if the products and mechanisms are similar to those of iodoethane.

In chapter 5 the study of the reaction of ozone with bromiodomethane, CH_2BrI , would provide a useful insight into the change in photochemistry that occurs between the reaction of CH_2ClI and of CH_2I_2 with ozone. In chapter 6 the reaction of bromochloromethane and dibromochloromethane with ozone was studied, and the study of bromodichloromethane¹³² provides interesting comparisons in terms of the products formed. In chapters 5-7 the reaction of O atoms with halogenated methanes was shown to proceed via elimination of HX or X_2 ; thus using triiodomethane, CHI_3 , as a precursor we should be able to produce formyl iodide as a product. The reaction of O atoms with CBr_3Cl could be studied and is expected to produce a carbonyl, whose subsequent photolysis could be studied. If, as expected the carbonyl COBrCl were produced its dissociation to either $\text{CO} + \text{BrCl}$ or $\text{ClCO} + \text{Br}$ could be compared with the similar products formed between O atoms and CBr_3F (chapter 7).

The study of the reaction of iodine cyanide, ICN , with ozone would extend the range of known reactions with iodine-containing compounds,^{19-21,47} and on the basis of the photochemical rearrangements reported for ICN ^{133,134} and NCO ,¹³⁵ and the existence of ONCl ¹³⁶ and NI ,¹³⁷ this reaction would be expected to produce species containing the elements ICNO (e.g. iodoso- and iodyl-, cyanate and isocyanate species). The photochemical interconversion between these species could thus be studied by wavelength-selective photolysis.

All the experiments reported in this thesis have involved varying the halogen elements. Interesting results would be obtained were sulfur atoms used instead of oxygen atoms; previously OCS has been used as a source of S atoms¹³⁸ in the reactions with NO ¹³⁹ and CH_4 ,¹⁴⁰ and CS_2 has been also used as a source in the reaction with H^{141} atoms. The experiments - in this thesis - are all based around halogenated alkanes, another area worth study would be the halogenated silanes and germanes.

Finally, during the course of this research various *ab initio* and semi-empirical calculations have provided valuable information. Additional calculations performed on the species studied in this thesis would greatly enhance the depth of the results, specifically with regard to distinguishing between competing mechanisms and to determining the geometry of complexes.

Table 8.1. Species detected after the reaction of oxygen atoms (ozone or O₂) with halogen-containing precursors (note: all the single iodine-containing precursors form a weak complex with ozone, e.g. [X-I...O₃]).

precursors	species detected
chapter 3	C ₂ H ₅ IO
C ₂ H ₅ I	C ₂ H ₅ OI C ₂ H ₅ IO ₂ CH ₃ COH...HI/(HOI)
C ₂ H ₅ Br	CH ₃ COH...HBr
(CH ₃) ₂ CHI	(CH ₃) ₂ CHIO (CH ₃) ₂ CHOI (CH ₃) ₂ CHIO ₂ (CH ₃) ₂ COH...HI
chapter 4	C ₂ F ₅ IO
C ₂ F ₅ I	C ₂ F ₅ IO ₂ C ₂ F ₅ OI CF ₃ COF...IF
CF ₃ CH ₂ I	CF ₃ CH ₂ IO CF ₃ CH ₂ IO ₂ CF ₃ COH...HI
CF ₂ HCF ₂ I	CF ₂ HCF ₂ IO CF ₂ HCF ₂ IO ₂ CF ₂ HCF ₂ OI CF ₂ HCOF...IF
CF ₃ CFHI	CF ₃ CFHIO CF ₃ CFHIO ₂ CF ₃ CFHOI CF ₃ COF...HI CF ₃ COH...IF

chapter 5	CH ₂ ClIO
CH ₂ ClI	CH ₂ ClOI
	CH ₂ ClIO ₂
	COHCl...HI
	OC...HCl...HI
CH ₂ I ₂	COH ₂ ...I ₂
<hr/>	
chapter 6	COHCl...HBr
CH ₂ BrCl	COHBr...HCl
	COBrCl...H ₂
	OC...HCl...HBr
	OC...HBr...HCl
	HBr...CO...HCl
CHBr ₂ Cl	COHCl...Br ₂
	COBrCl...HBr
	COHBr...BrCl
	OC...HCl...Br ₂
	OC...Br ₂ ...HCl
	OC...BrCl...HBr
	BrCl...CO...HBr
<hr/>	
chapter 7	COBrF...Br ₂
CBr ₃ F	FCO...Br
	FCO(O) _x
	COF ₂ ...Br ₂

APPENDIX A

Table A.1. Infrared bands /cm⁻¹ of ozone detected after co-deposition with a number of halogen-containing alkanes in argon matrices at 14 K.

precursor		ν_1	ν_2	ν_3	$\nu_1 + \nu_3$	
CH ₂ I ₂	¹⁶ O		702.1mw	1036.4br,vs		
	¹⁸ O			1016.8w	1997.1w	
					983.0vs	1993.3mw
					977.1sh,s	
CH ₂ BrCl	¹⁶ O	1104.2mw	704.0m	1037.6s	2110.9m	
				1025.1vw	2108.6ms	
				1005.8w		
CHBr ₂ Cl	¹⁶ O	1104.7mw	704.5m	1038vs	2110.5m	
				1027.0sh,w	2108.1m	
				1006.8w		
C ₂ H ₅ Br	¹⁶ O	1104.6w	704.2mw	1037br,vs	2110.8m	
					2108.6m	
	¹⁸ O	1042.9w	653.0w	979.7br,s	1995.4mw	
			649.0w		1991.5mw	
C ₃ H ₇ I	¹⁶ O	1104.7w	705.0ms	1040vs	2110.5m	
		¹⁸ O	1042w	664.9m	991.3w	1996.1m
			658.6w	979.8vs	1993.7m	
			652.7w			

REFERENCES

1. Whittle, E.; Dows, D.A.; Pimentel, G.C., *J. Chem. Phys.*, **22**, 1943, (1954).
2. Norman, I.; Porter, G., *Nature*, **174**, 508, (1954).
3. Lewis, G.N.; Lipkin, D., *J. Am. Chem. Soc.*, **64**, 2801, (1942).
4. Brown, H.C.; Pimentel, G.C., *J. Chem. Phys.*, **29**, 883, (1958).
5. Pimentel, G.C.; Ewing, G.E.; Thompson, W.E., *J. Chem. Phys.*, **32**, 927, (1960).
6. Okabe, H., *Photochemistry of Small Molecules*; Wiley, NY, (1976).
7. Moskovits, M.; Ozin, G.A., *Cryochemistry*; Wiley, NY, (1976).
8. Hallam, H., *Vibrational Spectroscopy of Trapped Species*; Wiley, NY, (1973).
9. Burnett, J.K.; Poliakoff, M.; Turner, J.J.; Dubost, H., in *Advances in Infrared and Raman Spectroscopy*, Vol. 2, Eds. Clark, R.J.H.; Hester, R.E.; Heyden, London, (1976).
10. Durig, J.R., *Analytical Applications of FTIR to Molecular and Biological Systems*; Reidel, Boston, (1980).
11. Downs, A.J.; Hawkins, M., in *Advances in Infrared and Raman Spectroscopy*, Vol. 10, Eds. Clark, R.J.H.; Hester, R.E.; Heyden, London, (1983).
12. Almond, M.J., Downs, A.J., *Spectroscopy of Matrix Isolated Species*, in *Advances in Infrared and Raman Spectroscopy*, Vol. 17, Eds. Clark, R.J.H.; Hester, R.E.; Wiley, NY, (1989).
13. Andrews, L.; Moskovits, M., *Chemistry and Physics of Matrix Isolated Species*; North-Holland, Amsterdam, (1989).
14. Almond, M.J., *Short-Lived Molecules*; Ellis Horwood, NY, (1990).
15. Andrews, L., *Appl. Spec.*, **33**, 199, (1979).
16. Jacox, M.E., *Rev. Chem. Intermed.*, **2**, 1, (1978).
17. Jacox, M.E., *J. Phys. Chem. Ref. Data*, **13**, 945, (1984); *ibid*, **17**, 269, (1988).
18. Perutz, R.N., 'Photochemical Reactions involving Matrix Isolated Atoms', *Chem. Rev.*, **85**, 77, (1985); *ibid.*, 'Photochemistry of Small Molecules in Low Temperature

Matrices', **85**, 97, (1985).

19. Hawkins, M.; Andrews, L.; Downs, A.J.; Drury, D.J., *J. Am. Chem. Soc.*, **106**, 3076, (1984).

20. Hawkins, M.; Andrews, L., *Inorg. Chem.*, **24**, 3285, (1985).

21. Andrews, L.; Hawkins, M.; Withnall, R., *Inorg. Chem.*, **24**, 4234, (1985).

22. *Laboratory Methods in Infrared Spectroscopy*, Eds. Miller, R.G.J.; Stace, B.C.; Heyden, London, (1972).

23. Barnes, A.J.; Orville-Thomas, W.J., *Vibrational Spectroscopy-Modern Times*; Elsevier, Amsterdam, (1977).

24. Wilson, E.B.; Decius, J.C.; Cross, P.C., *Molecular Vibrations*; Dover, NY, (1955).

25. Nakamoto, K., *Infrared & Raman Spectra of Inorganic and Coordination Compounds*; Wiley, NY, (1986).

26. Bell, R.J., *Introductory Fourier Transform Spectroscopy*; Academic Press, NY, (1972).

27. Martin, A.E., *Infrared Instrumentation and Techniques*; Elsevier, (1966).

28. Griffith, P.R., *Chemical Infrared Fourier Transform Spectroscopy*; Wiley, NY, (1975).

29. Griffiths, P.R., *Transform Techniques in Chemistry*; Plenum, NY, (1978).

30. Shriver, D.F.; Drezdson, M.A., *The Manipulation of Air-Sensitive Compounds*; Wiley, NY, (1986).

31. VAT Switzerland; Swagelock, Hoke, Nor-Cal Products Inc., ITL, Leybold-Heraeus, Edwards.

32. Bruker IFS Users' Manual, version 4/89, (1987).

33. Wayne, R.P., *Principles of Photochemistry*; Oxford Univ. Press, (1988).

34. Wayne, R.P., *Photochemistry of Atmospheres*; Oxford Univ. Press, (1990).

35. Calvert, J.G.; Pitts, J.N.Jr., *Photochemistry*; Wiley, NY, (1966).

36. Withnall R.; Hawkins, M.; Andrews, L., *J. Phys. Chem.*, **90**, 575, (1986).

37. Andrews, L.; Chi, F.K.; Arkell, A., *J. Am. Chem. Soc.*, **96**, 1997, (1974).

38. Downs, A.J.; Gaskill, G.P.; Saville, S.B., *Inorg. Chem.*, **21**, 3385, (1982).
39. Kugel, R.; Taube, H.J., *J. Phys. Chem.*, **79**, 2130, (1975).
40. Ogilvie, J.F.; Salares, V.R.; Newlands, M.J., *Canad. J. Chem.*, **53**, 269, (1975).
41. Roebbler, J.L., *J. Phys. Chem.*, **67**, 2391, (1963).
42. Schriver-Mazzuoli, L.; de Saxcá, A.; Lugez, C.; Camy-Peyret, C.; Schriver, A., *J. Chem. Phys.*, **102**, 690, (1995).
43. Barnes, A.J.; Hallam, H.E.; Howells, J.D.R., *J. Chem. Soc. Faraday Trans 2*, 1682, (1974).
44. Brosset, P.; Dahoo R.; Gauthier-Roy, B.; Abouaf-Marguin, L., *Chem. Phys.*, **172**, 315, (1993).
45. Brosset, P.; Dahoo, R.; Gauthier-Roy, B.; Abouaf-Marguin, L., *J. Chem. Phys.*, **172**, 315, (1993).
46. Walker, N.; Tevault, D.E.; Smardzewski, R.R., *J. Chem. Phys.*, **69**, 564, (1978).
47. Clark, R.J.H.; Dann, J.R., *J. Phys. Chem.*, **100**, 532, (1996).
48. Wiesenfeld, J.R., *Acc. Chem. Res.*, **15**, 110, (1982).
49. Herzberg, G., *Electronic Spectra and Electronic Structure of Polyatomic Molecules*; Van Nostrand, NY, (1966).
50. Withnall, R.; Hawkins, M.; Andrews, L., *J. Phys. Chem.*, **90**, 575, (1986).
51. Price, W. C.; Ed. In *Bond Energies Ionisation Potentials and Electron Affinities*; Edward Arnold Ltd., (1966).
52. Wong, S.F.; Vorburger, T.V; Woo, S. B., *Bull. Am. Phys. Soc.*, **16**, 213, (1971).
53. Robiette, A.G.; Parent, C.R.; Gerry, M.C.L., *J. Mol. Spec.*, **86**, 455, (1981).
54. Lugez. C.; Schriver, A.; Levant, R.; Schriver-Mazzuoli, L., *Chem. Phys.*, **181**, 129, (1994).
55. Hawkins, M.; Andrews, L., *J. Am. Chem. Soc.*, **105**, 2523, (1983).
56. Leone, S.R.; Klaassen, J.J.; Linder, J., *Abs. of Papers of the Am. Chem. Soc.*, **210**, 171, (1995).
57. Andrews, L.; Johnson, G.L., *J. Phys. Chem.*, **88**, 5887, (1984).

58. Gaufres R.; Béjaud-Bianchi, M., *Spectrochim. Acta.*, **27A**, 2249, (1971).
59. Levin and Lias, *Ionization Potential and Appearance Potential Measurements, 1971-1981*, U.S. Dept. of Commerce / National Bureau of Standards, NSRDS-NBS 71.
60. Personal communication from J.J. Klaassen and S.R. Leone.
61. Bach, S. B. H.; Ault, B. S., *J. Phys. Chem.*, **88**, 3600, (1984).
62. Nelander, B., *J. Mol. Struct.*, **69**, 59, (1980).
63. Pacansky, J.; Coufal, H., *J. Chem. Phys.*, **62**, 3298, (1980).
64. Dellepiane, G.; Overend, J., *Spectrochim. Acta*, **22**, 593, (1966).
65. Schriver, L., *J. Chem. Soc., Faraday Trans. 2*, **85**, 607, (1989).
66. Novak, M.J.; Szczepaniak, K.; Baran, J.W., *J. Mol. Struct.*, **47**, 307, (1978).
67. Francis, W.C.; Haszeldine, R. N., *J. Chem. Soc.*, 2151, (1955).
68. Clemitshaw, K.C.; Sodeau, J.R., *J. Phys. Chem.*, **93**, 3552, (1989).
69. Davis, S.R.; Liu, L.; *J. Phys. Chem.*, **97**, 3690, (1993).
70. Smardzewski, R.R.; Fox, W. B., *J. Phys. Chem.*, **79**, 219, (1975).
71. Kuo, J.C.; DesMarteau, D.D.; Fateley, W.G.; Hammaker, R.M.; Marsden, C.T.; Witt, J.D., *J. Raman Spec.*, **9**, 230, (1980).
72. Risgin, O.; Taylor, R.C., *Spectrochim. Acta*, **12**, 1036, (1959).
73. Smardzewski, R.R.; Fox, W. B., *J. Am. Chem. Soc.*, **96**, 304, (1974).
74. Smardzewski, R.R.; Fox, W. B., *J. Chem. Phys.*, **60**, 2104, (1974).
75. Jacox, M.E., *J. Phys. Chem.*, **87**, 4940, (1983).
76. Arkell, A., *J. Am. Chem. Soc.*, **87**, 4057, (1965).
77. Jacox, M.E., *J. Mol. Spec.*, **84**, 74, (1980).
78. Pacansky, J.; Waltman, R. J.; Ellinger, Y., *J. Phys. Chem.*, **98**, 4787, (1994).
79. Ottavianelli, E.; Maluendes, S.; Castro, E.; Jubert, A., *J. Mol. Struct.*, **210**, 305, (1990).

80. Ter Brake, J.; Driessen, A.J.; Mijlhoff, F.C.; Renes, G.H., *J. Mol. Struct.*, **81**, 277,(1982).
81. Loos, K.R.; Lord, R. C., *Spectrochim Acta*, **21**, 119, (1965).
82. Berney, C.V., *Spectrochim Acta*, **27A**, 663, (1971).
83. Dune, R.A., *Canad. J. Phys.*, **44**, 337,(1966).
84. Miller, J.H.; Andrews, L., *Inorg. Chem.*, **18**, 988, (1979).
85. Edgell, W.F.; Riethof, T.R.; Ward, C., *J. Mol. Spec.*, **11**, 92, (1963).
86. Berney, C.V., *Spectrochim Acta*, **25A**, 793, (1971).
87. Lugez, C.; Schriver, A.; Schriver-Mazzuoli, L.; Lasson, E.; Nielson, C.J., *J. Phys. Chem.*, **97**, 11617, (1993).
88. Schriver, L.; Gauthier-Roy, B.; Carrere, D.; Schriver, A.; Abouaf-Marguin, L., *Chem. Phys.*, **163**, 357, (1992).
89. Sablinskas, V.; Klæboe, P.; Nielsen, C.J.; Sülzle, D., *Analyst*, **117**, 365, (1992).
90. Dubost, H.; Abouaf-Marguin, L., *Chem. Phys. Lett.*, **17**, 269, (1972).
91. Leroi, G.E.; Ewing, G.E.; Pimentel, G.C., *J. Chem. Phys.*, **40**, 2298, (1964).
92. MOPAC v 6.0, Stewart, J.J.P., USAF Academy.
93. Wellington Davis, R.; Gerry M.C.L., *J. Mol. Spec.*, **97**, 117, (1983).
94. Suzuki, M.; Yamada, K.; Takami, M., *J. Mol. Spec.*, **88**, 207, (1981)
95. Andrews, L.; Arlinghaus, R.T.; Johnson, G.L., *J. Chem. Phys.*, **78**, 6347, (1983).
96. Barnes, A.J.; Hallam, H.E.; Schrimshaw, G.F.; *Trans. Faraday Soc.*, **65**, 3159, (1969); *ibid.* p.3172.
97. Schmitt, G.; Comes, F.J., *J. Photochem. & Photobiol. A: Chem.*, **41**, 13, (1987).
98. Porret, D.; Goodeve, C.F., *Trans. Faraday Soc.*, **33**, 690, (1937).
99. Baughaum, S.L.; Leone, S.R., *J. Chem. Phys.*, **72**, 6531, (1980).
100. Nelander, B., *J. Chem. Phys.*, **73**, 1026, (1980).
101. Harvey, K.B.; Ogilvie, J.F., *Canad. J. Chem.*, **40**, 85, (1962).

102. Perchard, J.P.; Cipriani, J.; Silvi, B.; Maillard, D., *J. Mol. Struct.*, **100**, 317, (1983).
103. Bouteiller, Y.; Abdelaoui, O; Schriver, A.; Schriver-Mazzuoli, L., *J. Chem. Phys.*, **102**, 1731, (1995); and references therein.
104. Giorgianni, S.; DeCarli, B.; Visinoni, R.; Gherseti, S., *Spec. Lett.*, **19**, 1207, (1986).
105. Weber, A.; Meister, A.G.; Cleveland, F.F., *J. Chem. Phys.*, **21**, 930, (1953).
106. Plyler, E.K.; Smith, W.H.; Acquista, N., *J. Res. Nat. Bur. Stand.*, **44**, 503, (1950).
107. Barnes, A.J.; Hallam, H.E.; Schrimshaw, G.F.; *Trans. Faraday Soc.*, **65**, 3150, (1969).
108. Overend, J.; Evans, J.C., *Trans. Farady Soc.*, **55**, 1817, (1960).
109. Itoh, K.; Kato, J.; Nakayama, Y.; Kutsuna, S.; Koike, K.; Ibusuki, T., *Chemosphere*, **29**, 1701, (1994).
110. Withnall, R.; Andrews, L., *J. Phys. Chem.*, **92**, 594, (1988).
111. Jacox, M.E.; Milligan, D.E., *J. Chem. Phys.*, **53**, 2688, (1970); *ibid.*, **47**, 1626, (1967).
112. Kwaitkowski, J.S.; Leszczyński, J., *Mol. Phys.*, **81**, 119, (1994).
113. Zhao, Y.; Francisco, J.S., *Mol. Phys.*, **77**, 1187, (1992).
114. Zhao, Y.; Francisco, J.S., *Mol. Phys.*, **79**, 1, (1993).
115. Francisco, J.S.; Goldstein, A.N.; Li, Z.; Zhao, Y.; Williams, I.H., *J. Phys. Chem.*, **94**, 4791, (1990).
116. Schneider, W.F.; Maricq, M.M.; Francisco, J.S., *J. Chem. Phys.*, **103**, 6601, (1995).
117. Francisco, J.S.; Williams, I.H., *J. Phys. Chem.*, **92**, 5347, (1992).
118. Wallington, T.J.; Ellerman, T.; Nielsen, O.J.; Sehested, J., *J. Phys. Chem.*, **98**, 2346 (1994); and references therein.
119. Meister, A.G.; Rosser, S.E.; Cleveland, F.F., *J. Chem. Phys.*, **18**, 346, (1950).
120. Ngai, L.H.; Mann, R.H., *J. Mol. Spec.*, **38**, 322, (1971).

121. Frank, A.J.; Hanrahan, R.J., *J. Phys. Chem.*, **82**, 2194, (1978).
122. Patty, R.R.; Lagemann, R.T., *Spectrochim. Acta*, **15**, 60, (1953).
123. Prochaska, F.T.; Andrews, L., *J. Phys. Chem.*, **82**, 1731, (1978).
124. Keelan, B.W.; Andrews, L., *J. Phys. Chem*, **83**, 2488, (1979).
125. Tevault, D.E.; Walker, N.; Smardzewski, R.R.; Fox, W.B., *J. Phys. Chem.*, **82**, 2733, (1978).
126. Jayanty, R.K.M.; Simonaitis, R.; Heicklen, J., *J. Photochem*, **4**, 381, (1975).
127. Ongoing research in this laboratory
128. Jacox, M.E., *J. Mol. Spec.*, **80**, 257, (1980).
129. Yarwood, G.; Niki, H.; Maker, P.D., *J. Phys. Chem.*, **95**, 4773, (1991).
130. Zhao, Y.; Francisco, J.S., *Chem. Phys. Lett.*, **199**, 65, (1992).
131. Maricq, M.M.; Szente, J.J.; Khitrov, G.A.; Francisco, J.S., *Chem. Phys. Lett.*, **199**, 71, (1992).
132. O'Neale, K., Studied in this laboratory, (1996).
133. Carr, B.R.; Chadwick, B.M.; Cobbold, D.G.; Grzybowski, J.M., Long, D.A., *J. Raman Spec.*, **4**, 421, (1976).
134. Carr, B.R.; Chadwick, B.M.; Cobbold, D.G.; Grzybowski, J.M., Long, D.A.; Marcus-Hanks, D.A.M., *Ber. Bunsen. Gesellschaft Phys. Chem.*, **82**, 98, (1978).
135. Bondybey, V.E.; English, J.H.; Matthews, C.W.; Contolini, R.J., *Chem. Phys. Lett.*, **82**, 208, (1981).
136. Cazzoli, G.; Degli Esposti, C.; Palmieri, P.; Simeone, S., *J. Mol. Spec.*, **97**, 165, (1983).
137. Becker, A.C.; Langen, J.; Oberhoffer, H.M.; Schuranth, U., *J. Chem. Phys.*, **84**, 2907, (1986).
138. Gunning, H.E.; Strausz, O.P., *Adv. Photochem.*, **4**, 143, (1966).
139. Hawkins, M.; Downs, A.J., *J. Phys. Chem.*, **88**, 3042, (1984).
140. Hawkins, M.; Almond, M.J.; Downs, A.J., *J. Phys. Chem.*, **89**, 3326, (1985).
141. Bohn, R.B.; Andrews, L.; Brabson, G.D., *J. Phys. Chem.*, **96**, 1582, (1992).